Title
Bridging Molecular Properties to Emergent Bulk Performance for Rational Design of Advanced Dynamic Materials

Permalink
https://escholarship.org/uc/item/6160q2zz

Author
Chung, Jaeyoon

Publication Date
2016

UNIVERSITY OF CALIFORNIA,
IRVINE

Bridging Molecular Properties to Emergent Bulk Performance for Rational Design of Advanced Dynamic Materials

DISSERTATION

submitted in partial satisfaction of the requirements
for the degree of

DOCTOR OF PHILOSOPHY

in Chemistry

by

Jaeyoon Chung

Dissertation Committee:
Professor Zhibin Guan, Chair
Professor Aaron P. Esser-Kahn
Professor Kenneth J. Shea

2016

DEDICATION

To

Ye Pei

my better half in every way

TABLE OF CONTENTS

LIST OF SCHEMES

Page

LIST OF FIGURES

LIST OF TABLES

ACKNOWLEDGMENTS

I would like to express my gratitude for Professor Zhibin Guan for allowing me the opportunity to work in his lab and for his support throughout my Ph.D. studies. His unwavering curiosity and enthusiasm for science have provided great discussions over the past years and his high standards have kept me aiming to exceed. I've learned a lot both about science and about professional development in the lab. I'd like to thank my thesis committee members: Professor Aaron Palmer Esser-Kahn and Professor Kenneth J. Shea. I also would like to thank Dr. Beniam Berhane and Dr. John Greaves for help in mass spectrometry, and also Dr. Philip Dennison for help on the NMR. I would also like to thank Dr. Jason Bemis of Asylum Research who helped me quite extensively on numerous aspects of operating the hardware and software of the AFM. The funding for my research was provided in part by grants from the US Department of Energy, Division of Materials Sciences, and the National Science Foundation. I sincerely thank these agencies for their financial support to make the research possible. I would also like to thank Allergan for providing me with the Allergan Graduate Fellowship, and the UC Regent for providing me with the Regent's Dissertation Fellowship.

I consider myself extremely fortunate to have worked in an environment that was very positive, incredibly supportive, and fostering of stimulating scientific conversations. For that I express my sincere thanks to current and former members of the Guan lab. In particular I want to thank Dr. Olivia Cromwell, James Neal, Dr. Davoud Mozhdehi, Dr. Greg Williams, and Dr. Aaron Kushner. As a student who entered with almost no organic chemistry experience, Aaron trained me well early on in the basics and organization of working in a chemistry hood. Greg was an exceptional role model in my early days in the Guan lab in terms of organization, presentation, conduct, and work ethic. Olivia first welcomed me into the lab, and has been a consistent mentor and great friend throughout the entire process. She always brought the most amazing positive energy and willing to lend a helping hand not just in science but also in professional development as well as everyday life. Davoud always brought an unparalleled zeal for science to every discussion, and constantly elevated the scientific level of conversation. James is an extraordinarily caring and intelligent person, and whatever small part I may have had in helping him in his early days through graduate school is among the most rewarding experiences of my Ph.D.

I am most grateful to my wife, Ye, by far the most attentive, supportive, and capable person that I know. Graduate school without her is simply unimaginable. I am grateful for my dog Scout, who lifts me up on a difficult day. I would like to thank my parents, Taeowan and Boksim, for always supporting me. I would like to thank my friends, in particular Ben, Ellen, Noah, Alan, Travis, Gary, and Glen for putting up with me and keeping me mostly sane throughout the process.

CURRICULUM VITAE

Jaeyoon Chung

1123 Frederick Reines Hall, Department of Chemistry

University of California, Irvine, CA 92617

Phone: (515)-559-4690

Email: jaeyooc@uci.edu

EDUCATION

Ph.D., Chemistry, University of California, Irvine, Irvine, CA *August 2016*

B.S. with Honors, Chemistry, California Institute of Technology, Pasadena, CA *June 2010*

RESEARCH EXPERIENCE

Vitrimer Materials from Dynamic Boronic Ester Bonds

University of California, Irvine, CA *Spring 2015 – Summer 2016*

Mentor: Professor Zhibin Guan

- Performed organic synthesis of di-boronic ester and tris-diol small molecules, tested various thermoset casting and curing conditions, and characterized by ^{1}H NMR, ^{11}B NMR and ES-MS
- Investigated dynamic mechanical properties through rheology and static tensile properties using Instron, and further characterized material through differential scanning calorimetry (DSC), thermogravimetric analysis (TGA).
- Investigated dynamic mechanical properties and activation energy of material flow from stress relaxation experiments and temperature sweep DMA experiments.

Malleable and Self-healing Materials from Tunable Dynamic Boronic Ester Bonds

University of California, Irvine, CA *Winter 2013 – Summer 2015*

Mentor: Professor Zhibin Guan

- Performed organic synthesis of di-boronic ester crosslinkers, and diol-based polymer through Ring-Opening Metathesis Polymerization (ROMP), and characterized by ^{1}H NMR, ^{13}C NMR, ES-MS, and gel-permeation chromatography (GPC).
- Investigated and calculated rates of trans-esterification using ^{1}H NMR peak coalescence and EXSY (exchange spectroscopy).

- Investigated dynamic mechanical properties through rheology and static tensile properties using Instron, and further characterized material through differential scanning calorimetry (DSC), thermogravimetric analysis (TGA), and stress-relaxation experiments.
- Probed variably dynamic properties of crosslinked materials through self-healing, reprocessibility, and malleability.

Correlation of Single Molecule Nano-mechanical Properties to Bulk Material Performance

University of California, Irvine, CA *Fall 2011 – Spring 2014*

Mentor: Professor Zhibin Guan

- Performed advanced organic and organometallic synthesis of biomimetic modular polymer through Acyclic Diene METathesis (ADMET) and characterized by ^{1}H NMR, ^{13}C NMR, various 2D NMR, ES-MS, MALDI-TOF, and GPC.
- Investigated through various single molecule force spectroscopic (SMFS) techniques on the atomic force microscope (AFM) and performed statistical analysis of data with IgorPro
- Synthesized, processed, and characterized bulk material via Instron tensile testing, differential scanning calorimetry (DSC), and dynamic mechanical analysis (DMA)
- Drew qualitative correlation between nano-mechanical properties to bulk tensile performance
- Resulted in a separate collaboration project with Prof. Dr. E.W. Meijer

Biochemical and Bioinformatic Studies of a Non-competitive Inhibitor of MraY

California Institute of Technology, Pasadena, CA *Summer 2010 – Summer 2011*

Mentor: Professor William (Bil) Clemons

- Designed E (inhibitor of MraY, essential protein in bacterial peptidoglycan pathway) / lysozyme protein fusion construct and expressed and purified protein
- Investigated effects of point mutations on inhibition capacity by performing DNA point mutations and growth and lysis assays after induction of protein E
- Wrote code in Python for bioinformatic search of proteins of *E.coli* similar to protein E based on certain criteria

Conformation Scanning of GTPase Pair Interactions with FRET Probes

California Institute of Technology, Pasadena, CA *Summer 2008; Summer 2009*

Mentor: Professor Shu-ou Shan

- Summer Undergraduate Research Fellow (SURF) 2009
- Performed basic biochemical techniques such as PCR amplification of DNA, primer design for DNA mutagenesis, cloning and ligation of DNA into vector
- Expressed and purified proteins with single cysteine mutations for dye labeling
- Labeled proteins with fluorescent probes (BODIPY-FL and coumarin dyes)

Summary of Technical Skills

- *Organic chemistry:* small molecule synthesis, workup and purification; characterization through ^{1}H NMR, ^{13}C NMR, ^{11}B NMR, 2D NMR (ROESY, NOESY, COSY, HMQC, HMBC, etc), ES-MS, MALDI-TOF.
- *Polymer chemistry:* polymer synthesis (ADMET, ROMP, etc); thermal and UV-curing of thermosets; characterization through ^{1}H NMR, GPC.
- *Material testing:* DSC, TGA, Instron (tensile), DMA (multi-frequency temperature sweep, stress relaxation, creep, tensile), rheology (time sweep, frequency sweep, time-temperature superposition (TTS)).
- *Other:* AFM imaging, AFM single molecule force spectroscopy.
- *Biochemistry:* Protein expression and purification, DNA cloning and ligation

TEACHING EXPERIENCE

Private Tutoring *Summer 2007*

- Designed and taught curricula for math ranging from Algebra to AP Calculus, and AP Chemistry to middle and high school students.

Graduate Teaching Assistant *Fall 2011 – Summer 2015*

Sophomore Organic Chemistry

- Led discussions sections; organized website management, led grading of midterms and final, prepared questions for weekly discussion, midterms and final examinations; advised students in office hours; held review sections for midterms and final.

Organic Chemistry Laboratory / General Chemistry Laboratory

- Taught laboratory sections; advised students in office hours; graded weekly experimental write-ups.

SERVICE TO THE DEPARTMENT

Safety Representative in Guan Lab (2015)

- Primary liaison between laboratory members and Environmental Health and Safety (EH&S)
- Supervision, delegation and management of: safe lab practices for group of 11 graduate students; training and orientation of eight new members; group coordination for EH&S safety inspection; drafting of SOPs; acquirement of PPE; assignment of Guan group jobs.

Member, Student Hosted Seminar Committee (2015)

- Hosted Prof. Stephen Craig from Duke on behalf of UC Irvine organic chemistry student body, coordinated schedule and introduced speaker to a room of >100 students and faculty.

AWARDS AND HONORS

- Allergan Graduate Fellowship (Fall 2015)
- Regents' Dissertation Fellowship (Spring 2015)
- Summer Undergraduate Research Fellowship, Cal Tech (Summer 2009)
- Best Poster Award, Gordon Research Conference, Bioinspired Materials (July 2014)

PUBLICATIONS

Zhang, X.; Lam, V. Q.; Mou, Y.; Kimura, T.; **Chung, J.**; Chandrasekar, S.; Winkler, J. R.; Mayo, S. L.; and Shan, S.- O. Direct visualization reveals dynamics of a transient intermediate during protein assembly. *Proc. Natl. Acad. Sci. U.S.A.* **2011**, *108*, 6450–6455.

Chung, J.; Kushner, A. M.; Weisman, A. C.; Guan, Z. Direct Correlation of Single Molecule Properties with Bulk Mechanical Performance for Biomimetic Design of Advanced Polymers. *Nature Mater.* **2014**, *13*, 1055–1062.

Cromwell, O. R‡.; **Chung, J‡.**; Guan, Z. Malleable and self-healing covalent polymer networks through tunable dynamic boronic ester bonds. *J. Am. Chem. Soc.,* **2015**, *137*, 6492–6495.

‡Co-first author.

Hosono, N.; Kushner, A. M.; **Chung, J.**; Palmans, A. R. A.; Guan, Z.; Meijer, E. W. Forced Unfolding of Single-Chain Polymeric Nanoparticles. *J. Am. Chem. Soc.* **2015**, *137*, 6880–6888. Highlighted in *Nature Chemistry* **2015**, *7*, 536.

Williams, G. A.; Ishige, R.; Cromwell, O. R.; **Chung, J.**; Takahara, A.; Guan, Z. Mechanically robust and self-healing superlattice nanocomposites by self-assembly of single-component "sticky" polymer-grafted nanoparticles. *Adv. Mater.,* **2015**, *27*, 3934–3941.

Zhao, R.; Zhang, Y.; **Chung, J.**; Shea, K.J. A Convenient Controlled Aqueous C1 Synthesis of Long-chain Aliphatic AB, AA and BB Macromers for the Synthesis of Polyesters with Tunable Hydrocarbon Chain Segments. ***ACS Macro Lett.*** 2016, *5*, 854.

PRESENTATIONS

Chung, J.; Zhang, X.; Shan, S.-O. Visualization of an Early Intermediate Preceding the Formation of a Stable Complex During Protein-Protein Interaction. [Oral presentation] ***SURF Seminar Day, California Institute of Technology***, Pasadena, CA, November 2009.

Chung, J.; Kushner, A.M.; Weisman, A.C.; Guan, Z. Direct correlation of single-molecule properties with bulk mechanical performance for the biomimetic design of polymers. [Oral presentation] ***UC Irvine Department of Chemistry Colloquium.*** 2013.

Chung, J*. (*Winner of best poster award*); Kushner, A.M.; Weisman, A.C.; Guan, Z**.** Direct correlation of single-molecule properties with bulk mechanical performance for the biomimetic design of polymers. [Poster presentation] ***Gordon Research Conference, Bioinspired Materials***, Newry, ME, June 2014.

Chung, J.; Cromwell, O.R.; Guan, Z. Dynamic bulk materials through tunably dynamic boronic ester bonds. [Poster presentation] ***Gordon Research Conference, Multifunctional Materials & Structures***. Ventura, CA, Feb. 2016.

Chung, J.; Cromwell, O.R.; Guan, Z. Dynamic bulk materials through tunably dynamic boronic ester bonds. [Oral presentation] ***251st ACS National Meeting, POLY division: Sustainable Polymers, Processes, & Applications***. San Diego, CA, March 2016.

ADDITIONAL INFORMATION

Affiliations

American Chemical Society (2012 – current)

Languages

Fluent in English and Korean

ABSTRACT OF THE DISSERTATION

Bridging Molecular Properties to Emergent Bulk Performance for Rational Design of Advanced Dynamic Materials

By

Jaeyoon Chung

Doctor of Philosophy in Chemistry

University of California, Irvine, 2016

Professor Zhibin Guan, Chair

The pursuit of dynamic molecular interactions to control macroscopic properties of polymers represents an exciting new direction to materials science. This new paradigm gives power to bottom-up rational design of materials to imbue remarkable macroscopic responses such as biomimetic adaptiveness, self-healing, and reprocessability. Thus, there is a critical need to establish a clear link between the mechanical and dynamic properties of advanced polymeric materials and the thermodynamic and kinetic parameters of its small molecule constituents, which is the goal of this dissertation.

In Chapter 2, we set out to directly correlate the fundamental mechanical properties of advanced dynamic materials to its individual molecular constituents. We used multi-cyclic single-molecule force spectroscopy (SMFS), paired with the unique capability of SMFS to derive the shape profile and the kinetic and thermodynamic parameters of the energy landscape of modular rupture and refolding, to characterize a *titin*-mimicking modular polymer. We found that a steep dissociative pathway accounted for the high plateau modulus, while a shallow associative well explained the slow dynamic recovery and energy-dissipative hysteresis.

In Chapter 3, we used variable small molecule kinetics to rationally design and directly correlate the advanced dynamic properties of dynamically crosslinked materials. Specifically, we crosslinked diol-based polymers with two variants of telechelic di-boronic esters, whose rates of transesterification vary by five orders of magnitude. It was found that the highly dynamic nature of the fast exchanging boronic ester imbued efficient self-healing and enhanced malleability, while the relatively inert nature of the slow exchanging boronic ester demonstrated little self-healing capability as well as diminished malleability, though both variants showed excellent reprocessibility at elevated temperatures.

In Chapter 4, we furthered the concept of Chapter 3 by moving to a dynamically crosslinked thermoset design. This was achieved through poly-condensation of telechelic boronic acids with multivalent diols. Though unfortunately the kinetic variability of boronic acid exchange and its emergent effect on bulk material was inconclusive, a boronic ester-based vitrimer material was nevertheless described, with a robust match between activation energies of molecular exchange and bulk material flow.

Chapter 1: Dynamic Bonds for Advanced Materials and their Correlation to Molecular Properties

1.1 Dynamic Molecular Processes in Dynamic Materials

It has been nearly a hundred years since Hermann Staudinger proposed his macromolecular hypothesis,[1] leading to the gradual acceptance of covalently linked long, organic polymeric species as a reality, and giving birth to the new field of polymer science.[2-8] From the emergence of the field, polymer science has been an interdisciplinary effort, but until the last few decades, there has been a disconnection between the chemists' and physicists' approach to polymer science. Polymer chemists have largely focused on refinement and control over the synthesis of polymeric species based on simple monomers, with focus on structure, uniformity and their effects on emergent performance. Consequently, polymer chemistry has enjoyed prolific advance in the ability to produce structures of wide variety and control.[5,6,9,10]

On the other hand, polymer physicists have largely been devoted to understanding of polymeric species, originally borrowing heavily from statistical physics to explain polymer behavior.[4] In classical works of polymer physics, individual polymer chains are often regarded as segments jointed by freely rotating chains,[7] so-called worm-like chains,[11] or reptating entangled polymer chains, [3] to name a few examples. Similarly, for ensemble viscoelastic behavior of bulk polymer melts, the Generalized Maxwell Models, which are depicted as circuits of springs and dashpots in series and parallel, may be used to predict their response to external oscillating stress.[8] These classical polymer physics methods and their refinements prove exceptionally powerful and can predict classical covalent polymers to remarkable effect.[2-5,8]

A striking feature of these classical approaches, however, is that often little to no attention is heeded to the chemical structure of the macromolecules in question. Consider, from the seminal *Principles of Polymer Chemistry* by Paul J. Flory: “The complexities of high polymers are far too great for a direct mechanistic deduction of properties from the detailed structures of the constituent molecules; even the constitution of polymers often is too complex for an exact description.”[2] A main reason that this has been possible as the dominant approach to understanding behavior of polymers is the simplicity and relative uniformity of their design. Traditionally, polymers have been designed to be static, with irreversible, permanent covalent bonds serving as the linkers between monomer units. The passive and static nature of these polymer chains allow their approximation as chemically non-descript chain entities and thus the small molecular contribution to the macromolecular whole has traditionally been rather unimportant. Chemical structure-to-property relationships in polymers certainly do exist, but the extent to which chemical structures are considered in understanding and predicting emergent properties of synthetic polymers often amount to empirical additivity of their constituent monomeric units, mainly used to predict thermal transition behavior.[12]

In the past few decades, there has been a shifting paradigm towards the incorporation of non-static molecular interactions and processes into polymeric materials for adaptive, responsive, or otherwise dynamic effect.[13-19] These molecular interactions may range from weak supramolecular interactions such as hydrogen bonds[20] to stronger supramolecular interactions such as metal-ligand interactions,[21] or reversible, dynamic covalent interactions.[16] Furthermore, covalent bonds that can be activated to be dynamic upon application of stimulus such as heat or light have also been incorporated into polymeric materials.[17,22] This shifting paradigm has allowed scientists and engineers to imbue remarkable macroscopic responses such as self-healing,[23-25] shape-memory,[26] malleability,[27] photoresponsive dynamic properties,[28] mechanoresponsive properties,[18,19] and electroresponsive properties,[29] to name a few.

From the chemists' point of view, this advance has brought about some changes in perspective. Firstly, rational bottom-up materials design has been given added complexity and benefit. That is, designing polymers first with consideration of the molecule, the molecular dynamic interaction and its effect on the final emergent material dynamic properties in mind, and then building the rest of the polymer around the dynamic small molecule species, has become a productive and efficient approach. This philosophy of material design has been employed for a large variety of functional purposes, including a few examples to be presented in the work of this thesis.[30,31] From the bottom-up view we rationally engineer novel material properties through molecular design. In Chapter 2 we describe the use of a molecular, sacrificial hydrogen bonding motif for biomimetic enhancement of material toughness.[30] In Chapter 3 we describe the use of dynamic boronic ester exchange in order to design self-healing materials.[31] In Chapter 4 we extend the boronic ester exchange motif to a reprocessable dynamic thermoset, i.e. vitrimer design.

For the rest of the sections in the introduction, some backgrounds on the dynamic materials concepts for each individual project will be covered. These include: for Chapter 2, the biomimetic concepts pertaining to muscle protein *titin* mimicking synthetic organic material; for Chapter 3, the concept, history, and overview of the examples for self-healing materials; and for Chapter 4, the concept and precedent examples of strong organic glass-forming materials, so-called vitrimers. We close the chapter with a section on conclusions and outlook.

1.2 ***Titin*-mimicking Synthetic Materials**

Biomimetics is an interdisciplinary realm of study in which scientists and engineers elucidate mechanistic details of nature's design philosophies, distill them down to simple concepts, and implement them in synthetic systems in the laboratory.[32,33] The primary workhorse of living organisms is the protein, where nature has developed a highly diverse set of remarkable materials through eons of evolution largely with the 20 naturally occurring amino acids as their monomeric units. Though synthetic materials are now capable of carrying out a wide variety of exciting dynamic functions due in large part to the aforementioned smart materials revolution, a baseline property of any material is its mechanical performance, namely its strength, toughness, elasticity, ductility, durability, et cetera. Fortunately nature has an abundance of biomaterials that provide inspiration in these design concepts. Specifically, elastomeric proteins, materials in the body that respond to mechanical stimuli, are used for mechanical and structural function and can provide strength, toughness and elasticity.[34] Examples of these types of proteins include elastin, resilin, byssus, and *titin*.[34] In this portion of the introduction, we will focus on the muscle protein *titin*,[35] and in particular its design element that provides its desirable toughness.

1.2.1 ***Titin* Nanomechanics demonstrates Molecular Mechanism for its Toughness**

Titin, so named for its titanic size (~3 MDa), is a linear polymer of immunoglobulin (Ig) and fibronectin-III (Fn-3) modules, crosslinked and processed in such a way as to provide a load-bearing matrix. The molecular mechanism responsible for these material properties was revealed starting with a pair of pioneering works by Gaub[36] and Bustamante[37] nearly two decades ago. Gaub and co-workers used the atomic force microscope (AFM) not for its traditional imaging purposes, but as a tool to bridge the substrate surface and the AFM tip with a single molecule of *titin*. They found repeated rupture forces in the regime of 150 and 300 pN, with regularly spaced increases in contour length of 25 – 28 nm between each rupture (Figure 1.1a). This gave rise to a pN-nm force-extension plot with 'sawtooth' like patterns, a feature that is now a hallmark of single molecule force spectroscopic (SMFS) studies. In the same study, the authors performed cyclic approach-retraction experiments on the same molecule of *titin*, and sawtooth patterns were confirmed to reemerge after repeated cycles, demonstrating the refolding of modules after rupture upon relaxation of external stress.[36] Concurrent work by Bustamante and co-workers demonstrated similar results using optical laser tweezers in lieu of the AFM.[37] Subsequent protein nanomechanical work followed, in which recombinant proteins with selected modular repeats of immunoglobulin components of *titin* were engineered in order to more specifically tease out each domain's mechanical strength. In particular, a homo-polypeptide of the immunoglobulin I27 and I28 domain were studied by Fernandez and co-workers, more accurately determining the rupture forces of these domains to be approximately 204 ± 26 and 257 ± 27 pN, respectively (at 600 nm/s pulling rate).[38]

These studies were complemented by the computational equivalent of SMFS, or steered molecular dynamics (SMD) pioneered by Schulten and co-workers.[39] When a single domain of I27 was pulled from one terminus to the other through SMD, nine hydrogen bonds were identified as the units bearing the load. Specifically, three cooperative hydrogen bonds between beta strands A and B arranged in anti-parallel conformation were first ruptured, revealing an intermediate before complete rupture of the module. Then the six cooperative hydrogen bonds between beta strands A' and G arranged in parallel conformation ruptured, followed by rapid unfolding of the entire domain revealing its entire hidden length (Figure 1.1b).[40] This intermediate along the path of complete unfolding of the module was confirmed in a parallel SMFS study by Fernandez and co-workers.[41]

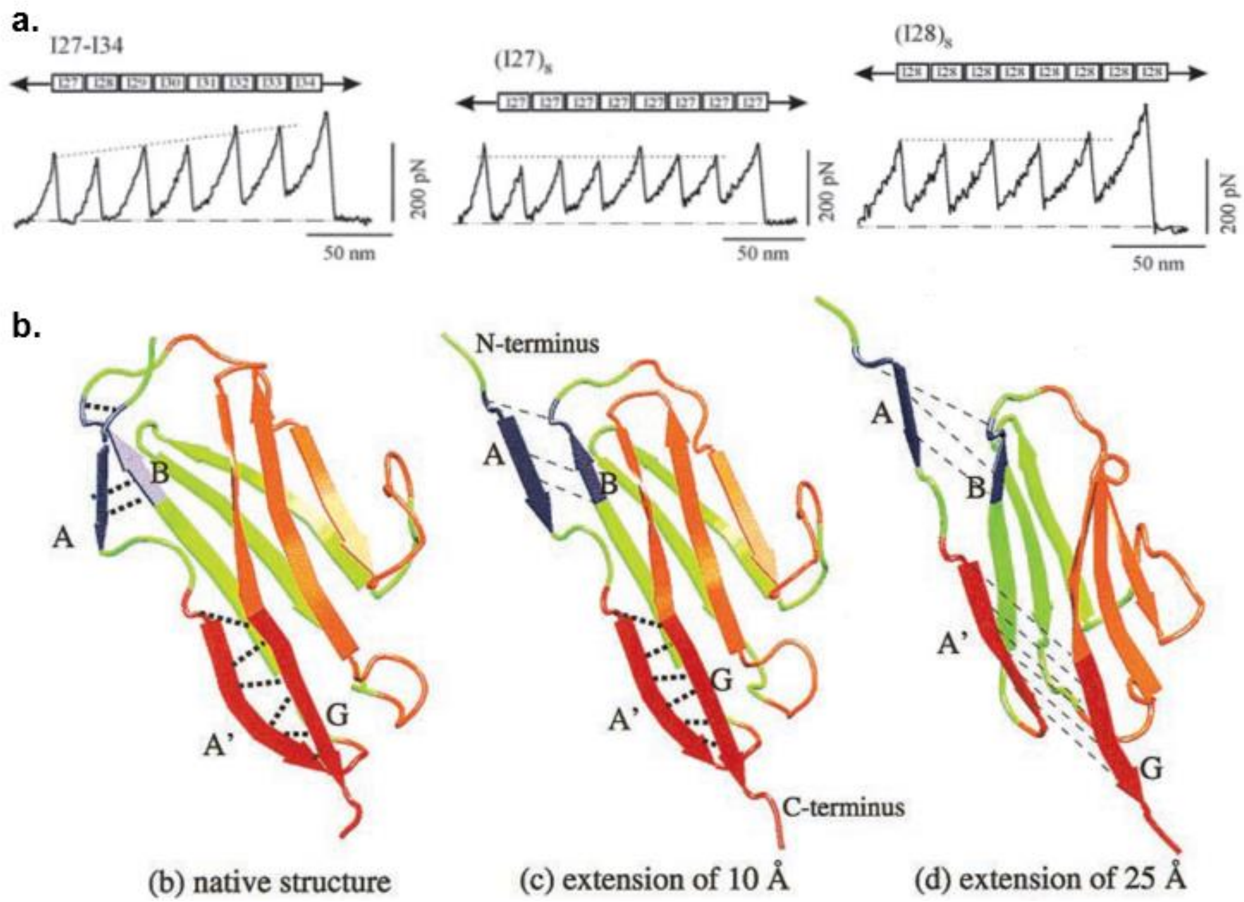

Figure 1.1 *Titin* nanomechanics. a. Single molecule force spectroscopy (SMFS) studies of recombinant *titin* heteropolymer of I27-I34 domains (left) and homopolymers of I27 (middle) and I28 (right). Force histograms for the latter show a narrow single peak centered at 204 pN and 257 pN for I27 and I28, respectively. b. Steered molecular dynamics (SMD) simulations for the I27 domain shows cooperative load on three hydrogen bonds in anti-parallel conformation between beta strands A and B, followed by load on six hydrogen bonds in parallel conformation between beta strands A' and G leading to failure. Figure adapted and reprinted from refs 38 & 40.

This series of experiments provide a picture for the molecular mechanism that lends the stretchability, strength and toughness of *titin*. First is its strength: what would normally be a weak interaction in the form of hydrogen bonds is provided moderate strength in the form of high rupture forces through cooperativity. What is revealed after the cooperative rupture is a long hidden length, allowing each domain to be stretched far beyond its initial length without catastrophic damage to the material. Taken together in a modular repeat, a relatively large amount of force is constantly required to persist through a long extension before all the domains are ruptured, ultimately resulting in a large amount of energy dissipated before catastrophic failure, the materials basis for toughness. Finally, these ruptured modules rejoin upon relaxation of external stress, allowing for the toughness to be restored with time, a feature frequently referred to in the literature as passive elasticity.[42]

1.2.2 Synthetic *Titin*-mimicking Tough Materials

In our lab, we have taken these design principles and incorporated them into organic polymers for synthetic replication of material toughness. The ureidopyrimidinone motif, more commonly referred to as UPy, is a supramolecular moiety that dimerizes strongly in nonpolar solvents through four cooperative hydrogen bonds, similar to the load-bearing six cooperative hydrogen bonds in the beta sheets of the I27 domain. The UPy motif was first described by Meijer and co-workers in 1997[20,43] and has since then found widespread usage as a supramolecular motif in polymer systems. The dimerization strength of this unit in nonpolar solvents are in the range of 11 – 12 kcal/mol ($K_D = 5.7 \times 10^7$ M^{-1} in chloroform, and $K_D = 5.9 \times 10^8$ M^{-1} in toluene),[44] showing a range that provides a promise for reversibility, adaptability and strength, but lying well below the covalent bonding regime, therefore not competing with any permanent bonds in the module to be broken upon rupture from external stress.

The original UPy-module mimic to the *titin* protein developed in the Guan lab was a simple design that combined the concepts of cooperative H-bonds as the basis for a reversible material and a hidden length (poly(tetramethylene oxide) pre-polymer) upon rupture (Figure 1.2a).[45] This polymer successfully demonstrated the biomimetic integration of the strength and toughness and dynamic elasticity both in single molecule and in bulk, but suffered a few drawbacks of non-uniformity; e.g. the non-uniform length of the hidden length between modules, three different pulling orientations of the UPy-module leading to two sets of rupture forces, and re-dimerization between random neighboring partners after rupture.

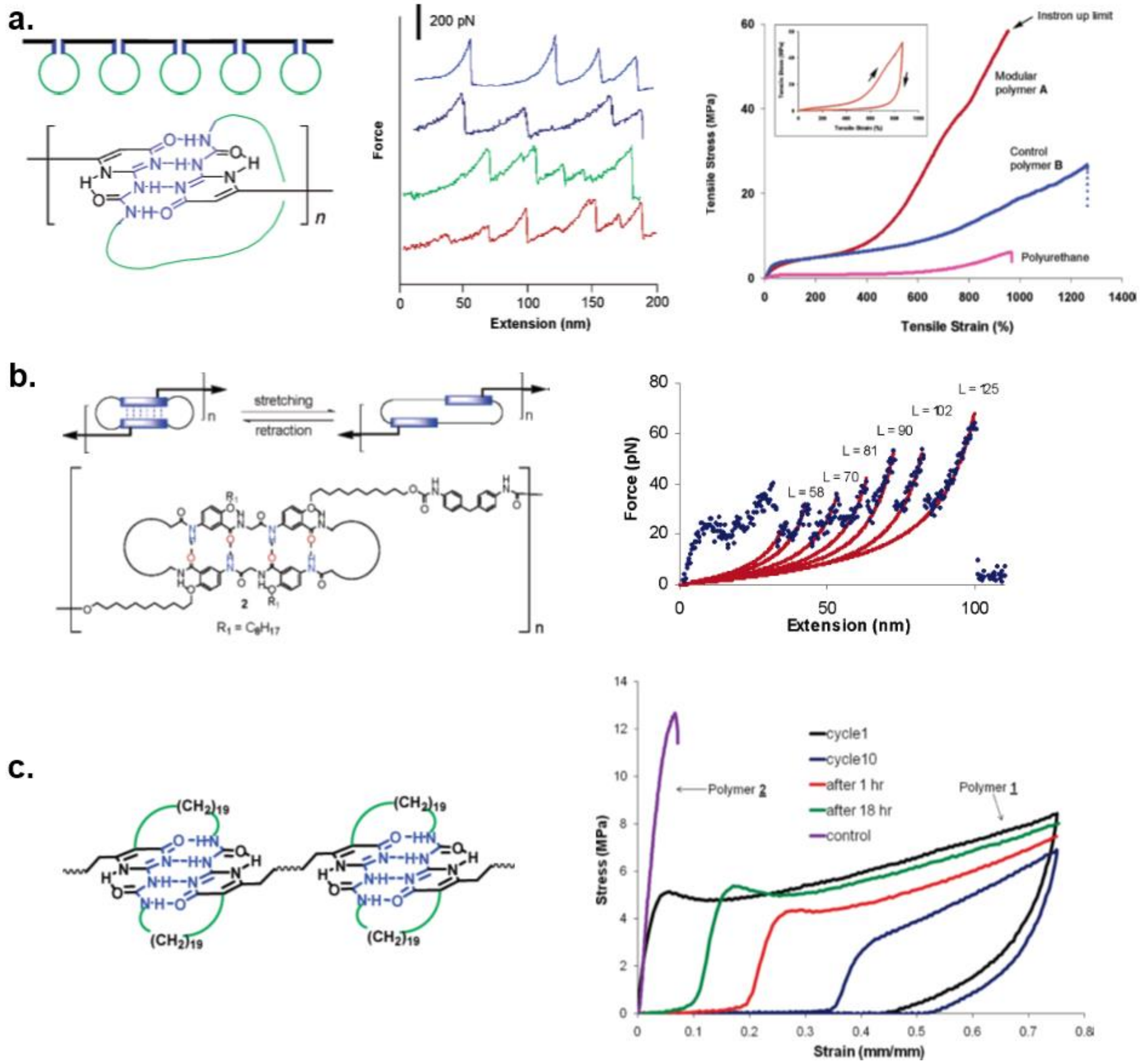

Figure 1.2 Guan lab *titin* mimicking synthetic materials. a. First generation of *titin* mimicking materials was a modular repeat of ureidopyrimidinone (UPy) and poly(tetramethylene oxide) units (left). SMFS studies showed high rupture forces up to ~200 pN, but showed rather large variability. This was attributed to the different possibilities of the pulling orientation of the UPy dimer units (middle). The bulk mechanical properties (red) show extraordinary combination of extensibility and toughness (right). b. Next iteration design featured a modular repeat of a peptidomimetic quadruple hydrogen bonding unit enclosed in a double closed loop (DCL) arm architecture (left). SMFS shows controlled modular spacing between rupture of each unit (right). c. The UPy-DCL design features both the UPy core and the double closed loop arms in modular repeat (left). Bulk mechanical properties show strength, toughness and elasticity as well as slow

recovery of dimension and mechanical properties after removal of external stress (right). Figure adapted and reprinted from refs. 45, 46 & 48.

The next synthetic iteration eliminated these issues by employing a so-called "double closed loop" (DCL) architecture, installing hydrocarbon loops around the self-dimerizing hydrogen bonded units for controlled rupture and re-dimerization (Figure 1.2b). This design allowed for a monodisperse hidden length, a set dimerization partner per module, and a uniform pulling orientation. In initial employment of the DCL design, the UPy core was abandoned in favor of a self-dimerizing unit consisting entirely of amide hydrogen bonds, for a greater biomimetic analogy to a beta sheet structure.[46] In a follow up study, 4, 6, and 8 hydrogen bonds were employed as the self-dimerizing core units and paired with SMFS as well as SMD, predictably showing higher rupture strength with increasing number of hydrogen bonds in the dimerizing core.[47] Generally, this amide-based hydrogen-bonded self-dimerizing unit proved thermodynamically less stable than UPy, and a UPy-DCL design was ultimately employed in condensed solid material,[48] showing robust strength, extensibility and toughness (Figure 1.2c).[48,49]

In a somewhat different approach, protein engineering aided by bioinformatics screening guided the design for a protein-based material utilizing similar biomimetic concepts. The bioinformatics search screened for proteins with properties known for mechanical stability, including the C-terminal and N-terminal strands of the beta sheets in cooperative hydrogen bonds aligned in parallel conformation. The chosen protein, Af1521, had an additional advantage over the hydrogen bonds in the immunoglobulin domains of *titin*, which is that the load-bearing hydrogen bonds between the C- and N-terminal beta strands were deeply buried in the hydrophobic pocket, leading to complete shielding from water.[50] A linear modular repeat of this protein showed rupture forces as high as 522 ± 50 pN (at 4000 nm/s pulling rate), almost doubling the rupture force of I32 of ~300 pN, the strongest of the well-studied domains of *titin*.[41,51] Through SMD and

SMFS it was shown that the hydrophobic burial of the load-bearing strands was crucial for the mechanical strength, as when portions of the protein were deleted through protein engineering to expose those strands to water, the average rupture force was severely compromised at 247 ± 76 pN (at 1000 nm/s pulling rate).[50]

1.3 Self-healing Materials

All materials, as part of their lifecycles, inevitably experience degradation through fatigue and damage that start as microcracks that propagate can ultimately cause irreversible, catastrophic failure. The traditional engineering approach has been to combat these unavoidable elements of fatigue, damage, and failure by delaying them, that is, through development of mechanically robust materials. As onset of damage and its ability to propagate is delayed, naturally the lifetime of the material in question is lengthened. We saw, in the previous section, one of nature's design strategies for said approach: the use of sacrificial weak and dynamic bonds for enhanced stretchability and toughness. Self-healing, another one of nature's mechanisms, is a fundamentally different approach to tackle this dilemma. Instead of delaying the onset of imperfections of a material's lifecycle, it reverses them as they arise. Naturally, this salient feature is a prime target of mimicry into synthetic materials, as it has the obvious implications of extending the material's lifetime. This enhanced lifetime can further extrapolate to more durable, safer, less wasteful, and more recyclable materials.[23-25]

Wound healing as employed in biology is a multi-step process involving a complex interplay between multiple cell types and proteins.[52] The first and immediate response is hemostasis, or blood clotting, where platelets are rushed to the wound site and glued by fibrin to patch the wound site together.[53] This is quickly followed by inflammation, where cells damaged by the wound process are removed through phagocytosis.[54] Then new cells and tissue are proliferated, forming new extracellular matrices (ECM) through fibroblast growth and secretion of collagen and fibronectin. Finally the provisional ECM is remodeled through collagen realignment and removal of unneeded cells through apoptosis.[55]

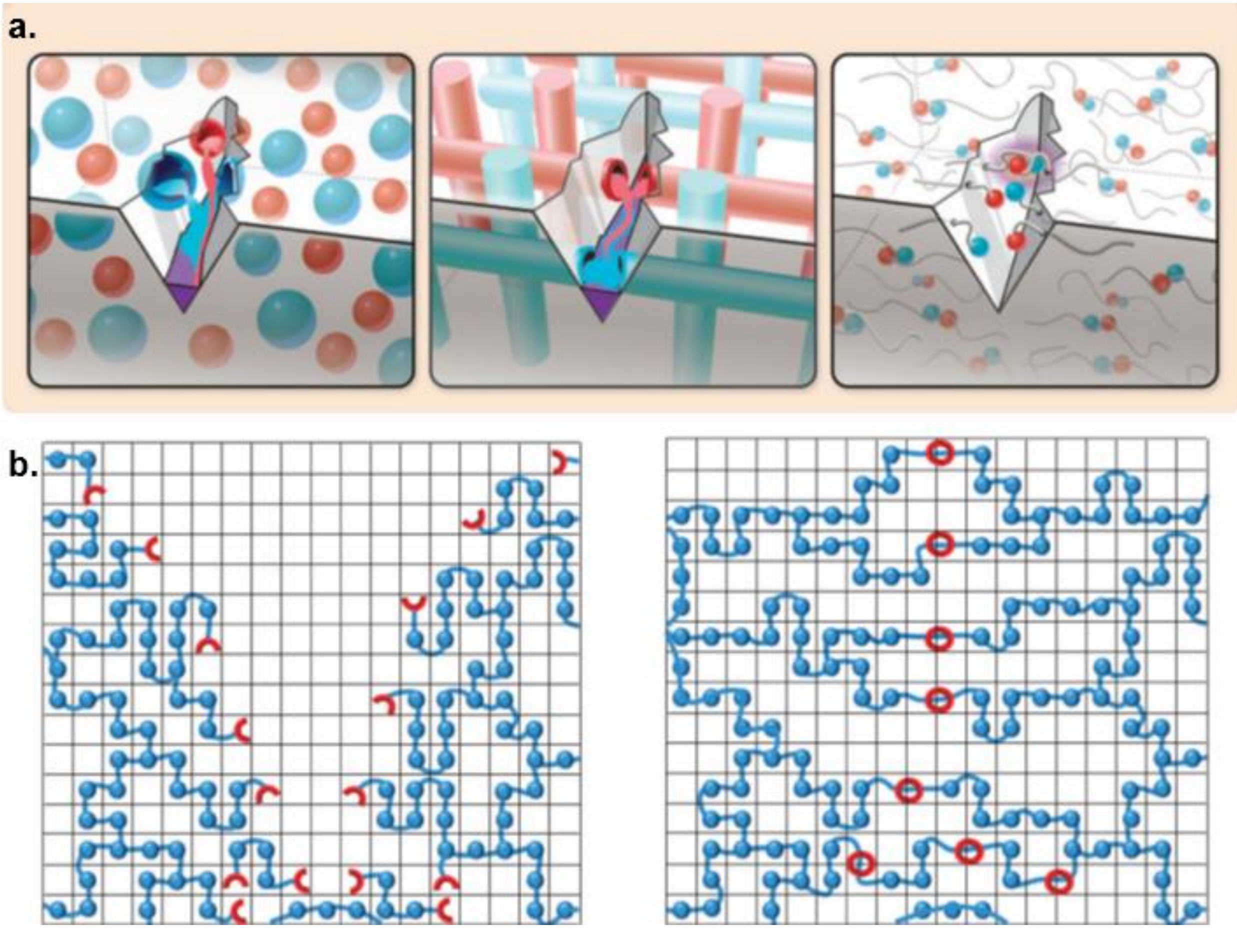

Figure 1.3 Self-healing types and concepts. a. Three main categories of self-healing include capsule-based (left), vascular (middle), and intrinsic (right). Capsule based self-healing materials flow healant upon damage to crack site initiated by capsule rupture. Healant solidifies through polymerization and fills the crack with solid material. Vascular self-healing materials also flow healant to damaged site, but through capillary action in a network of vascular channels. Intrinsic self-healing materials seal the damaged surface through dynamic chemistry. b. Simplified schematic for intrinsic self-healing. Damage causes polymer chains to take up less volume, and polymer chains move towards each other to maximize entropy. This allows reactive functional groups in polymer chains to find each other and react, sealing the damaged interface and causing healing. Reprinted from refs. 23 & 24.

This process is rather complex, and in the spirit of biomimicry, for synthetic materials the concepts are distilled and the process for material healing is necessarily far simpler. Self-healing synthetic polymeric materials are broadly divided into three categories: microencapsulated composite materials, vascular networks, and so-called 'intrinsic' self-healing materials (Figure 1.3a). In terms of the healing process, the microencapsulation and vascular methods of healing (*vide infra*) is closer to the biological approach in its initial clotting and inflammation stages as it generally involves immediate delivery of needed material to the damaged site, which solidifies over time to fill the damaged interfaces with healed material. The intrinsic approach to healing (*vide infra*) borrows concepts more closely to the later stages of wound healing, which involve the reformation and remodeling of networks to be homogeneous with the rest of the material (Figure 1.3b).[23-25]

1.3.1 Intrinsic Self-healing Materials

Intrinsic self-healing materials are so named because the chemical structure of the polymers themselves intrinsically contain the necessary chemical functional groups for healing when damage occurs to the material.[23] The chemical functional groups in question must have a dynamic component, which can traverse across damaged interfaces and stitch them back together. Since the chemical functionalities that perform the healing chemistry are intrinsic to the polymer structure and are nearly always reversible, healing through many repeated cycles at a single location is possible.[56]

When damage occurs, two interfaces are generated at the site of the defect. The creation of the defect is accompanied by either chain slippage or chain breakage in order to create the negative volume of the damaged site.[24] As polymer chains now occupy a smaller physical space after damage, the system is temporarily set out of equilibrium due to an entropic loss of freedom of the polymer chains in a smaller volume. If the newly created interfaces are in poor registry or a long physical distance between the damaged surfaces are allowed to persist for too long, new equilibria at each interface will result instead of healing.[57] When in good registry and close physical proximity of the damaged interfaces, however, the restoration of a new equilibrium is the driving force of the healing process, wherein segmental movement of the polymer chains can reoccupy the defect volume, physically adjoining the damaged interfaces.[58] Then dynamic chemistry can reform broken bonds, restoring mechanical properties and aiding in reentanglement of chains, homogenizing the damaged area and repairing the network.

Damage to a material such as a microcrack necessarily generates a discontinuity in the volume of the sample. In the encapsulation and vascular methods to self-healing (*vide infra*), the negative volume of the defect is filled through redirection of liquid healant that is sequestered from the rest of the material until damage occurs, which solidifies and restores continuity in the sample volume. As discussed in the above paragraph, in the intrinsic self-healing approach, new material flow into the negative volume of the damaged site depends not upon liquid flow but upon polymer flow, which is almost universally less facile. Consequently, the temperature at which healing can be effective in intrinsic self-healing materials depends critically on the T_g of the polymer chains (and T_m in semi-crystalline materials) as good polymer chain mobility is an essential requirement for reactive chain ends to find each other and perform the required healing chemistry.[24]

Intrinsic self-healing materials were first demonstrated in 2002 by Wudl and co-workers, who used Diels-Alder reactions as the dynamic chemistry to effect healing (Figure 1.4).[56] Utilizing the fact that the equilibrium between the Diels-Alder and retro-DA reactions could be affected through heating, the authors synthesized a network from tetra-furan and tris-maleimide monomers. Full mechanical characterizations showed that the material showed mechanical properties comparable with commercial epoxies. A pre-crack was generated and tested to fracture, after which the samples were re-aligned and heated to 120 to 150 ºC for 2 hours and allowed to cool to room temperature. The healed samples were tested again, which showed an approximately 50% healing of fracture load. A second healing cycle showed 80% recovery of the fracture load compared to the first cycle, demonstrating the possibility of healing through multiple cycles. Other materials have since utilized the on-off equilibrium of a chemical reaction to effect healing. Examples include other cycloaddition-reversion pairs used for self-healing include coumarin[59] or anthracene[60] dimerization, and the formation and reversion of hindered ureas from isocyanates and bulky amines.[61]

a.

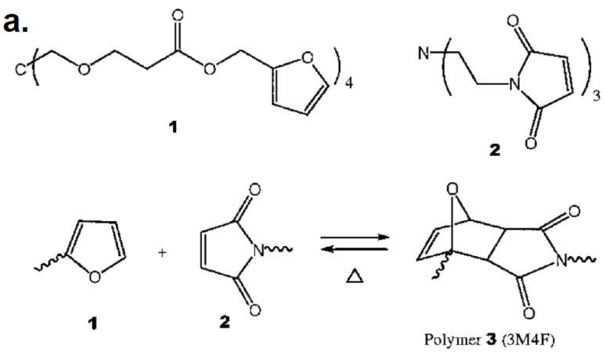

c.

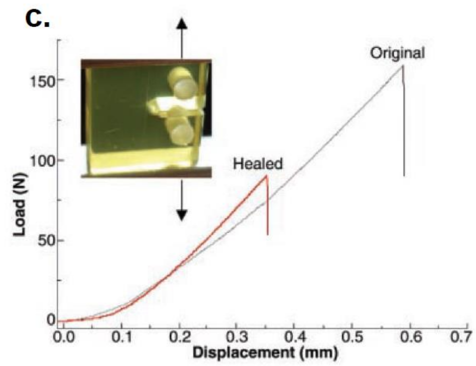

b.

Properties	Polymer **3**	Epoxy resins
Tensile		
Strength (MPa)	68*	27 to 88
Modulus (GPa)	—	2.4
Elongation (%)	1.6 to 4.7	3 to 6
Compression		
Strength (MPa)	121*	102 to 170
Modulus (GPa)	3.1	3.4†
Flexural		
Strength (MPa)	143*	88 to 143
Modulus (GPa)	—	

d.

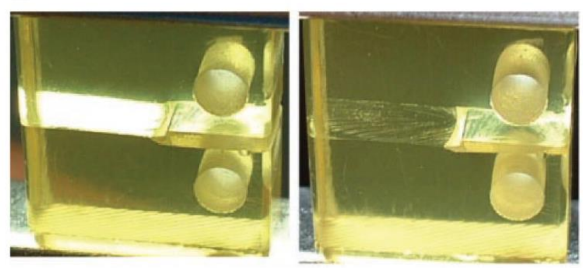

Figure 1.4 Diels-Alder based intrinsic self-healing material. a. Monomers used and schematic representation of networked formed through pervasive Diels-Alder reaction. b. Comparison of virgin material with commercial epoxies shows robust mechanical properties. c. Tensile properties of original and self-healed material mechanical properties. d. Failed sample before (left) thermal treatment for healing and after (right). Adapted and reprinted from ref. 56.

Whereas the above examples took advantage of a shifting chemical equilibrium to form or break covalent chemical bonds, a ubiquitous source of energy such as UV-light can also be harnessed to create reactive functionalities for self-healing. A polyurethane network film with oxetane-substituted chitosan moieties was synthesized and was found to heal upon irradiation with UV light (302 nm) (Figure 1.5).[62] Though the exact mechanism for healing was not elucidated, the authors concluded that reactive chain ends that reacted both through the oxetane and chitosan were involved, as healing was not observed in films without either component. The healing capability was observed through IR and optical imaging where a microscopic crack was shown to disappear after irradiation for 30 minutes. The irradiation intensity was rather minor, which the authors estimate to be roughly on the order of the UV exposure from the sun in summertime, indicating favorable industrial applicability.

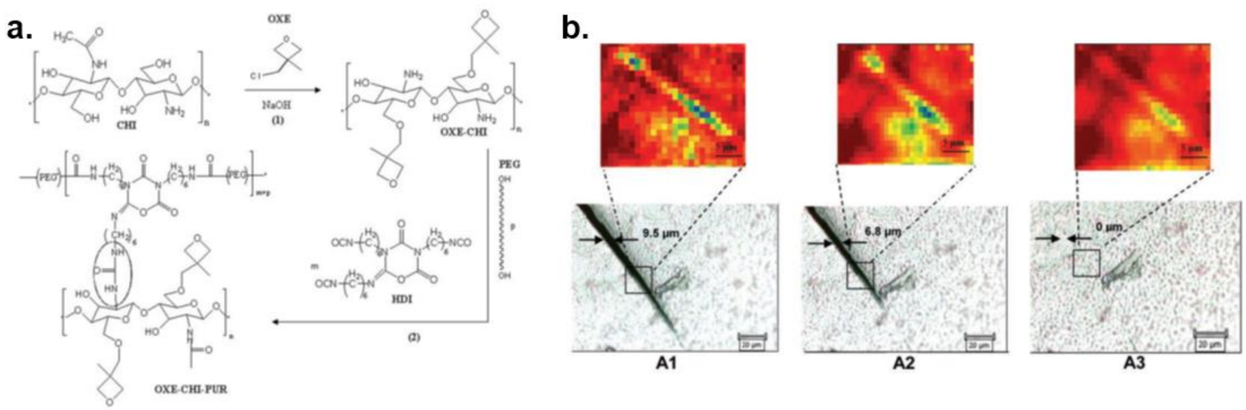

Figure 1.5 Oxetane-chitosan polyurethane intrinsic self-healing material. a. Schematic for synthesis of the oxetane-substituted chitosan polyurethane network polymer. b. IR (top) and optical (bottom) images of a disappearance of a microcrack after UV-irradiation. Left to right: 0, 15, and 30 minutes after UV irradiation. Adapted and reprinted from ref. 62.

In the previous examples, formation or breakage of new bonds is the driving force for dynamic chemistry. A thermodynamically neutral reaction that occurs rapidly at room temperature can be utilized to produce a spontaneously self-healing material at ambient conditions. In a simple example, commercial polybutadiene was covalently crosslinked with standard radical conditions and impregnated with low quantity of Grubbs G2 catalyst (50 – 100 ppm), allowing the pervasive olefins in the network to be constantly shuffled around within the matrix (Figure 1.6).[63] With one olefin exchanging for another, the reactants and products are completely thermodynamically equivalent, and therefore no external stimulus such as light or heat is required in order to bias the formation or breakage of bonds or for the reaction to proceed. Furthermore, commercial polybutadiene has an extremely low T_g allowing free polymer chain dynamics at any reasonable service temperature. Indeed, at 75 ppm Grubbs G2 catalyst with 20 kPa pressure between the manually cut interfaces, healing was quantitative in 3 hours at room temperature and even showed substantial (~90% of ultimately strength) healing even at 5 ºC over 24 hours. Other examples that take advantage of a thermodynamically neutral exchange to form equivalent species include disulfide exchange,[64,65] siloxane exchange,[66] radical shuffling reactions of trithiocarbonates[67] or thiuram disulfide[68] moieties.

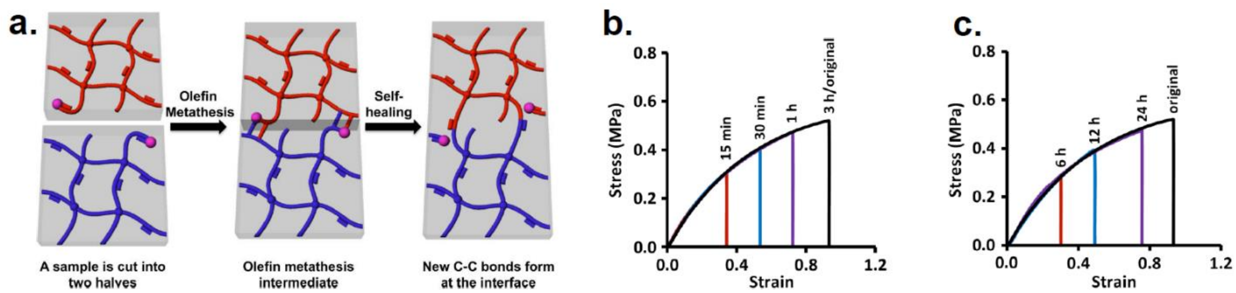

Figure 1.6 Olefin metathesis based intrinsic self-healing material. a. Concept cartoon depicting healing process. Ruthenium catalyzed olefin metathesis occurs across damaged interface and results in healed material. b. Self-healing tensile plots at room temperature with 75 ppm embedded Grubbs catalyst and 20 kPa pressure. Healing is quantitative at 3 hours. c. Self-healing tensile plots at 5 ºC with 75 ppm embedded Grubbs catalyst and 20 kPa pressure. All the original Young's modulus and approximately 90% of the original ultimate strength is restored in 24 hours. Adapted and reprinted from ref. 63.

The above examples have dealt with the formation, breakage, and dynamic exchange of covalent bonds. Covalent bonds offer the advantage of bond strength which often correspond to mechanical robustness, but can be energetically more intensive to initiate shuffling and thus slower to remodel the network for effective healing.[24] Supramolecular chemistry provides an effective solution to this dilemma, as association-dissociation dynamics through non-covalent means is generally faster and inherently reversible.[69] This means that healing dynamics can be quite rapid when supramolecular chemistry is employed, however they are often limited to low T_g materials for their full effect to manifest in healing systems, and thus usually comes at the expense of the mechanical robustness and stability of healing systems based on covalent bonds.

Arguably the simplest of supramolecular interactions is the hydrogen bond, ubiquitous not only in biology but also in synthetic polymers, including polyurethanes, polyureas, polyaramides and polyamides, which constructively use hydrogen bonds for structural and mechanical stability. Cordier et al in 2008 first describe the use of hydrogen bonding supramolecular interactions for self-healing materials, where cheap, readily available fatty di- and tri-acids were first condensed with diethylene triamine and then by urea to produce a mixture of relatively small molecular weight oligomers with an abundance of amide and urea functional groups (Figure 1.7a).[57] The resulting mixture of compounds was plasticized with dodecane to lower the glass transition temperature (T_g ~8 ºC) for rubber-like properties at ambient conditions. These hydrogen bonds spontaneously crosslinked the oligomers producing a supramolecular elastomer in the condensed phase. Behaving like a classical rubber, the material showed good extensibility approaching 600%, and a moderate ultimate strength of ~3 MPa. The material showed quick and high efficiency healing at room temperature, however, the material showed very low initial stiffness.

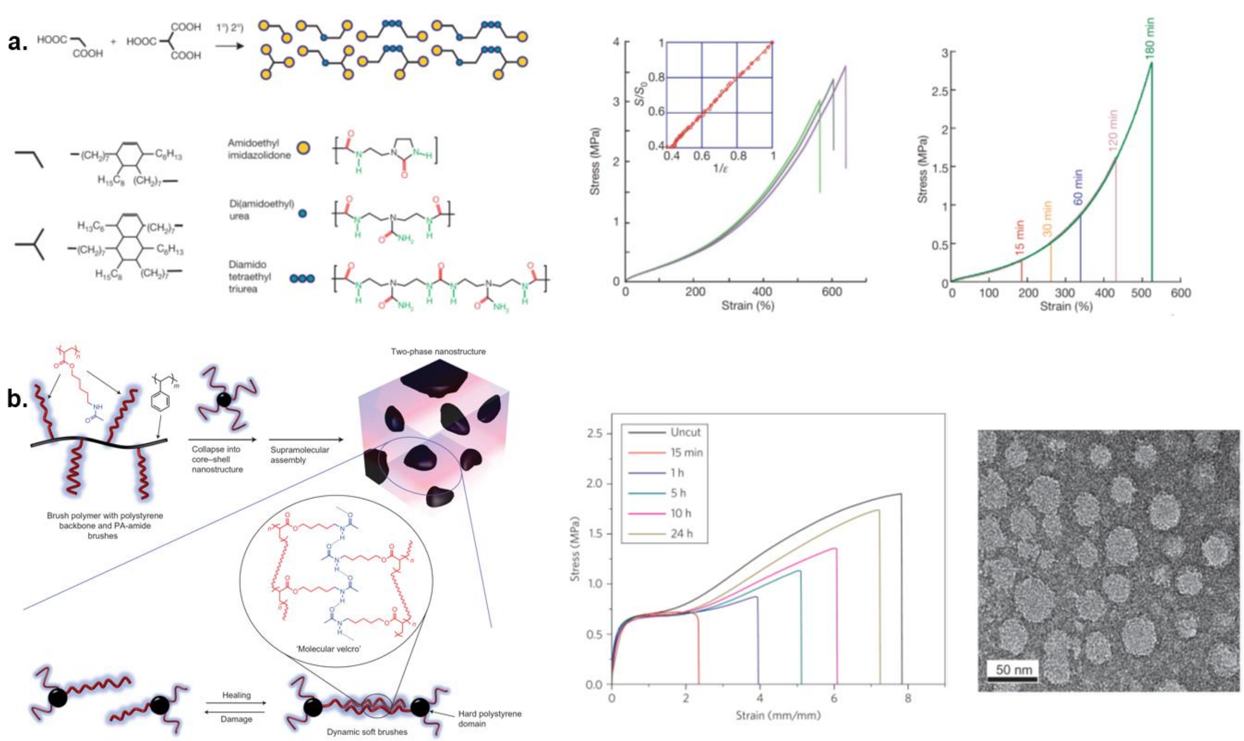

Figure 1.7 Self-healing materials based on hydrogen bonds. a. Concept design of supramolecular hydrogen bonded elastomer. Condensation products of di- and tri- fatty acids with an abundance of amide and urea hydrogen bonding units self-assemble into supramolecular rubber (left). Triplicate test results of virgin supramolecular material shows elastomeric properties (middle). Self-healing of material at room temperature shows near quantitative healing in 3 hours (right). b. Concept design of self-healing material toughened through thermoplastic elastomer design (left). Material recovers nearly all of its mechanical properties after 24 hours of healing, with a notably higher stiffness (middle). Transmission electron micrograph (TEM) stained with uranyl acetate shows phase-separated microstructure to combine stiffness and healing capability (right). Adapted and reprinted from refs. 57 & 70.

To address the low stiffness of the hydrogen-bonded self-healing material, Guan and co-workers employed a thermoplastic elastomer design to phase separate a hard phase for mechanical integrity and a soft phase for self-healing properties (Figure 1.7b).[70] Specifically, a bottle-brush system was employed with a polystyrene backbone and a soft designer polyacrylate brush with pendant amides. In appropriate processing conditions, the polystyrene backbone underwent a hydrophobic collapse to a spherical structure while the long polyacrylate brushes extended out of the spheres like coronas free to interact with each other and provide healing through the amide hydrogen bonding. The resulting material was able to retain the robust self-healing capabilities of hydrogen bond-based design while also enjoying the mechanical stiffness of thermoplastic elastomer design. This concept has been expanded to other phase-separated structures, including block-co-polymer,[71] core-shell nanostructure,[72] and silica nanocomposite designs,[73] the latter of which exhibited an unexpected mechanochromic property through condensed-phase photonic crystal like effects.

Another common supramolecular interaction used to effect self-healing is the metal-ligand interaction.[21] Reported in 2011, Rowan, Weder and co-workers designed a macromonomer with a poly(ethylene-co-butylene) linker telechelically end-capped by Mebip ligands (Figure 1.8a).[74] When $Zn(NTf)_2$ salt was added a high molecular weight linear supramolecular polymer was formed through Zn-ligand interactions, which formed an entangled melt. Ultraviolet light of 320

– 390 nm was pulsed twice for 30 seconds onto the sample after damage, which caused healing of the material. The mechanism was shown to be through an absorption of 341 nm UV light from the Zn-Mebip ligand complex, dissipating much of the absorbed energy through heat, causing high localized heating up to 220 ºC, temporarily liquefying the hard phase where the metal ligand pairs reside, dissociating the Mebip ligand from the metal center, and triggering the necessary dynamics for self-healing to occur. In other example, Mozhdehi et al designed a thermoplastic elastomer system wherein metal ligand (Zn-imidazole) interaction lie in the soft matrix instead of the hard phase, allowing ambient healing without external stimulus (Figure 1.8b).[75] These two contrasting examples utilizing the same metal salt demonstrate the potency of metal ligand complexes as a dynamic motif with a wide spectrum of variability in strength and on-off rates.

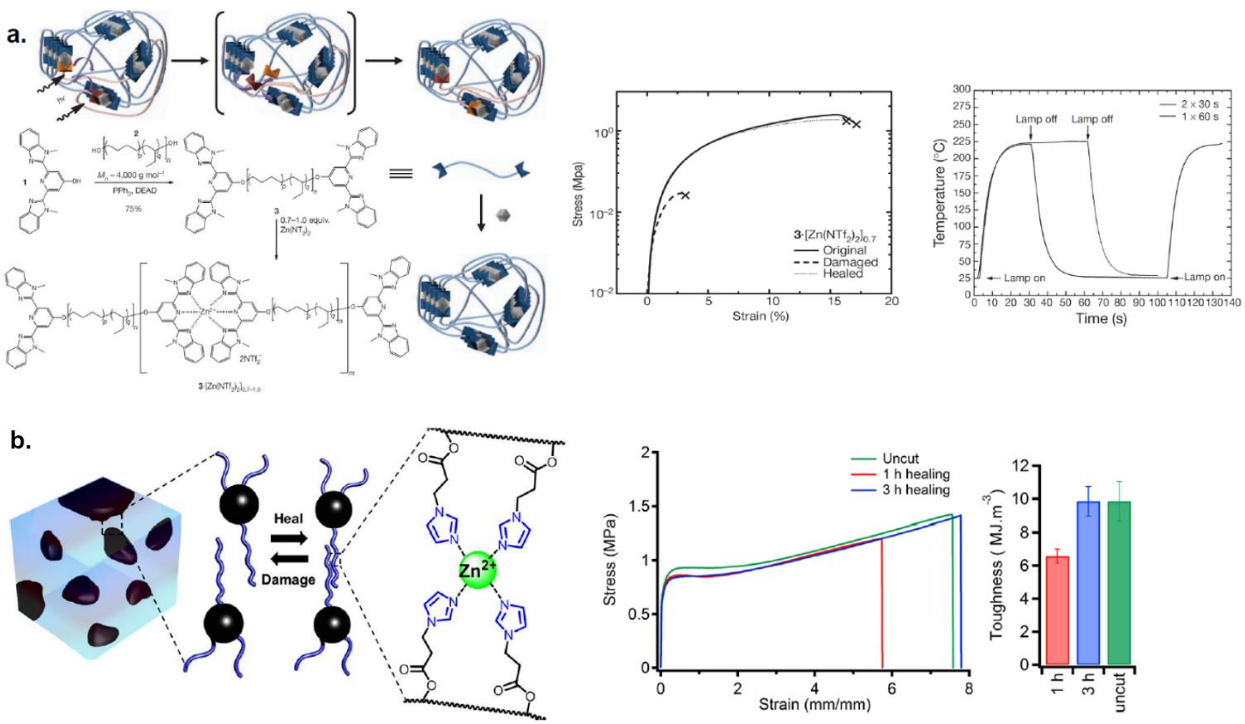

Figure 1.8 Self-healing materials based on metal-ligand interactions. a. Concept design of a self-healing metallopolymer linearly assembled through Zn^{2+} - Mebip interactions (left). For 0.7 equivalent of metal to telechelic bis-Mebip macromonomer, self-healing is quantitative upon UV light irradiation (middle). Local temperature at site of light irradiation rises to above 200 ºC for healing to occur which is necessary as the metal-ligand interaction lies in the hard phase (right). b. Concept design of a multi-phase metallopolymer wherein the Zn^{2+} - imidazole ligand interaction

lies in the soft matrix (left). Healing at room temperature shows quantitative recovery of toughness after 3 hours of healing (right). Adapted and reprinted from refs. 74 & 75.

Additionally, pi-pi stacking interactions are used for self-healing, where a pair of donor-acceptor aromatic species are chosen with complementary electron densities in the pi system strengthening the pi-pi interaction and promoting specificity in the interactions. In one example, a linear oligomer of pi-electron-poor aromatic bisimides were mixed with pi-electron-rich telechelic pyrene compounds which supramolecularly assembled into a gel. Initial demonstration of healing was shown through ESEM images where small cracks were shown to disappear at relatively high temperatures of 80 ºC.[76] A follow up example, which combined pi-pi stacking and hydrogen bonding interactions, demonstrated robust healing of mechanical properties including Young's modulus and toughness, but healing had to be conducted at 100 ºC.[77]

1.3.2 Capsule-based Self-healing Materials

In the capsule-based self-healing approach, a polymer matrix, often hardened epoxy, is embedded with capsules of varying size dispersed throughout the matrix. As the material is physically damaged, the capsules at the damage site burst open, spilling out its contents and filling the space of the newly formed crack. Here a variety of different mechanisms can occur, but typically the liquid monomer that was spilled comes into contact with catalyst that was dispersed in the matrix, triggering crosslinking through polymerization and subsequent hardening to seal the crack. In general, capsule-based self-healing materials are capable of healing strong, hard materials such as epoxies, and do not require external intervention to bring damaged surfaces together. However, a fundamental limitation of the approach is that healing cannot occur in the same location more than once without manual addition of additional monomer, as rupture of a microcapsule (and spillage of its contents) is irreversible.[23] A few additional considerations are universal to this type of self-healing material.

First, the encapsulation method must be robust. This is particularly true since the capsules embedded in the final polymer matrix often have reactive chemical species enclosed inside them, which is necessary for the healing to occur once the capsules rupture in the final material. Designing an emulsion polymerization condition in which these reactive chemical species not only stay inside the emulsion droplets (which ultimately become the inside of the capsules), but also is minimally reactive to solvent including water can be somewhat challenging. Typically the encapsulation is performed either through in situ polymerization or interfacial polymerization. In in situ polymerization, monomers first oligomerize in one phase, which switches polarity as oligomers and migrate to the other phase, finishing polymerization and forming a membrane capsule around the second phase. In interfacial polymerization, the two components necessary for polymerization of the capsule reside in the two different phases, and when they meet at the interface, they polymerize for form a membrane. Urea-formaldehyde (UF)[78] microcapsules are commonly synthesized through the former method, while polyurethane (PU)[78] and polyacrylate (PA)[79] capsules are common in the second. These and other methods of encapsulation are reviewed in several publications.[80,81]

The size and thickness of the capsules are some of the other general considerations for encapsulated self-healing materials. Capsule sizes normally lie in the micron range, but nanocapsule self-healing materials also exist.[82] Naturally, greater size capsules lead to greater volume of enclosed healant, and thus a greater capacity for healing larger damages. It comes at the cost of a larger, potentially detrimental effect on the overall properties of the material, including surface roughness. Conversely, smaller capsules can offer greater homogeneity to the final material at the cost of lower volume of healant per capsule, and thus requiring greater amount of capsule. Thickness of capsule walls must be carefully balanced, primarily as it correspond to its response to external damage. Too thick and capsules may not burst with damage, failing to heal when needed, and too thin and it may rupture prematurely before crack formation, or permeate healant material out to the matrix, causing leakage before desired healing. Finally, the capsule-to-matrix bonding interaction is also of due consideration, as with poor interaction between the interfaces, propagating cracks may simply deflect off the capsules and avoid triggering the healing event.[25]

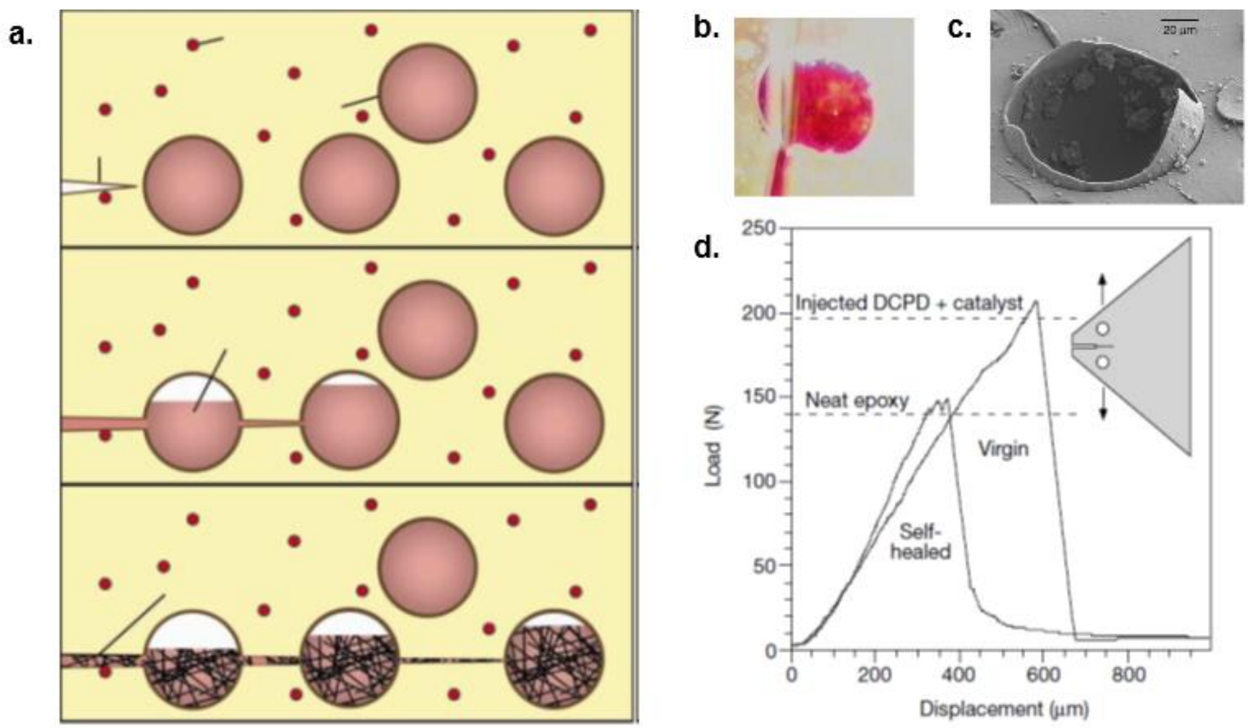

Figure 1.9 Capsule-based self-healing. a. Design concept for the mechanism of capsule-based healing. As a microcrack propagates throughout the material, it bursts microcapsules containing DCPD monomer, which spills into the crack, comes into contact with Grubbs catalyst embedded in the epoxy, and polymerizes and hardens for healing. b. Optical micrograph of a rupturing capsule filled with red dye, and c. Scanning electron micrograph (SEM) of a ruptured capsule demonstrate the viability of the approach. d. Fracture tests on virgin and self-healed sample shows recovery of ~60% fracture load after healing. Adapted and reprinted from ref. 83.

The possibility of synthetic self-healing materials gathered widespread attention when a capsule-based approach to self-healing was reported in 2001 (Figure 1.9).[83] Specifically, an epoxy network (diglycedyl ether of bisphenol A (DGEBA) hardened with diethylenetriamine (DETA)) was dispersed with first generation Grubbs (Grubbs G1) catalyst and dispersed with UF microcapsules filled with dicyclopentadiene monomer (DCPD). In this system, upon crack formation, UF microcapsules burst along the crack, filling the space with DCPD which comes into contact with Grubbs G1 catalyst, and initiates ring-opening metathesis polymerization (ROMP)[10] to form crosslinked poly-DCPD within the crack space.

Modeling guided the design of synthesis of the microcapsules of appropriate compliance and thickness, and optical and scanning electron spectroscopy confirmed rupture of capsules upon crack propagation. Healing efficiency was tested by way of measuring fracture toughness of virgin and healed samples of tapered double cantilever beam (TDCB) specimens. Specifically, pre-cracks were formed and load applied in perpendicular orientation. Critical load for propagation of the crack was recorded for the virgin sample, after which the sample was allowed to sit without external load and manual intervention for 48 hr at room temperature. The sample was tested again to measure the critical load for propagation of the crack of the healed sample. The results showed 75% maximum, 60% average recovery of fracture load upon healing. As expected, control samples missing either the Grubbs G1 catalyst and/or microcapsules containing DCPD monomer did not exhibit any healing.[83]

After this initial demonstration, several variations and improvements to the DCPD microcapsule design have been developed. The DCPD capsule – Grubbs catalyst pair have been employed in a variety of host matrices, including various epoxies,[84,85] fiber-reinforced epoxy,[86,87] and block co-polymers.[88] Additionally, to address catalyst stability in an amine-containing epoxy network, the Grubbs catalyst was encapsulated in wax.[89] This approach allowed near quantitative healing of the material with an order of magnitude lower catalyst loading, but mechanical properties were rather compromised, including a non-linear ductile fracture behavior. Different catalysts have been employed to address catalyst stability, notably a cheap tungsten ROMP catalyst (WCl_6).[90] Though this catalyst demonstrated improved lifetime and thermal stability, poor dispersion led to low healing efficiency.

In another example, the poor interfacial interactions between microcapsules and the epoxy network of the original system was addressed through incorporation of dimethylnorbornene ester (DNE) as co-monomers to DCPD, allowing favorable hydrogen-bonding interaction between the interfaces for improved strength after healing.[91] Another monomer-catalyst healing pair includes ring-opening polymerization of epoxides, catalyzed at high temperatures through imidazole compounds. In this case the UF microcapsules were enclosed with DGEBA monomers.[92] This eliminated the need for DCPD monomers, allowing complete homogeneity between the network formed through healing and the original host network. However, a high energy input in the form of heating at 140 ºC was required for healing to occur.

A multi-capsule approach has also been employed, wherein distinct capsule types enclose different chemical components, sequestered so that they do not react until damage occurs. After rupture of the capsules, mixing of the different components in the causes healing through polymerization. This method has been employed to encapsulate vinyl-polydimethylsiloxane (PDMS) and hydrosilyl-PDMS, encapsulated in discrete UF microcapsules that reacting through Pt-catalyzed hydrosilylation for network formation upon damage.[93] The tear strength of the material after healing was recovered by at least 70%. In another example, Lewis acid catalysis was also used as catalysts to initiate healing, wherein $BF_3 \cdot OEt_2$ and DGEBA were encapsulated in distinct PA microcapsules, resulting in 80% recovery of impact strength.[94]

1.3.3 Vascular Self-healing Materials

Conceptually, vascular systems for self-healing share much in common with capsule-based self-healing materials. In vascular systems, however, healing agents are encapsulated inside hollow capillaries or channels instead of spherical capsules, which similarly erupt with damage so that the pressurized liquid inside the capillaries can flow out its content to fill the damaged area.[23] This process initiates polymerization, hardening the crack formed from damage and thus effecting healing. This class of self-healing materials has been dubbed 'vascular' because it is reminiscent of blood vessels delivering the required healing reagents to the wound site for healing, the process of which was briefly described in a previous section. Though the mechanisms of the body are clearly more complex, the similarities in the process make this class of self-healing materials arguably the most biomimetic. Additionally, capillary action is capable of delivering healing agents to the same site more than once, allowing for finite but repeated cycles of healing, though often to diminished results with increasing cycles. An inherent drawback of this system is that vascular networks tend to require a high level of engineering, causing the whole system to be much more labor and cost-intensive than the other systems.[25]

The first example of a vascular self-healing material precedes all other types in the 1990s, when Dry and Sottos used glass pipettes filled with either one-component cyanoacrylate adhesive, or two component amine-DGEBA epoxy adhesive, as a simple vascular network and applied epoxy coating around it.[95] The release of healant upon fiber pulling was examined to favorable results. The concept was expanded so that the thin (15 μm) hollow glass fibers (HGFs) were used both as channels for delivering two part epoxy components and also as a means of reinforcing epoxy composites.[96] Though some flow of healing chemicals into the crack was observed, healing was minimal as HGFs were too thin to deliver much healant efficiently leading to difficulties in curing. To address this limitation, thicker (60 μm) borosilicate HGFs were used, leading to improved delivery of healing agents and self-healing capability.[97] Though these HGF approaches are collectively easier to implement, they are generally somewhat limited in potential; notably only a 1D vascular network can be fabricated through this method.

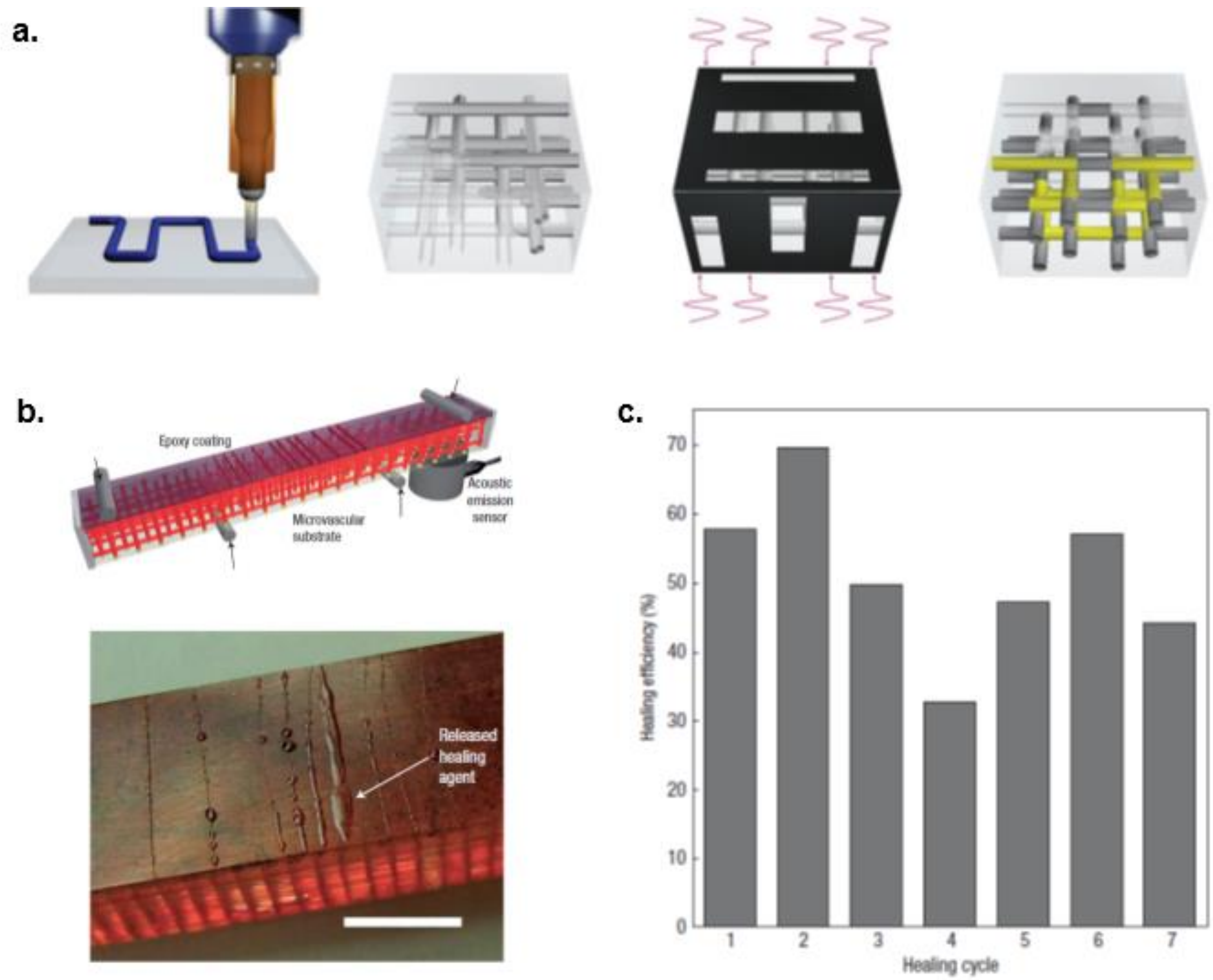

Figure 1.10 Vascular self-healing. a. Fabrication method of vascular network inside epoxy. First a robotic direct-write of organic ink creates a sacrificial scaffold. After pouring in thermosetting monomers at low temperature, and curing, high temperature and vacuum vaporizes the fugitive ink scaffold and creates microchannels. b. Schematic (top) and epoxy material (bottom) with vascular networks as created by this method. c. Healing can occur through many cycles at ~40% average healing over up to seven cycles. Adapted and reprinted from refs. 98 & 99.

To design more complex systems for vascular networks, more sophisticated engineering methods are required. In one method, a so-called "fugitive organic ink" is 3D printed using a robotic device and solidified at low temperatures such as a dry ice/acetone bath to form a structural scaffold of the 3-dimensional vascular network (Figure1.10a). After infiltration and hardening of the desired resin around this scaffold, the heating and application of vacuum removes the fugitive ink, leaving follow vascular networks around the resin.[98] This method was utilized to assemble a 3D vascular scaffold filled with DCPD in an amine-hardened epoxy matrix dispersed with Grubbs catalyst (Figure 1.10b).[99] Recovery of fracture toughness through four-point bending tests was performed to measure healing performance. Average healing capability was somewhat lower at than the equivalent capsule-based healing method at ~40%, however unlike the capsule-based design healing could be performed many cycles, reporting healing up to seven cycles with fractures in the same location with 10-mol% embedded Grubbs catalyst (Figure 1.10c). This system suffered the same catalyst stability issues of the capsule-based healing material, and to address this problem a two-component design with delivery of two healing agents (epoxy resin and amine hardener; delivered through four independent vascular systems) was produced, showing enhanced healing (~60%) of fracture toughness across up to 16 intermittent cycles.[100]

The direct-write assembly of fugitive organic inks suffers the limitation that epoxy hardening must be amenable to low temperature curing, as at elevated temperatures the fugitive ink scaffold liquefies. An alternative method, vaporization of sacrificial components (VaSC), addresses this limitation by relying on high-temperature depolymerization and evaporation of PLA for vascular scaffold generation.[101] In this method, PLA fibers are weaved into glass preforms for a defined 3D structure, and epoxy matrix is cured around it. With embedded tin catalyst and application of vacuum, at 200 ºC PLA is depolymerized and evaporated. VaSC vascular networks were tested for self-healing of delamination damage of epoxy composites reinforced with glass fibers in two orientations – parallel and herringbone. Both orientations of fiber reinforcement showed good healing efficiency, but the herringbone orientation was noticeably better, averaging over 100% recovery of fracture toughness.[102]

1.4 Vitrimers: Organic Networks with Vitreous Fluidity

In a relatively new development, the past five years have seen the use of associative dynamic covalent chemistry as applied to hard, epoxy-like materials for a new class of dynamic materials called vitrimers. Vitrimers are so named due to their glass-like (vitreous) Arrhenian fluidity in a permanently crosslinked organic network. These materials boast epoxy-like mechanical durability and creep resistance at service temperature, while also displaying the convenient reprocessability of thermoplastics at highly elevated temperatures. Unlike thermoplastics, however, vitrimers also enjoy the robust solvent and temperature resistance of thermosets, as they do not dissolve in solvent even at highly elevated temperatures.[27]

Several emergent properties are common to qualify a material as a vitrimer. One, though essentially devoid of creep or dynamic behavior at service temperature, the material gains malleability and reprocessability at highly elevated temperatures due to activation of dynamic chemistry. These materials therefore exhibit two distinct transition temperatures; one is the traditional glass transition temperature, T_g, which represents the temperature at which polymer chain segments gain significant mobility. The second, the topology-freezing temperature, T_v, represents the onset temperature at which topology-remodeling dynamic chemistry gains significant kinetics. Consequently, the material above T_v flows in accordance with the Arrhenius law governing exchange chemistry kinetics, resulting in glass-like flow properties. Additionally, the material must be solvent resistant at all temperatures, provided the solvent cannot chemically react with the material itself. This criterion can be met when the dynamic chemistry proceeds by an associative mechanism instead of dissociative, a distinguishing feature of vitrimers. This allows the crosslinking density of the material to be fully preserved at any temperature regardless of chain mobility or chemical kinetics, as the equilibrium never features a temporarily broken bond favoring depolymerization. Finally, though not a requirement, vitrimers are often designed with epoxy-like structure, and thus exhibit strong and brittle mechanical properties.[27]

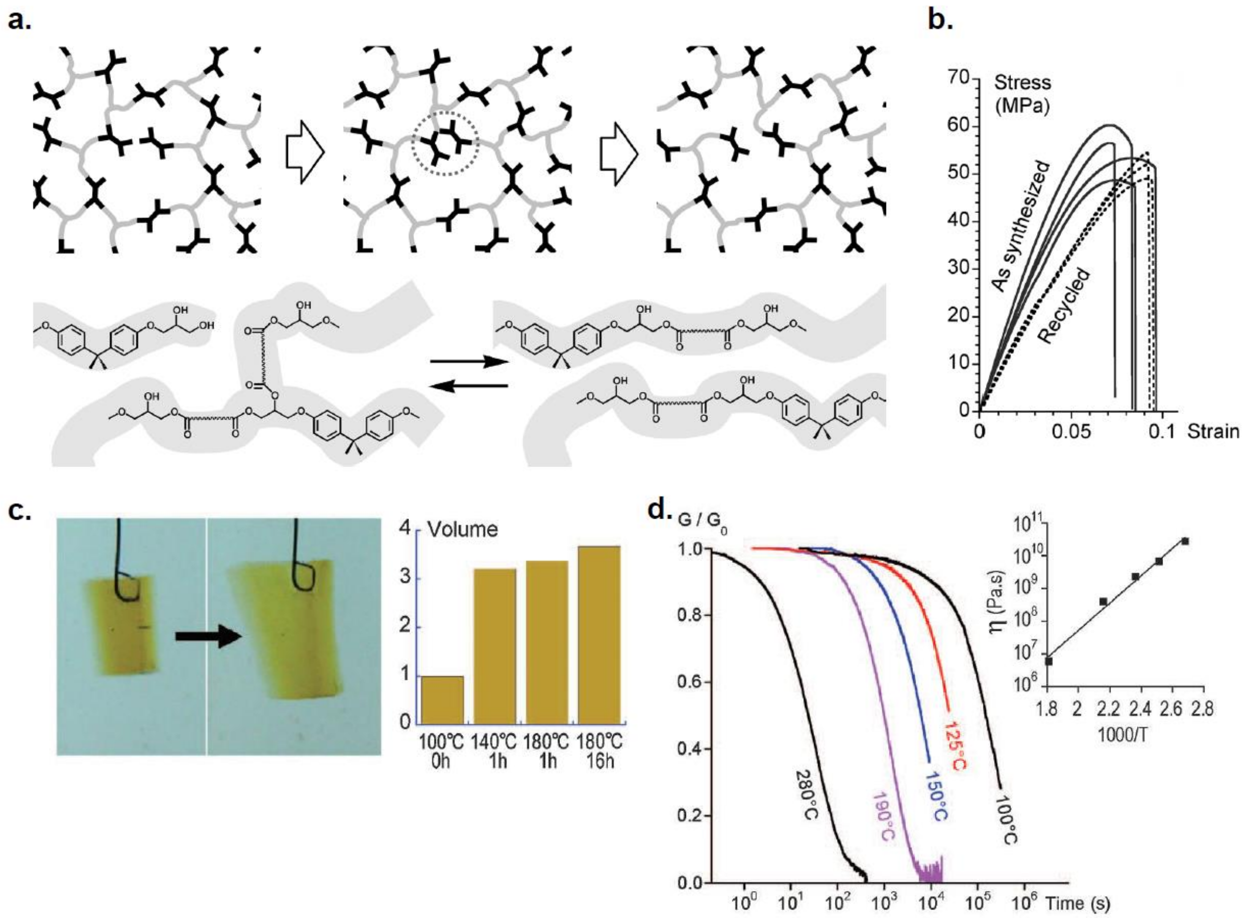

Figure 1.11 Epoxy trans-esterification vitrimer. a. Design concept. The covalent bond exchange that provides the material's properties proceeds by an associative mechanism and full network connectivity is preserved at all times (top). Molecular design involves epoxy monomer hardened with carboxylic acids that can trans-esterify through embedded Zinc catalyst (bottom). b. Mechanical properties of material shows typical epoxy-like strength, and materials reprocessed after catastrophic failure retain their original mechanical properties. c. When sample is immersed in trichlorobenzene solvent at elevated temperatures, the material swells significantly, but no mass loss through dissolution is observed. d. The material relaxes stress gradually at highly elevated temperatures, demonstrating malleability through network reorganization. Furthermore, temperature dependent stress-relaxation rates match well to an Arrhenius fit, showing silica-like gradual flow. Adapted and reprinted from ref. 103.

The term vitrimer was coined by Leibler and co-workers who in 2011 used classical chemistry between epoxy monomer (DGEBA) and multivalent carboxylic acids to form a polyester network (Figure 1.11).[103] The thermosetting chemistry was catalyzed by zinc acetate which stayed in the final network to continue to remodel the network through zinc catalyzed trans-esterification. Two network materials were synthesized, one with soft di- and tri-carboxylic acids creating a soft elastomeric material, and other with the more rigid glutaric anhydride, creating a final network with strong, epoxy-like mechanical properties. The authors demonstrated robust reprocessability, insolubility of the network at high temperatures, two thermal transition temperatures shown through dilatometry, and glass-like fluidity with an excellent match between activation energies of material flow and chemical exchange.

Following Leibler's initiative, most examples of to date vitrimers that have been reported in the literature utilize an exchange reaction across a carbonyl group. For example, utilizing an analogous trans-esterification motif with an organic catalyst, Ji and co-workers cleverly utilized the multiple thermal transitions of the vitrimer (T_g and T_v) in order to create a multi-shape memory material that could be fixed at two temperatures: one between T_g and T_v, and the other above T_v.[104] In another example utilizing trans-esterification, Hillmyer and co-workers described a crosslinked polylactide with chemical exchange catalyzed by tin, notably relaxing stress at much quicker rates than the previous trans-esterification examples.[105] Curiously, there was significant incongruity between the activation energies of molecular exchange (83 kJ/mol) and material flow as determined by stress relaxation (150 kJ/mol).

A few examples of catalyst-free trans-carbonylation reactions exist for vitrimer design. In one example, polyhydroxyurethanes vitrimers have been reported with robust reprocessability and glass-like flow.[106] In sharp contast to the example shown in the polylactide vitrimer, here the activation energy of molecular exchange (148 kJ/mol) was noticeably higher than that calculated for material flow (111 kJ/mol). Here the difference was attributed to strain-activated twisting of the urethane dihedral angle in bulk sample, lowering the activation energy. This conclusion was qualitatively backed by DFT calculations. In another example, Du Prez and co-workers synthesized poly(vinylogous urethane) networks through catalyst-free polymerization of cyclohexane dimethanol bisacetoacetate, m-xylylene diamine, and tris(2-aminoethyl)amine with a slight excess (5-mol%) excess of amine groups in the final network to allow exchange chemistry to occur.[107] The molecular exchange and bulk flow activation energies matched well at approximately 60 kJ/mol.

In a final example, crosslinked triazolium ionic network materials were synthesized through the catalyst-free thermal curing of α-azide-ω-alkyne and 1,6-dibromohexane (Figure 1.12).[108] High temperature curing led to the Huisgen dipolar cycloaddition reaction for a linear polymer with triazole rings which spontaneously crosslinked with the dibromoalkane compound to form triazolium bromide salts, forming a crosslinked network in one pot. The reprocessability and stress-relaxation behavior of the network was shown to be due to trans-alkylation reactions on the triazolium ring which was confirmed through small molecule studies with iodide counterions. The stress relaxation activation energy was found to be 140 kJ/mol with the bromide counterion. The rate of flow of the material was found to depend upon the counterion, where bromide showed the fastest relaxation, iodide slower, and mesylate prohibitively slow for practical application without network degradation. As a poly(ionic liquid), the material can also be utilized as a solid electrolyte, showing ion conducting capabilities. Counterion effect was also seen in conduction capabilities, showing the same trend as stress relaxation, i.e. bromide > iodide >> mesylate.

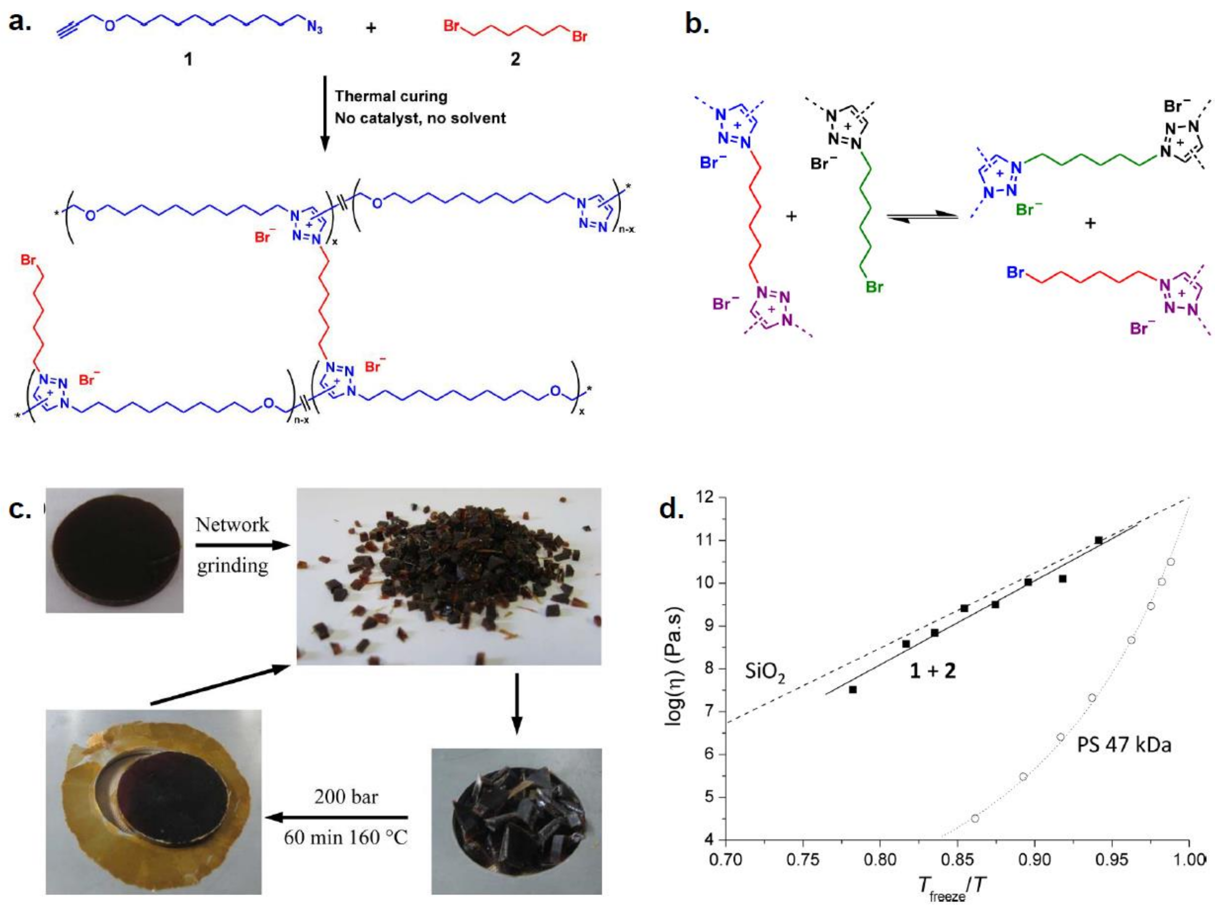

Figure 1.12 Triazolium trans-alkylation vitrimer. a. Network synthesis involves catalyst-free azide-alkyne cycloaddition and alkylation in one pot to form crosslinked, ion-conducting triazolium-linked networks. b. Proposed mechanism of exchange involves trans-alkylation across trazolium rings. c. Bulk sample can be reprocessed into a homogeneous material after grinding the network to small pieces. d. Arrhenius fit of stress relaxation timescales produces fragility plot with inorganic silica-like gradual viscosity change. Adapted and reprinted from ref. 108.

1.5 Conclusion, Outlook, and Goal of the Thesis

In the sections above we described a few examples of the power of incorporating dynamic chemistry into organic materials for functional benefit. In Section 1.2 we saw how nature utilized the design philosophy of sacrificial weak bonds in modular repeats in order to increase the toughness of a linear polymer chain, specifically for the muscle protein *Titin*. It was shown that this strategy could be incorporated into synthetic materials in the form of a unit capable of dynamically dimerizing through hydrogen bonds. In Section 1.3 it was shown that various strategies could be utilized for self-healing material design. We place our emphasis here on the intrinsic self-healing materials, as the use of dynamic chemistry for advanced material properties is most relevant in this case. In Section 1.4 we saw an extension of the intrinsic self-healing material design, wherein associative dynamic covalent chemistry could give rise to a set of materials with a productive combination of the benefits of both thermosets and thermoplastics, with an interesting glass-like fluidity. All these examples covered above demonstrate only a very small fraction of biomimetic, self-healing, and vitrimer materials, subfields which are themselves only a small scope of the potential of dynamic materials.

The vast expanse in the functional capability of organic polymer materials through the introduction of these dynamic chemical motifs into polymers cannot be understated. However, this shift in perspective brings about another, perhaps slightly more understated outlook for polymer chemists. Namely, with incorporation of dynamic chemistry into organic polymer structures, thorough understanding of the molecular dynamic interaction now becomes instrumental in understanding the emergent polymeric material behavior. The kinetics and thermodynamics of small molecule chemistry, a domain of chemistry easily accessible by the traditional organic chemist, must be complemented to polymer physics in order to understand and predict the behavior of this new generation of materials. This allows chemists an unprecedented opportunity to not only design and synthesize novel dynamic materials, but to enhance understanding of polymer behavior through understanding chemical properties. In other words, a direct experimental linkage between small molecule properties and the emergent properties of its solid bulk material is an area in need of examination and elucidation.

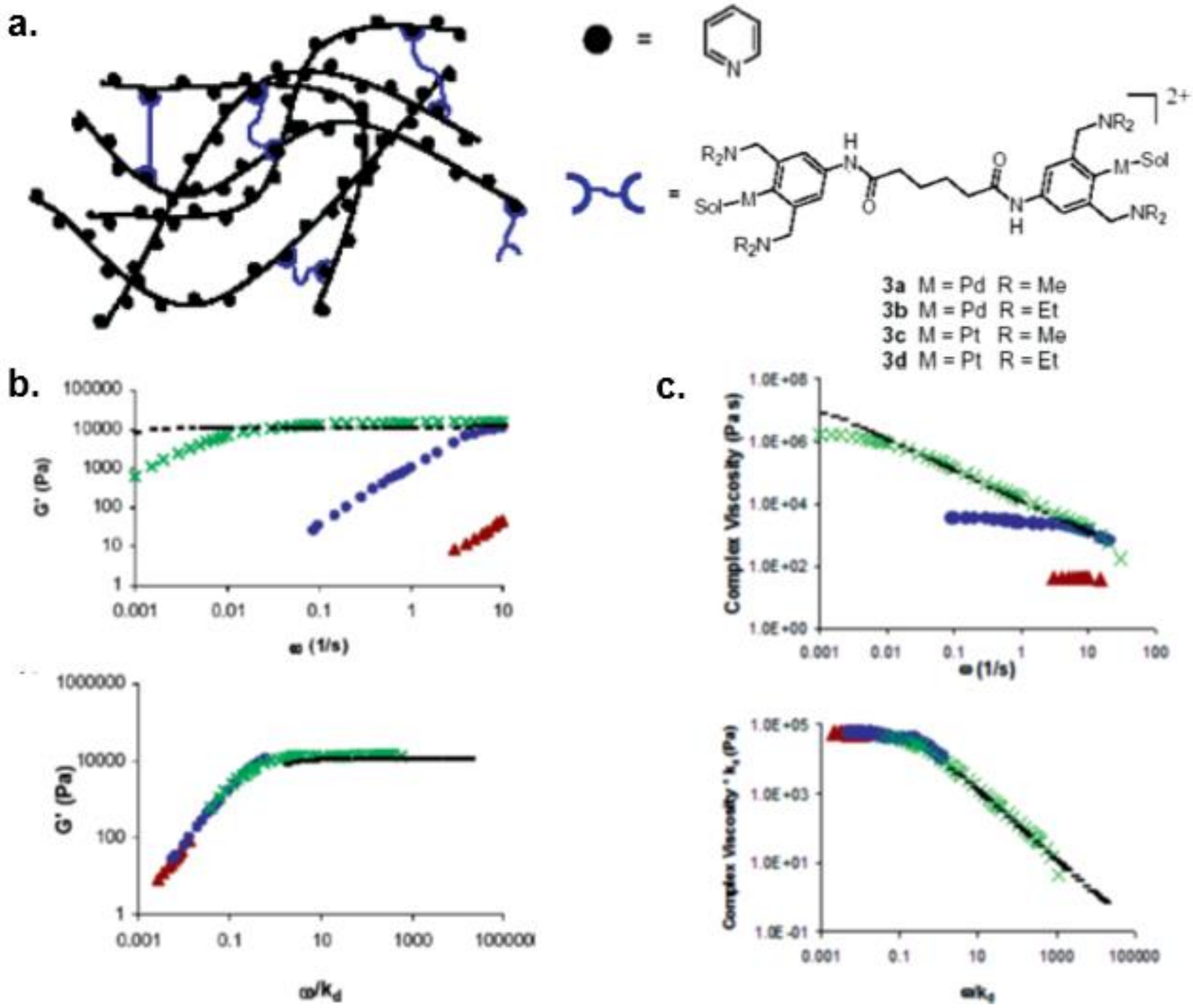

Figure 1.13 Physical organic chemistry of supramolecular networks. a. Concept design for organogel employed by Craig and co-workers for study. b. Frequency-dependent storage modulus G' for the four molecular species of different rates (top), when scaled to the molecular rate of exchange collapses to a single master curve (bottom). c. Similarly, frequency dependent complex viscosity for the four species (top), when scaled to the rate of exchange of small molecule, collapses to a master curve (bottom). Adapted and reprinted from ref. 112.

The possibilities of this linkage is demonstrated in a series of work by Stephen Craig and co-workers.[109-112] Starting first with orthogonal kinetic / thermodynamic control of a supramolecular interaction,[110] the team of workers ultimately show a near perfect scaling relationship between molecular kinetics of constituent small molecules to aggregate rheological properties.[112] In the same work, a very nice quantitative relationship is shown between the dissociation kinetics of the molecules (a small molecule property) to the relaxation timescale of the bulk network (an aggregate bulk response).[112] This correlation is explained through the transient network models,[113,114] wherein supramolecular kinetics can be viewed as analogous to the effects of chain entanglement / de-entanglement kinetics. These works serve as testaments to the powerful implications that in the new generation of materials fueled by dynamic chemistry, understanding of various aspects of small molecule chemistry can directly translate to understanding of bulk polymer behavior.

Nevertheless, these are a limited set of works, and the crosslinked networks here are unentangled gels, wherein near ideal polymer chain behavior can be assumed. Whether such a molecule-to-bulk viewpoint can be robustly applied in understanding and predicting behavior of organic polymer materials in solid bulk remains to be tested. A few notable works address this issue; notably as was noted in Section 1.4, a match between the dynamics of the small molecule and the bulk material flow can be achieved through the activation energy.[103,107,115] In order to continue on the track of enhancing our polymer structure-property relationship, there is a critical emerging need to elucidating – through chemical understanding – how molecular properties affect emergent organic polymer material performance.

In addition to add to the materials scientists' growing repertoire of dynamic materials with incorporated dynamic chemistry, a primary aim of this thesis is address this deficiency. In Chapter

2 we investigate the correlation between the nano-mechanical responses of a single supramolecular chemical module to the bulk mechanical performance of solid material.[30] In other words, we elucidate the molecule-to-bulk *mechanical to mechanical* correlation. In Chapter 3 we probe the relationship between the properties of molecular dynamic exchange to the bulk self-healing performance.[31] In another context, we elucidate the molecule-to-bulk *dynamic to dynamic* correlation. In Chapter 4, we aimed to investigate the relationship between the molecular properties to both mechanical and dynamic properties of bulk material. Conclusions in this particular case remain unresolved.

1.6 References

(1) Staudinger, H. *Ber. Deut. Chem. Ges.* **1920**, 1073.

(2) Flory, P. J. *Principles of Polymer Chemistry*; 1st ed.; Cornell University Press: Ithaca, NY, 1953.

(3) Doi, M.; Edwards, S. F. *The theory of polymer dynamics*; Oxford University Press: Oxford, UK, 1986.

(4) Rubinstein, M.; Colby, R. H. *Polymer Physics*; Oxford University Press: Oxford, 2003.

(5) Cowie, J. M. G. *Polymers: Chemistry & Physics of Modern Materials*; 2nd ed.; Chapman and Hall: New York, NY, 1991.

(6) Odian, G. *Principles of Polymerization*; 4th ed.; John Wiley & Sons, Inc.: Hoboken, NJ, 2004.

(7) Flory, P. J. *Statistical mechanics of chain molecules*; Interscience Publishers: New York, 1969.

(8) Christensen, R. M. *Theory of Viscoelasticity: an Introduction*; 2nd ed.; Academic Press: New York, NY, 1982.

(9) Matyjaszewski, K.; Xia, J. Atom Transfer Radical Polymerization *Chemical Reviews* **2001**, *101*(9), 2921-2990.

(10) Bielawski, C. W.; Grubbs, R. H. In *Controlled and Living Polymerizations*; Wiley-VCH Verlag GmbH & Co. KGaA: 2010, p 297-342.

(11) Kratky, O.; Porod, G. X-ray investigation of dissolved chain molecules *Rec. Trav. Chim. Pays-Bas* **1949**, *68*1106-1123.

(12) Van Krevelen, D. W.; Hoftyzer, P. J. *Properties of Polymers: Their Estimation and Correlation with Chemical Structure*; Elsevier Scientific Publishing Company: Amsterdam, 1976.

(13) Aida, T.; Meijer, E. W.; Stupp, S. I. Functional Supramolecular Polymers *Science* **2012**, *335*(6070), 813-817.

(14) Brunsveld, L.; Folmer, B. J. B.; Meijer, E. W.; Sijbesma, R. P. Supramolecular Polymers *Chemical Reviews* **2001**, *101*(12), 4071-4098.

(15) De Greef, T. F. A.; Smulders, M. M. J.; Wolffs, M.; Schenning, A. P. H. J.; Sijbesma, R. P.; Meijer, E. W. Supramolecular Polymerization *Chemical Reviews* **2009**, *109*(11), 5687-5754.

(16) Rowan, S. J.; Cantrill, S. J.; Cousins, G. R. L.; Sanders, J. K. M.; Stoddart, J. F. Dynamic Covalent Chemistry *Angewandte Chemie International Edition* **2002**, *41*(6), 898-952.

(17) Wojtecki, R. J.; Meador, M. A.; Rowan, S. J. Using the dynamic bond to access macroscopically responsive structurally dynamic polymers *Nat Mater* **2011**, *10*(1), 14-27.

(18) Caruso, M. M.; Davis, D. A.; Shen, Q.; Odom, S. A.; Sottos, N. R.; White, S. R.; Moore, J. S. Mechanically-Induced Chemical Changes in Polymeric Materials *Chemical Reviews* **2009**, *109*(11), 5755-5798.

(19) Black, A. L.; Lenhardt, J. M.; Craig, S. L. From molecular mechanochemistry to stress-responsive materials *Journal of Materials Chemistry* **2011**, *21*(6), 1655-1663.

(20) Sijbesma, R. P.; Beijer, F. H.; Brunsveld, L.; Folmer, B. J. B.; Hirschberg, J. H. K. K.; Lange, R. F. M.; Lowe, J. K. L.; Meijer, E. W. Reversible Polymers Formed from Self-Complementary Monomers Using Quadruple Hydrogen Bonding *Science* **1997**, *278*(5343), 1601-1604.

(21) Whittell, G. R.; Hager, M. D.; Schubert, U. S.; Manners, I. Functional soft materials from metallopolymers and metallosupramolecular polymers *Nat Mater* **2011**, *10*(3), 176-188.

(22) Roy, D.; Cambre, J. N.; Sumerlin, B. S. Future perspectives and recent advances in stimuli-responsive materials *Progress in Polymer Science* **2010**, *35*(1–2), 278-301.

(23) Blaiszik, B. J.; Kramer, S. L. B.; Olugebefola, S. C.; Moore, J. S.; Sottos, N. R.; White, S. R. Self-Healing Polymers and Composites *Annual Review of Materials Research* **2010**, *40*(1), 179-211.

(24) Yang, Y.; Urban, M. W. Self-healing polymeric materials *Chemical Society Reviews* **2013**, *42*(17), 7446-7467.

(25) Diesendruck, C. E.; Sottos, N. R.; Moore, J. S.; White, S. R. Biomimetic Self-Healing *Angewandte Chemie International Edition* **2015**, *54*(36), 10428-10447.

(26) Liu, C.; Qin, H.; Mather, P. T. Review of progress in shape-memory polymers *Journal of Materials Chemistry* **2007**, *17*(16), 1543-1558.

(27) Denissen, W.; Winne, J. M.; Du Prez, F. E. Vitrimers: permanent organic networks with glass-like fluidity *Chemical Science* **2016**, *7*(1), 30-38.

(28) Otsuka, H.; Nagano, S.; Kobashi, Y.; Maeda, T.; Takahara, A. A dynamic covalent polymer driven by disulfide metathesis under photoirradiation *Chemical Communications* **2010**, *46*(7), 1150-1152.

(29) Wang, Q.; Gossweiler, G. R.; Craig, S. L.; Zhao, X. Cephalopod-inspired design of electro-mechano-chemically responsive elastomers for on-demand fluorescent patterning *Nature Communications* **2014**, *5*.

(30) Chung, J.; Kushner, A. M.; Weisman, A. C.; Guan, Z. Direct correlation of single-molecule properties with bulk mechanical performance for the biomimetic design of polymers *Nature Materials* **2014**, *13*(11), 1055-1062.

(31) Cromwell, O. R.; Chung, J.; Guan, Z. Malleable and Self-Healing Covalent Polymer Networks through Tunable Dynamic Boronic Ester Bonds *Journal of the American Chemical Society* **2015**, *137*(20), 6492-6495.

(32) Vincent, J. F. V.; Bogatyreva, O. A.; Bogatyrev, N. R.; Bowyer, A.; Pahl, A.-K. Biomimetics: its practice and theory *Journal of The Royal Society Interface* **2006**, *3*(9), 471-482.

(33) Fratzl, P. Biomimetic materials research: what can we really learn from nature's structural materials? *Journal of the Royal Society Interface* **2007**, *4*(15), 637-642.

(34) Tatham, A. S.; Shewry, P. R. Elastomeric proteins: biological roles, structures and mechanisms *Trends in Biochemical Sciences* **2000**, *25*(11), 567-571.

(35) Granzier, H. L.; Labeit, S. The Giant Protein Titin: A Major Player in Myocardial Mechanics, Signaling, and Disease *Circulation Research* **2004**, *94*(3), 284-295.

(36) Rief, M.; Gautel, M.; Oesterhelt, F.; Fernandez, J. M.; Gaub, H. E. Reversible Unfolding of Individual Titin Immunoglobulin Domains by AFM *Science* **1997**, *276*(5315), 1109-1112.

(37) Kellermayer, M. S. Z.; Smith, S. B.; Granzier, H. L.; Bustamante, C. Folding-Unfolding Transitions in Single Titin Molecules Characterized with Laser Tweezers *Science* **1997**, *276*(5315), 1112-1116.

(38) Li, H.; Oberhauser, A. F.; Fowler, S. B.; Clarke, J.; Fernandez, J. M. Atomic force microscopy reveals the mechanical design of a modular protein *Proceedings of the National Academy of Sciences* **2000**, *97*(12), 6527-6531.

(39) Lu, H.; Schulten, K. Steered molecular dynamics simulations of force-induced protein domain unfolding *Proteins: Structure, Function, and Genetics* **1999**, *35*453-463.

(40) Lu, H.; Schulten, K. The Key Event in Force-Induced Unfolding of Titin's Immunoglobulin Domains *Biophysical Journal* **2000**, *79*(1), 51-65.

(41) Marszalek, P. E.; Lu, H.; Li, H.; Carrion-Vazquez, M.; Oberhauser, A. F.; Schulten, K.; Fernandez, J. M. Mechanical unfolding intermediates in titin modules *Nature* **1999**, *402*(6757), 100-103.

(42) Benichou, I.; Givli, S. The hidden ingenuity in titin structure *Applied Physics Letters* **2011**, *98*(9), -.

(43) Beijer, F. H.; Sijbesma, R. P.; Kooijman, H.; Spek, A. L.; Meijer, E. W. Strong Dimerization of Ureidopyrimidones via Quadruple Hydrogen Bonding *Journal of the American Chemical Society* **1998**, *120*(27), 6761-6769.

(44) Söntjens, S. H. M.; Sijbesma, R. P.; van Genderen, M. H. P.; Meijer, E. W. Stability and Lifetime of Quadruply Hydrogen Bonded 2-Ureido-4[1H]-pyrimidinone Dimers *Journal of the American Chemical Society* **2000**, *122*(31), 7487-7493.

(45) Guan, Z.; Roland, J. T.; Bai, J. Z.; Ma, S. X.; McIntire, T. M.; Nguyen, M. Modular Domain Structure: A Biomimetic Strategy for Advanced Polymeric Materials *Journal of the American Chemical Society* **2004**, *126*(7), 2058-2065.

(46) Roland, J. T.; Guan, Z. Synthesis and Single-Molecule Studies of a Well-Defined Biomimetic Modular Multidomain Polymer Using a Peptidomimetic β-Sheet Module *Journal of the American Chemical Society* **2004**, *126*(44), 14328-14329.

(47) Guzmán, D. L.; Roland, J. T.; Keer, H.; Kong, Y. P.; Ritz, T.; Yee, A.; Guan, Z. Using steered molecular dynamics simulations and single-molecule force spectroscopy to guide the rational design of biomimetic modular polymeric materials *Polymer* **2008**, *49*(18), 3892-3901.

(48) Kushner, A. M.; Vossler, J. D.; Williams, G. A.; Guan, Z. A Biomimetic Modular Polymer with Tough and Adaptive Properties *Journal of the American Chemical Society* **2009**, *131*(25), 8766-8768.

(49) Kushner, A. M.; Gabuchian, V.; Johnson, E. G.; Guan, Z. Biomimetic Design of Reversibly Unfolding Crosslinker to Enhance Mechanical Properties of 3D Network Polymers *Journal of the American Chemical Society* **2007**, *129*(46), 14110-14111.

(50) Guzmán, D. L.; Randall, A.; Baldi, P.; Guan, Z. Computational and single-molecule force studies of a macro domain protein reveal a key molecular determinant for mechanical stability *Proceedings of the National Academy of Sciences* **2010**, *107*(5), 1989-1994.

(51) Carrion-Vazquez, M.; Oberhauser, A. F.; Fowler, S. B.; Marszalek, P. E.; Broedel, S. E.; Clarke, J.; Fernandez, J. M. Mechanical and chemical unfolding of a single protein: A comparison *Proceedings of the National Academy of Sciences* **1999**, *96*(7), 3694-3699.

(52) Stadelmann, W. K.; Digenis, A. G.; Tobin, G. R. Physiology and healing dynamics of chronic cutaneous wounds *Am. J. Surg.* **1998**, *176*26S-36S.

(53) Versteeg, H. H.; Heemskerk, J. W. M.; Levi, M.; Reitsma, P. H. New Fundamentals in Hemostasis *Physiological Reviews* **2013**, *93*(1), 327-358.

(54) Eming, S. A.; Krieg, T.; Davidson, J. M. Inflammation in Wound Repair: Molecular and Cellular Mechanisms *Journal of Investigative Dermatology*, *127*(3), 514-525.

(55) Midwood, K. S.; Williams, L. V.; Schwarzbauer, J. E. Tissue repair and the dynamics of the extracellular matrix *The International Journal of Biochemistry & Cell Biology* **2004**, *36*(6), 1031-1037.

(56) Chen, X.; Dam, M. A.; Ono, K.; Mal, A.; Shen, H.; Nutt, S. R.; Sheran, K.; Wudl, F. A Thermally Re-mendable Crosslinked Polymeric Material *Science* **2002**, *295*(5560), 1698-1702.

(57) Cordier, P.; Tournilhac, F.; Soulie-Ziakovic, C.; Leibler, L. Self-healing and thermoreversible rubber from supramolecular assembly *Nature* **2008**, *451*(7181), 977-980.

(58) Wool, R. P.; O'Connor, K. M. A theory crack healing in polymers *Journal of Applied Physics* **1981**, *52*(10), 5953-5963.

(59) Ling, J.; Rong, M. Z.; Zhang, M. Q. Photo-stimulated self-healing polyurethane containing dihydroxyl coumarin derivatives *Polymer* **2012**, *53*(13), 2691-2698.

(60) Froimowicz, P.; Frey, H.; Landfester, K. Towards the Generation of Self-Healing Materials by Means of a Reversible Photo-induced Approach *Macromolecular Rapid Communications* **2011**, *32*(5), 468-473.

(61) Ying, H.; Zhang, Y.; Cheng, J. Dynamic urea bond for the design of reversible and self-healing polymers *Nat Commun* **2014**, *5*.

(62) Ghosh, B.; Urban, M. W. Self-Repairing Oxetane-Substituted Chitosan Polyurethane Networks *Science* **2009**, *323*(5920), 1458-1460.

(63) Lu, Y.-X.; Guan, Z. Olefin Metathesis for Effective Polymer Healing via Dynamic Exchange of Strong Carbon–Carbon Double Bonds *Journal of the American Chemical Society* **2012**, *134*(34), 14226-14231.

(64) Yoon, J. A.; Kamada, J.; Koynov, K.; Mohin, J.; Nicolaÿ, R.; Zhang, Y.; Balazs, A. C.; Kowalewski, T.; Matyjaszewski, K. Self-Healing Polymer Films Based on Thiol–Disulfide Exchange Reactions and Self-Healing Kinetics Measured Using Atomic Force Microscopy *Macromolecules* **2011**, *45*(1), 142-149.

(65) An, S. Y.; Noh, S. M.; Nam, J. H.; Oh, J. K. Dual Sulfide–Disulfide Crosslinked Networks with Rapid and Room Temperature Self-Healability *Macromolecular Rapid Communications* **2015**n/a-n/a.

(66) Zheng, P.; McCarthy, T. J. A Surprise from 1954: Siloxane Equilibration Is a Simple, Robust, and Obvious Polymer Self-Healing Mechanism *Journal of the American Chemical Society* **2012**, *134*(4), 2024-2027.

(67) Amamoto, Y.; Kamada, J.; Otsuka, H.; Takahara, A.; Matyjaszewski, K. Repeatable Photoinduced Self-Healing of Covalently Crosslinked Polymers through Reshuffling of Trithiocarbonate Units *Angewandte Chemie International Edition* **2011**, *50*(7), 1660-1663.

(68) Amamoto, Y.; Otsuka, H.; Takahara, A.; Matyjaszewski, K. Self-Healing of Covalently Crosslinked Polymers by Reshuffling Thiuram Disulfide Moieties in Air under Visible Light *Advanced Materials* **2012**, *24*(29), 3975-3980.

(69) Lehn, J.-M. Toward complex matter: Supramolecular chemistry and self-organization *Proceedings of the National Academy of Sciences* **2002**, *99*(8), 4763-4768.

(70) Chen, Y.; Kushner, A. M.; Williams, G. A.; Guan, Z. Multiphase design of autonomic self-healing thermoplastic elastomers *Nature Chemistry* **2012**, *4*(6), 467-472.

(71) Chen, Y.; Guan, Z. Multivalent hydrogen bonding block copolymers self-assemble into strong and tough self-healing materials *Chemical Communications* **2014**, *50*(74), 10868-10870.

(72) Chen, Y.; Guan, Z. Self-assembly of core-shell nanoparticles for self-healing materials *Polymer Chemistry* **2013**, *4*(18), 4885-4889.

(73) Williams, G. A.; Ishige, R.; Cromwell, O. R.; Chung, J.; Takahara, A.; Guan, Z. Mechanically Robust and Self-Healable Superlattice Nanocomposites by Self-Assembly of Single-Component “Sticky” Polymer-Grafted Nanoparticles *Advanced Materials* **2015**, *27*(26), 3934-3941.

(74) Burnworth, M.; Tang, L.; Kumpfer, J. R.; Duncan, A. J.; Beyer, F. L.; Fiore, G. L.; Rowan, S. J.; Weder, C. Optically healable supramolecular polymers *Nature* **2011**, *472*(7343), 334-337.

(75) Mozhdehi, D.; Ayala, S.; Cromwell, O. R.; Guan, Z. Self-Healing Multiphase Polymers via Dynamic Metal-Ligand Interactions *Journal of the American Chemical Society* **2014**.

(76) Burattini, S.; Colquhoun, H. M.; Fox, J. D.; Friedmann, D.; Greenland, B. W.; Harris, P. J. F.; Hayes, W.; Mackay, M. E.; Rowan, S. J A self-repairing, supramolecular polymer system: healability as a consequence of donor-acceptor [small pi]-[small pi] stacking interactions *Chemical Communications* **2009**(44), 6717-6719.

(77) Burattini, S.; Greenland, B. W.; Merino, D. H.; Weng, W.; Seppala, J.; Colquhoun, H. M.; Hayes, W.; Mackay, M. E.; Hamley, I. W.; Rowan, S. J. A Healable Supramolecular Polymer Blend Based on Aromatic Ï€âˆ'Ï€ Stacking and Hydrogen-Bonding Interactions *Journal of the American Chemical Society* **2010**, *132*(34), 12051-12058.

(78) Cho, S. H.; Andersson, H. M.; White, S. R.; Sottos, N. R.; Braun, P. V. Polydimethylsiloxane-Based Self-Healing Materials *Advanced Materials* **2006**, *18*(8), 997-1000.

(79) Xiao, D. S.; Yuan, Y. C.; Rong, M. Z.; Zhang, M. Q. Hollow polymeric microcapsules: Preparation, characterization and application in holding boron trifluoride diethyl etherate *Polymer* **2009**, *50*(2), 560-568.

(80) Esser-Kahn, A. P.; Odom, S. A.; Sottos, N. R.; White, S. R.; Moore, J. S. Triggered Release from Polymer Capsules *Macromolecules* **2011**, *44*(14), 5539-5553.

(81) Yow, H. N.; Routh, A. F. Formation of liquid core-polymer shell microcapsules *Soft Matter* **2006**, *2*(11), 940-949.

(82) Blaiszik, B. J.; Sottos, N. R.; White, S. R. Nanocapsules for self-healing materials *Composites Science and Technology* **2008**, *68*(3–4), 978-986.

(83) White, S. R.; Sottos, N. R.; Geubelle, P. H.; Moore, J. S.; Kessler, M. R.; Sriram, S. R.; Brown, E. N.; Viswanathan, S. Autonomic healing of polymer composites *Nature* **2001**, *409*(6822), 794-797.

(84) Brown, E. N.; White, S. R.; Sottos, N. R. Retardation and repair of fatigue cracks in a microcapsule toughened epoxy composite—Part II: In situ self-healing *Composites Science and Technology* **2005**, *65*(15–16), 2474-2480.

(85) Brown, E. N.; Kessler, M. R.; Sottos, N. R.; White, S. R. In situ poly(urea-formaldehyde) microencapsulation of dicyclopentadiene *J. Microencapsul.* **2003**, *20*719-730.

(86) Kirkby, E. L.; Rule, J. D.; Michaud, V. J.; Sottos, N. R.; White, S. R.; Månson, J.-A. E. Embedded Shape-Memory Alloy Wires for Improved Performance of Self-Healing Polymers *Advanced Functional Materials* **2008**, *18*(15), 2253-2260.

(87) Kessler, M. R.; Sottos, N. R.; White, S. R. Self-healing structural composite materials *Composites Part A: Applied Science and Manufacturing* **2003**, *34*(8), 743-753.

(88) Chipara, M. D.; Chipara, M.; Shansky, E.; Zaleski, J. M. Self-healing of high elasticity block copolymers *Polymers for Advanced Technologies* **2009**, *20*(4), 427-431.

(89) Rule, J. D.; Brown, E. N.; Sottos, N. R.; White, S. R.; Moore, J. S. Wax-Protected Catalyst Microspheres for Efficient Self-Healing Materials *Advanced Materials* **2005**, *17*(2), 205-208.

(90) Kamphaus, J. M.; Rule, J. D.; Moore, J. S.; Sottos, N. R.; White, S. R. A new self-healing epoxy with tungsten (VI) chloride catalyst *Journal of The Royal Society Interface* **2008**, *5*(18), 95-103.

(91) Wilson, G. O.; Caruso, M. M.; Schelkopf, S. R.; Sottos, N. R.; White, S. R.; Moore, J. S. Adhesion Promotion via Noncovalent Interactions in Self-Healing Polymers *ACS Applied Materials & Interfaces* **2011**, *3*(8), 3072-3077.

(92) Yuan, L.; Liang, G.; Xie, J.; Li, L.; Guo, J. Preparation and characterization of poly(urea-formaldehyde) microcapsules filled with epoxy resins *Polymer* **2006**, *47*(15), 5338-5349.

(93) Keller, M. W.; White, S. R.; Sottos, N. R. A Self-Healing Poly(Dimethyl Siloxane) Elastomer *Advanced Functional Materials* **2007**, *17*(14), 2399-2404.

(94) Xiao, D. S.; Yuan, Y. C.; Rong, M. Z.; Zhang, M. Q. Self-healing epoxy based on cationic chain polymerization *Polymer* **2009**, *50*(13), 2967-2975.

(95) Dry, C. *Compos. Struct.* **1996**, *35*263-269.

(96) Bleay, S. M.; Loader, C. B.; Hawyes, V. J.; Humberstone, L.; Curtis, P. T. A smart repair system for polymer matrix composites *Composites Part A: Applied Science and Manufacturing* **2001**, *32*(12), 1767-1776.

(97) Pang, J. W. C.; Bond, I. P. A hollow fibre reinforced polymer composite encompassing self-healing and enhanced damage visibility *Composites Science and Technology* **2005**, *65*(11–12), 1791-1799.

(98) Therriault, D.; White, S. R.; Lewis, J. A. Chaotic mixing in three-dimensional microvascular networks fabricated by direct-write assembly *Nat Mater* **2003**, *2*(4), 265-271.

(99) Toohey, K. S.; Sottos, N. R.; Lewis, J. A.; Moore, J. S.; White, S. R. Self-healing materials with microvascular networks *Nature Materials* **2007**, *6*(8), 581-585.

(100) Toohey, K. S.; Hansen, C. J.; Lewis, J. A.; White, S. R.; Sottos, N. R. Delivery of Two-Part Self-Healing Chemistry via Microvascular Networks *Advanced Functional Materials* **2009**, *19*(9), 1399-1405.

(101) Esser-Kahn, A. P.; Thakre, P. R.; Dong, H.; Patrick, J. F.; Vlasko-Vlasov, V. K.; Sottos, N. R.; Moore, J. S.; White, S. R. Three-Dimensional Microvascular Fiber-Reinforced Composites *Advanced Materials* **2011**, *23*(32), 3654-3658.

(102) Patrick, J. F.; Hart, K. R.; Krull, B. P.; Diesendruck, C. E.; Moore, J. S.; White, S. R.; Sottos, N. R. Continuous Self-Healing Life Cycle in Vascularized Structural Composites *Advanced Materials* **2014**, *26*(25), 4302-4308.

(103) Montarnal, D.; Capelot, M.; Tournilhac, F.; Leibler, L. Silica-Like Malleable Materials from Permanent Organic Networks *Science* **2011**, *334*(6058), 965-968.

(104) Pei, Z.; Yang, Y.; Chen, Q.; Wei, Y.; Ji, Y. Regional Shape Control of Strategically Assembled Multishape Memory Vitrimers *Advanced Materials* **2016**, *28*(1), 156-160.

(105) Brutman, J. P.; Delgado, P. A.; Hillmyer, M. A. Polylactide Vitrimers *ACS Macro Letters* **2014**, *3*(7), 607-610.

(106) Fortman, D. J.; Brutman, J. P.; Cramer, C. J.; Hillmyer, M. A.; Dichtel, W. R. Mechanically Activated, Catalyst-Free Polyhydroxyurethane Vitrimers *Journal of the American Chemical Society* **2015**, *137*(44), 14019-14022.

(107) Denissen, W.; Rivero, G.; Nicolaÿ, R.; Leibler, L.; Winne, J. M.; Du Prez, F. E. Vinylogous Urethane Vitrimers *Advanced Functional Materials* **2015**n/a-n/a.

(108) Obadia, M. M.; Mudraboyina, B. P.; Serghei, A.; Montarnal, D.; Drockenmuller, E. Reprocessing and Recycling of Highly Crosslinked Ion-Conducting Networks through Transalkylation Exchanges of C–N Bonds *Journal of the American Chemical Society* **2015**, *137*(18), 6078-6083.

(109) Serpe, M. J.; Craig, S. L. Physical Organic Chemistry of Supramolecular Polymers *Langmuir* **2007**, *23*(4), 1626-1634.

(110) Yount, W. C.; Juwarker, H.; Craig, S. L. Orthogonal Control of Dissociation Dynamics Relative to Thermodynamics in a Main-Chain Reversible Polymer *Journal of the American Chemical Society* **2003**, *125*(50), 15302-15303.

(111) Yount, W. C.; Loveless, D. M.; Craig, S. L. Small-Molecule Dynamics and Mechanisms Underlying the Macroscopic Mechanical Properties of Coordinatively Crosslinked Polymer Networks *Journal of the American Chemical Society* **2005**, *127*(41), 14488-14496.

(112) Yount, W. C.; Loveless, D. M.; Craig, S. L. Strong Means Slow: Dynamic Contributions to the Bulk Mechanical Properties of Supramolecular Networks *Angewandte Chemie International Edition* **2005**, *44*(18), 2746-2748.

(113) Green, M. S.; Tobolsky, A. V. A New Approach to the Theory of Relaxing Polymeric Media *The Journal of Chemical Physics* **1946**, *14*(2), 80-92.

(114) Tanaka, F.; Edwards, S. F. Viscoelastic properties of physically crosslinked networks. 1. Transient network theory *Macromolecules* **1992**, *25*(5), 1516-1523.

(115) Capelot, M.; Unterlass, M. M.; Tournilhac, F.; Leibler, L. Catalytic Control of the Vitrimer Glass Transition *ACS Macro Letters* **2012**, *1*(7), 789-792.

Chapter 2: Direct Correlation of Single Molecule Properties with Bulk Mechanical Performance for Biomimetic Design of Advanced Polymers

2.1 Introduction

2.1.1 Utilizing Single Molecule Force Spectroscopy for Molecule-to-bulk Correlation

Understanding how the molecular structure of polymers relates to their emergent macroscopic properties has been critical to their development into a wide range of useful materials including plastics, fibers, and elastomers.[116-118] While numerous polymers have been synthesized to fulfill a myriad of technological applications, rational design of polymers with the ability to independently control key mechanical property variables such as Young's modulus, yield stress, toughness, and elasticity remains a fundamental challenge.[117] To truly make rational design of advanced polymeric materials possible, there is a critical need to understand how the mechanical response of individual polymer chains can be directly linked to the mechanical property profiles observed in the condensed bulk material. Many theoretical[119,120] and experimental[111,116,117,121,122] studies have resulted in substantial progress towards this goal. For example, Buehler *et al*.[119] revealed the molecular mechanism for the exceptional strength and toughness of spider silk using computational studies, while Craig *et al*.[111] demonstrated a quantitative correlation between molecular exchange rates of crosslinkers with bulk dynamic properties of organogels. Nevertheless, it remains a major challenge to directly correlate the detailed single molecule nanomechanical behavior in solution to emergent bulk mechanical properties in the solid state.

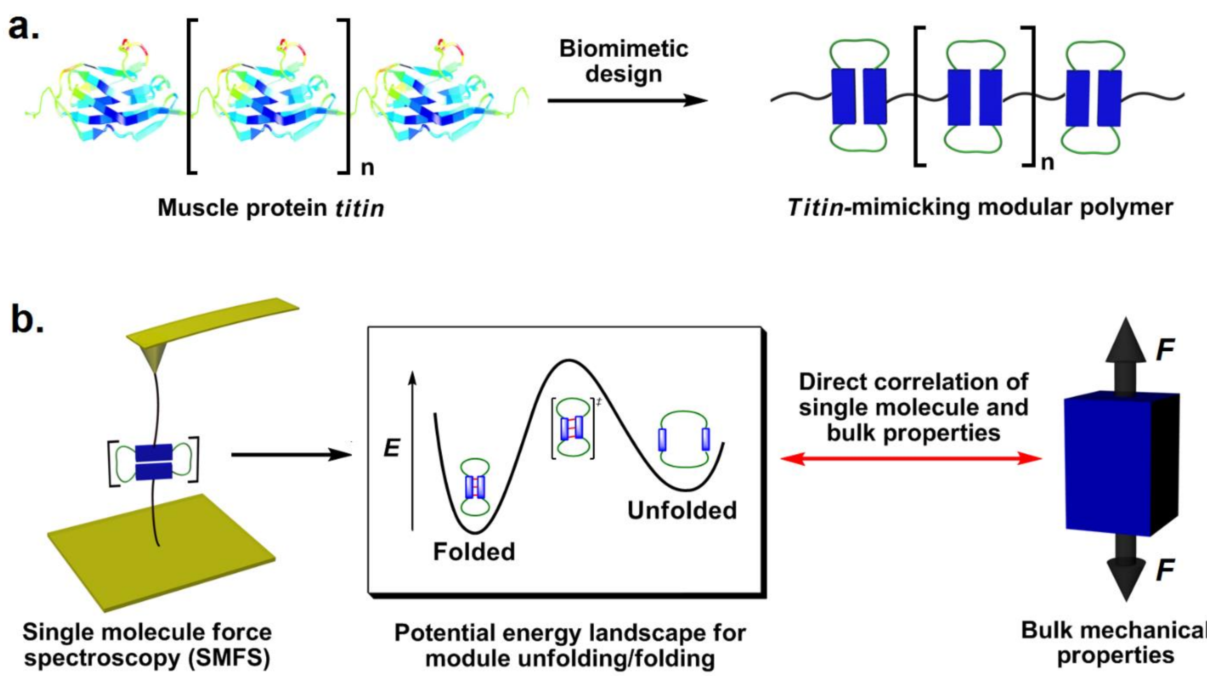

Figure 2.1 Biomimetic modular polymer is synthesized and studied in single molecule and bulk levels**.** **a.** Our biomimetic design of a modular polymer composed of a linear tandem array of stiff and reversibly unfolding monomers, which displays tough and adaptive properties similar to *titin*. **b.** SMFS reveals nano-mechanical properties, enabling derivation of the potential energy landscape, which is then directly correlated to bulk mechanical performance of the polymer.

Single molecule force spectroscopy (SMFS) provides a powerful means to investigate the mechanical force-induced behavior of various chemo-physical events on the level of individual molecules.[123] A key advantage of SMFS characterization lies in its ability to provide information about the energy landscape of molecular processes that would not be available through traditional ensemble averaging techniques. To date, valuable molecular-level insights of protein unfolding gained both experimentally by SMFS[36,37,41,51,123-126] and computationally by steered molecular dynamics (SMD[40,127,128]), have inspired the de novo design of new bio-engineered protein-based materials.[50,129] Synthetic oligomers and polymers have also been investigated by SMFS, which has aided in the understanding of their nanomechanical properties.[45,46,121,130-133] However, a direct mechanistic link between the energy landscape of a single molecule obtained by SMFS and the mechanical performance of a synthetic bulk polymer has not yet been reported. In this chapter, we employed SMFS studies to quantitatively derive the complete potential energy landscape governing both unfolding and re-folding dynamics of a biomimetic modular polymer (Figure 2.1b). This provide an unprecedented opportunity to directly correlate single molecule nanomechanical behavior to the emergent advanced mechanical properties of the bulk material, demonstrating the feasibility of bottom-up rational design of high-performance polymeric materials.

2.1.2 Our Biomimetic Design of the Protein *Titin*, SB-UPy-DCL Modular Polymer

The biomimetic modular polymer employed in this study was designed to mimic the modular muscle protein *titin*, using a strongly dimerizing 2-ureido-4-[1H]-pyrimidinone (UPy)[20,43] core with a double closed loop (DCL) architecture (Figure 2.1a). We have previously reported the linearly repeating modular design of energy-dissipative UPy modules for biomimetic material design,[45] and further demonstrated the use of a DCL module for dynamic materials.[48,49] In this work, to improve the solubility and to reduce non-specific π-π stacking interactions between UPy-DCL modules, we introduced a "stack-blocking" (SB) design to minimize co-facial attractive interactions between the planar aromatic UPy modules.[44,134]

2.2 Results and Discussion

2.2.1 Synthesis of SB-UPy-DCL Monomer and Oligomer

The synthesis of (SB-UPy-DCL) monomer (**2.9**) (Scheme 2.1) and its oligomers (**2.12**) (Scheme 2.2) are shown below. Monomer **2.9** was synthesized in a convergent synthesis starting with δ-valerolactone, which was ring opened and benzyl protected to produce carboxylic acid **2.1**. The compound was then converted to the acid chloride, reacted with Meldrum's acid, then refluxed in ethanol to synthesize β-ketoester **2.2**. The doubly-α position of **2.2** was alkylated with 11-bromoundecene to form compound **2.3**. The compound was then condensed with guanidine carbonate to form isocytosine **2.4**. For the other half of the UPy module, 1,6-diisopropylaniline was iodinated to form **2.5**, which was Ullman ether coupled with 10-undecen-1-ol to form compound **2.6**. The compound was converted to the isocyanate with phosgene and then coupled to **2.4** to make the UPy core **2.7**. Compound **2.7** dimerizes spontaneously in non-polar solvent which allows ring-closing methathesis with Grubbs catalyst followed by hydrogenolysis to assemble the SB-UPy-DCL architecture in **2.8**. Finally the free alcohols were acylated to create SB-UPy-DCL α,ω-diene monomer **2.9**. Details of the synthesis and characterization are provided in the Experimental section.

For SMFS studies, linear oligomers of SB-UPy-DCL modules (**2.12**) were synthesized via acyclic diene metathesis (ADMET) polymerization[135] with thiol groups attached at both ends of each polymer chain to promote chemisorption of the chain to the gold-coated cantilever and substrate surface, thus improving the chance of pulling from the ends of the oligomer. This design was inspired by many protein-based AFM-SMFS studies in which thiols from cysteine residues present in the protein domains can serve as anchors to the cantilever and substrate surface. We note in later SMFS studies that not all force-extension curves displayed thiol-gold rupture in the end of single molecule force spectra, suggesting that some may have been physically adsorbed. Similar observations have been made in many previous AFM-SMFS studies, without compromising the integrity of the data analysis.[125,136]

Scheme 2.1 Synthesis of SB-UPy-DCL Monomer

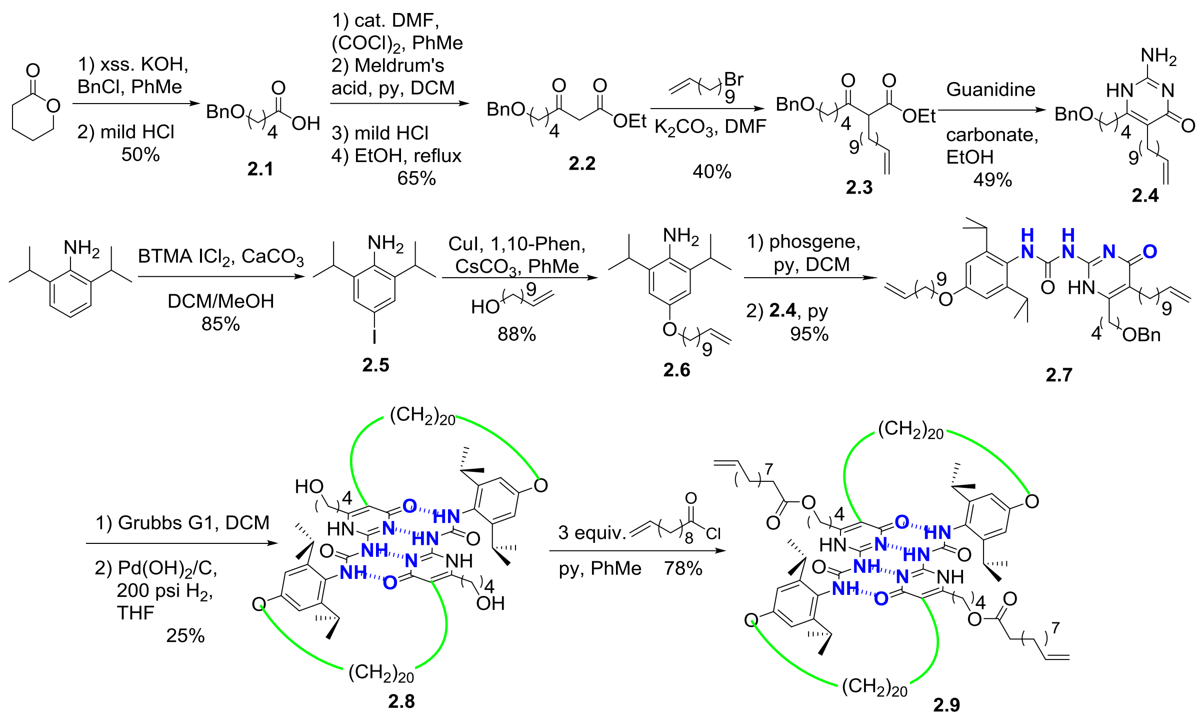

Scheme 2.2 Synthesis of SB-UPy-DCL Oligomer

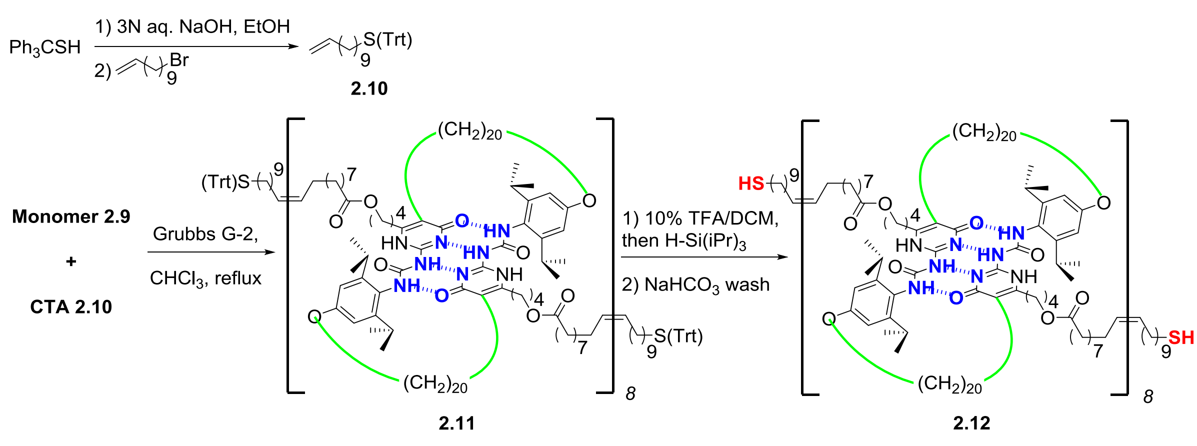

2.2.2 Single Molecule Force Spectroscopy Data Acquisition and Analysis of SB-UPy-DCL Oligomer

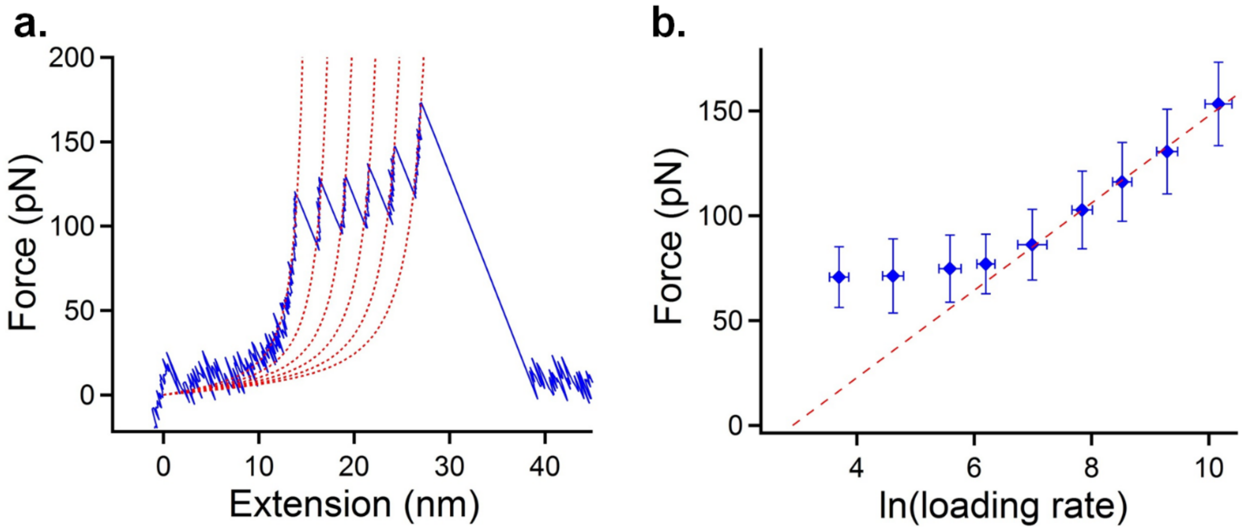

Figure 2.2 SMFS pulling experiments show robust saw-tooth patterns in force spectra and Bell-Evans fit derives dissociative kinetics. **a.** A representative single molecule force spectrum (blue) and its WLC model fit (red; l_p = 0.42 nm) at 30,000 pN/s loading rate. **b.** Semi-logarithmic plot of most probable rupture force versus loading rate shows both quasi- and non-equilibrium regions of the Bell-Evans model. Error bars in both axes represent the width at half-height of the Gaussian fit. Dotted red line: Bell-Evans model out-of-equilibrium linear fit. See Experimental for details of data acquisition and analysis.

With the synthesized oligomer **2.12**, single molecule pulling experiments were first carried out at a variety of loading rates (60 to 60,000 pN/s), allowing the extraction of the kinetic parameters governing the force-induced unfolding of individual UPy modules. The force curves thus obtained were selected for analysis based on the presence and quality of evenly-spaced saw-tooth patterns well-fitted to a single persistence length (0.38 ± 0.08 nm) according to the worm-like chain (WLC) model of polymer elasticity, described by the equation:

$$F(x) = \frac{k_B T}{l_p}\left[\frac{1}{4}\left(1-\frac{x}{L_c}\right)^{-2} - \frac{1}{4} + \frac{x}{L_c}\right]$$

where l_p is the persistence length and L_c is the contour length.[137,7,138] A representative curve is shown in Figure 2.2a. From the WLC fit, the increase in contour length (ΔL_c) of the oligomer following each rupture event was binned and fitted to a histogram (Figure 2.3), and was derived to be 2.95 ± 0.43 nm, which is in excellent agreement with the modeled increase in length between the folded and fully extended states of individual SB-UPy-DCL modules (2.85 nm; Figure 2.4), confirming that the observed saw-tooth patterns result from the sequential rupture of UPy-DCL modules in oligomer **2.12**. Further, the histogram of ΔL_c exhibits a well-defined mono-modal Gaussian shape (Figure 2.3), confirming a potential energy landscape consisting of a single transition state between folded and unfolded states.[50]

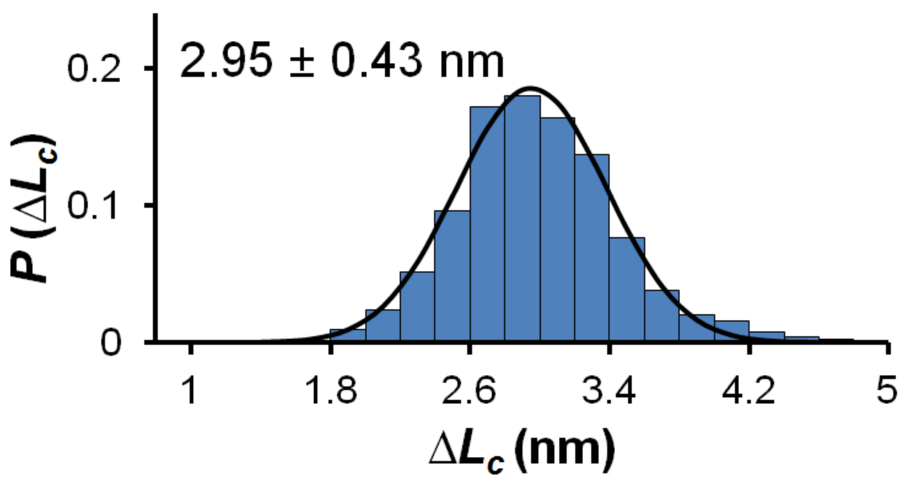

Figure 2.3 Histogram and Gaussian fit of increase in contour length (ΔL_c) per rupture event yields ΔL_c = 2.95 ± 0.43 nm, close to the dimer separation of 2.85 nm at full extension obtained from modeling.

a.

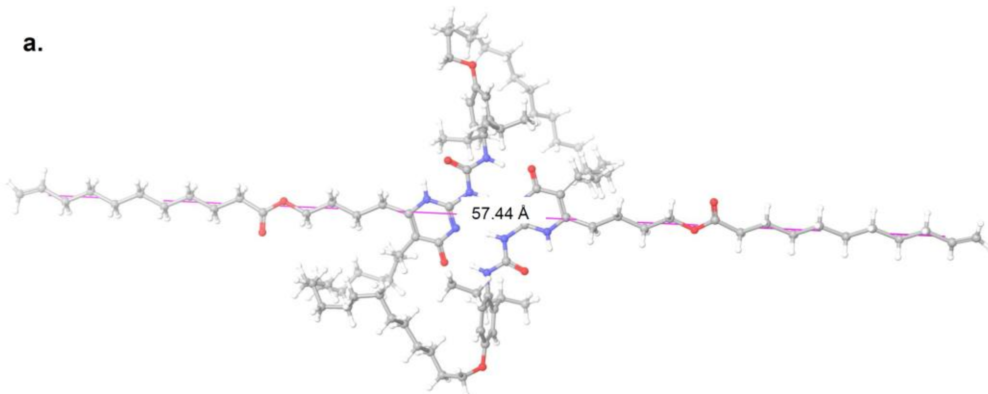

b.

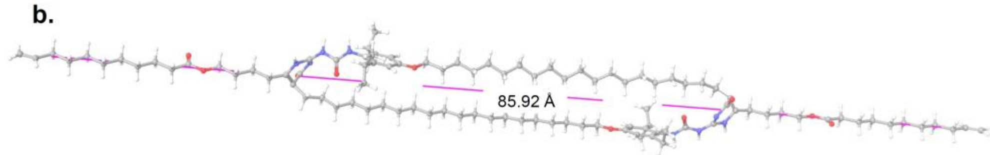

Figure 2.4 Molecular model and end-to-end distances along the pulling axis of dimerized (**a.**) and ruptured (**b.**) SB-UPy-DCL monomer generated from MacroModel.

At each loading rate, both rupture force and natural logarithm of loading rate were binned and fitted to a Gaussian (Figures 2.5 and 2.6; Table 2.1), and plotted as a single data point on a semi-logarithmical plot of rupture force vs. loading rate (Figure 2.2b). The plot shows a clear transition from the quasi-equilibrium to non-equilibrium regime in the range of loading rates that was studied. A Bell-Evans model least squares linear fit in the non-equilibrium regime was performed with the five highest loading rate data points. From the linear fit, $\Delta x_u^{\ddagger}$ was derived from the slope, while k_u^0 was derived from the x-intercept according to the equation:

$$F_{rupture} = \left(\frac{k_B T}{\Delta x_u^{\ddagger}}\right) ln\, \mu + \left(\frac{k_B T}{\Delta x_u^{\ddagger}}\right) ln \left(\frac{\Delta x_u^{\ddagger}}{k_u^0 k_B T}\right)$$

where μ is the loading rate.

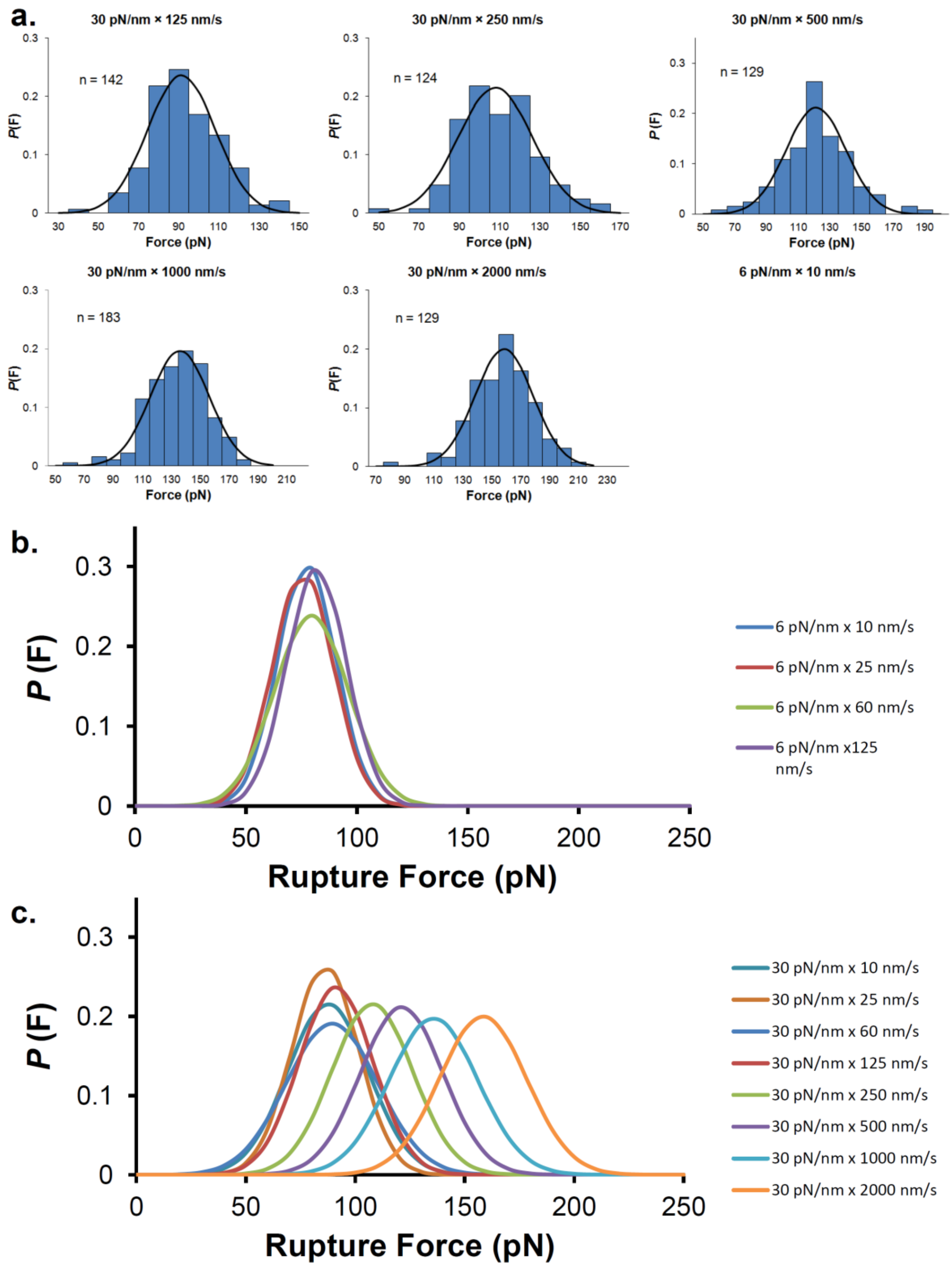

Figure 2.5 Pulling mode rupture forces. **a.** Histograms and Gaussian fits of rupture force at various out-of-equilibrium loading rates. Gaussian fits for most probable rupture force for pulling SMFS experiments are shown in **b.** (6 pN/nm cantilever) and in **c.** (30 pN/nm cantilever).

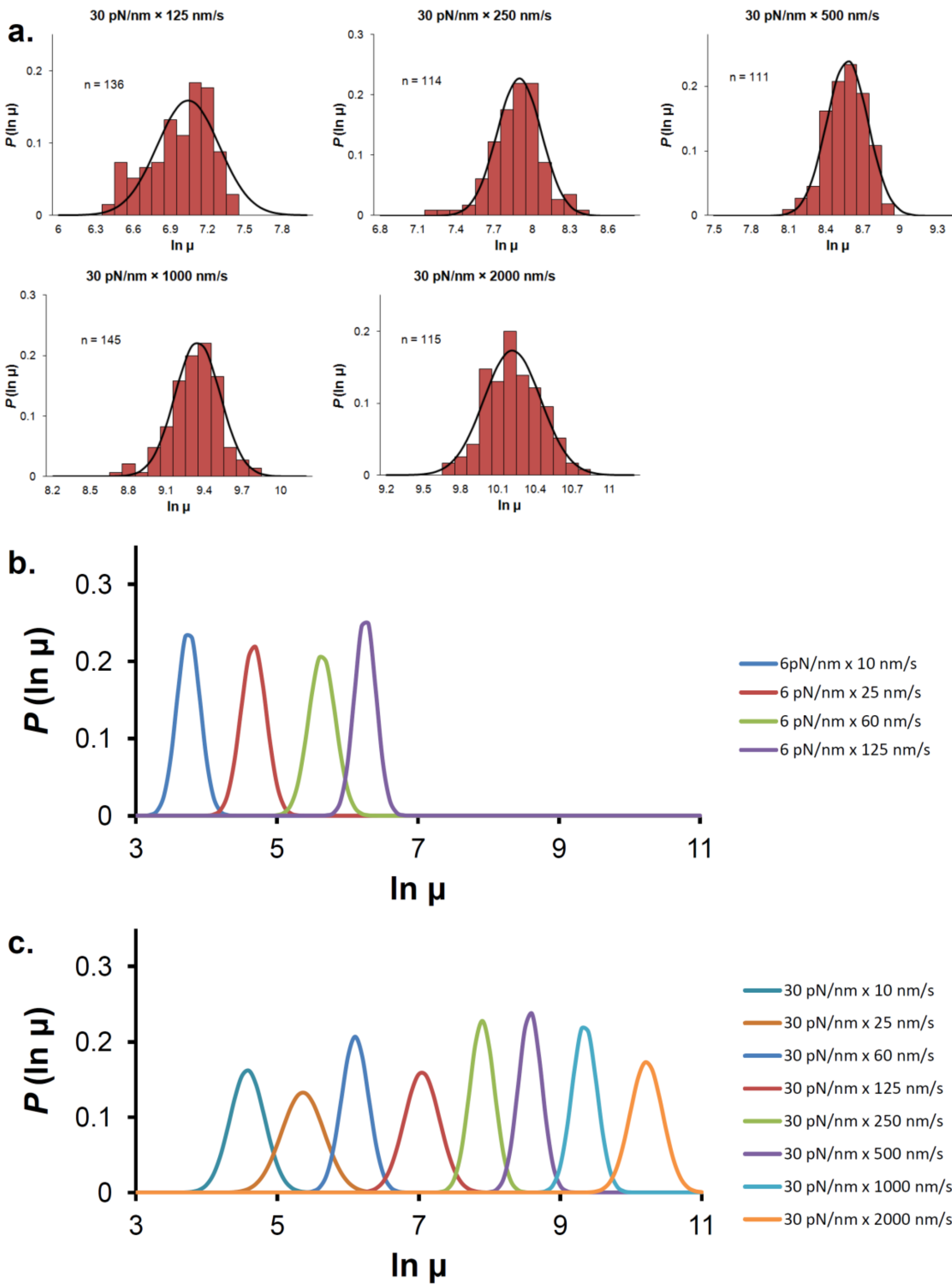

Figure 2.6 Pulling mode loading rates. **a.** Histograms and Gaussian fits for the natural logarithm of loading rate at various out of equilibrium loading rates. **b. and c.** Gaussian fits for natural logarithm of loading rate for pulling SMFS experiments with 6 pN/nm (**b.**) and 30 pN/nm cantilevers (**c.**).[139]

Table 2.1 Summary of Pulling SMFS Experimental Data

Spring const. (pN/nm)	**Ret. Velocity (nm/s)**	**Gaussian center ln μ**	**Gaussian width ln μ**	**Gaussian center Force (pN)**	**Gaussian width Force (pN)**
6	10	3.70	0.17	70.7	14.5
6	25	4.62	0.18	71.3	17.7
6	60	5.59	0.19	74.9	16.0
6	125	6.20	0.15	77.1	14.2
30	10	4.53	0.25	83.4	17.8
30	25	5.31	0.30	83.9	15.8
30	60	6.05	0.19	84.3	21.1
30	125	6.99	0.25	86.2	16.8
30	250	7.84	0.18	103	18.5
30	500	8.52	0.17	116	18.8
30	1000	9.29	0.18	131	20.2
30	2000	10.2	0.23	153	19.9

Consistent with the Bell-Evans model,[140,141] at high loading rates the system is fully out of equilibrium, and the rupture force is found to respond linearly with the natural logarithm of the loading rate (Figure 2.2b). As the loading rate is lowered below a critical threshold, the rupture forces begin to converge at a single value, finally reaching a plateau representing the quasi-equilibrium regime. The data was fitted to both the Bell-Evans model[140,141] and the less frequently used dynamic two-state model by Diezemann and Janshoff[142] in order to quantify the dimensions of the dissociative pathway of the potential energy profile. The rate of spontaneous unfolding in the absence of external force (k_u^0) was found to be 0.49 ± 0.09 or 0.88 ± 0.2 s^{-1} depending on the model (Table 2.2). Both values are close to the solution phase value reported by Meijer *et al.*, 0.6 ± 0.3 s^{-1} in toluene.[44] Furthermore, the reaction coordinate distance from the folded to the transition state ($\Delta x_u^{\ddagger}$) was found to be 2.0 ± 0.08 Å (Table 1), also in good agreement with previous UPy-based SMFS studies.[133]

Table 2.2 Kinetic and Thermodynamic Pparameters of SB-UPy-DCL Oligomer Derived from SMFS.

	***Bell-Evans*[140,141]**	***Diezemann-Janshoff*[142]**
k_u^0 (s^{-1})	0.88 ± 0.2	0.49 ± 0.09
$\Delta x_u^{\ddagger}$ (Å)	2.0 ± 0.08	2.0 ± 0.08
$\Delta x_f^{\ddagger}$ (Å)	-	12.2 ± 0.65
ΔG^0 (kJ/mol)	-	–58 ± 3

2.2.3 Cyclic Single Molecule Force Spectroscopy Data Acquisition and Analysis of SB-UPy-DCL Oligomer

Next, cyclic single molecule pulling-relaxation experiments were conducted to examine the refolding of SB-UPy-DCL modules and to quantify the dimensions of the associative potential energy well, as the load-rate-dependent forces observed during pulling can only provide dissociative kinetic information for the potential energy well. For this purpose, single oligomers **2.12** were repeatedly stretched and relaxed at different velocities, with a 0.5 s pause between each cycle (Figure 2.7a). This allowed examination of the out-of-equilibrium behavior of the rejoining forces imposed on the modules during the relaxation cycle. Re-folding events appear as a saw-tooth transition on the retraction cycle of the force-extension curve,[131] accompanied by a corresponding decrease in contour length (Figure 2.7c). Even at the low pulling and retraction velocities (25 nm/s), a significant hysteresis between the pulling and relaxation cycles was observed (Figure 2.7c). At relatively high velocities (500 nm/s), this hysteresis became much more pronounced (Figure 2.7b). Despite very large hysteresis, the modules re-fold quantitatively when the polymer is allowed to relax, as demonstrated by complete recovery of saw-tooth patterns between cycles (Figure 2.7b). As predicted by the two-state dynamic model described by Diezemann and Janshoff[142], the most probable rejoining forces (Figure 2.8; Table 2.3) decreased logarithmically with increasing retraction rate, following the opposite trend as in the rupture mode.

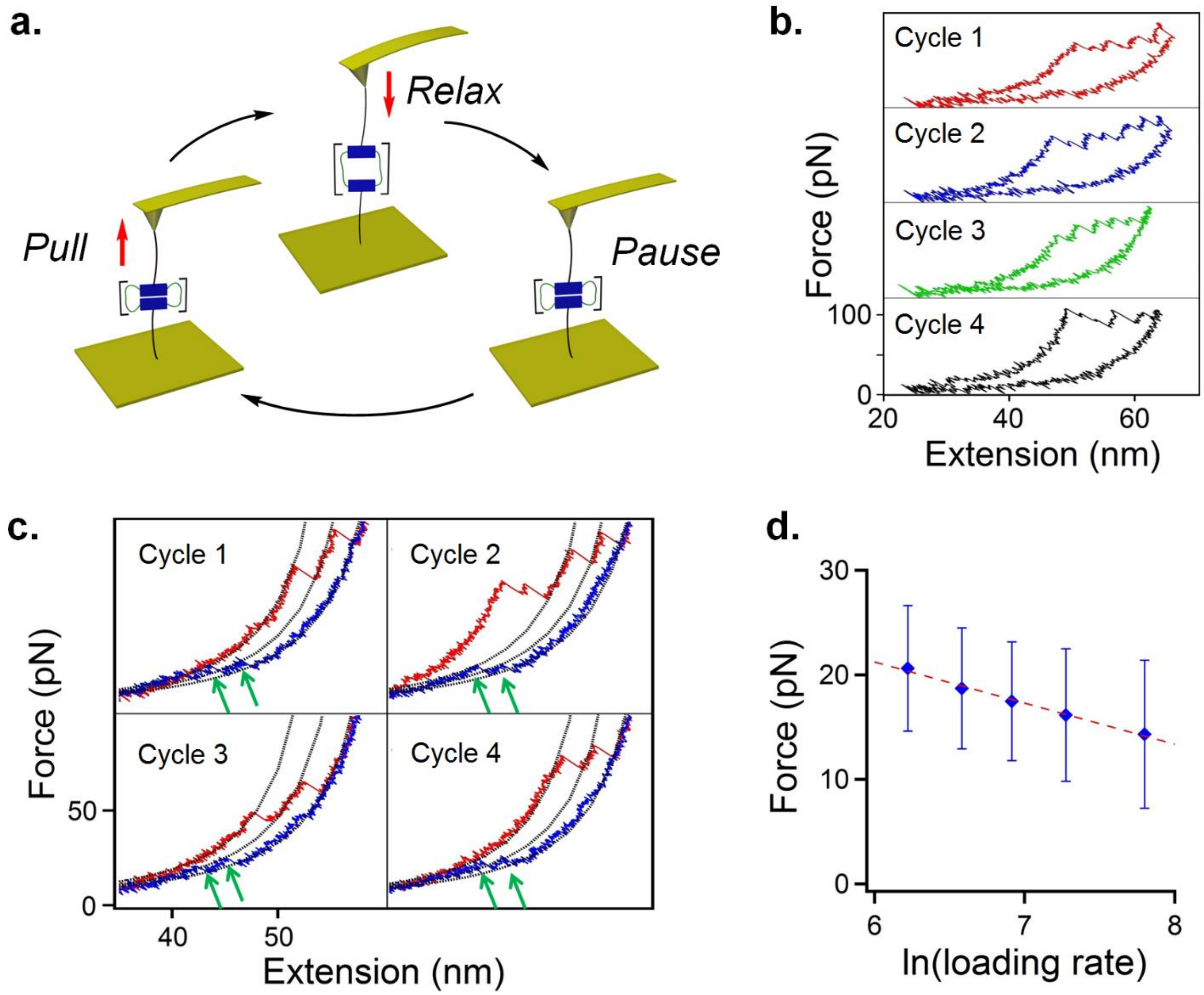

Figure 2.7 Cyclic SMFS experiments demonstrates re-folding of modules and fit of rejoining forces derives associative kinetics. **a.** Schematic representation of cyclic SMFS experiments. Single oligomer molecules were repeatedly pulled and retracted at a given velocity ranging from 125 to 500 nm/s for up to 10 cycles with 0.5 s pause between cycles. **b.** Representative multi-cyclic SMFS results show refolding and recovery of saw-tooth patterns between cycles at 500 nm/s pulling and relaxation velocity. **c.** Representative cyclic SMFS results at 25 nm/s pulling and relaxation velocity. Red and blue curves represent extension and retraction curves, respectively. Green arrows highlight rejoining events as exemplified by saw-tooth patterns on the retraction curve. Gray lines represent the WLC model fits of each cycle. Note that WLC model fit to a given contour length matches both saw-tooth patterns on extension (red) as well as saw-tooth patterns on retraction (blue) in all cycles. The increase in contour length between saw-tooth patterns in each cycle is approximately 3 nm in all cycles, in good agreement with the value extracted from pulling experiments as discussed above. **d.** Semi-logarithmic plot of most probable rejoining force versus loading rate. Error bars represent the width of the Gaussian fit. The width of potential energy well $\Delta x_f^{\ddagger}$ was derived from the linear fit in the non-equilibrium region (dotted red line).

Manual determination of loading rate on the rejoining path from the force versus time curve was omitted due to low signal-to-noise ratio in the lower pN portion of the force-retraction curve. Instead, the simpler equation of $\mu = k_c \times v$, where k_c is the cantilever spring constant measured by the thermal tuning method and v is the velocity, was used. A semi-logarithmic plot of most probable rejoining force versus loading rate was constructed, from which a least squares linear fit of the data was obtained in a similar manner to the pulling experiments. From the slope of the linear fit was derived $\Delta x_f^{\ddagger}$ according to the equation (Equation 16 in ref. 42):

$$F_{rejoin} = -\left(\frac{k_B T}{\Delta x_f^{\ddagger}}\right) ln\, \mu - \left(\frac{k_B T}{\Delta x_f^{\ddagger}}\right) ln\, z_r$$

where $z_r = \frac{e^{-\gamma} \Delta x_f^{\ddagger}}{k_f^0 k_B T}$. F_{rejoin} is the most probable rejoining force, k_f^0 is the folding rate in the absence of external force, $\Delta x_f^{\ddagger}$ is the distance on the reaction coordinate diagram from the transition state to the unfolded energy well, μ is the loading rate, and $\gamma = 0.577215$ is the Euler constant. We note the Euler constant only serves to offset the intercepts, and has no effect on the slope from which $\Delta x_f^{\ddagger}$ is derived.

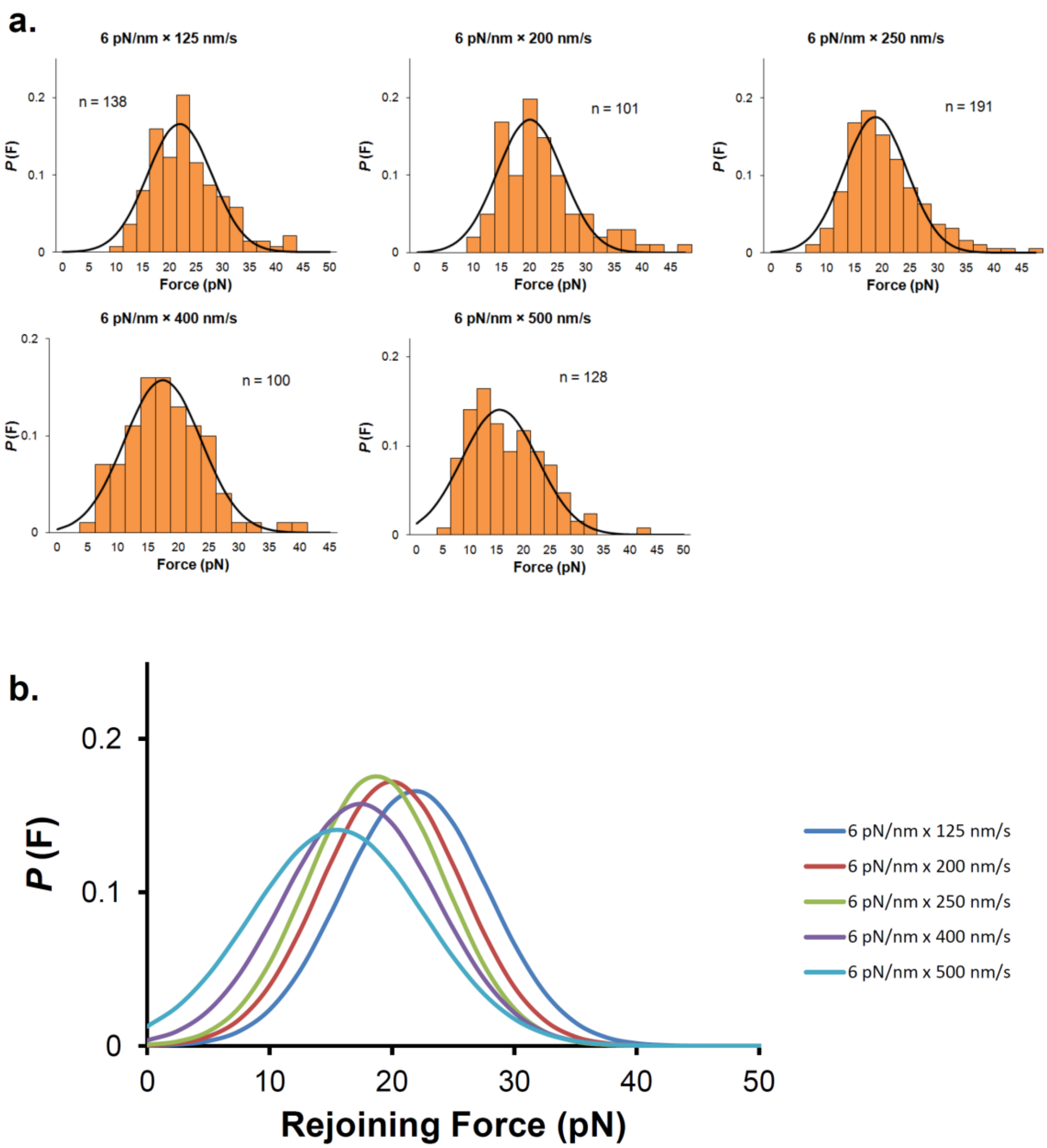

Figure 2.8 Cyclic SMFS rejoining forces. **a.** Histograms and Gaussian fits for rejoining force at various retraction rates. **b.** Gaussian fits for rejoining force for retraction cycle of cyclic SMFS experiments.

Table 2.3 Summary of Cyclic SMFS Data

Spring Const. (pN/nm)	**Velocity (nm/s)**	**ln μ**	**Gaussian Center Force (pN)**	**Gaussian Width Force (pN)**
6	125	5.65	20.6	6.0
6	200	6.06	18.7	5.8
6	250	6.32	17.4	5.7
6	400	6.84	16.2	6.3
6	500	7.08	14.3	7.1

Based on the quasi-equilibrium rupture force and the kinetic parameters obtained in the above study, we can extract the equilibrium free energy (ΔG^0) for the unfolding of a single SB-UPy-DCL module. The two-state potential energy surface constructed from the described results depicts a distance between the folded and unfolded states of 14.2 Å on the extension coordinate. According to the dynamic model proposed by Diezemann and Janshoff,[142] the inter-coordinate distance between the folded and unfolded states in combination with the quasi-equilibrium rupture force can be used to calculate the equilibrium constant between the two states according to the equation:

$$F_{eq} = \frac{k_B T}{Q_{BA}} \times ln(1 + K_{eq})$$

where F_{eq} is the rupture force in the quasi-equilibrium regime, k_B is the Boltzmann constant, T is the temperature in Kelvin, and Q_{BA} is the distance along the reaction coordinate between the bound and unbound states. Using this method, K_{eq} is calculated to be $(1.5 \pm 0.7) \times 10^{10}$, or $\Delta G^0 = -58 \pm 3$ kJ/mol at ambient temperature (Table 2.2, also see Figure 2.9), agreeing reasonably well with Meijer *et al*.'s value of $\Delta G^0 = -50$ kJ/mol measured by fluorescence spectroscopy.[44]

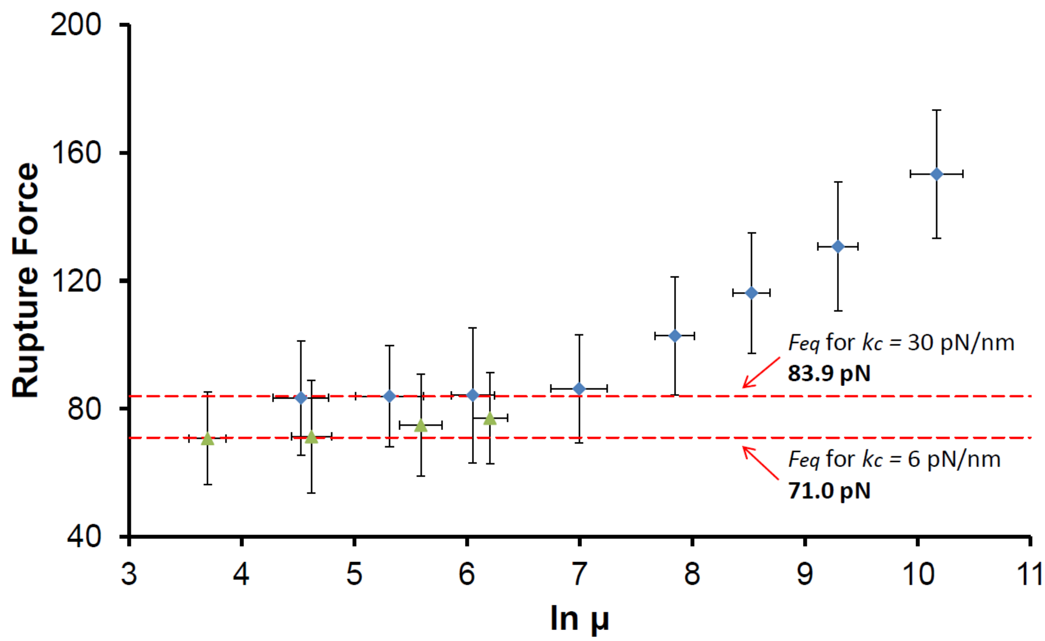

Figure 2.9 Derivation of quasi-equilibrium regime rupture force. Red lines denote the equilibrium rupture forces with 30 pN/nm and 6 pN/nm cantilevers.

In order to correlate single molecule with bulk properties, we further synthesized high molecular weight SB-UPy-DCL modular polymer and characterized its bulk mechanical properties. Monomer **2.9** was polymerized by ADMET under vacuum to remove ethylene byproduct in order to form high molecular weight polymer (M_n = 33 kDa, M_w/M_n = 2.1; See Scheme 2.3).

Scheme 2.3 Synthesis of Bulk SB-UPy-DCL Material

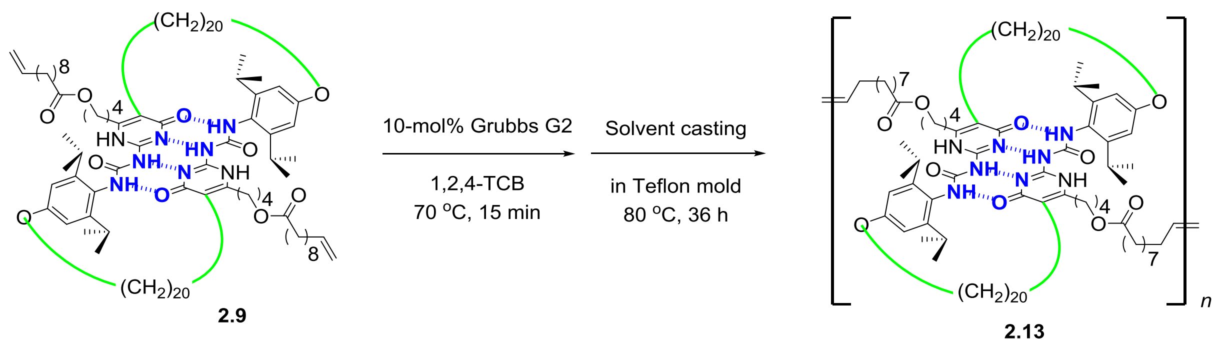

Tensile testing of resulting films revealed a strong and tough material, with high Young's modulus and yield strength (~250 and ~20 MPa at room temperature, respectively), and extensibility at break of over three times its original length (Figure 2.10).

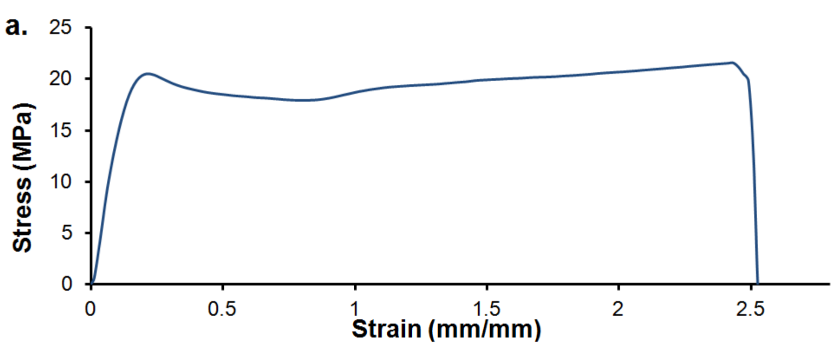

Figure 2.10 Static tensile behavior of bulk SB UPy-DCL material at room temperature. Young's modulus is ~250 MPa, yield strength is ~20 MPa, and strain at break is ~250%.

After yield, the material undergoes homogeneous deformation, with modest strain hardening. A very large hysteresis was observed within each pulling-retraction cycle, resulting in extremely high toughness for the material. The material also showed an unusual dynamic behavior as demonstrated by the time- and temperature-dependent recovery of plastic deformation. Following a large plastic deformation, the sample gradually recovered with time and the recovery process was greatly accelerated by heating the sample at 80 ºC (Figure 2.11a). Critically, this high toughness and recoverable tensile plastic deformation occurred below the glass transition temperature (*vide infra*), as observed with the previously reported system[48] (Figure 2.11a). The unique combination of high Young's modulus (~250 MPa), high toughness (~45 MJ/m^3), and recovery of tensile properties after plastic deformation clearly distinguishes our biomimetic modular polymer from traditional rubbers (e.g., polybutadiene),[143] plastics (e.g., poly(methyl methacrylate)),[144] and thermoplastic elastomers (e.g., styrene-butadiene-styrene block co-polymer (SBS)).[145] As load-rate dependence is the critical link between single molecule and bulk behaviors,[141,146-148] we performed further tensile testing at strain rates varying between 0.1 to 100 mm/min, and found that both the yield and the post-yield plateau stresses (4.5 ± 0.4 to 9.7 ±0.4 MPa) increased with increasing strain rate (Figure 2.11b).

We then characterized the dynamic response of our material using dynamic mechanical analysis (DMA). We observed two peaks in G" and tan δ, with the α transition occurring at approximately 80 ºC (Figure 2.11c), and the β transition at approximately –25 ºC (Figure 2.11d). The shift in tan δ peak with frequencies ranging from 0.1 to 20 Hz observed by DMA resulted in a linear Arrhenius plot for both transitions (Figure 2.11e). The activation energies associated with the α and β transitions were thus calculated to be 380 ± 10, and 77 ±2 kJ/mol, respectively.

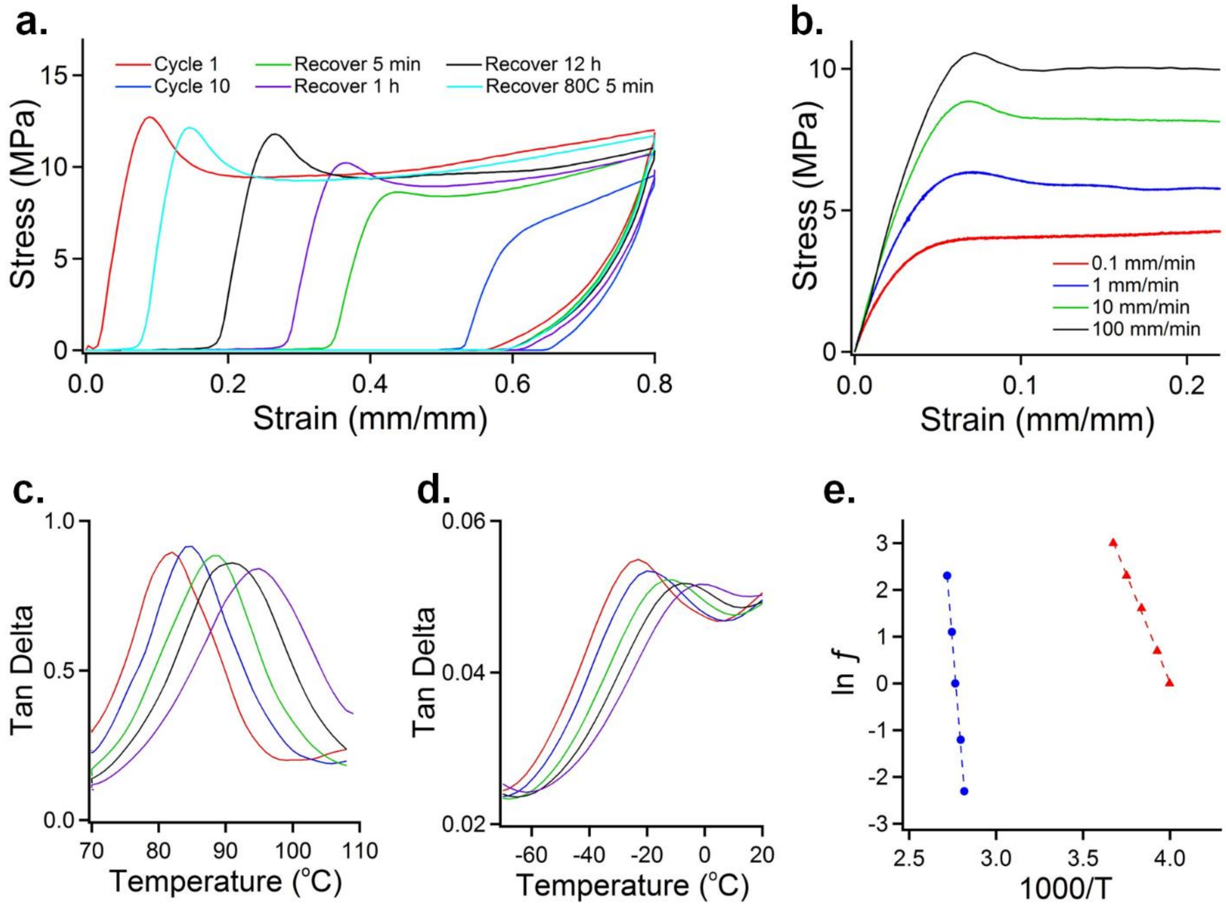

Figure 2.11 Mechanical characterization of bulk SB-UPy-DCL material demonstrates high strength, toughness, and slow dynamic recovery of properties. **a.** Tensile testing at 60 ºC of SB UPy-DCL film. The material shows high strength and toughness (cycle 1, red), much of which is temporarily lost after multiple cycles of pulling (cycle 10, blue). Recovery of strength and stiffness happens quickly (5 m recovery, green), while full recovery of dimension happens much more slowly (12 h recovery, black). Recovery of both strength and dimension is greatly enhanced when heated to near T_g (80 ºC recovery 5 m, cyan). **b.** Strain-rate dependent tensile testing of SB UPy-DCL film (strain rate: 0.1, 1, 10, and 100 mm/min). At higher strain rates the material exhibits higher yield and post-yield stresses. **c.** Multi-frequency (0.1, 0.3, 1, 3, and 10 Hz) temperature sweep of SB UPy-DCL material using DMA. The α transition occurs at approximately 80 to 100 ºC. **d.** Multi-frequency (1, 2, 5, 10, 20 Hz) temperature sweep of SB UPy-DCL material using DMA. The β transition occurs at approximately –25 to 0 ºC. **e.** Arrhenius plot of α (blue) and β (red) transitions based on frequency-dependent shift of tan δ peak. Activation energy for α transition is 380 ± 10 kJ/mol, while activation energy for β transition is 77 ± 2 kJ/mol.

2.2.4 Molecule-to-bulk Correlation of *Titin* Biomimetic Concepts

Clearly, the extracted kinetic parameters confirm that the nanomechanical response of individual oligomers observed in SMFS is indeed attributable to the biomimetic modular design. First, the linear array of SB-UPy-DCL modules rupture sequentially when pulled from the chain ends (Figure 2.2a), providing the familiar saw-tooth profile observed for both the immunoglobulin[36,41] and fibronectin-III[124] domains of *titin*. With each rupture effectively increasing the contour length of the molecule, the oligomer is able to sustain an average load in the 100-150 pN range throughout extension, resulting in enhanced energy dissipation compared to a simple linear polymer chain. Second, the recovery of the saw-tooth patterns between multiple pulling cycles of the same molecule (Figure 2.7b) illustrates that the ruptured UPy dimers re-fold when stress on the oligomer is relaxed, confirming that the *titin*-like passive elasticity is retained in our synthetic analog. Third, the complete potential energy profile derived from our quantitative SMFS data for a single modular rupture and re-folding event illustrates an asymmetric double-well potential with a steep and short pathway towards rupture and, in sharp contrast, a shallow, broad pathway towards re-folding (Figure 2.12). The potential energy profile displays a comparatively larger distance to the transition state on the re-folding pathway than the rupture pathway, such that even a small external force can significantly affect the dynamic module's re-folding rate, allowing the ruptured state to persist under the small load experienced during retraction. This combination of short $\Delta x_u^{\ddagger}$ and long $\Delta x_f^{\ddagger}$ is a key feature of the mechanical proteins that inspired our design, and results in a characteristic energy-dissipating hysteresis between an extension-retraction cycle.[36,124,149]

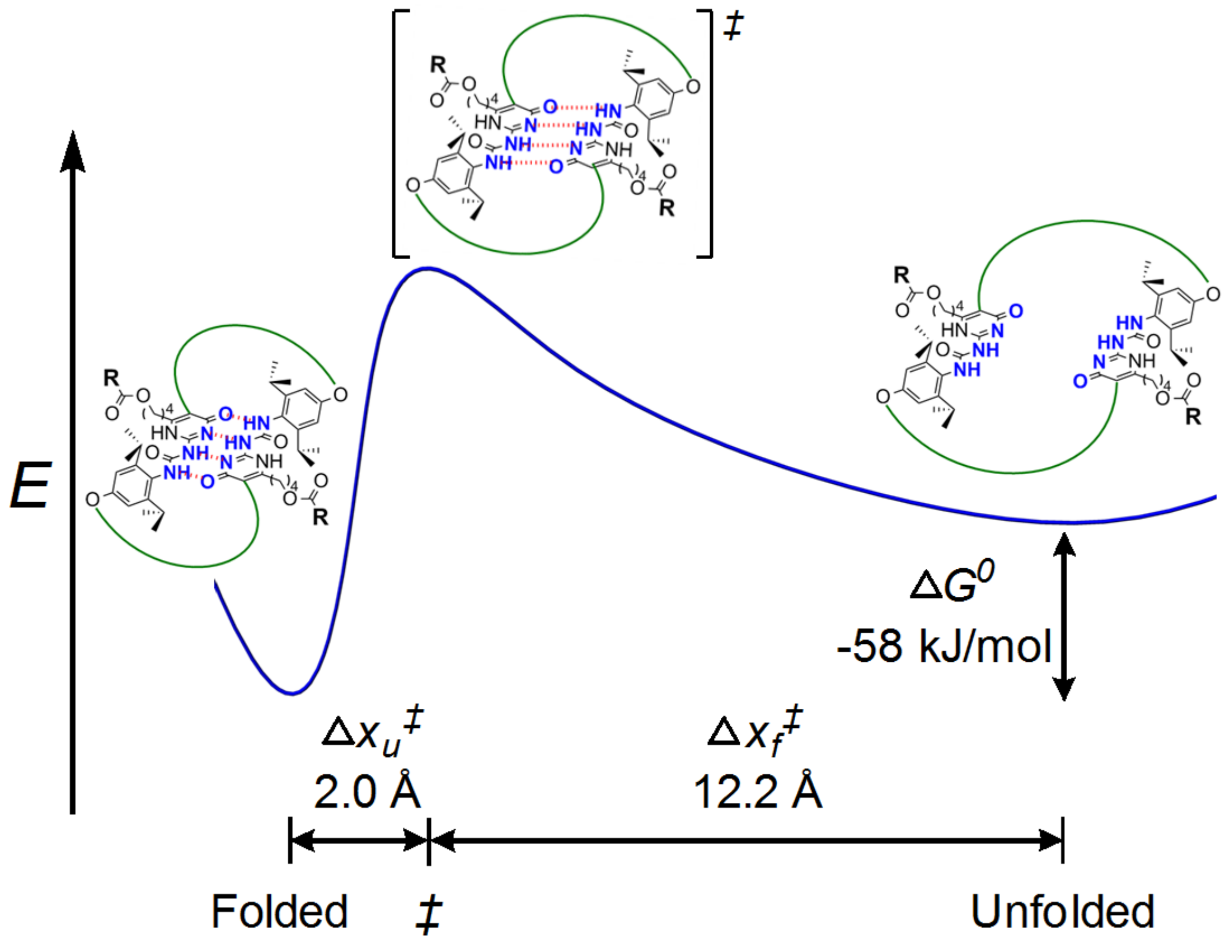

Figure 2.12 The potential energy landscape constructed for SB-UPy-DCL unfolding based on SMFS data bridges the nanomechanical and emergent bulk properties. The two-state potential energy profile of SB-UPy-DCL rupture depicts an asymmetric energy diagram with a sharp dissociative well and a shallow, compliant associative well. The steep dissociative pathway contributes to high rupture strength while the shallow associative pathway causes slow re-folding dynamics on the AFM timescale, resulting in energy-dissipative hysteresis in pull-relax cycles. These factors translate to high post-yield stress, dynamic strain recovery after plastic deformation, and high energy dissipation in the bulk material (Figure 4a), providing the first example of direct correlation between single molecule nanomechanical properties and bulk mechanical performance for a synthetic polymer.

Critically, the extracted kinetic parameters from SMFS studies allow us to construct the quantitative potential energy landscape for SB-UPy-DCL folding-unfolding (Figure 2.12), which provides an opportunity to directly correlate the observed bulk behavior under load to the nanomechanical properties of individual polymer chains in our biomimetic modular polymer. As described above, we derived a short distance to the transition state on the rupture pathway. According to Bell's equation for the rate of unfolding under an external force:[140]

$$k_u(F) = k_u^0 \cdot exp\,(\frac{F\Delta x_u^{\ddagger}}{k_B T})$$

the rate of unfolding grows exponentially relative to the product of external force F and $\Delta x_u^{\ddagger}$. Consequently, with a short and steep well (small $\Delta x_u^{\ddagger}$), a higher force is required to significantly affect the unfolding rate, ultimately resulting in a high average rupture force.[149] The observed distance to the unfolding transition state ($\Delta x_u^{\ddagger}$ = 2.0 ± 0.1 Å, Figure 2.12) is typical for cooperative H-bond failure in synthetic systems[131,133] and mechanically robust proteins alike.[36,123,124] This property provides a direct explanation for the high post-yield plateau modulus observed in the SB-UPy-DCL bulk material (Figure 2.11a).

We also observed a slow elastic recovery of dimension and mechanical properties after extension of the bulk material (Figure 4a), which can be linked to the long distance to the transition state on the re-folding pathway ($\Delta x_f^{\ddagger}$ = 12.2 ± 0.65 Å, Figure 2.12), and results in *titin*-like passive elasticity at both the bulk and single molecule scales. The rate of re-folding is affected by external force following the equation[140,149]:

$$k_f(F) = k_f^0 \cdot exp\,(-\frac{F\Delta x_f^{\ddagger}}{k_B T})$$

where k_f^0 is the binding rate in the absence of external load and $k_f(F)$ is the force-dependent folding rate. Thus, analogous to the rupture kinetics, the rate of re-folding shows a similar exponential dependence on the product of external force and distance to the transition state. With a long distance between the transition and unfolded states, even a low force can significantly slow down re-folding. This observed single molecule behavior (Figure 2.12) can be correlated to the slow and temperature-dependent dynamic recovery of dimension and strength of our bulk polymer. In the bulk phase, various weak intermolecular interactions are felt by individual SB-UPy-DCL modules, which significantly slows down the re-dimerization of unfolded UPy modules, hence the bulk recovery. These intermolecular forces decrease with increasing temperature and chain mobility, allowing for more facile UPy re-dimerization and faster recovery at temperatures closer to the glass transition temperature (80 ºC, Figure 2.11b).

Finally, the combination of high rupture force and quantitative passive re-folding observed at the single molecule level (Figure 2.7b) can be associated with the large energy dissipation during plastic deformation, as well as the slow but complete recovery of strength, strain, and toughness observed during the course of the load-relaxation-recovery cycle in the bulk experiment (Figure 2.11a). The asymmetric energy diagram displays a shallow, broad pathway towards re-dimerization complementing a steep and short pathway towards rupture (Figure 2.12). In the natural as well as our synthetic system, this type of individual module response produces not only extreme toughness when many modules are connected in a linear load-bearing chain, but also results in a highly adaptive elastomeric material: tensile behavior remains fairly constant across a large stress and strain range. In the case of *titin,* this dynamic property allows mammalian muscle to act as a shock absorber and retain its programmed functionality across the wide range of mechanical strains experienced by the muscle tissue.[150]

2.3 Conclusions and Outlook

In this study, we have shown the first example of the use of SMFS to directly correlate molecular potential energy profile to bulk mechanical behavior. The SMFS data enabled us to construct the complete, asymmetric potential energy profile of the rupture and re-folding of each individual module within a dynamic modular polymer of the SB-UPy-DCL motif. Furthermore, we demonstrated that the detailed potential energy landscape derived from SMFS can qualitatively describe the ultimate bulk material properties. The approach we have described here should be applicable to the study of other polymeric materials for elucidating the molecular mechanism for their bulk behavior. With further advancement in SMFS methodology, we envision that SMFS will serve not only as a tool for mechanistic elucidation but also as a guide for rational, *de novo* design of advanced polymer materials.

2.4 References

(1) van Krevelen, D. W.; te Nijenhuis, K. *Properties of polymers: Their correlation with chemical structure; their numerical estimation and prediction from additive group contributions*; 4th ed.; Elsevier: Oxford, UK, 2009.

(2) Hearle, J. W. S. *Polymers and their properties: Fundamentals of structure and mechanics*; Halstead Press: New York, 1982; Vol. 1.

(3) Flory, P. J. *Principles of polymer chemistry*; Cornell University Press: Ithaca, 1953.

(4) Keten, S.; Xu, Z.; Ihle, B.; Buehler, M. J. Nanoconfinement controls stiffness, strength and mechanical toughness of β-sheet crystals in silk *Nat Mater* **2010**, *9*(4), 359-367.

(5) Meijer, H. E. H.; Govaert, L. E. Mechanical performance of polymer systems: The relation between structure and properties *Progress in Polymer Science* **2005**, *30*(8–9), 915-938.

(6) Yount, W. C.; Loveless, D. M.; Craig, S. L. Small-Molecule Dynamics and Mechanisms Underlying the Macroscopic Mechanical Properties of Coordinatively Crosslinked Polymer Networks *Journal of the American Chemical Society* **2005**, *127*(41), 14488-14496.

(7) Serpe, M. J.; Craig, S. L. Physical Organic Chemistry of Supramolecular Polymers *Langmuir* **2006**, *23*(4), 1626-1634.

(8) Halary, J.-L.; Lauprêtre, F.; Monnerie, L. *Polymer materials: Macroscopic properties and molecular interpretations*; John Wiley & Sons, Inc.: Hoboken, New Jersey, 2011.

(9) Janshoff, A.; Neitzert, M.; Oberdörfer, Y.; Fuchs, H. Force Spectroscopy of Molecular Systems—Single Molecule Spectroscopy of Polymers and Biomolecules *Angewandte Chemie International Edition* **2000**, *39*(18), 3212-3237.

(10) Rief, M.; Gautel, M.; Oesterhelt, F.; Fernandez, J. M.; Gaub, H. E. Reversible Unfolding of Individual Titin Immunoglobulin Domains by AFM *Science* **1997**, *276*(5315), 1109-1112.

(11) Marszalek, P. E.; Lu, H.; Li, H.; Carrion-Vazquez, M.; Oberhauser, A. F.; Schulten, K.; Fernandez, J. M. Mechanical unfolding intermediates in titin modules *Nature* **1999**, *402*(6757), 100-103.

(12) Oberhauser, A. F.; Marszalek, P. E.; Erickson, H. P.; Fernandez, J. M. The molecular elasticity of the extracellular matrix protein tenascin *Nature* **1998**, *393*(6681), 181-185.

(13) Kellermayer, M. S. Z.; Smith, S. B.; Granzier, H. L.; Bustamante, C. Folding-Unfolding Transitions in Single Titin Molecules Characterized with Laser Tweezers *Science* **1997**, *276*(5315), 1112-1116.

(14) Rief, M.; Gautel, M.; Schemmel, A.; Gaub, H. E. The Mechanical Stability of Immunoglobulin and Fibronectin III Domains in the Muscle Protein Titin Measured by Atomic Force Microscopy *Biophysical Journal* **1998**, *75*(6), 3008-3014.

(15) Carrion-Vazquez, M.; Oberhauser, A. F.; Fowler, S. B.; Marszalek, P. E.; Broedel, S. E.; Clarke, J.; Fernandez, J. M. Mechanical and chemical unfolding of a single protein: A comparison *Proceedings of the National Academy of Sciences* **1999**, *96*(7), 3694-3699.

(16) Lee, H.; Scherer, N. F.; Messersmith, P. B. Single-molecule mechanics of mussel adhesion *Proceedings of the National Academy of Sciences* **2006**, *103*(35), 12999-13003.

(17) Lu, H.; Isralewitz, B.; Krammer, A.; Vogel, V.; Schulten, K. Unfolding of Titin Immunoglobulin Domains by Steered Molecular Dynamics Simulation *Biophysical Journal* **1998**, *75*(2), 662-671.

(18) Lu, H.; Schulten, K. The Key Event in Force-Induced Unfolding of Titin's Immunoglobulin Domains *Biophysical Journal* **2000**, *79*(1), 51-65.

(19) Chabria, M.; Hertig, S.; Smith, M. L.; Vogel, V. Stretching fibronectin fibres disrupts binding of bacterial adhesins by physically destroying an epitope *Nat Commun* **2010**, *1*135.

(20) Lv, S.; Dudek, D. M.; Cao, Y.; Balamurali, M. M.; Gosline, J.; Li, H. Designed biomaterials to mimic the mechanical properties of muscles *Nature* **2010**, *465*(7294), 69-73.

(21) Guzmán, D. L.; Randall, A.; Baldi, P.; Guan, Z. Computational and single-molecule force studies of a macro domain protein reveal a key molecular determinant for mechanical stability *Proceedings of the National Academy of Sciences* **2010**, *107*(5), 1989-1994.

(22) Roland, J. T.; Guan, Z. Synthesis and Single-Molecule Studies of a Well-Defined Biomimetic Modular Multidomain Polymer Using a Peptidomimetic β-Sheet Module *Journal of the American Chemical Society* **2004**, *126*(44), 14328-14329.

(23) Guan, Z.; Roland, J. T.; Bai, J. Z.; Ma, S. X.; McIntire, T. M.; Nguyen, M. Modular Domain Structure: A Biomimetic Strategy for Advanced Polymeric Materials *Journal of the American Chemical Society* **2004**, *126*(7), 2058-2065.

(24) Zhang, W.; Zou, S.; Wang, C.; Zhang, X. Single Polymer Chain Elongation of Poly(N-isopropylacrylamide) and Poly(acrylamide) by Atomic Force Microscopy *The Journal of Physical Chemistry B* **2000**, *104*(44), 10258-10264.

(25) Janke, M.; Rudzevich, Y.; Molokanova, O.; Metzroth, T.; Mey, I.; Diezemann, G.; Marszalek, P. E.; Gauss, J.; Bohmer, V.; Janshoff, A. Mechanically interlocked calix[4]arene dimers display reversible bond breakage under force *Nat Nano* **2009**, *4*(4), 225-229.

(26) Ortiz, C.; Hadziioannou, G. Entropic Elasticity of Single Polymer Chains of Poly(methacrylic acid) Measured by Atomic Force Microscopy *Macromolecules* **1999**, *32*(3), 780-787.

(27) Zou, S.; Schönherr, H.; Vancso, G. J. Force Spectroscopy of Quadruple H-Bonded Dimers by AFM: Dynamic Bond Rupture and Molecular Time−Temperature Superposition *Journal of the American Chemical Society* **2005**, *127*(32), 11230-11231.

(28) Sijbesma, R. P.; Beijer, F. H.; Brunsveld, L.; Folmer, B. J. B.; Hirschberg, J. H. K. K.; Lange, R. F. M.; Lowe, J. K. L.; Meijer, E. W. Reversible Polymers Formed from Self-Complementary Monomers Using Quadruple Hydrogen Bonding *Science* **1997**, *278*(5343), 1601-1604.

(29) Beijer, F. H.; Sijbesma, R. P.; Kooijman, H.; Spek, A. L.; Meijer, E. W. Strong Dimerization of Ureidopyrimidones via Quadruple Hydrogen Bonding *Journal of the American Chemical Society* **1998**, *120*(27), 6761-6769.

(30) Kushner, A. M.; Gabuchian, V.; Johnson, E. G.; Guan, Z. Biomimetic Design of Reversibly Unfolding Crosslinker to Enhance Mechanical Properties of 3D Network Polymers *Journal of the American Chemical Society* **2007**, *129*(46), 14110-14111.

(31) Kushner, A. M.; Vossler, J. D.; Williams, G. A.; Guan, Z. A Biomimetic Modular Polymer with Tough and Adaptive Properties *Journal of the American Chemical Society* **2009**, *131*(25), 8766-8768.

(32) Söntjens, S. H. M.; Sijbesma, R. P.; van Genderen, M. H. P.; Meijer, E. W. Stability and Lifetime of Quadruply Hydrogen Bonded 2-Ureido-4[1H]-pyrimidinone Dimers *Journal of the American Chemical Society* **2000**, *122*(31), 7487-7493.

(33) Hentschel, J.; Kushner, A. M.; Ziller, J.; Guan, Z. Self-Healing Supramolecular Block Copolymers *Angewandte Chemie International Edition* **2012**, *51*(42), 10561-10565.

(34) Wagener, K. B.; Boncella, J. M.; Nel, J. G. Acyclic diene metathesis (ADMET) polymerization *Macromolecules* **1991**, *24*(10), 2649-2657.

(35) Rief, M.; Pascual, J.; Saraste, M.; Gaub, H. E. Single molecule force spectroscopy of spectrin repeats: low unfolding forces in helix bundles *Journal of Molecular Biology* **1999**, *286*(2), 553-561.

(36) Kratky, O.; Porod, G. X-ray investigation of dissolved chain molecules. *Rec. Trav. Chim. Pays-Bas* **1949**, *68*1106-1123.

(37) Flory, P. J. *Statistical mechanics of chain molecules*; Interscience Publishers: New York, 1969.

(38) Marko, J. F.; Siggia, E. D. Stretching DNA *Macromolecules* **1995**, *28*(26), 8759-8770.

(39) Friedsam, C.; Wehle, A., K.; Kűhner, F.; Gaub, H. Dynamic single-molecule force spectroscopy: bond rupture analysis with variable spacer length *J. Phys.: Condens. Matter* **2003**, *15*(18), S1709-S1723.

(40) Bell, G. I. Models for the Specific Adhesion of Cells to Cells *Science* **1978**, *200*(4342), 618-627.

(41) Evans, E.; Ritchie, K. Dynamic strength of molecular adhesion bonds *Biophysical Journal* **1997**, *72*(4), 1541-1555.

(42) Diezemann, G.; Janshoff, A. Dynamic force spectroscopy: Analysis of reversible bond-breaking dynamics *Journal of Chemical Physics* **2008**, *129*(8), 084904.

(43) Cowie, J. M. G. *Polymers: Chemistry & Physics of Modern Materials*; 2nd ed.; Blackie Academic & Professional: Glasgow, UK, 1991.

(44) Brostow, W. *Performance of plastics*; Hanser/Gardner Publications, Inc.: Cincinnati, 2000.

(45) Holden, G.; Kricheldorf, H. R.; Quirk, R. P. *Thermoplastic elastomers*; 3rd ed.; Hanser Gardner Publications, Inc.: Cincinnati, 2004.

(46) Kramers, H. A. Brownian motion in a field of force and the diffusion model of chemical reactions. *Physica (Utrecht)* **1940**, *7*284-304.

(47) Glasstone, S.; Laidler, K. J.; Eyring, H. *The Theory of Rate Processes*; McGraw-Hill: New York, 1941.

(48) Roetling, J. A. Yield stress behaviour of poly(ethyl methacrylate) in the glass transition region *Polymer* **1965**, *6*(11), 615-619.

(49) Rief, M.; Fernandez, J. M.; Gaub, H. E. Elastically Coupled Two-Level Systems as a Model for Biopolymer Extensibility *Physical Review Letters* **1998**, *81*(21), 4764-4767.

(50) Benichou, I.; Givli, S. The hidden ingenuity in titin structure *Appl. Phys. Lett.* **2011**, *98*091904.

2.5 Experimental

General Experimental Information: Unless otherwise noted, reactions were carried out with stirring with a magnetic stirbar at room temperature. Anhydrous solvents were purified through a column of alumina according to the method described by Pangborn *et al*. before use[151]. All commercial reagents were used as received unless otherwise noted. Flash column chromatography was performed by forced flow of indicated solvent systems over 32 – 63u silica gel from Dynamic Adsorbents (Norcross, GA). ^{1}H NMR and ^{13}C NMR spectra were recorded at 500 and 125 MHz, respectively, on Bruker GN-500 or CRYO-500 spectrometers. ^{1}H NMR and ^{13}C NMR chemical shifts are reported as δ values in ppm relative to TMS or residual solvent: $CDCl_3$ (7.26 ppm; 77.0 ppm), or CD_2Cl_2 (5.30 ppm; 54.0 ppm). ^{1}H NMR data are reported as follows: chemical shift in ppm, multiplicity (s = singlet, d = doublet, t = triplet, q = quartet), coupling constants in Hz, and relative integration in number of protons. Multiplets (m) are reported over the range of chemical shift at which they appear. For ^{13}C NMR spectra, only chemical shift values are reported. Mass Spectra were obtained on Micromass LCT (ES-MS, low resolution), Micromass Autospec (ES-MS and GC-MS, high resolution), and Perseptive Biosystems DE STR (MALDI-TOF) instruments. Gel Permeation Chromatography (GPC) traces were obtained on an Agilent 1100 SEC system using a PLGel Mixed-C column from Polymer Labs (Amherst, MA). THF was used as eluting solvent at a flow rate of 1.0 mL/min. Number averaged and weight averaged molecular weight distributions (M_n and M_w, respectively) of samples were measured with respect to polystyrene (PS) standards purchased from Aldrich (Milwaukee, WI). Single molecule force spectroscopy experiments were performed on an Asylum MFP-3D atomic force microscope (AFM) with an Olympus Biolever (nominal spring constants ~30 and ~6 pN/nm) and a gold-coated silicon wafer assembled in a closed fluid cell.

5-(Benzyloxy)pentanoic acid (2.1) A solution of freshly distilled δ-valerolactone (88.2 mL; 95.2 g, 0.951 mol), finely ground KOH (350 g, 4.76 mol), and benzyl chloride (391 mL; 430 g, 3.04 mol) in toluene (1.5 L) was prepared in a 3-neck round-bottom flask equipped with a mechanical stirrer in one neck, a reflux condenser in another, and sealed with a septum on the third. The solution was heated to reflux for 18 h, then cooled to room temperature, after which DI-water (1 L) was added, and the mixture stirred for an additional hour. The aqueous layer was collected, washed with Et_2O (1 × 1 L), and concentrated HCl (12.1 M) was added until the pH reached 4-5. The resulting mixture was extracted with Et_2O (3 × 0.5 L), after which the combined ethereal layers were washed with brine (1 L), then the solvent evaporated *in vacuo*. The light yellow oily residue was co-distilled with toluene (2 × 150 mL), then dried and purified by vacuum distillation (lit. b.p. ca. 130 °C at 7.5 mtorr). A small amount of white impurity has a tendency to clog the distilling apparatus, and may be brought over by heat gun with no water flow, and the desired distillate collected separately. Yield: 99.1 g (50%) clear oil.

^{1}H NMR (500 MHz, $CDCl_3$) δ 11.09 (br. s, 1H), 7.36–7.25 (m, 5H), 4.50 (s, 2H), 3.49 (t, J = 6.1, 2H), 2.39 (t, J = 7.3, 2H), 1.76–1.73 (m, 2H), 1.72–1.65 (m, 2H). ^{13}C NMR (125 MHz, $CDCl_3$) δ 179.1, 138.4, 128.4, 127.65, 127.57, 72.9, 69.7, 33.6, 29.0, 21.5. ES-MS m / z calcd for $C_{12}H_{16}O_3$ $(M+Na)^+$ 231.0997, found 231.1003.

Ethyl 7-(benzyloxy)-3-oxoheptanoate (2.2) To a solution of compound **2.1** (40.0 g, 192 mmol) in anhydrous toluene (200 mL) was added catalytic DMF (0.15 mL; 1.9 mmol), followed by dropwise addition of oxalyl chloride (23.6 mL; 34.9 g, 275 mmol) over 1.5 h via an addition funnel. The resulting solution was stirred for an additional 30 min, heated to 55 °C for 2 h, then concentrated *in vacuo* to afford 5-(benzyloxy)pentanoyl chloride, and the light yellow oil was used in the next step without any further purification. Yield: 43.0 g (99% crude).

In a separate flask, a solution of 2,2-dimethyl-1,3-dioxane-4,6-dione (Meldrum's acid, 23.3 g, 162 mmol) and anhydrous pyridine (30.0 mL; 30.5 g, 386 mmol) in anhydrous DCM (600 mL) was prepared and chilled to 0 °C. A 1:1 v/v solution of 5-(benzyloxy)pentanoyl chloride (43.0 g, 190 mmol) in anhydrous DCM was added dropwise using an addition funnel, and the reaction was allowed to come to room temperature overnight, then transferred to a separatory funnel and washed with 0.1 M HCl (600 mL). The aqueous layer was extracted with DCM (3 × 300 mL), and the organic layers were combined, dried over Na_2SO_4, filtered, and the solvent evaporated *in vacuo* to afford a dark red oil. Absolute ethanol (500 mL) was added to the residue, and mixture was heated to reflux for 16 h. The solvent was evaporated *in vacuo* and the residue purified by flash chromatography (0 to 18% EtOAc in hexanes; product fractions 14–18% EtOAc). Yield: 34.7 g (65% over two steps), light yellow oil.

^{1}H NMR (500 MHz, $CDCl_3$) δ 7.36–7.25 (m, 5H), 4.49 (s, 2H), 4.19 (q, J = 7.0, 2H), 3.47 (t, J = 6.0, 2H), 3.42 (s, 2H), 2.57 (t, J = 7.1, 2H), 1.74–1.66 (m, 2H), 1.66 – 1.60 (m, 2H), 1.27 (t, J = 7.1, 3H). ^{13}C NMR (125 MHz, $CDCl_3$) δ 202.7, 167.2, 138.5, 128.4, 127.65, 127.55, 72.9, 69.9, 61.4, 49.3, 42.7, 29.0, 20.3, 14.1. ES-MS *m / z* calcd for $C_{16}H_{22}O_4$ $(M+Na)^+$ 301.1416, found 301.1412.

Ethyl 2-(5-(benzyloxy)pentanoyl)tridec-12-enoate (2.3) To a solution of compound **2.2** (2.00 g, 7.19 mmol) in DMF (24 mL) was added K_2CO_3 (1.99 g, 14.37 mmol) and 11-bromoundec-1-ene (1.73 mL; 1.84 g, 7.90 mmol), and suspension was stirred for 16 h at room temperature. Following removal of solvent under reduced pressure, the residue was partitioned between Et_2O and DI-water (30 mL each). The aqueous layer was extracted with Et_2O (1 × 30 mL), after which the ethereal layers were combined and washed with brine (30 mL), dried with $MgSO_4$, filtered, and the solvent evaporated *in vacuo.* The residue thus obtained was purified by flash chromatography (0 to 8% EtOAc in hexanes; product fractions 6–8% EtOAc; dialkylated side-product also elutes at 6%; the desired product elutes slightly later) to obtain the desired compound as a yellow liquid. Yield: 1.22g (40%).

^{1}H NMR (500 MHz, $CDCl_3$) δ 7.36–7.25 (m, 5H), 5.81 (ddt, *J* = 16.8, 10.0, 6.8, 1H), 4.99 (d, *J* = 17.3, 1H), 4.93 (d, *J* = 9.9, 1H), 4.49 (s, 2H), 4.17 (q, *J* = 7.1, 2H), 3.47 (t, *J* = 6.1, 2H), 3.40 (t, *J* = 7.3, 1H), 2.58 (dt, *J* = 17.5, 7.1, 1H), 2.50 (dt, *J* = 17.6, 7.1, 1H), 2.03 (t, *J* = 6.9, 2H), 1.83–1.80 (m, 2H), 1.69 (quintet, *J* = 7.2, 2H), 1.61 (quintet, *J* = 6.7, 2H), 1.39–1.33 (m, 2H), 1.30–1.23 (m, 15H). ^{13}C NMR (125MHz, $CDCl_3$) δ 205.4, 170.0, 139.2, 138.5, 128.4, 127.6, 127.5, 114.1, 72.9, 70.0, 61.2, 59.2, 41.5, 33.8, 29.5, 29.43, 29.36, 29.3, 29.1, 29.0, 28.9, 28.2, 27.5, 20.3, 14.1. ES-MS *m* / *z* calcd for $C_{27}H_{42}O_4$ $(M+Na)^+$ 453.2981, found 453.2960.

2-Amino-6-(4-(benzyloxy)butyl)-5-(undec-10-enyl)pyrimidin-4(1H)-one (2.4) Compound **2.3** (1.21 g, 2.81 mmol) was dissolved in absolute ethanol (14 mL) in a round-bottom flask equipped with a reflux condenser, to which guanidine carbonate (0.515 g, 2.81 mmol) was added, and the solution was heated to reflux for 24 h. The solvent was removed *in vacuo*, and the resulting residue was dissolved in a small volume of DCM, loaded onto a silica gel column, followed by purification via flash chromatography (0 to 5% methanol in DCM; product fraction 4–5% methanol). Yield: 0.587 g (49%) white solid.

^{1}H NMR (500 MHz, $CDCl_3$) δ 7.35–7.25 (m, 5H), 6.71 (br. s, 1H), 5.80 (ddt, *J* = 17.0, 10.1, 6.8, 1H), 4.98 (d, *J* = 17.1, 1H), 4.91 (d, *J* = 10.1, 1H), 4.48 (s, 2H), 3.52–3.47 (m, 2H), 2.46 (t, *J* = 6.7, 2H), 2.31 (t, *J* = 7.3, 2H), 2.03 (q, *J* = 7.0, 2H), 1.71–1.65 (m, 4H), 1.42–1.32 (m, 2H), 1.30–1.20 (m, 14H). ^{13}C NMR (125 MHz, $CDCl_3$) δ 154.3, 139.2, 138.2, 128.5, 127.8, 127.7, 114.1, 73.1, 70.4, 33.8, 29.9, 29.7, 29.6, 29.5, 29.2, 29.1, 28.9, 25.7, 25.1. ES-MS *m* / *z* calcd for $C_{26}H_{39}N_3O_2$ $(M+Na)^+$ 448.2940, found 448.2921.

4-Iodo-2,6-diisopropylaniline (2.5) A solution of 2,6-diisopropyl aniline (12.7 g, 71.8 mmol) was prepared in a 2:1 mixture of DCM and methanol (360 mL / 180 mL) in a round-bottom flask. Benzyltrimethylammonium dichloroiodate (25 g, 71.8 mmol) and $CaCO_3$ (7.91 g, 79.0 mmol) were the added, and the suspension was stirred for 18 h. Upon completion, $CaCO_3$ was filtered, and the filtrate concentrated *in vacuo*. Aqueous $NaHSO_3$ solution (5% w/v; 300 mL) was added to the residue and extracted with Et_2O (3 × 300 mL). The combined ethereal layers were dried with Na_2SO_4, filtered, and evaporated *in vacuo*. The residue was purified by flash chromatography (0 to 5% EtOAc in hexanes; product fractions 4–5% EtOAc) to obtain pure 4-iodo-2,6-diisopropylaniline as an orange liquid. Yield: 18.07 g (85%).

^{1}H NMR (500 MHz, $CDCl_3$) δ 7.28 (s, 2H), 3.73 (br. s, 2H), 2.84 (septet, J = 6.8, 2H), 1.24 (d, J = 6.9, 12H). ^{13}C NMR (125 MHz, $CDCl_3$) δ 140.1, 135.0, 131.7, 81.1, 27.9, 22.2. ES-MS m / z calcd for $C_{12}H_{18}NI$ (M^+) 303.0484, found 303.0480.

2,6-Diisopropyl-4-(undec-10-enyloxy)aniline (2.6) In a round-bottom flask, compound **2.5** (1.00 g, 3.30 mmol) was dissolved in anhydrous toluene (10 mL) and 10-undecene-1-ol (2.64 mL; 2.24 g, 13.2 mmol), cesium carbonate (2.15 g, 6.60 mmol), anhydrous 1,10-phenanthroline (0.472 g, 2.64 mmol), and copper (I) iodide (0.252 g, 1.32 mmol) were added sequentially. The mixture was stirred (for large scale reactions, a mechanical stirrer was used) for 48 h while heating to reflux. The reaction mixture was cooled to room temperature, and filtered through a 1.5 × 3 cm pad of silica gel, eluting with EtOAc. The filtrate was concentrated *in vacuo* and purified by flash chromatography (0 to 70% DCM in hexanes; product fractions 30–70% DCM). The resulting oil was further purified by vacuum distillation (0.1 torr, 110-130 °C). Yield: 1.00 g (88%) of dark red oil.

[1]H NMR (500 MHz, CD_2Cl_2) δ 6.56 (s, 2H), 5.81 (ddt, *J*= 17.0, 10.2, 6.1, 1H), 4.97 (d, *J*= 17.1, 1H), 4.90 (d, *J*= 10.2, 1H), 3.85 (t, *J* = 6.6, 2H), 3.41 (br. s, 2H), 2.92 (septet, *J* = 6.8, 2H), 2.02 (q, *J* = 7.0, 2H), 1.70 (quintet, *J* = 7.0, 2H), 1.45–1.39 (m, 2H), 1.38–1.27 (m, 22H). [13]C NMR (125 MHz, $CDCl_3$) δ 152.4, 139.3, 134.3, 133.7, 114.1, 109.4, 68.4, 33.8, 29.6, 29.55, 29.46, 29.4, 29.1, 28.9, 28.2, 26.1, 22.5. GC-MS *m* / *z* calcd for $C_{23}H_{39}NO$ (M^+) 345.3032, found 345.3035.

1-(6-(4-(Benzyloxy)butyl)-4-oxo-5-(undec-10-enyl)-1,4-dihydropyrimidin-2-yl)-3-(2,6-diisopropyl-4-(undec-10-enyloxy)phenyl)urea (2.7) In a round-bottom flask, compound **2.6** (6.94 g, 20.1 mmol) was dissolved in anhydrous DCM (80 mL), and the solution was cooled to 0 °C in an ice bath. Phosgene (13.5 mL, 1.93 M in toluene; 2.58 g, 26.1 mmol) was added, followed by anhydrous pyridine (6.47 mL; 6.36 g, 80.4 mmol), and the reaction was stirred for 2 h at 0 °C. Dry nitrogen gas was then bubbled through the mixture for 10 min to remove unreacted phosgene, after which the reaction mixture was filtered. The solvent was then removed *in vacuo*, the filtrate re-suspended in benzene, filtered again, and the filtrate once again evaporated *in vacuo*. The resulting residue was dissolved in anhydrous pyridine (80 mL), then added to a round-bottom flask charged with compound **2.4** (5.70 g, 13.4 mmol), and allowed to react for 17 h. After removal of solvent *in vacuo*, the residue was purified by flash chromatography (0 to 10% EtOAc in hexanes; product fractions 8–10% EtOAc). Yield: 10.1 g (95%) viscous red-orange liquid.

[1]H NMR (500 MHz, $CDCl_3$) δ 13.02 (s, 1H), 12.52 (s, 1H), 11.72 (s, 1H), 7.32–7.24 (m, 5H), 6.73 (s, 2H), 5.82 (ddt, *J* = 17.1, 10.4, 6.6, 1H), 5.80 (ddt, *J* = 17.1, 10.5, 6.6, 1H), 5.00 (d, *J* = 17.1, 1H), 4.98 (d, *J* = 17.1, 1H), 4.94 (d, *J* = 9.2, 1H), 4.92 (d, *J* = 8.9, 1H), 4.46 (s, 2H), 3.96 (t, *J* = 6.5, 2H), 3.44 (t, *J* = 5.8, 2H), 3.16 (septet, *J* = 6.8, 2H), 2.49 (t, *J* = 7.1, 2H), 2.29 (t, *J* = 7.3, 2H), 2.08–1.99 (m, 4H), 1.81–1.77 (m, 2H), 1.70–1.61 (m, 4H), 1.49–1.43 (m, 2H), 1.40–1.15 (m, 36H). [13]C NMR (125 MHz, $CDCl_3$) δ 172.2, 158.7, 156.8, 153.5, 148.1, 146.3, 139.3, 138.3, 128.4,

127.59, 127.55, 124.1, 118.4, 114.11, 114.08, 109.3, 73.0, 69.6, 67.8, 33.8, 31.6, 30.2, 29.6, 29.54, 29.50, 29.47, 29.44, 29.42, 29.3, 29.14, 29.10, 28.94, 28.91, 26.1, 24.7, 24.2, 23.0, 22.7, 14.1. ES-MS *m* / *z* calcd for $C_{50}H_{76}N_4O_4$ $(M+Na)^+$ 819.5764, found 819.5743. MALDI-TOF *m* / *z* calcd for $C_{50}H_{76}N_4O_4$ $(M+H)^+$ 797.6, found 797.9.

Stack-blocked UPy-DCL diol (2.8) Compound **2.7** (2.00 g, 5.32 mmol) was dissolved in degassed, anhydrous DCM (140 mL) in a two-neck round-bottom flask equipped with a reflux condenser in one neck and sealed with a septum in the other. Upon heating the solution to reflux, Grubbs generation I catalyst (104.0 mg, 0.12 mmol) in degassed, anhydrous DCM (10 mL) was added over 30 s. After heating at reflux for 15 min, the reaction mixture was allowed to cool to room temperature, then directly loaded onto a silica gel column for purification by flash chromatography (0 to 4% EtOAc in chloroform; product fraction 4% EtOAc). The product fractions were pooled and evaporated *in vacuo* to produce light brown solid (1.1 g). This solid was then dissolved in degassed, anhydrous THF (30 mL). After degassing for an additional 5 min, $Pd(OH)_2$ on activated carbon (0.2 g, 0.53 mmol) was added under nitrogen, and the solution was degassed for an additional 10 min, then purged pressurized with H_2 to 300 psi. The mixture was stirred at room temperature for 18h,then filtered with suction over celite, the celite bed washed further with chloroform, and the filtrate evaporated under reduced pressure. The resulting solid was dissolved in a minimum volume of chloroform, and loaded onto a silica gel column. Flash chromatography (0 to 10% acetone in DCM), and the pure fractions combined and evaporated to afford the product as a white solid. Yield: 0.70 g (37% over two steps).

^{1}H NMR (500 MHz, $CDCl_3$) δ 13.01 (s, 2H), 12.51 (s, 2H), 11.74 (s, 2H), 6.75 (s, 4H), 4.00 (t, *J* = 6.1, 4H), 3.62 (t, *J* = 6.0, 4H), 3.16 (septet, *J* = 6.7, 4H), 2.52 (t, *J* = 7.4, 4H), 2.32–2.26 (m, 4H), 1.82–1.78 (m, 4H), 1.68–1.63 (m, 4H), 1.59–1.48 (m, 6H), 1.40–1.15 (m, 92H). ^{13}C NMR (125

MHz, $CDCl_3$) δ 172.2, 158.7, 156.8, 153.4, 148.2, 146.2, 124.1, 118.6, 109.2, 67.4, 62.1, 31.9, 30.3, 30.0, 29.7, 29.63, 29.60, 29.4, 29.3, 29.2, 29.10, 29.05, 29.0, 28.94, 28.90, 28.8, 28.6, 28.5, 25.7, 25.5, 24.24, 24.17, 23.0. MALDI-TOF *m* / *z* calcd for $C_{82}H_{136}N_8O_8$ $(M+H)^+$ 1362.1, found 1362.5.

Stack-blocked UPy-DCL ADMET monomer (2.9) To a vial charged with compound **2.8** (328 mg, 0.241 mmol) dissolved in anhydrous toluene (6 mL), 10-undecenoyl chloride (155 μL; 146 mg, 0.722 mmol) was added, followed by anhydrous pyridine (85 μL; 83.8 mg, 1.06 mmol). After stirring for 20 h at room temperature, the mixture was filtered, and the filtrate evaporated *in vacuo*. The residue was purified via flash chromatography (0 to 2% EtOAc in chloroform; product fractions 1–2% EtOAc). Yield: 320 mg (78%) off-white solid.

^1H NMR (500 MHz, $CDCl_3$) δ 13.07 (s, 2H), 12.53 (s, 2H), 11.72 (s, 2H), 6.75 (s, 4H), 5.80 (ddt, *J* = 16.9, 10.2, 7.3, 2H), 4.98 (d, *J* = 17.1, 2H), 4.92 (d, *J* = 10.1, 2H), 4.06–4.03 (m, 4H), 4.00 (t, *J* = 6.1, 4H), 3.16 (septet, *J* = 6.6, 4H), 2.51–2.47 (m, 4H), 2.32–2.24 (m, 8H), 2.03 (q, *J* = 7.0, 4H), 1.80 (quintet, *J* = 6.5, 4H), 1.67–1.63 (m, 8H), 1.61–1.43 (m, 8H), 1.39–1.17 (m, 108H). ^{13}C NMR (125 MHz, $CDCl_3$) δ 173.8, 172.2, 158.7, 156.9, 153.5, 148.1, 148.0, 145.8, 139.2, 124.1, 118.6, 114.1, 109.3, 109.2, 76.8, 67.4, 63.4, 34.2, 33.8, 31.9, 30.3, 30.0, 29.7, 29.63, 29.58, 29.44, 29.35, 29.33, 29.29, 29.2, 29.12, 29.06, 28.99, 28.95, 28.89, 28.8, 28.6, 28.5, 28.2, 28.1, 25.7, 25.5, 24.9, 24.5, 24.25, 24.22, 23.0, 22.7, 14.1. ES-MS *m* / *z* calcd for $C_{104}H_{172}N_8O_{10}$ $(M+Na)^+$ 1716.3, found 1717.9.

1-(*S*-trityl)mercaptoundec-10-ene (2.10) Triphenylmethanethiol (1.00 g, 3.60 mmol) was suspended in a mixture of 3N aqueous NaOH (1.20 mL, 3.60 mmol) and ethanol (8 mL), and stirred for 10 min. 11-bromoundec-1-ene (800 μL; 844 mg, 3.60 mmol) was added, and mixture stirred for 21 h at room temperature. The reaction was quenched by addition of saturated aqueous NH_4Cl (5 mL), then diluted with DCM (5 mL). The organic layer was separated, and the aqueous layer was extracted with DCM (3 × 5 mL). The organic layers were combined and dried over $MgSO_4$, filtered, and concentrated *in vacuo*. The resulting residue was purified by flash chromatography (0 to 2% EtOAc in hexanes; product fractions 1–2% EtOAc) to isolate the pure product as a white, waxy solid. Yield: 1.22 g (78%).

^{1}H NMR (500 MHz, $CDCl_3$) δ 7.42–7.40 (m, 6H), 7.29–7.27 (m, 6H), 7.22–7.18 (m, 3H), 5.81 (ddt, *J* = 17.0, 10.2, 6.7, 1H), 4.98 (dd, *J* = 17.0, 2.0, 1H), 4.92 (dd, *J* = 10.0, 1.0, 1H), 2.13 (t, *J* = 7.3, 2H), 2.03 (q, *J* = 7.0 Hz), 1.37 (septet, *J* = 7.8, 4H), 1.28–1.10 (m, 10H). ^{13}C NMR (125 MHz, $CDCl_3$) δ 145.1, 139.2, 129.6, 127.8, 126.5, 114.1, 66.3, 33.8, 32.0, 29.4, 29.3, 29.15, 29.08, 29.0, 28.9, 28.6. ES-MS *m* / *z* calcd for $C_{30}H_{36}S$ $(M+Na)^+$ 451.2435, found 451.2425.

Bis-1-(*S*-trityl)mercaptoundec-10-ene-end-capped SB-UPy-DCL ADMET oligomer (n = 8) (2.11) In a round bottom flask, monomer **2.9** (137 mg, 0.081 mmol) and chain transfer agent **2.10** (8.6 mg, 0.02 mmol) were dissolved in chloroform (1.5 mL), to which Grubbs generation 2 catalyst (3.40 mg, 0.004 mmol) was added. The mixture was heated to reflux for 1 h, allowed to come to room temperature, and precipitated out of ethanol (~50 mL). After stirring in ethanol for 1 h, the solvent was decanted, and the precipitant re-dissolved in a minimum volume of chloroform, after which the solvent was removed *in vacuo*. GPC M_n : 15.0 kDa; PDI: 2.6.

Bis-undec-10-ene-1-thiol-end-capped SB-UPy-DCL ADMET oligomer (n = 8) (2.12) In a scintillation vial, oligomer **2.11** (150 mg) was dissolved in 10% TFA in DCM (220 µL TFA in 2 mL DCM), and stirred for 10 min., followed by addition of triisopropylsilane until the solution was no longer yellow (~100 µL), and stirred for an additional 10 min. The reaction was quenched by addition of saturated aqueous $NaHCO_3$ solution (2 mL), after which the organic phase was extracted. The aqueous layer was extracted with DCM (3 × 1 mL), and the combined organic phase was dried over $MgSO_4$, filtered, and concentrated *in vacuo*. The residue was precipitated out of ethanol (~50 mL), and stirred for 1 h. The solvent was decanted, and the precipitant was re-dissolved in a minimum volume of chloroform. The solvent was then removed *in vacuo* to afford oligomer **2.12** as a light brown film. GPC M_n: 30.2 kDa; PDI: 1.6.

SB-UPy-DCL ADMET polymer (2.13). In a round bottom flask, monomer **1** (250 mg, 0.147 mmol) was dissolved in 1,2,4-trichlorobenzene (2 mL) and heated to 70 °C under argon, and Grubbs generation 2 catalyst (16 mg, 0.018 mmol) was added. Vacuum (30 torr) was immediately applied, and fine bubbling due to ethylene evolution was observed. After 10 min, high vacuum (0.1 torr) was applied. After fine bubbling ceased and only large bubbles were observed, the mixture was transferred to a PTFE dish in an argon-purged vacuum oven. Vacuum (30 torr) was applied, and solvent slowly evaporated for 36 h at 80 °C. The resulting film was removed and subjected to bulk mechanical testing. GPC M_n : 33.0 kDa; PDI: 2.1.

Molecular modeling of SB-UPy-DCL monomer

Maestro MacroModel was used in order to generate a reasonable minimum energy conformation of dimerized and ruptured end-to-end distances of SB-UPy-DCL monomer. For both dimerized and ruptured forms, the minimum energy conformation was generated in AMBER* force field[152] with $CHCl_3$ solvation.

The UPy-dimerization H-bond distance and angle values (N – H ⋯ N distance and angle: 2.989 Å and 175°, respectively; N – H ⋯ O distance and angle: 2.720 Å and 165°, respectively) were taken from the X-ray crystal structure of SB-UPy-DCL compound,[30] and these values were used for energy minimization constraints with an extremely large force constant (5000 kJ/(mol Å^2)) to lock the values in place. Then the ends of the monomer were 'pulled' by placing an additional constraint of 150 Å end-to-end distance with a force constant of 5 kJ/(mol Å^2) [46]. The minimized energy conformation showed an end-to-end distance of 57.4 Å in the dimerized state.

For the ruptured SB-UPy-DCL monomer, a constraint of 150 Å end-to-end distance with a force constant of 5 kJ/(mol Å^2) was placed with no additional constraints. This yielded an end-to-end distance of 86.9 Å in the ruptured SB-UPy-DCL monomer.

Therefore the modeled difference in distance between the dimerized and extended forms of SB-UPy-DCL is 2.85 nm.

We also note that the difference in distance between unfolded and folded of 2.85 nm agrees with simple estimate based on bond angle and distance. The 20 carbon-carbon single bonds in the DCL architecture corresponds to 1.54 Å × 20 × sin(109.5°) = 2.5 nm. When we add also the length of the stack-blocking aryl group due to free bond rotation in the direction of pulling, this adds an additional 3-5 angstroms to make 2.8-3.0 nm.

Pulling SMFS experimental procedure. A 0.1 mg/ml sample of oligomer **2.12** in toluene was prepared and injected into in a closed fluid cell assembled with a Biolever (Olympus) and a gold-coated silicon wafer as the sample surface. SMFS studies were performed on an Asylum MFP-3D AFM with Igor Pro 6.22A software. The spring constant of each cantilever was found by the thermal tuning method[153]. Over 2000 force curves each were obtained at 10, 25, 60, 125, 250, 500, 1000 and 2000 nm/s pulling speed with Biolever nominal spring constant 30 pN/nm, and at 10, 25, 60, 125 nm/s pulling speed with Biolever nominal spring constant 6 pN/nm. The following parameters were used for the experiment: dwell towards surface, 5.0 s; surface trigger point, 500 pN.

Cyclic SMFS experiments and data analysis. A 0.1 mg/ml solution of oligomer **2.12** in toluene was injected into a closed fluid cell assembled with a Biolever (Olympus) and a gold-coated silicon wafer as sample surface. All cyclic SMFS studies were performed with Biolever nominal spring constant 6 pN/nm, whose accurate spring constants were measured by the thermal tuning method[153]. Cyclic SMFS studies were designed using the ForceRampSimple panel on Igor Pro 6.22A software on an Asylum MFP-3D AFM. The surface trigger was set to 500 pN, and the pull-off distance usually varied somewhere between 100–200 nm and was determined experimentally. Extension and retraction velocities were always set to be equal, and were varied between 125, 200, 250, 400, and 500 nm/s. Pause after retraction was set to 0.5 seconds for all loading rates before the next cycle. Maximum extension before retraction was aimed to be around 60 – 70 nm away from the surface, corresponding to a slightly shorter distance than the fully extended and ruptured distance of an 8-mer according to the MacroModel results. For data analysis, only rejoining forces were examined on the retraction path as described in the text.

Error correction in loading rate in cyclic SMFS experiments. In order to correct for the systematic errors introduced in calculating $\Delta x_f^{\ddagger}$ from simplifying the loading rate to $\mu = k_c \times v$, we employed methods reported by Ray *et al*.[154] to estimate the error in determining $\Delta x^{\ddagger}$ (equation 27 in ref. 6). For F^* (most probable force) the values for Gaussian center force from Table S2 were used, and for k_c the values determined from the thermal tuning method (4.03 pN/nm) was used. $F^{\ddagger}$ and F_p were calculated as described in ref. 6 using the uncorrected $\Delta x_f^{\ddagger}$ (1.05 nm) and l_p (0.38 nm), respectively. L_c was set to be 60 nm on average based on our maximum extension parameter on ForceRampSimple. Errors using equation 27 in ref. 6 were calculated separately for each Gaussian center force, and averaged together to obtain 18.5 % average error for $\Delta x_f^{\ddagger}$. When this error percentage is employed, $\Delta x_f^{\ddagger} = 1.22 \pm 0.65$ nm.

Derivation of equilibrium rupture force. As described in the main text, Diezemann and Janshoff's method of extracting K_{eq} requires the extrapolation of the equilibrium rupture force to a cantilever spring constant of $k_c = 0$.[142] As predicted by the authors, a higher cantilever spring constant manifests as a higher apparent equilibrium rupture force. From the data obtained in the rupture mode, the three lowest loading rate data points obtained with the 30 pN/nm cantilever were treated as being in the quasi-equilibrium regime and was averaged to obtain 83.9 ± 0.26 pN equilibrium rupture force with the 30 pN/nm cantilever. The lowest two loading rate data points obtained with the 6 pN/nm cantilever were treated as if in the quasi-equilibrium regime for an average equilibrium rupture force of 71.0 ± 0.30 pN with the 6 pN/nm cantilever. A linear extrapolation (of F_{eq} versus k_c) to $k_c = 0$ provided the equilibrium rupture force of 67.8 ± 0.40 pN.

Tensile testing of bulk polymer 2.13. The bulk static tensile properties of the SB-UPy-DCL polymer were measured using an Instron 3365 with a 500 N load cell with a pulling rate of 100 mm/min. Sample dimensions were measured (l,w,t: 12.0 x 3.4 x 0.20 mm) and the sample was pulled at ambient temperature until break.

Multi-cyclic and dimensional recovery tensile testing. Temperature was controlled during the experiment with an Instron SFL 3119-506 ‘Heatwave’ chamber. The dimensions of the sample used were 13.0 x 3.4 x 0.15 mm (l,w,t). The sample was loaded onto the Instron and equilibrated for 1 h at 60 ^{o}C, following which a multi-cyclic tensile test was performed for ten cycles at 100 mm/min, 80% maximum strain each cycle. The sample was then allowed to recover at 60 ^{o}C for 5 min, 1 h, and 12 h before an additional cycle was performed. For the final recovery, the sample was heated to 80 ^{o}C for 5 min, following which the sample was re-equilibrated at 60 ^{o}C for 30 minutes before the last cycle was performed.

Dynamic Mechanical Analysis. Multi-frequency temperature sweep tests were performed using a TA Instruments DMA Q800 with attached cryo accessory. Sample dimensions were measured (l,w,t: 10.5 x 1.85 x 0.2 mm) and loaded into furnace, after which the sample was equilibrated at the lower boundary temperature for 1 h. The temperature was then incremented by 1 ^{o}C and kept isothermal for 3 min with frequency sweep, until the upper bound temperature was reached. On initial run, temperature was swept from -80 to 100 ^{o}C with 3 ^{o}C increments in order to identify the two transitions. Following this, for analysis of the alpha transition the temperature was swept between 70 to 110 ^{o}C with 1 ^{o}C increment at 0.1, 0.3, 1, 3, and 10 Hz (Figure 4b). For analysis of beta transition, the temperature was swept between -75 to 25 ^{o}C with 1 ^{o}C increment at 1, 2, 5, 10, and 20 Hz.

2.6 References for Experimental

(1) Pangborn, A. B.; Giardello, M. A.; Grubbs, R. H.; Rosen, R. K.; Timmers, F. J. Safe and Convenient Procedure for Solvent Purification *Organometallics* **1996**, *15*(5), 1518-1520.

(2) Weiner, S. J.; Kollman, P. A.; Case, D. A.; Singh, U. C.; Ghio, C.; Alagona, G.; Profeta, S.; Weiner, P. A new force field for molecular mechanical simulation of nucleic acids and proteins *Journal of the American Chemical Society* **1984**, *106*(3), 765-784.

(3) Chung, J.; Kushner, A. M.; Weisman, A. C.; Guan, Z. Direct correlation of single-molecule properties with bulk mechanical performance for the biomimetic design of polymers *Nature Materials* **2014**, *13*(11), 1055-1062.

(4) Roland, J. T.; Guan, Z. Synthesis and Single-Molecule Studies of a Well-Defined Biomimetic Modular Multidomain Polymer Using a Peptidomimetic β-Sheet Module *Journal of the American Chemical Society* **2004**, *126*(44), 14328-14329.

(5) Hutter, J. L.; Bechhoefer, J. Calibration of atomic-force microscope tips *Review of Scientific Instruments* **1993**, *64*(7), 1868-1873.

(6) Ray, C.; Brown, J. R.; Akhremitchev, B. B. Correction of Systematic Errors in Single-Molecule Force Spectroscopy with Polymeric Tethers by Atomic Force Microscopy *The Journal of Physical Chemistry B* **2007**, *111*(8), 1963-1974.

(7) Diezemann, G.; Janshoff, A. Dynamic force spectroscopy: Analysis of reversible bond-breaking dynamics *Journal of Chemical Physics* **2008**, *129*(8), 084904.

2.7 Chapter 2 Spectra

5-(Benzyloxy)pentanoic acid (2.1)

^{1}H NMR (500 MHz, $CDCl_3$):

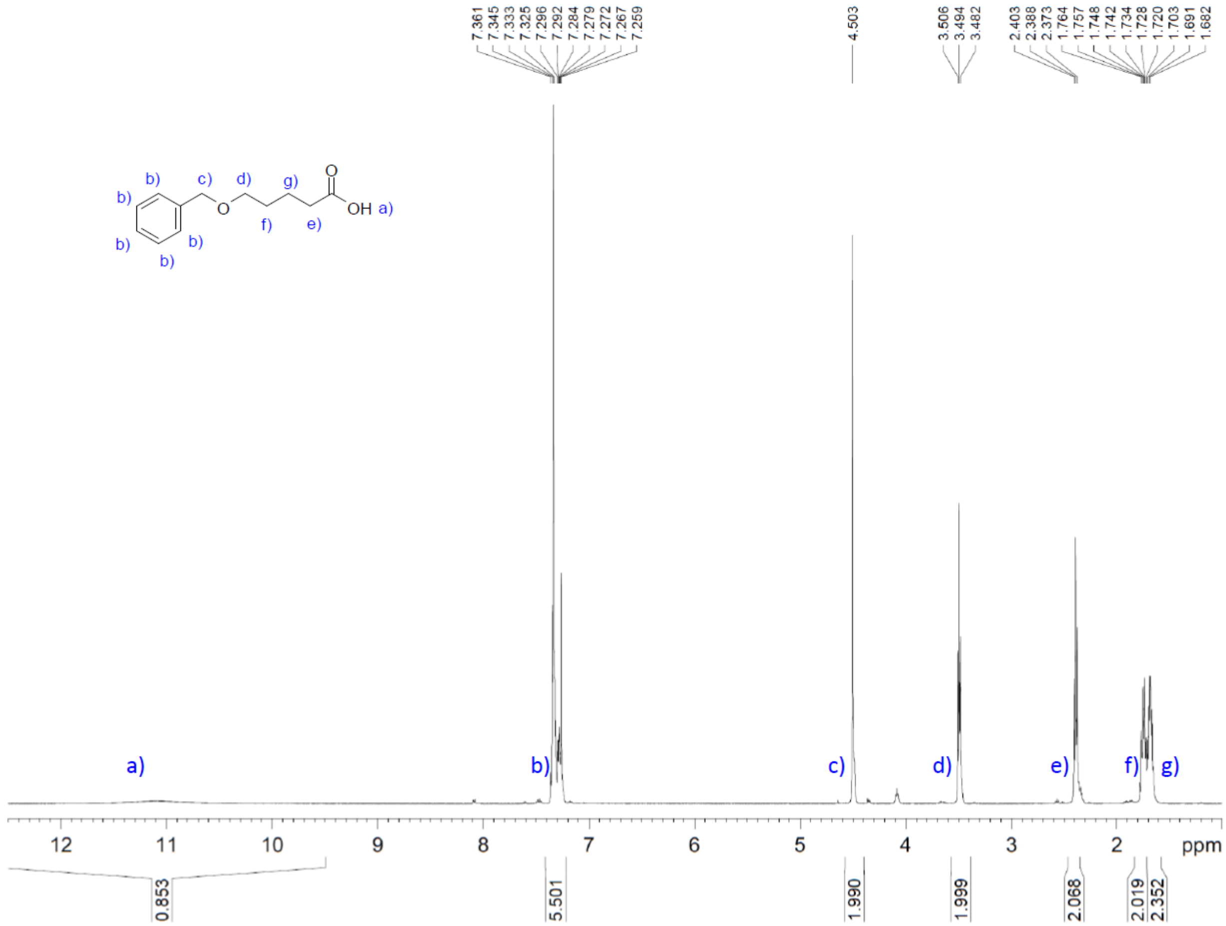

^{13}C NMR (125 MHz, $CDCl_3$):

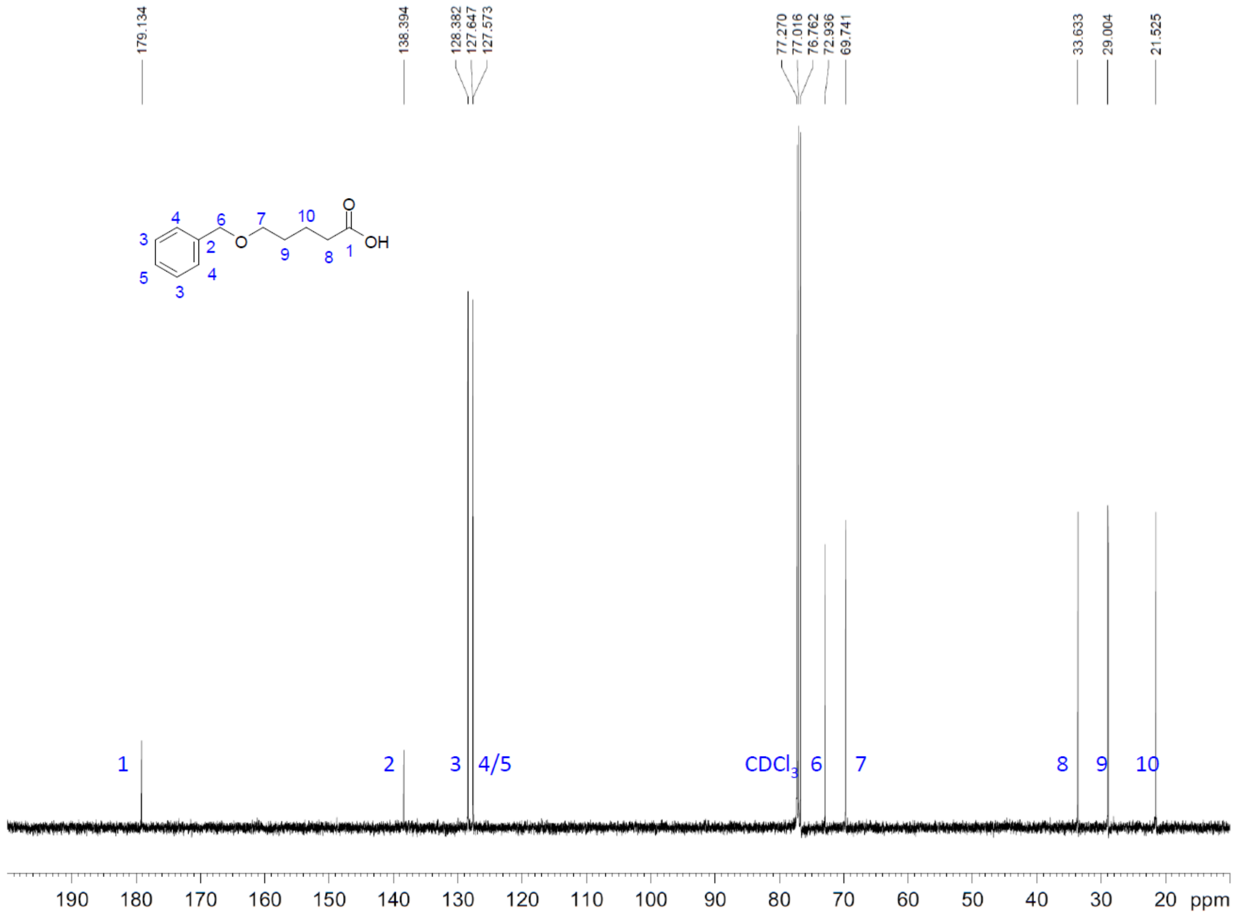

ES-MS (High Resolution):

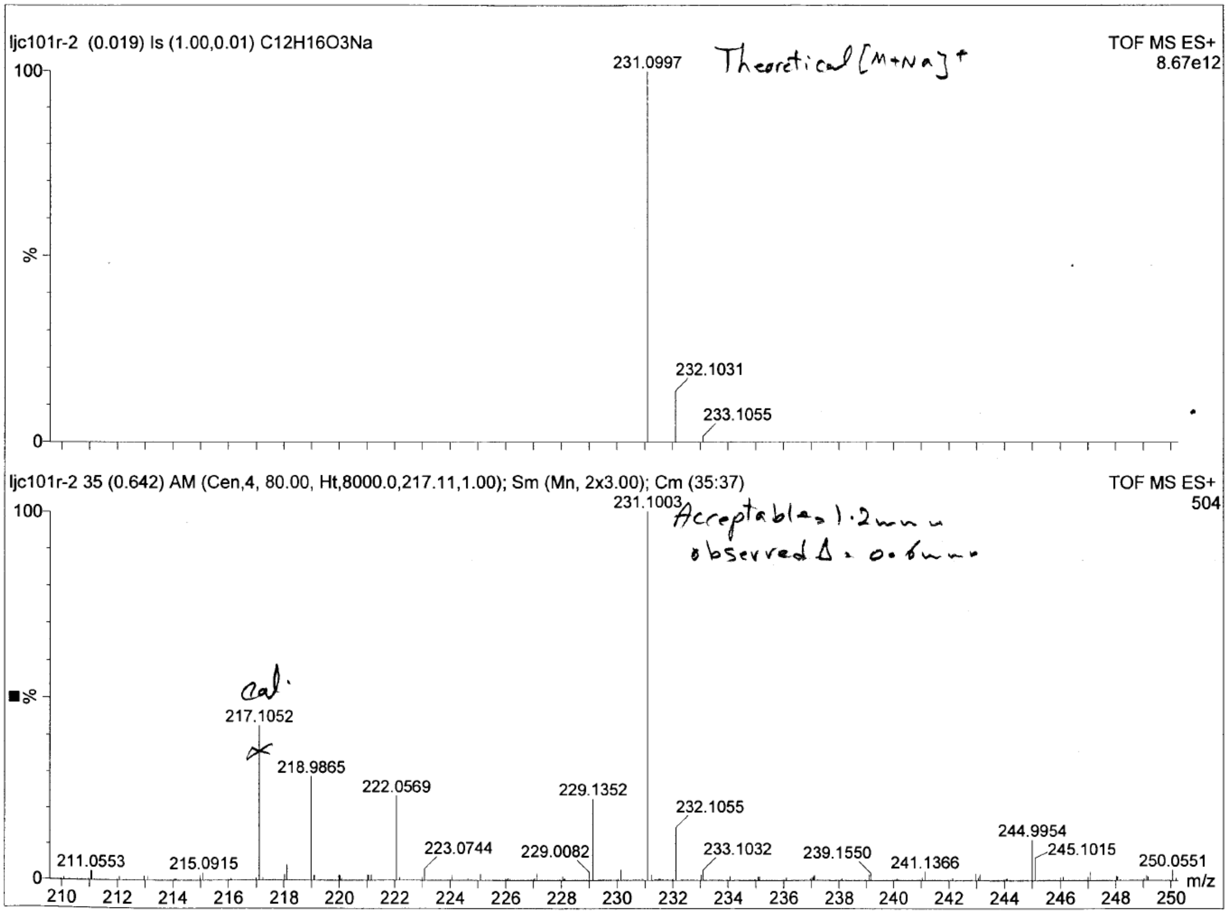

Ethyl 7-(benzyloxy)-3-oxoheptanoate (2.2)

^{1}H NMR (500 MHz, $CDCl_3$):

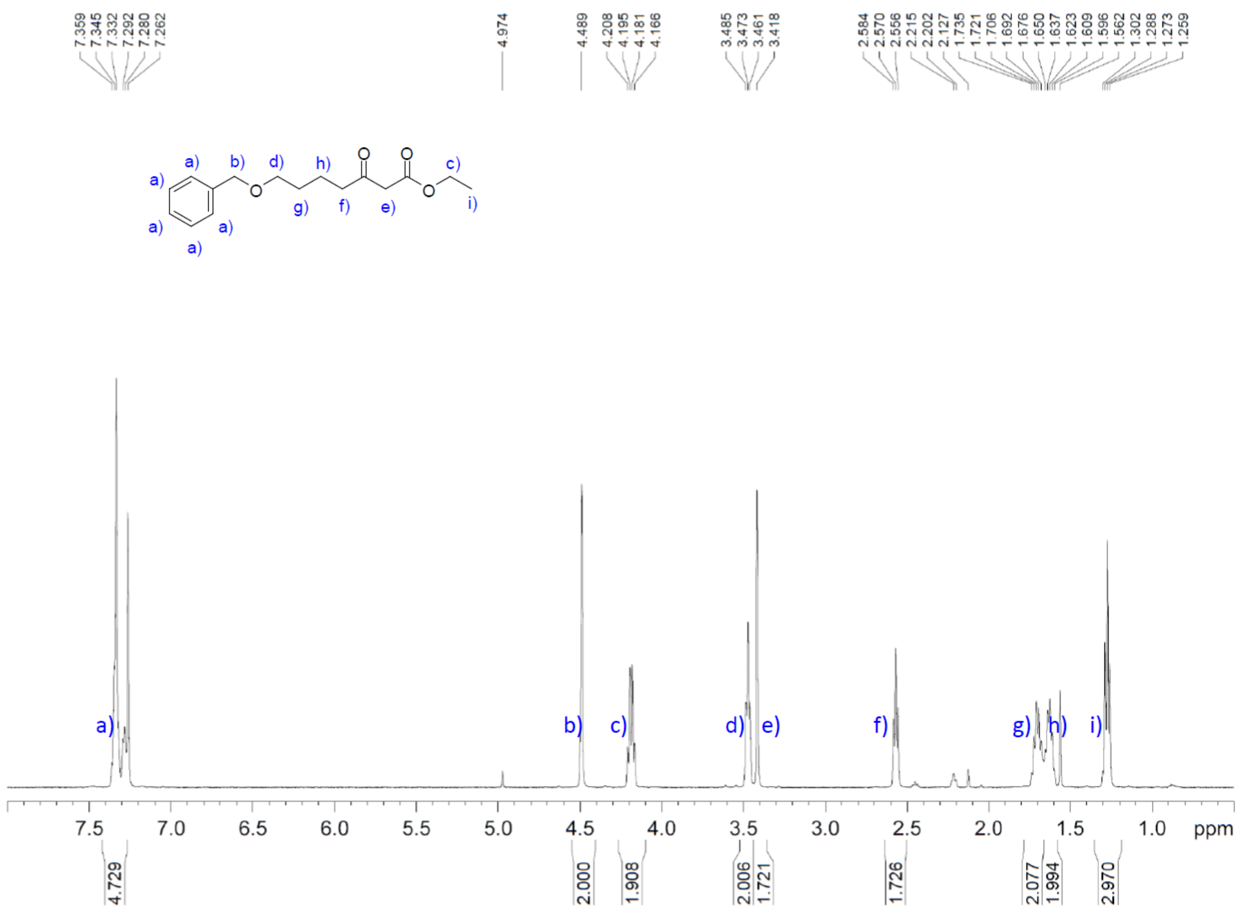

[13]C NMR (125 MHz, $CDCl_3$):

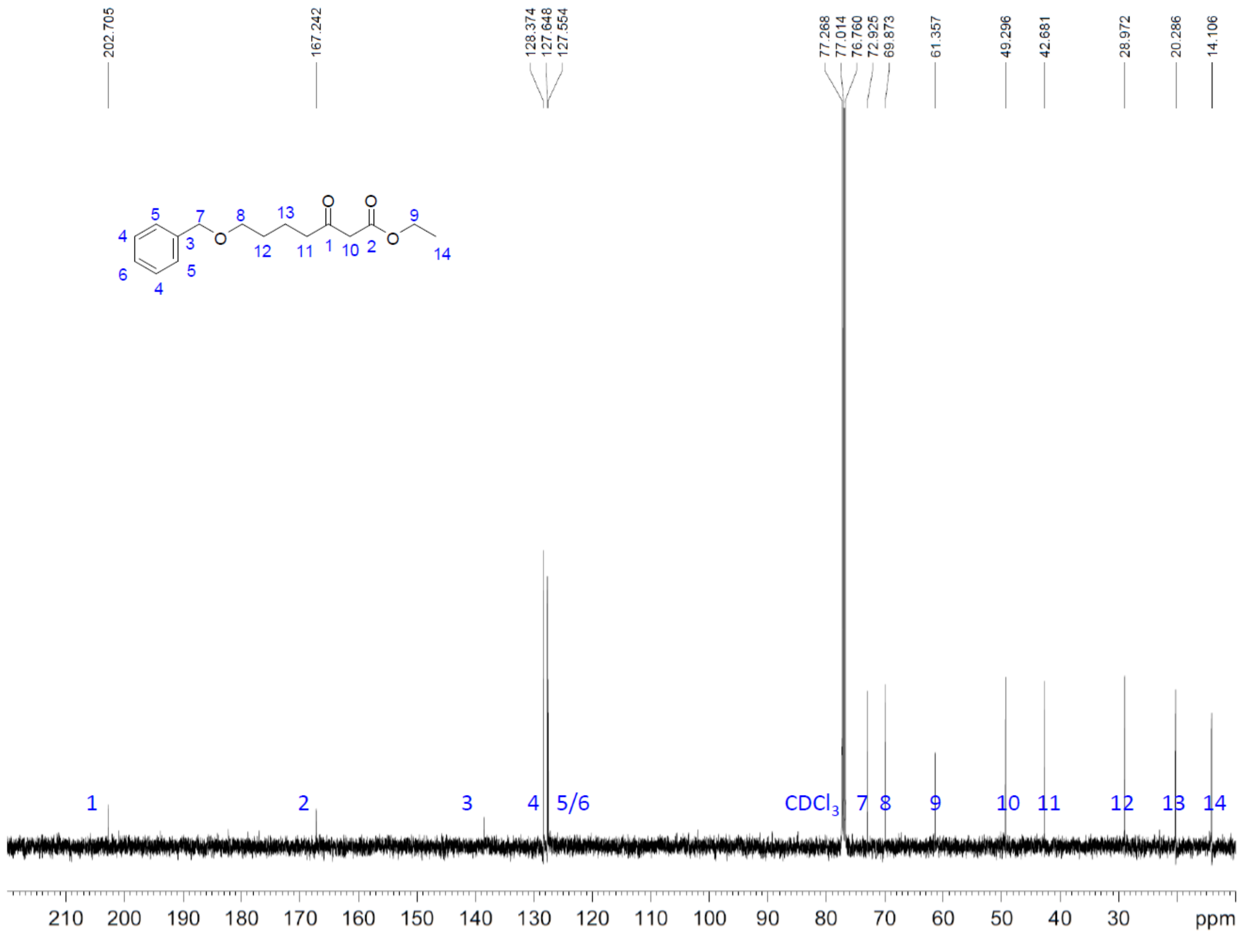

ES-MS (High Resolution):

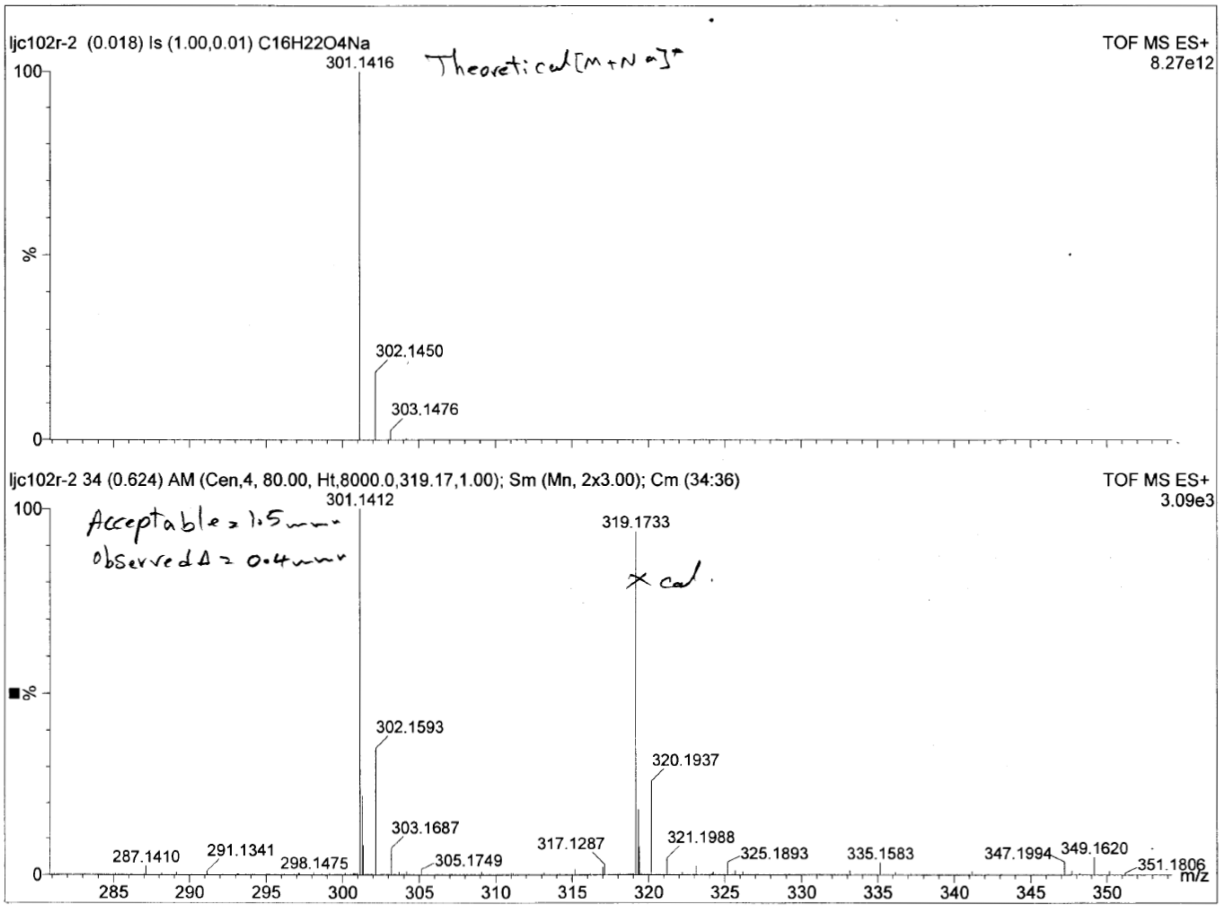

Ethyl 2-(5-(benzyloxy)pentanoyl)tridec-12-enoate (2.3)

^{1}H NMR (500 MHz, $CDCl_3$):

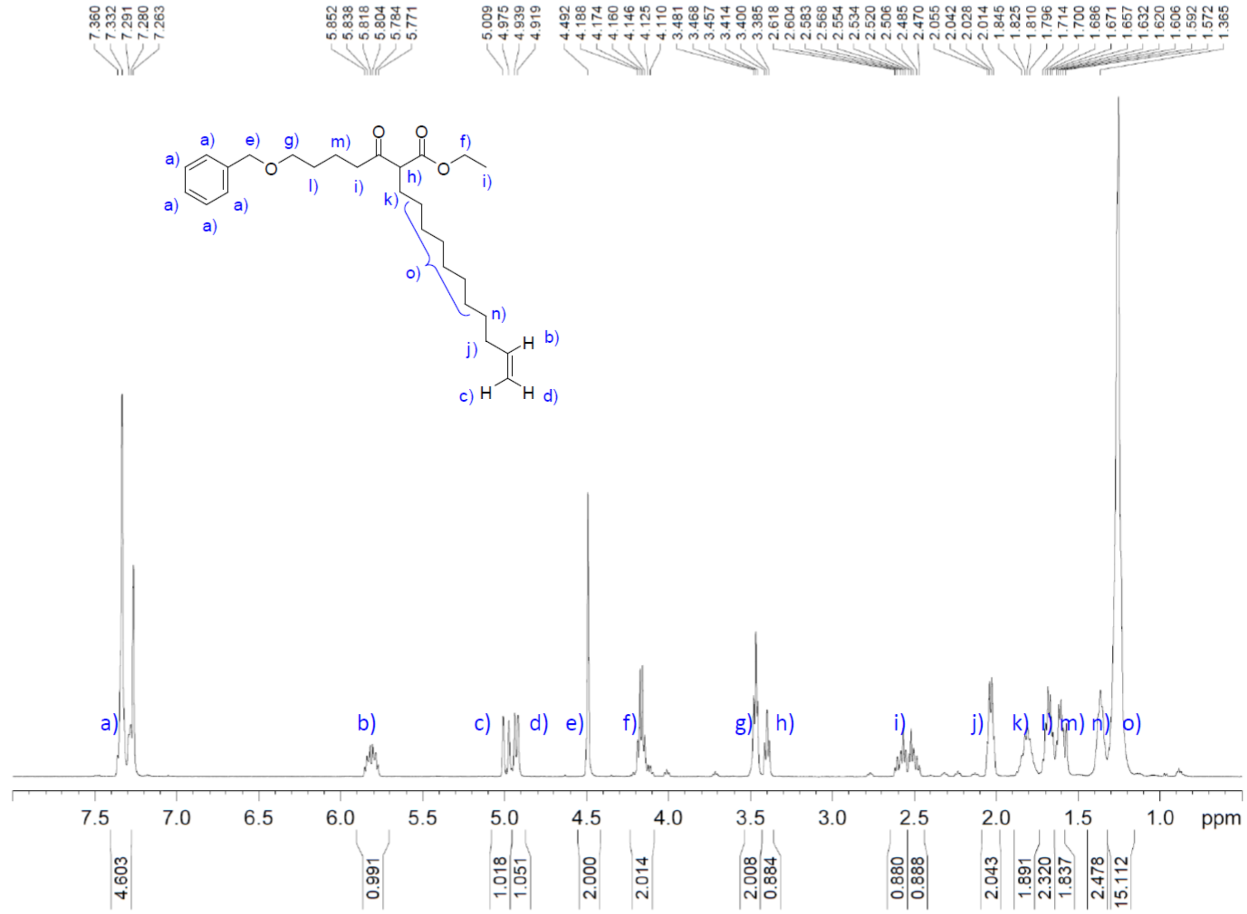

^{13}C NMR (500 MHz, $CDCl_3$):

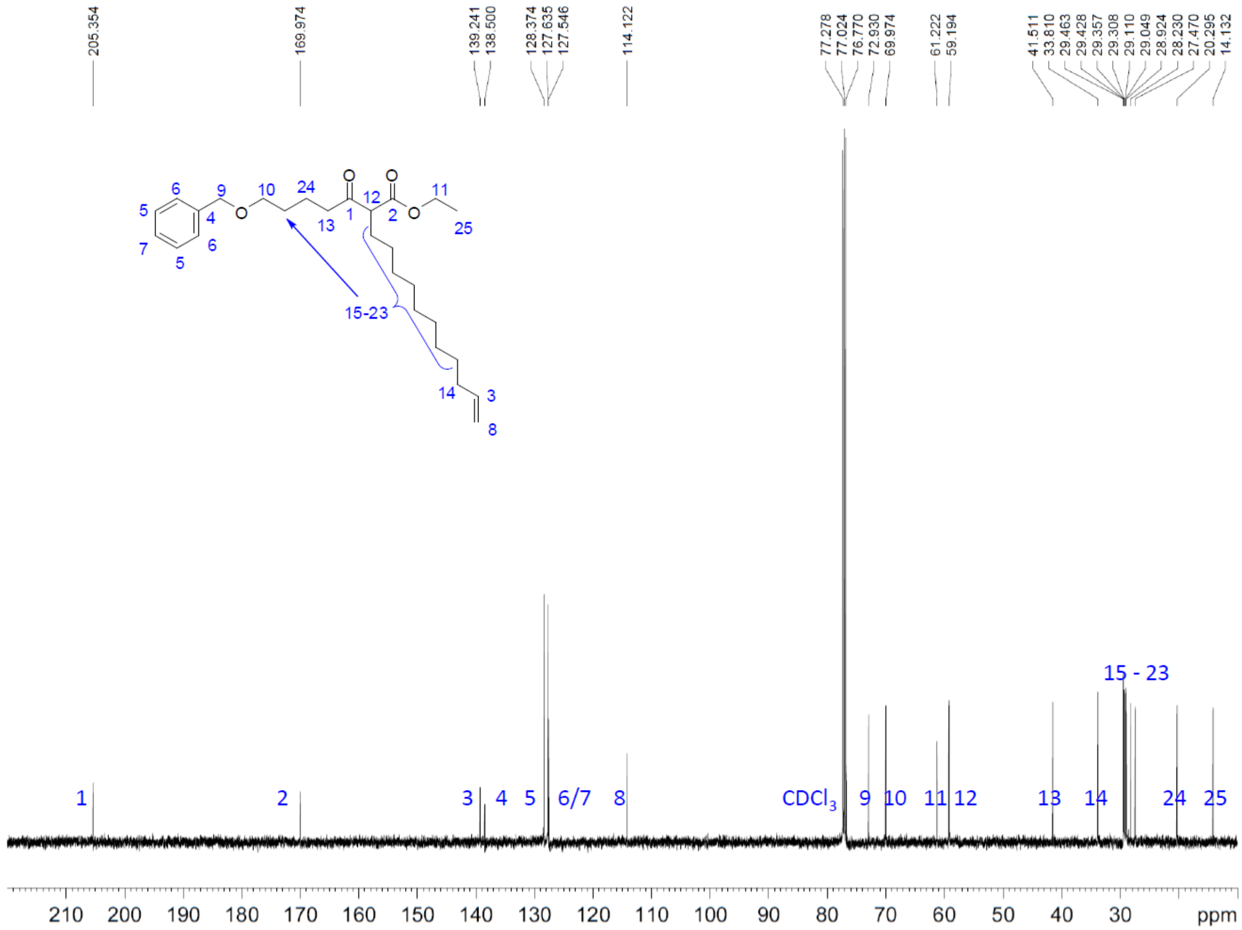

ES-MS (High Resolution):

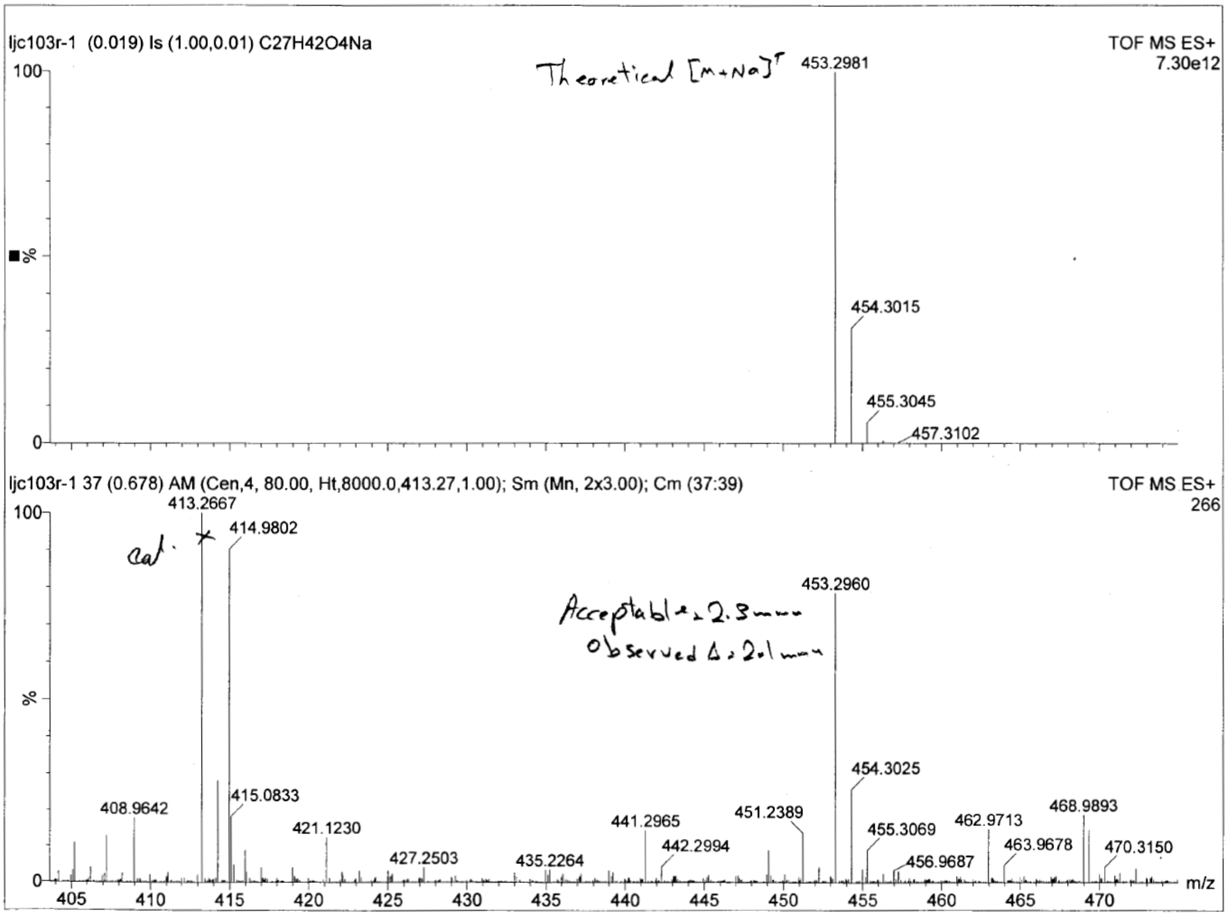

2-Amino-6-(4-(benzyloxy)butyl)-5-(undec-10-enyl)pyrimidin-4(1H)-one (2.4)

^{1}H NMR (500 MHz, $CDCl_3$):

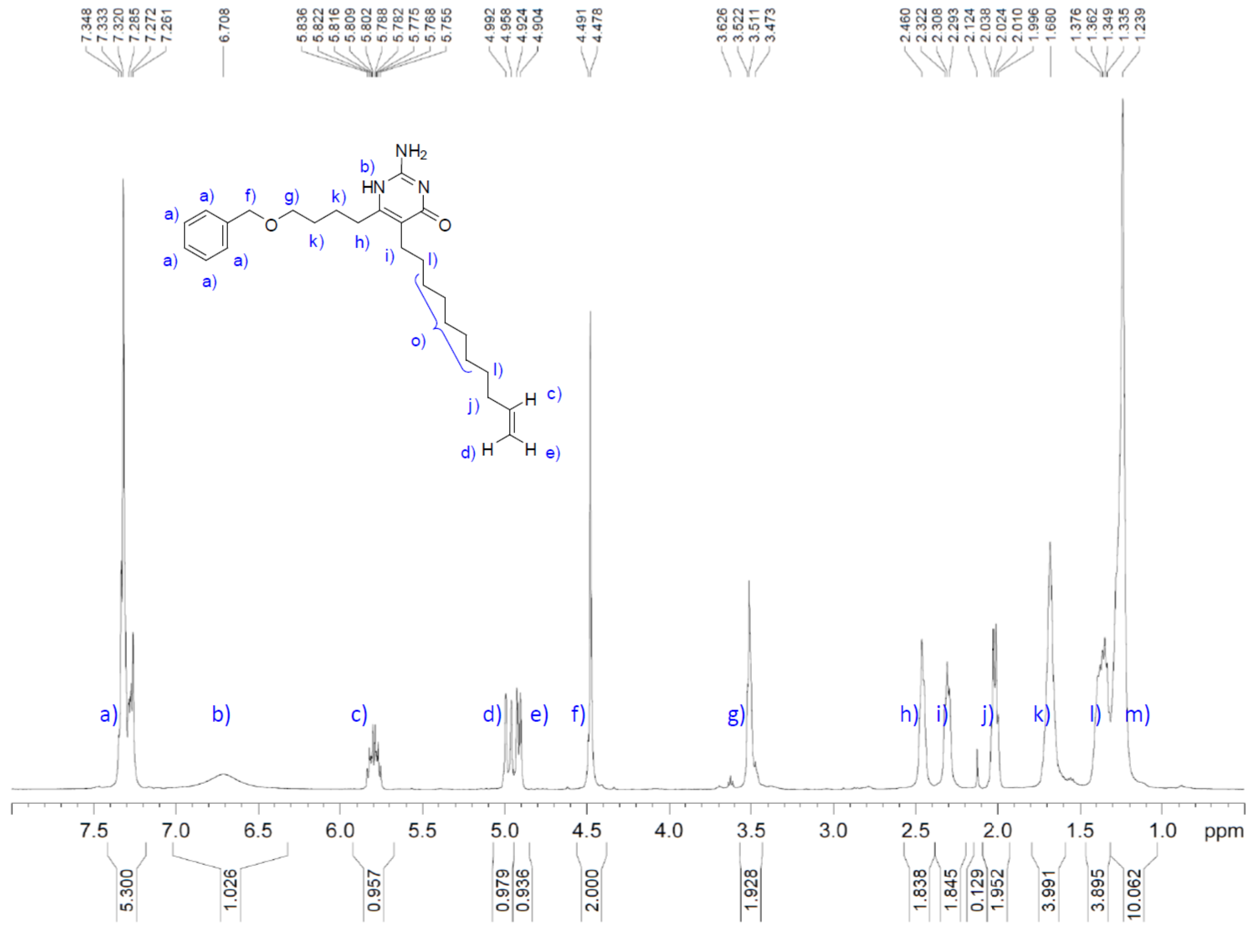

^{13}C NMR (125 MHz, $CDCl_3$):

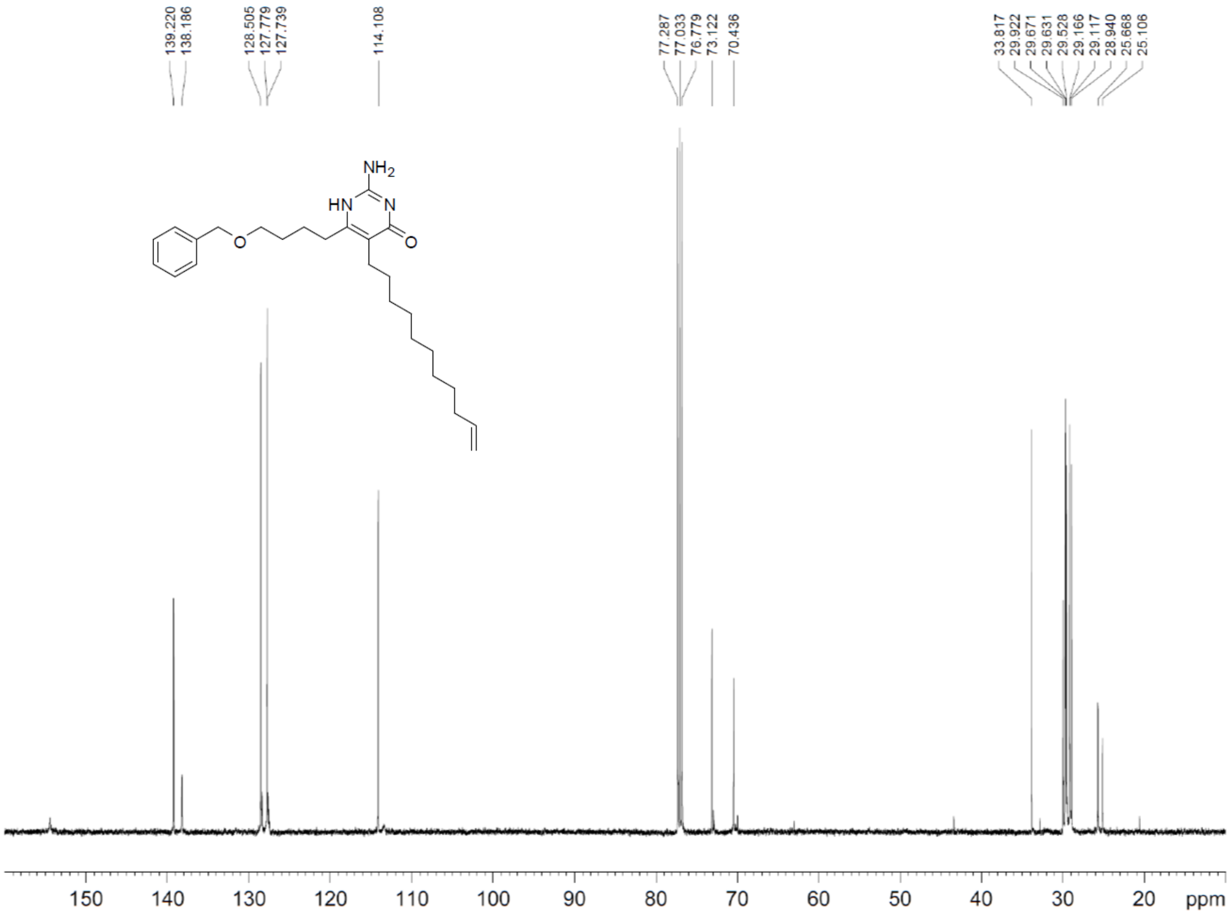

ES-MS (High Resolution):

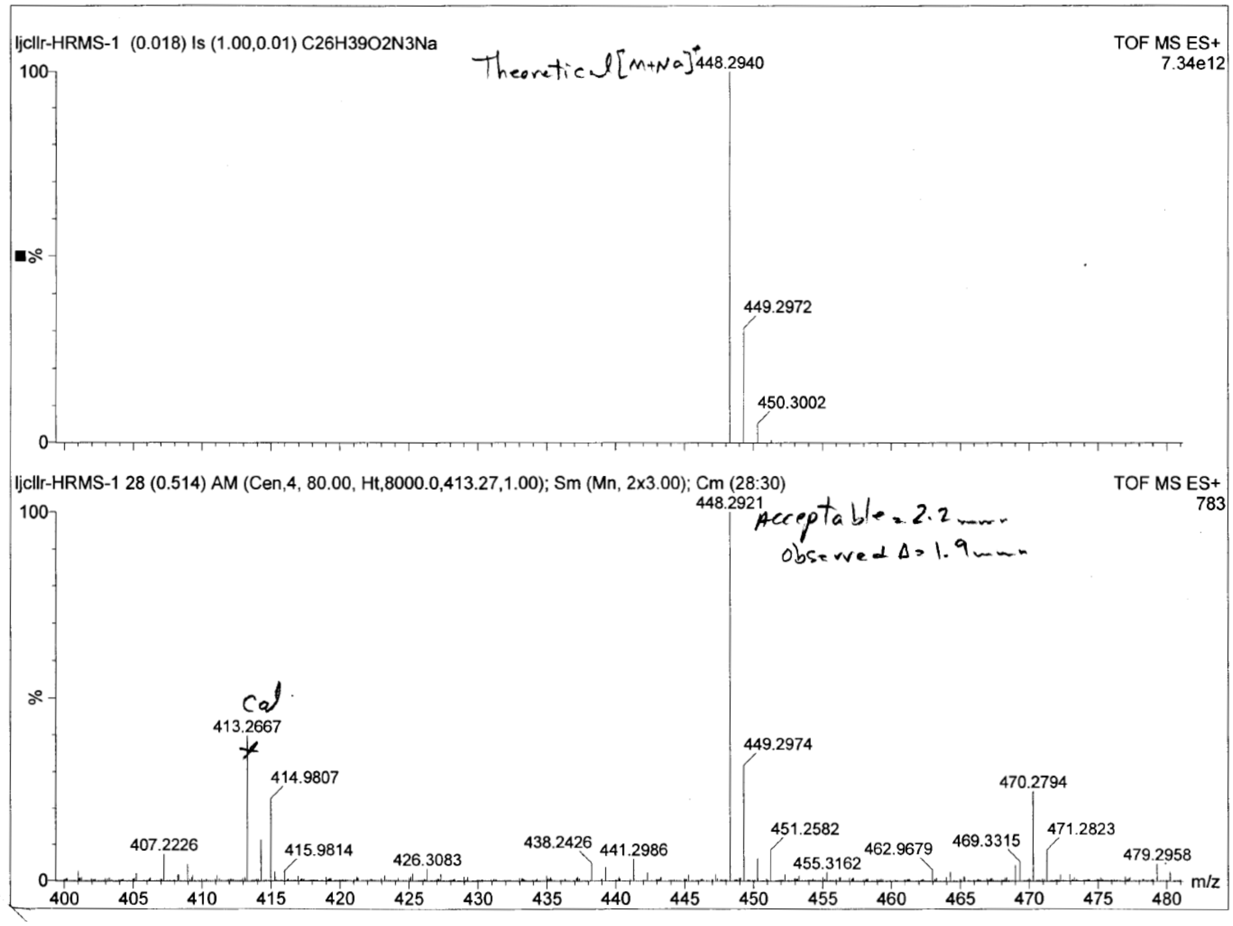

4-Iodo-2,6-diisopropylaniline (2.5)

^{1}H NMR (500 MHz, $CDCl_3$):

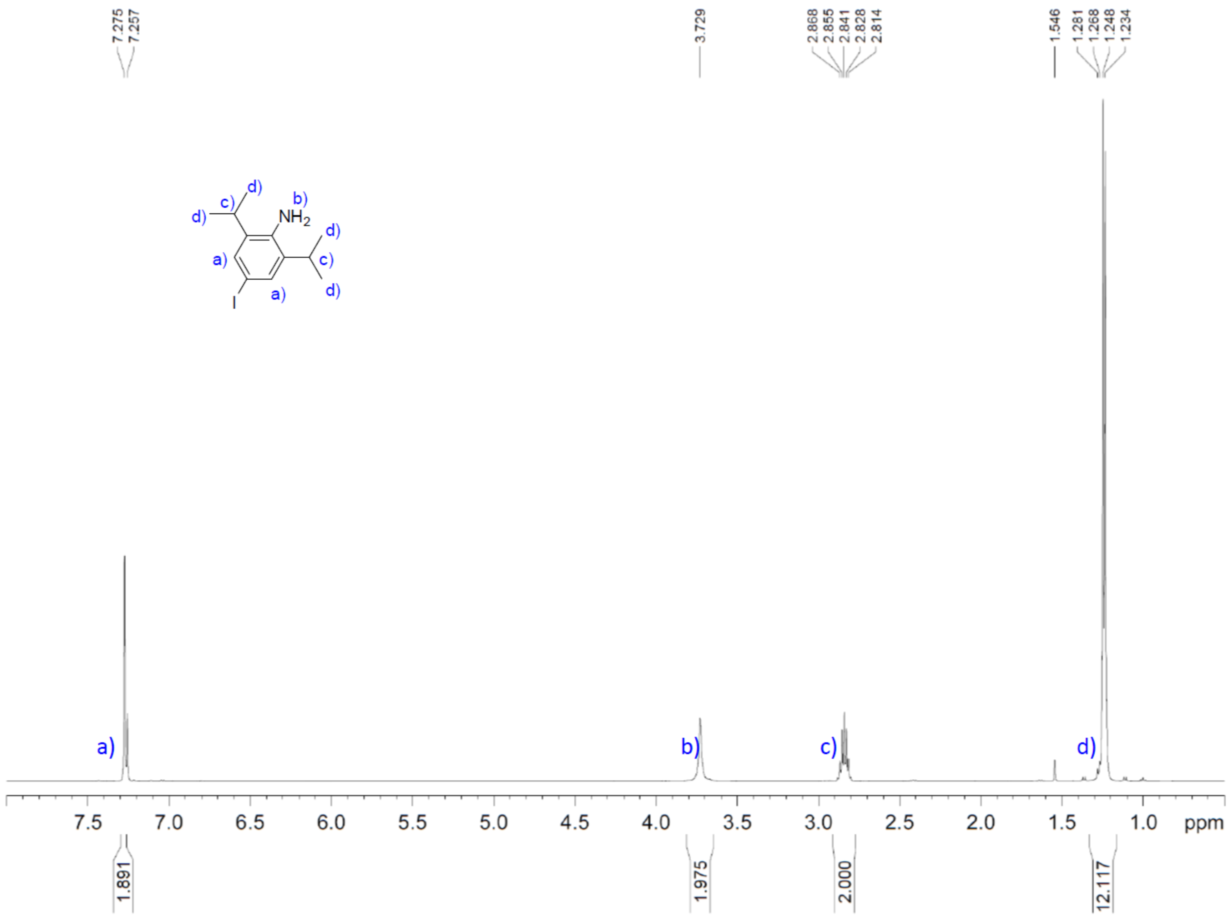

^{13}C NMR (125 MHz, $CDCl_3$):

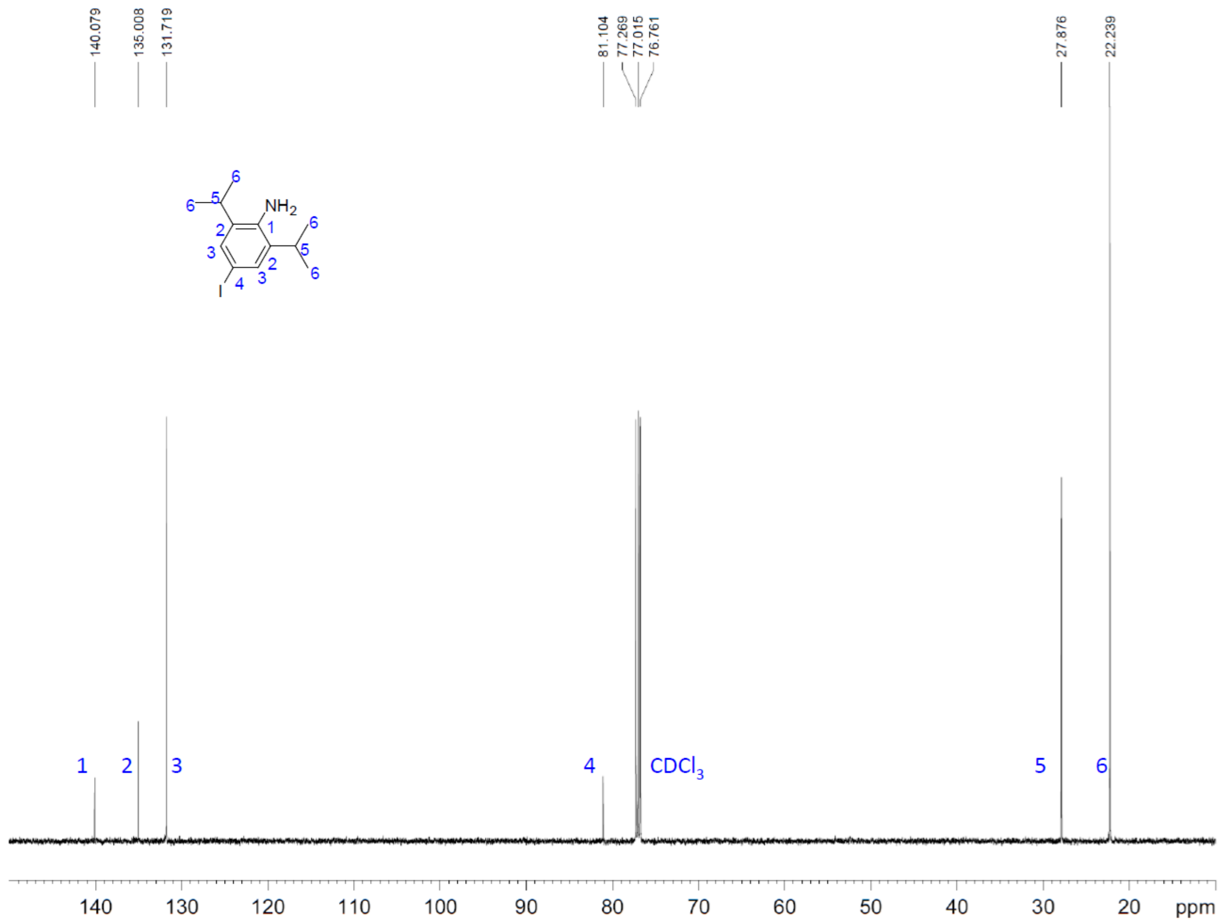

ES-MS (High Resolution):

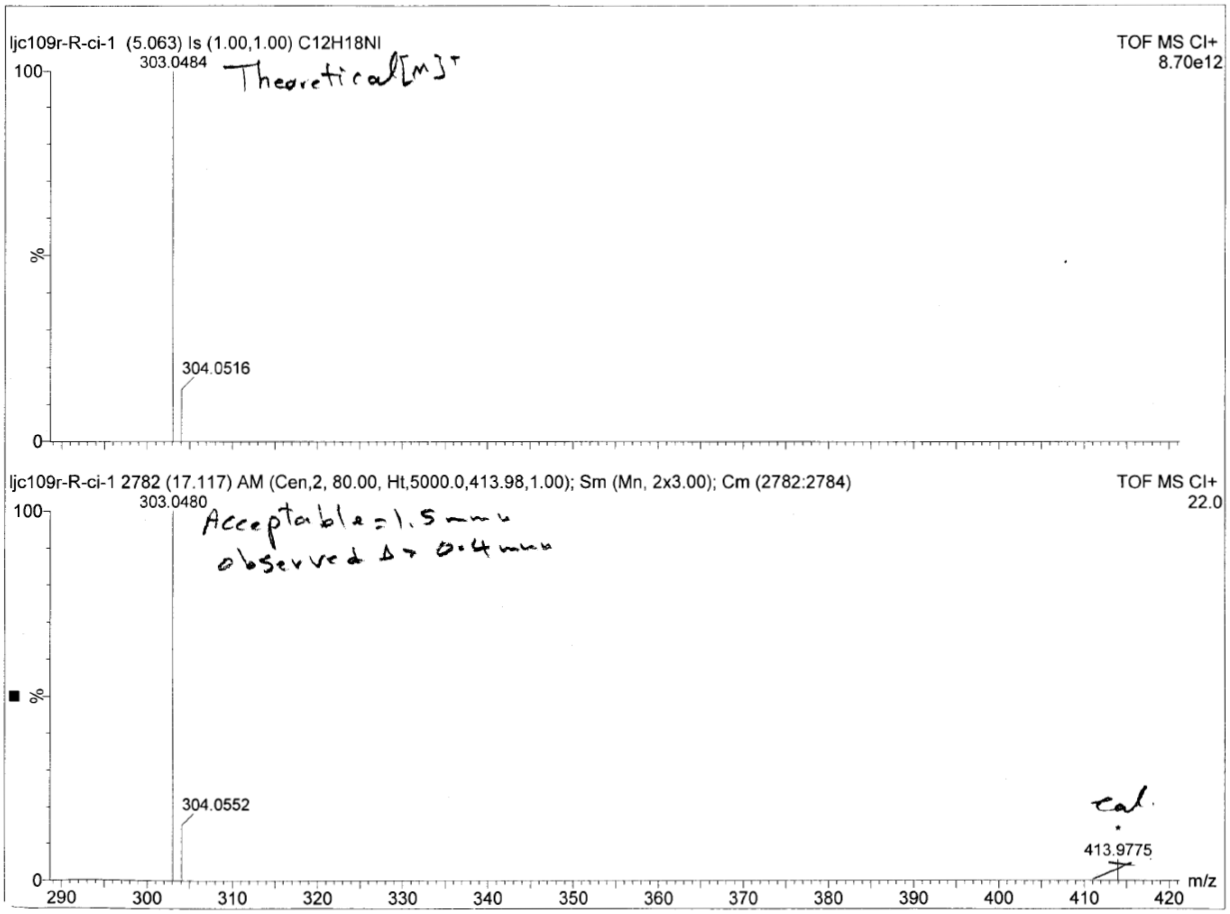

2,6-Diisopropyl-4-(undec-10-enyloxy)aniline (2.6)

^{1}H NMR (500 MHz, CD_2Cl_2):

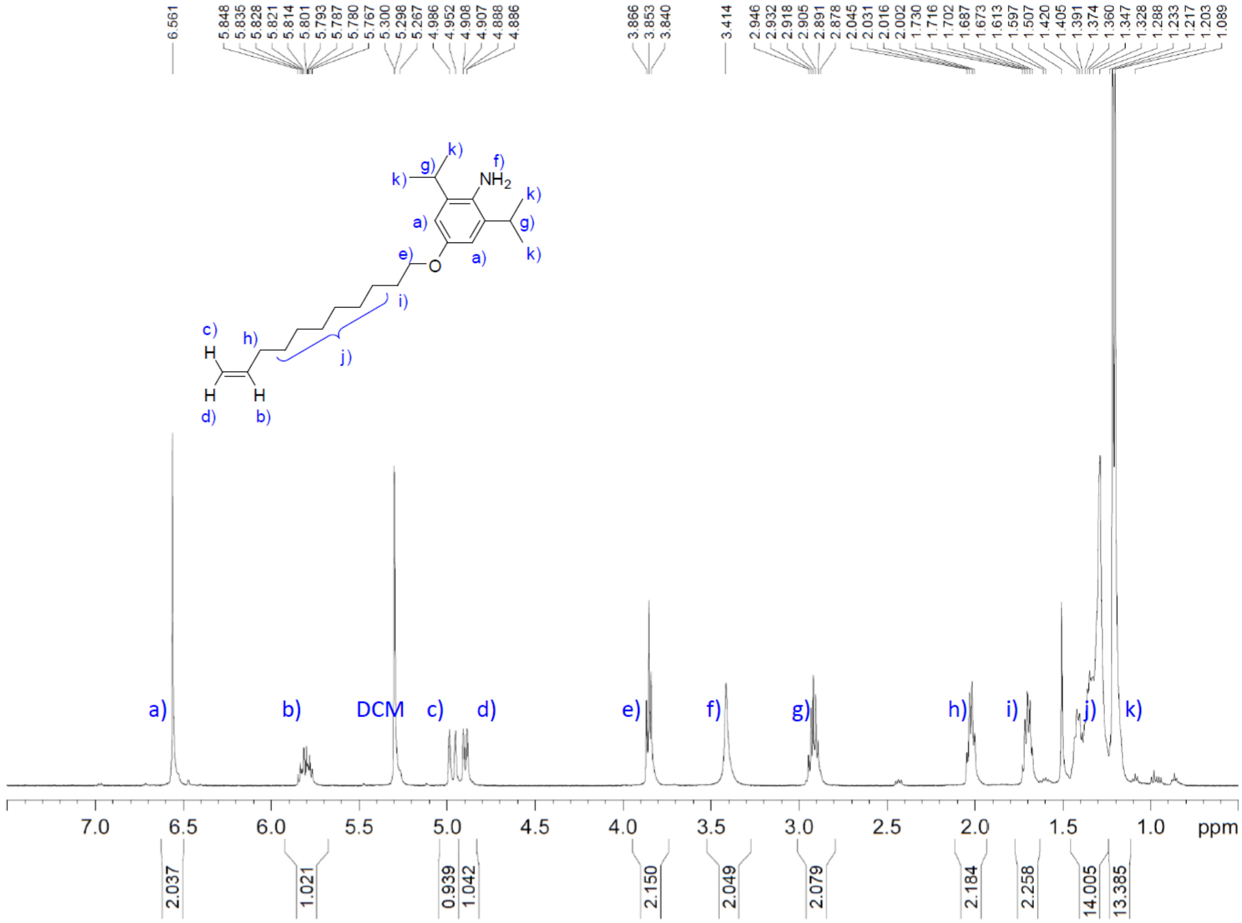

^{13}C NMR (125 MHz, CDCl$_3$):

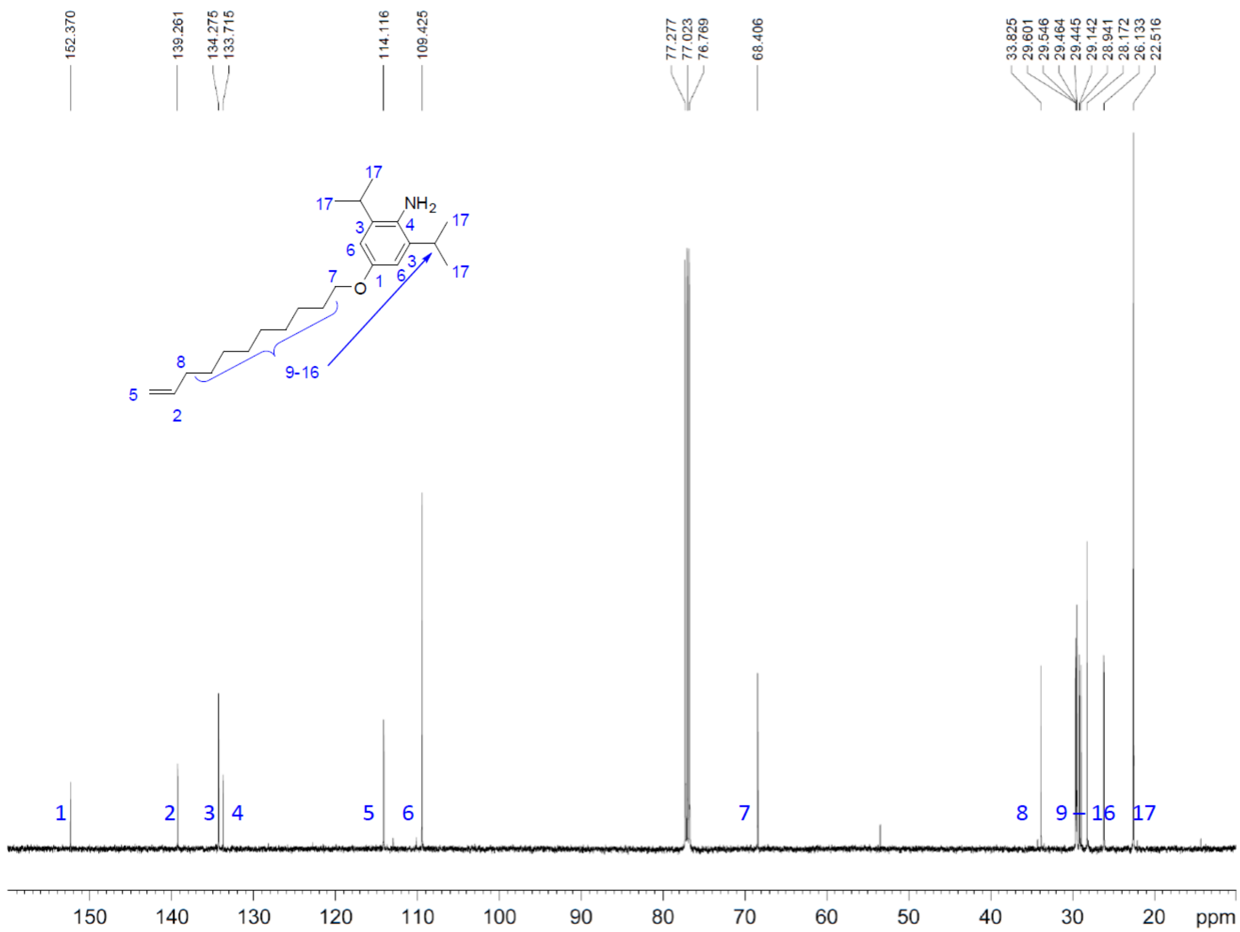

GC-MS (High Resolution):

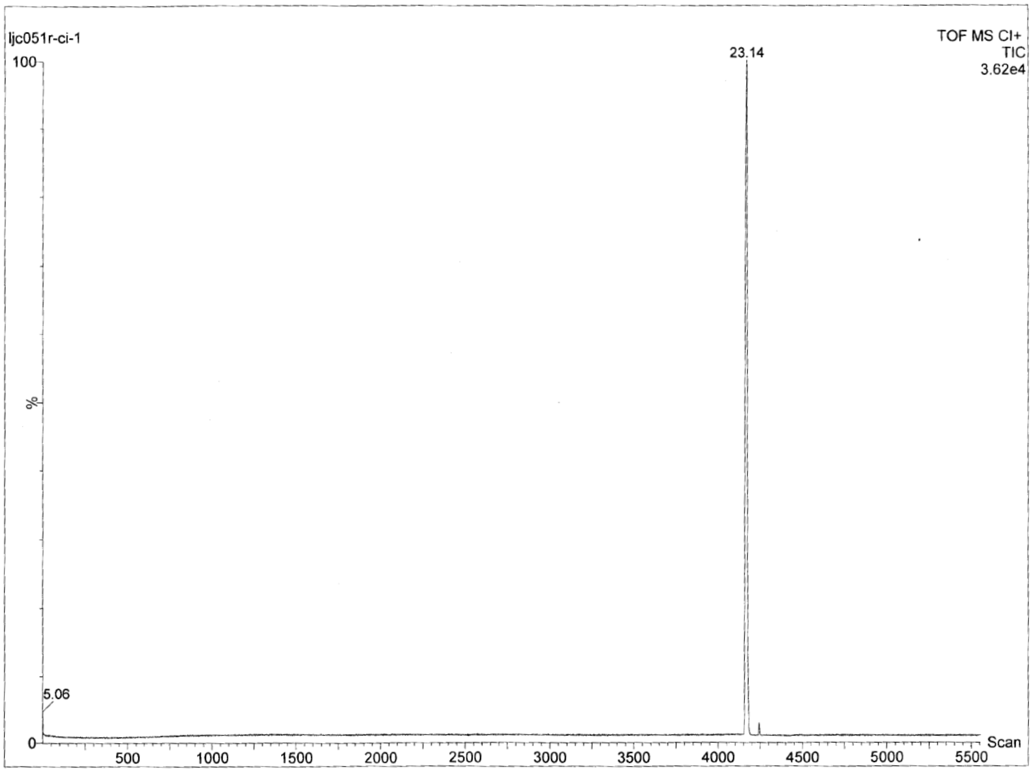

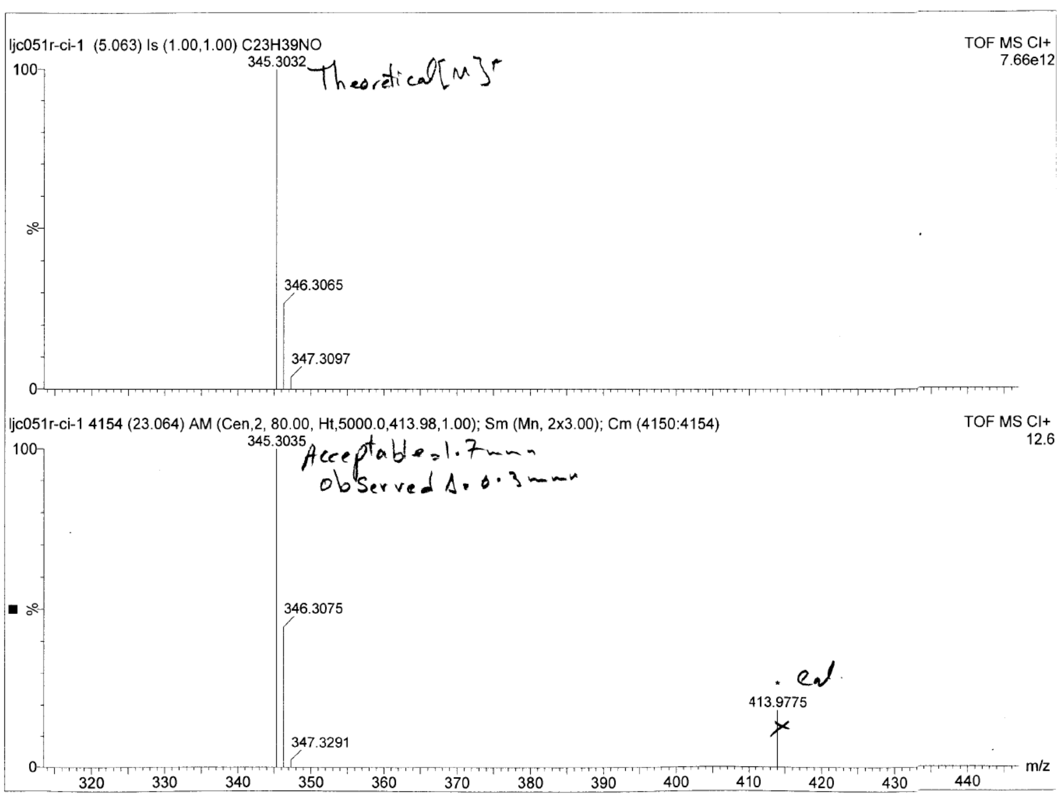

1-(6-(4-(Benzyloxy)butyl)-4-oxo-5-(undec-10-enyl)-1,4-dihydropyrimidin-2-yl)-3-(2,6-diisopropyl-4-(undec-10-enyloxy)phenyl)urea (2.7)

^{1}H NMR (500 MHz, $CDCl_3$):

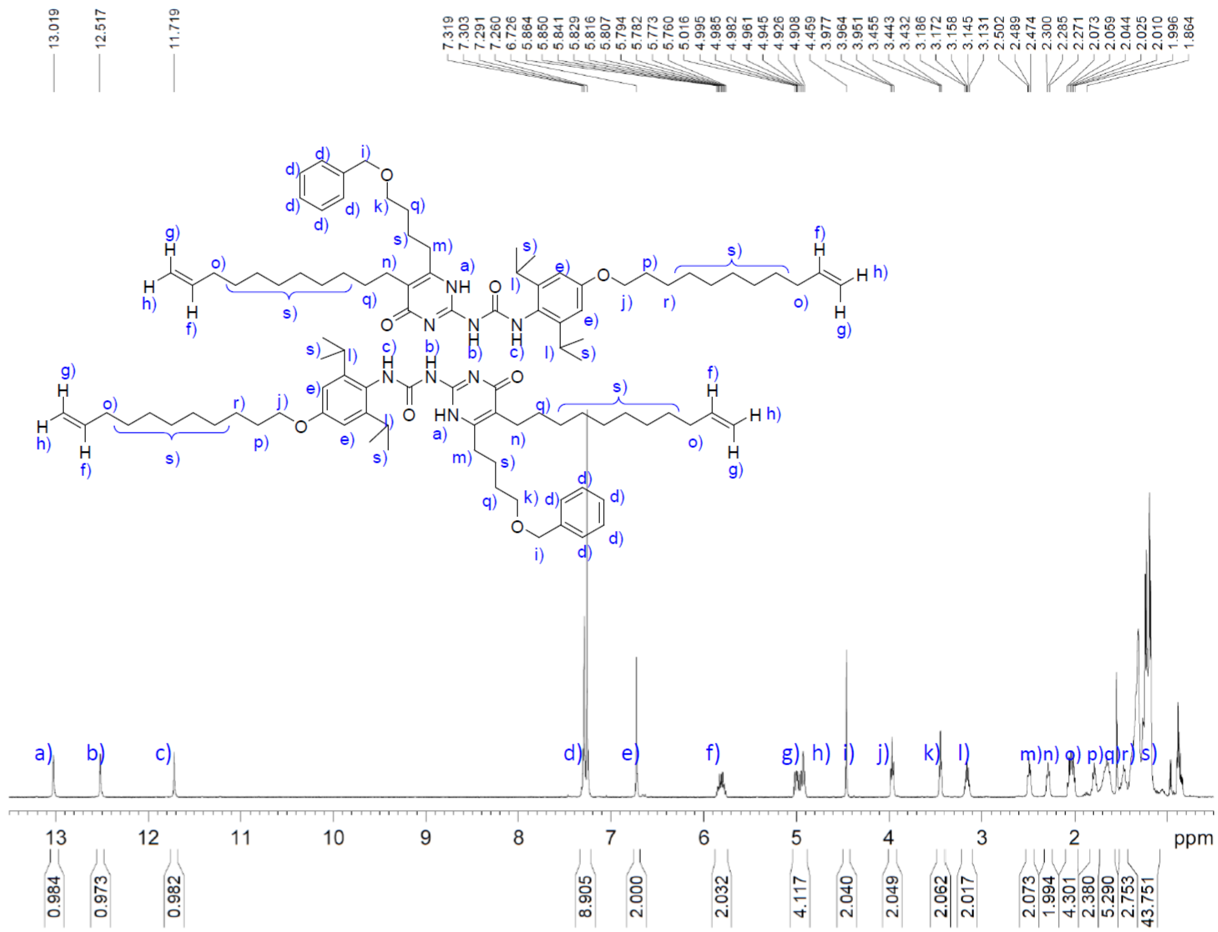

[13]C NMR (125 MHz, $CDCl_3$):

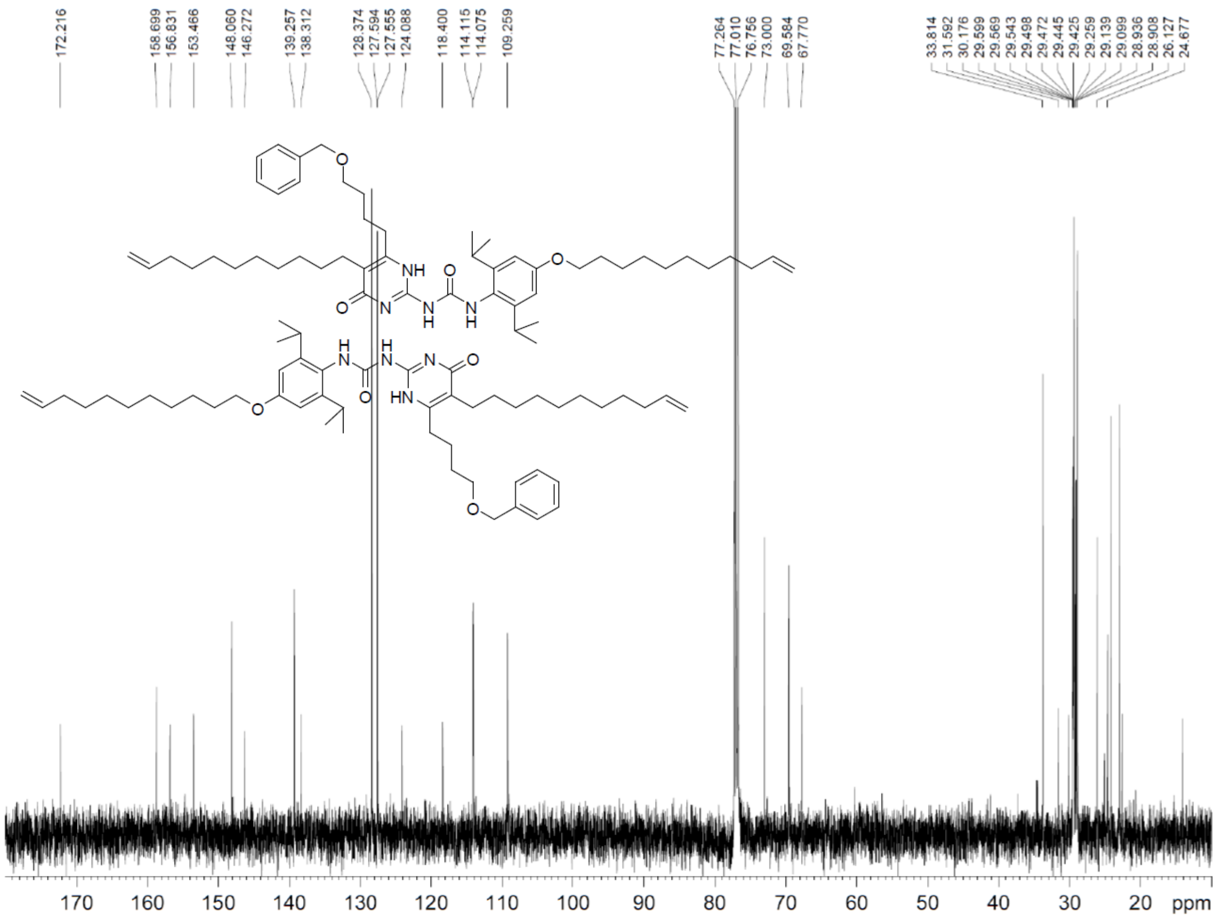

ES-MS (High Resolution):

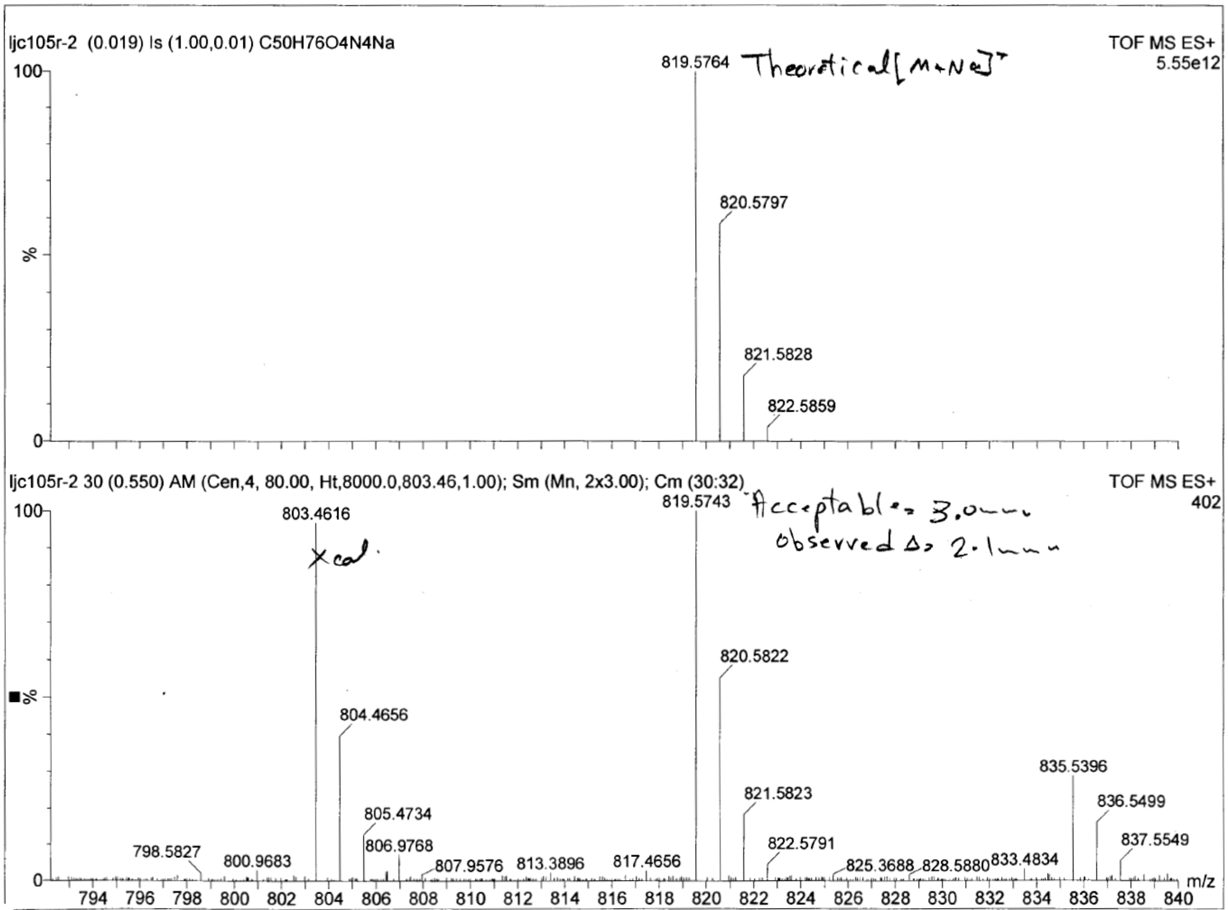

MALDI-TOF:

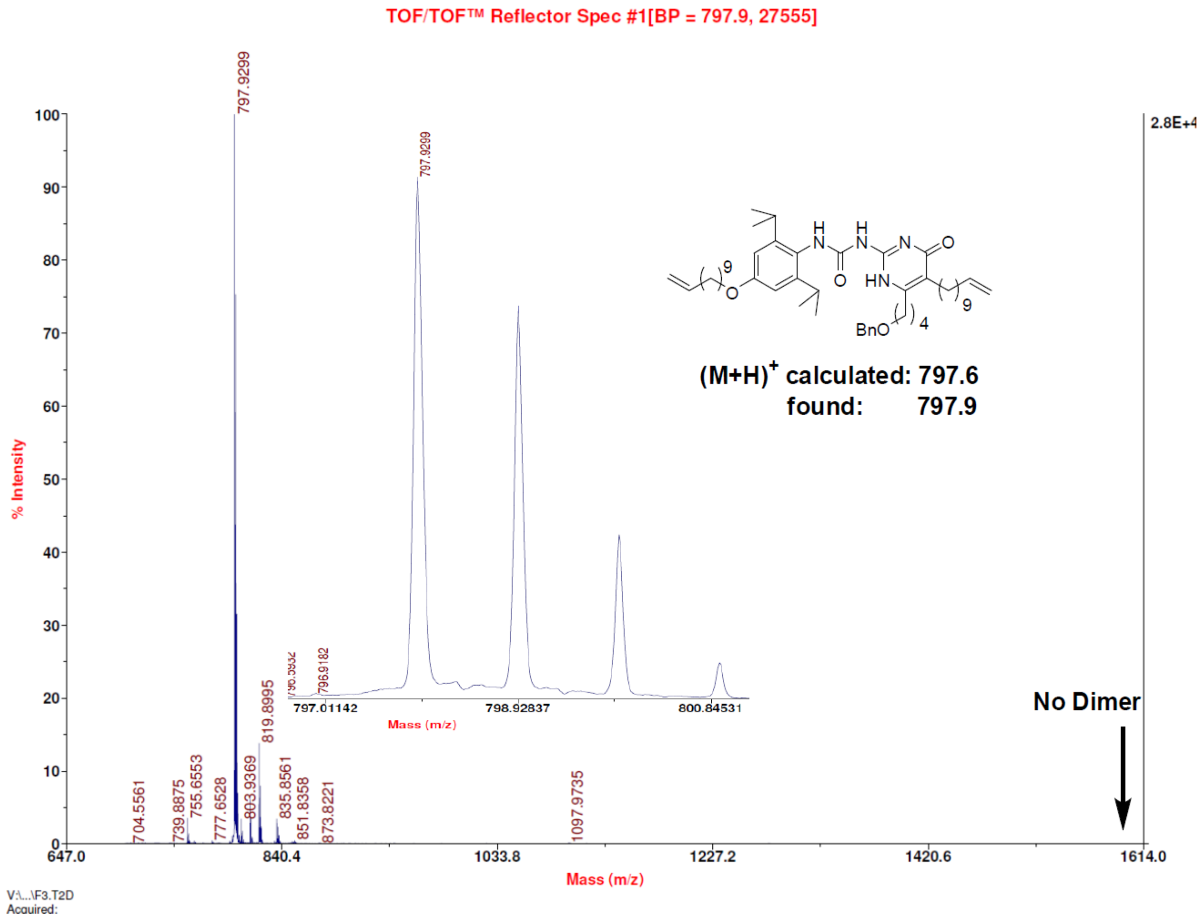
TOF/TOF™ Reflector Spec #1[BP = 797.9, 27555]
% Intensity
Mass (m/z)
2.8E+4
797.9299
819.8995
1097.9735
797.01142
798.92837
800.84531
(M+H)+ calculated: 797.6
found: 797.9
No Dimer
BnO
HN
V:\...\F3.T2D
Acquired:

Stack-blocked UPy-DCL diol (2.8)

^{1}H NMR (500 MHz, $CDCl_3$):

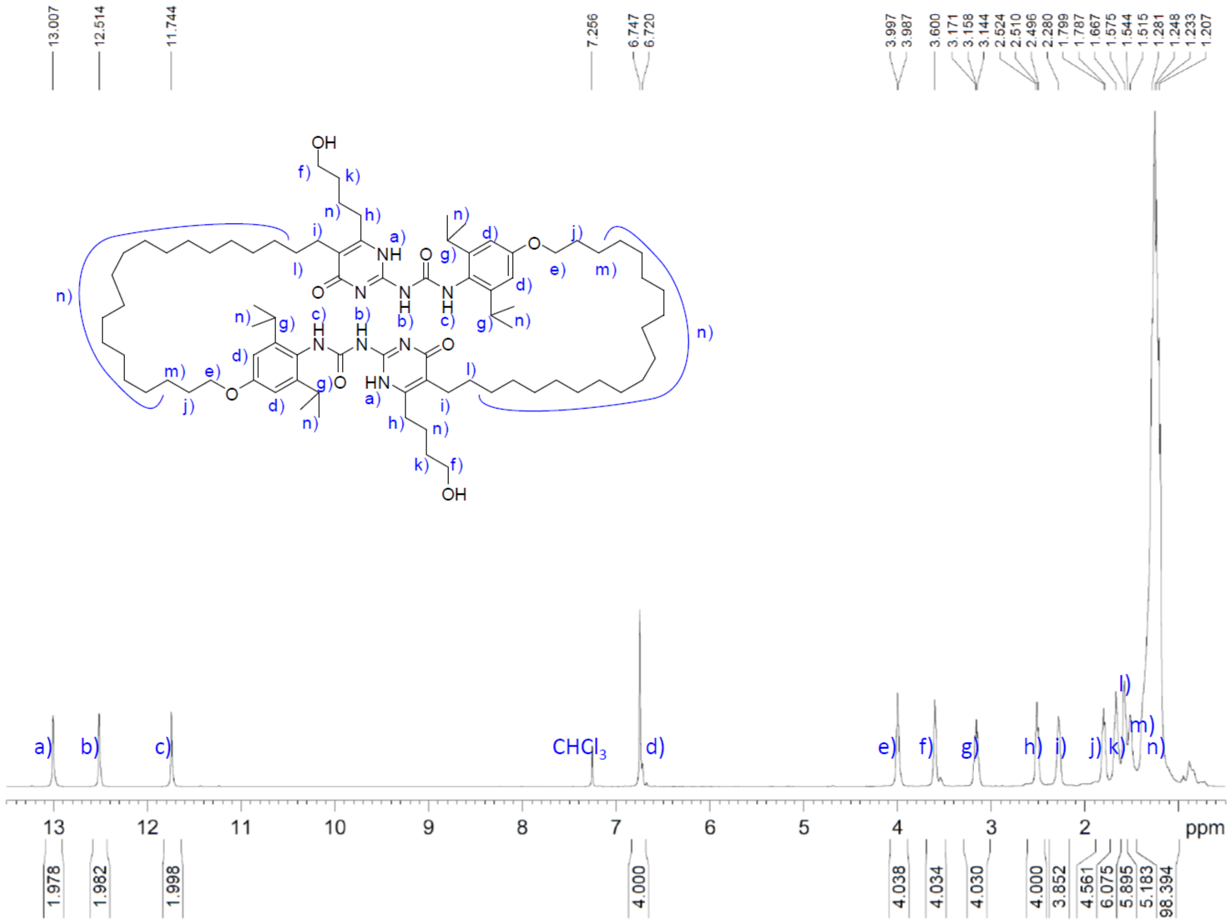

^{13}C NMR (125 MHz, CDCl$_3$):

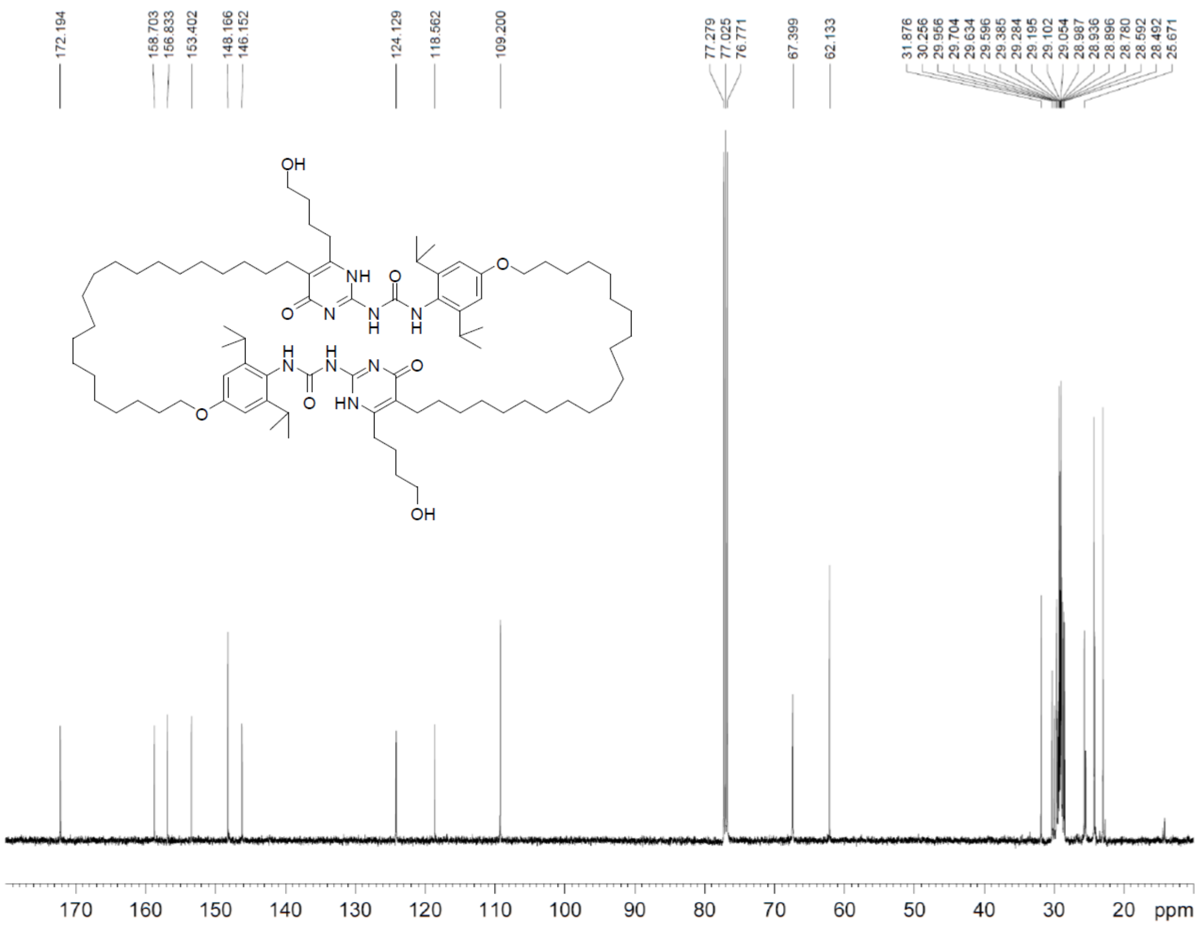

MALDI-TOF:

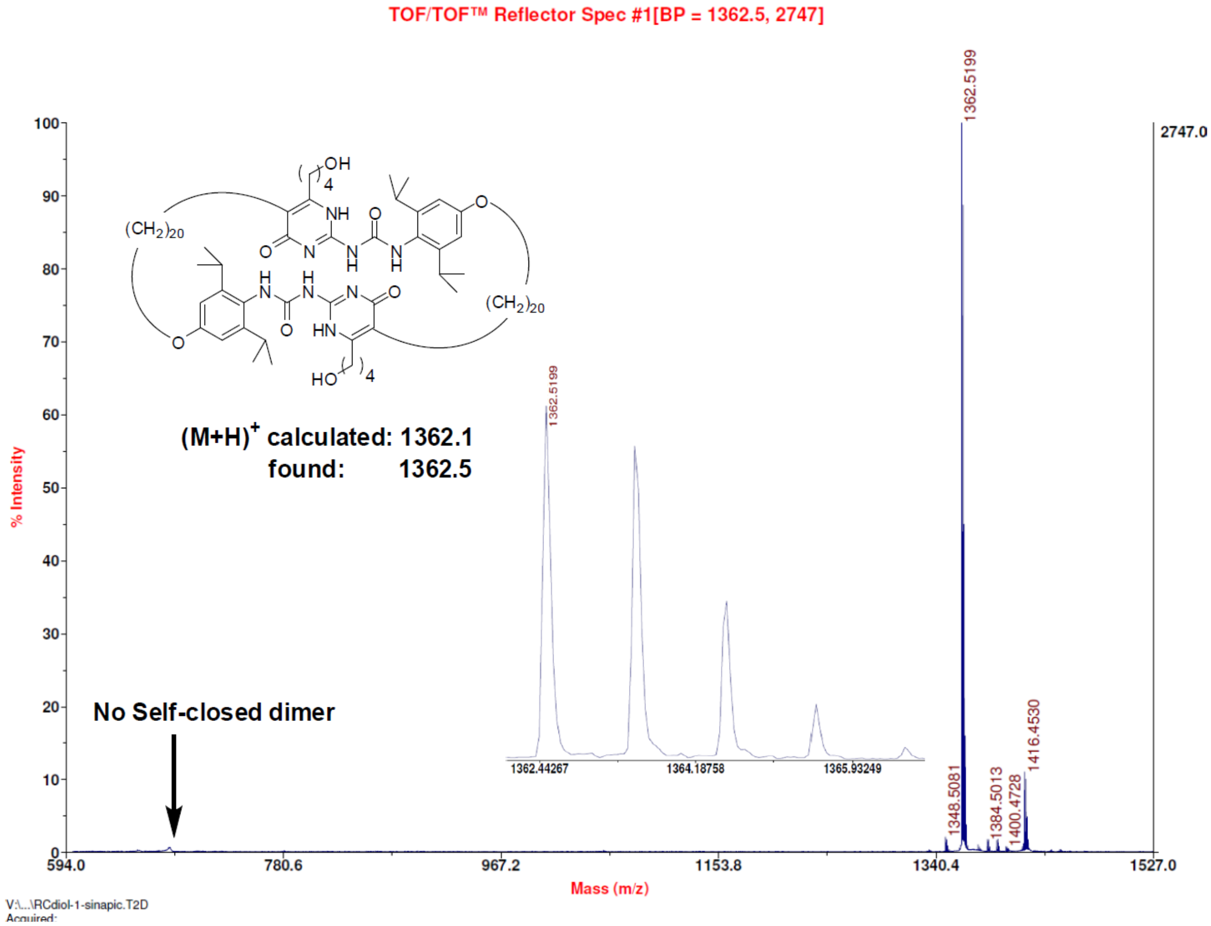

TOF/TOF™ Reflector Spec #1[BP = 1362.5, 2747]
1362.5199
2747.0
(M+H)+ calculated: 1362.1
found: 1362.5
No Self-closed dimer
1362.44267
1364.18758
1365.93249
1348.5081
1384.5013
1400.4728
1416.4530
% Intensity
Mass (m/z)
594.0
780.6
967.2
1153.8
1340.4
1527.0
V:\...\RCdiol-1-sinapic.T2D

Stack-blocked UPy-DCL ADMET Monomer (2.9)

^{1}H NMR (500 MHz, $CDCl_3$):

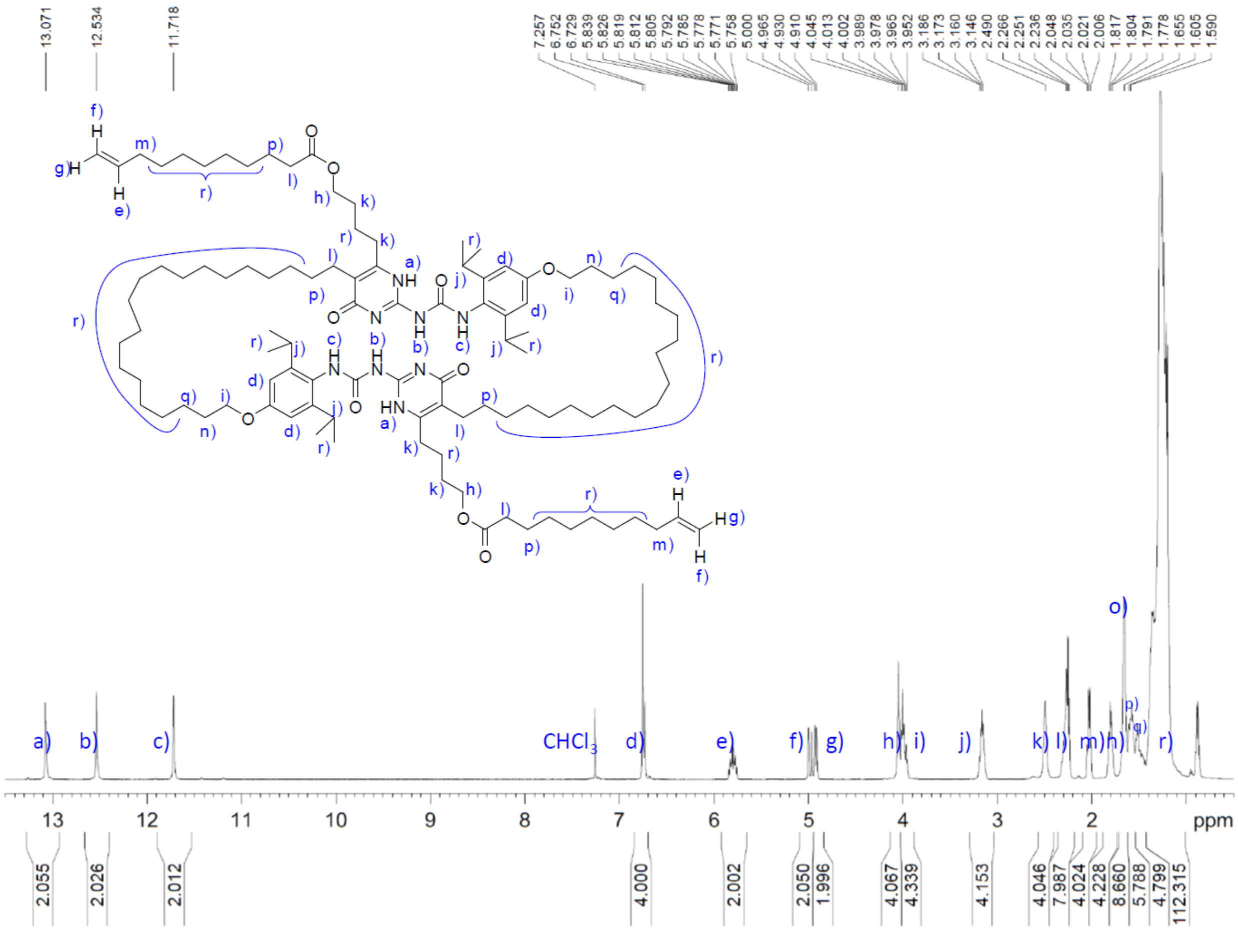

COSY (500MHz, $CDCl_3$):

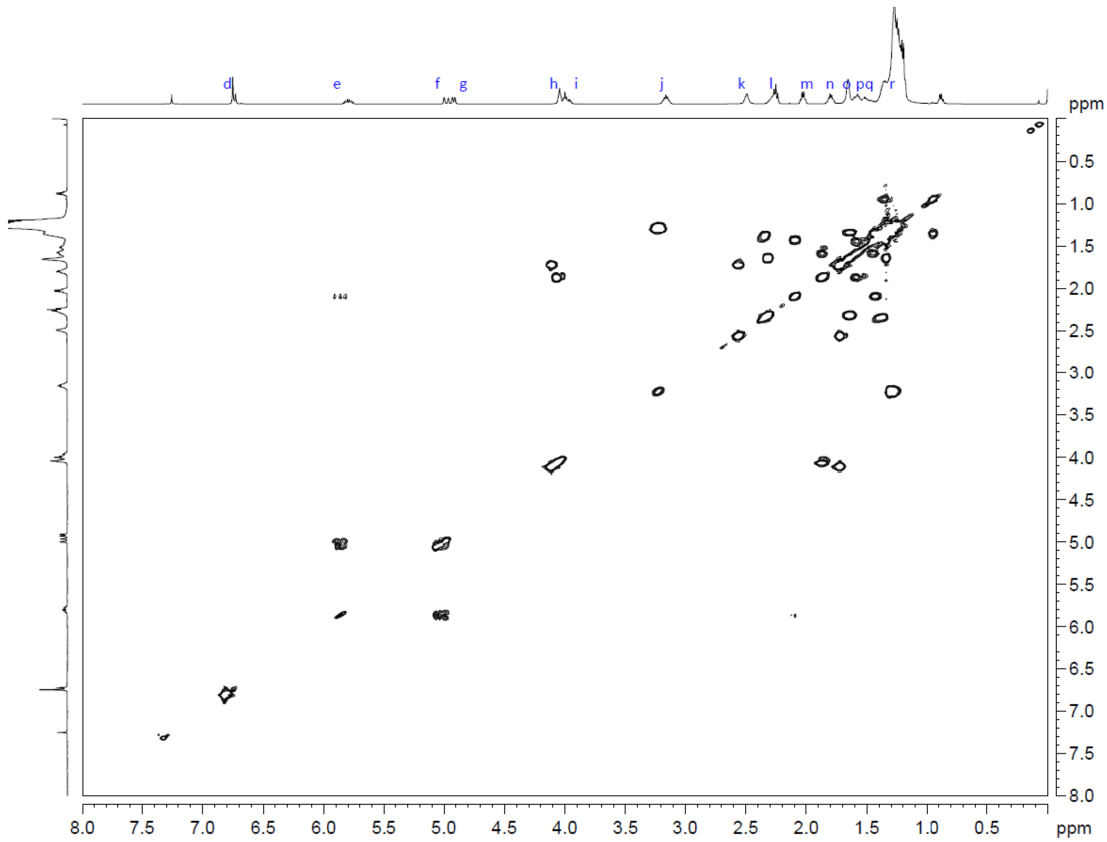

ROESY (500 MHz, $CDCl_3$):

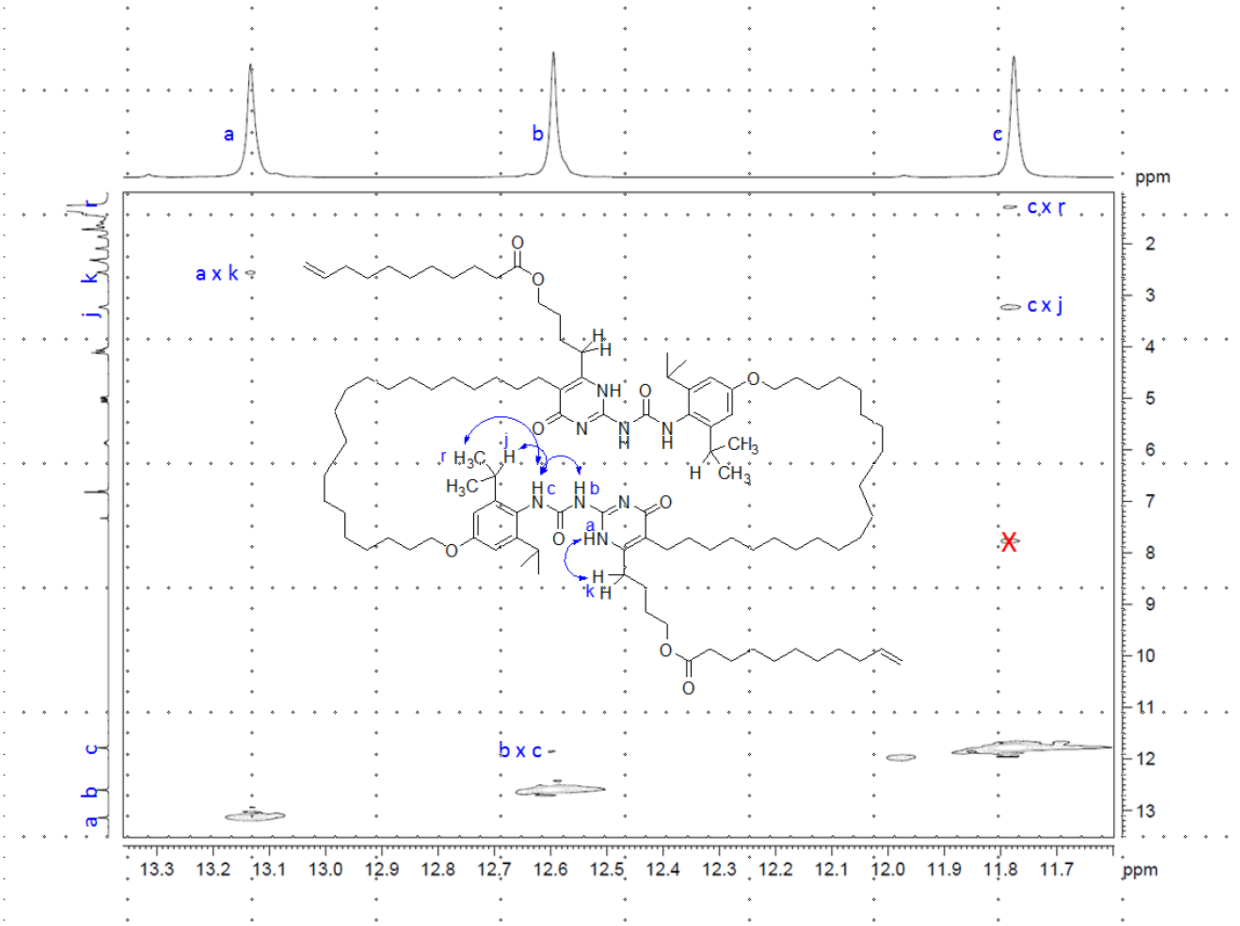

[13]C NMR (125 MHz, CDCl₃):

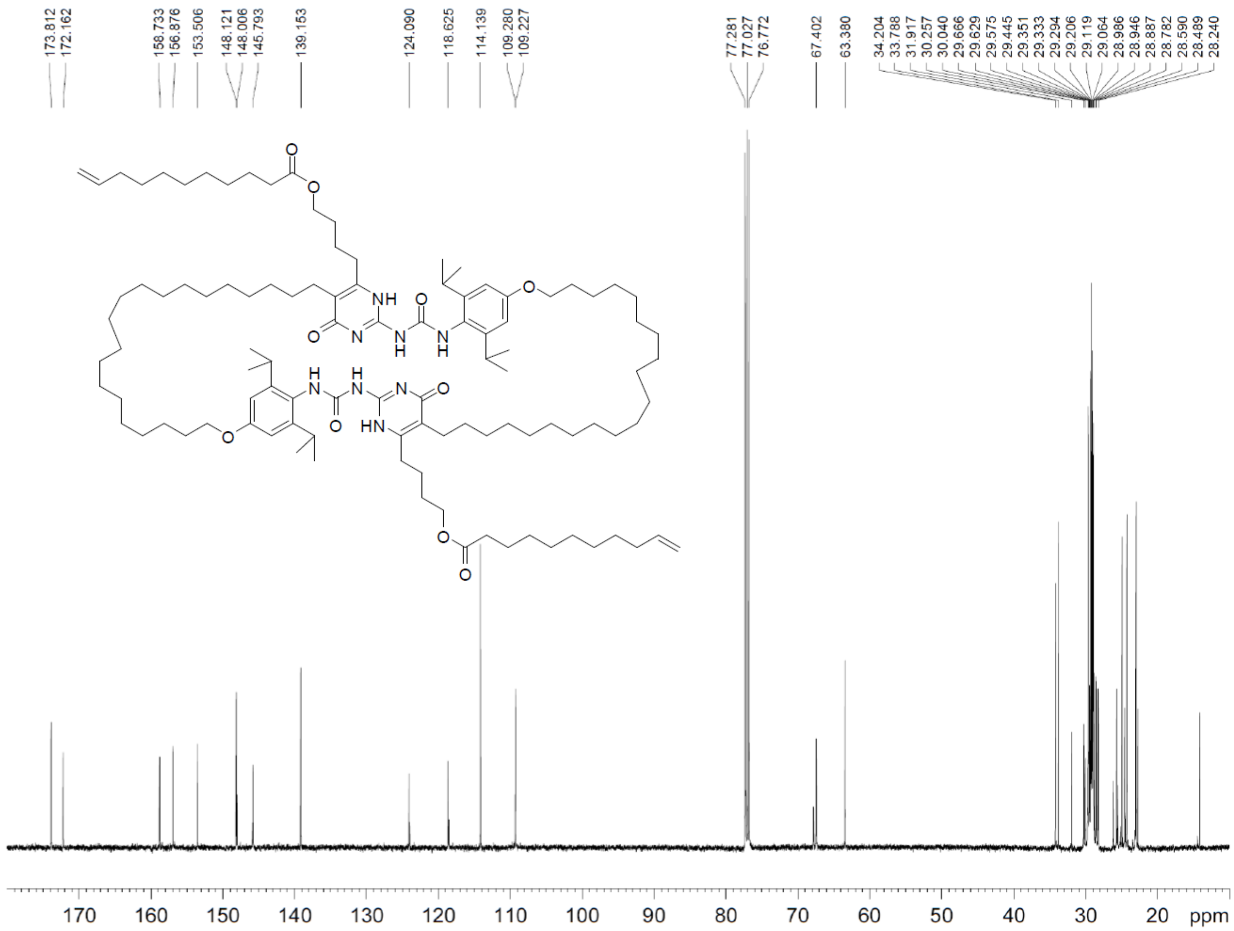

ES-MS (Low Resolution):

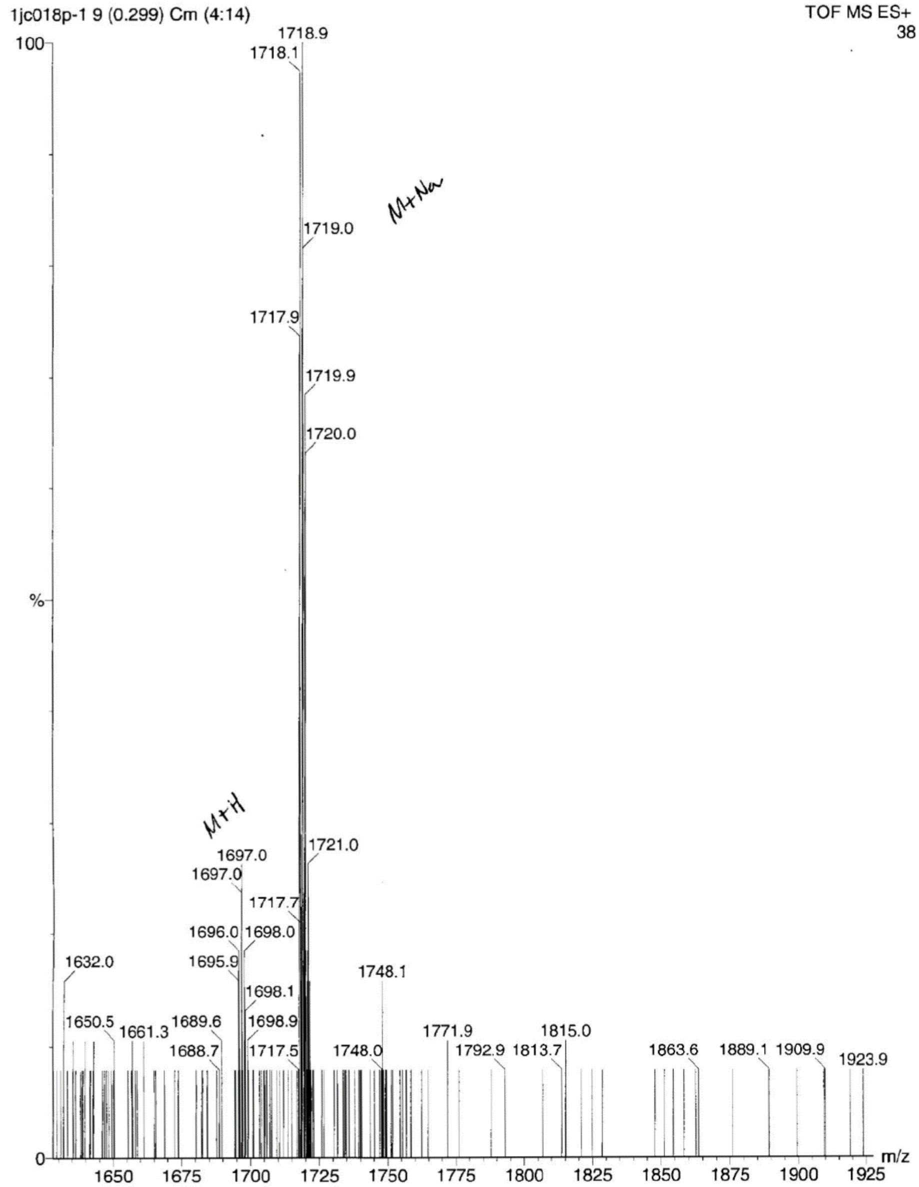

1-(*S*-trityl)mercaptoundec-10-ene (2.10)

^{1}H NMR (500 MHz, CDCl$_3$):

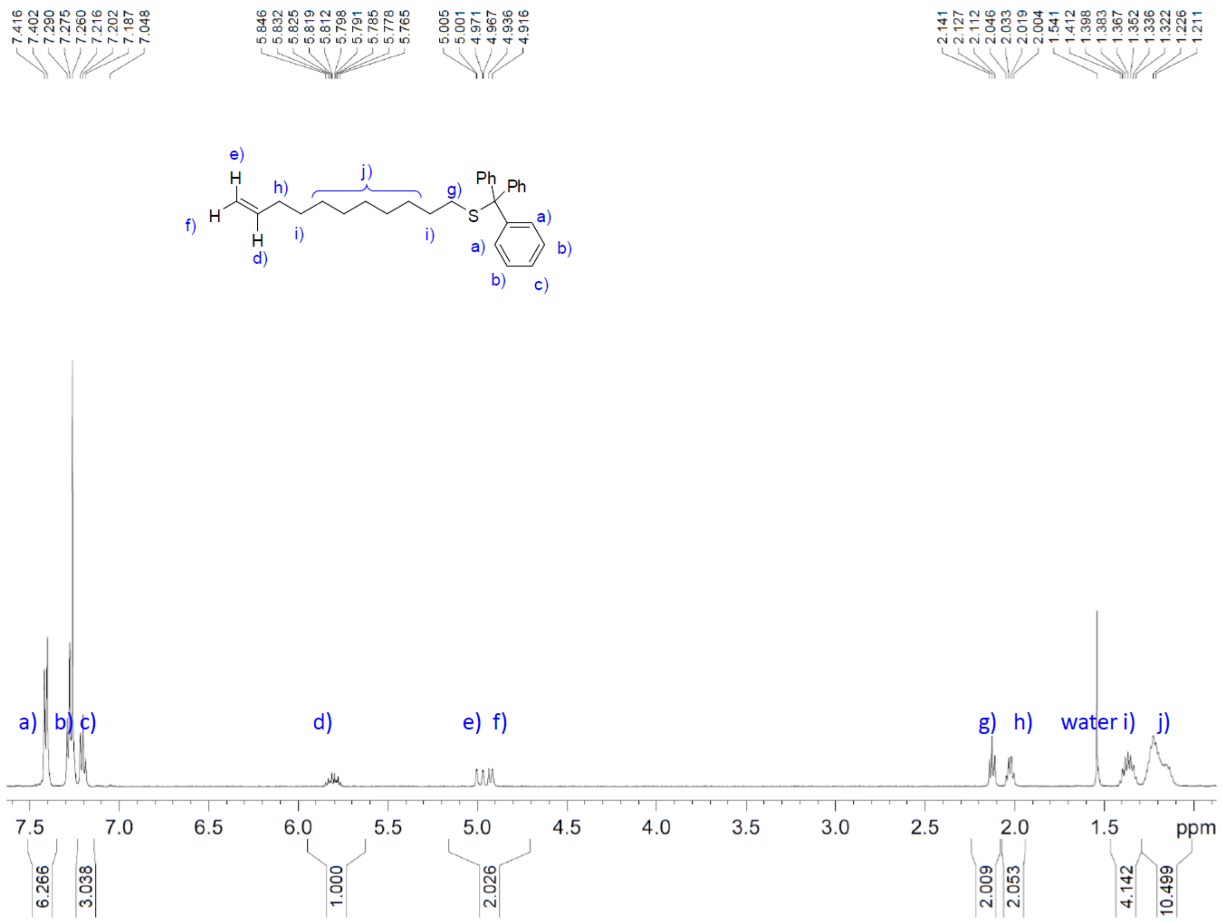

[13]C NMR (125 MHz, CDCl3):

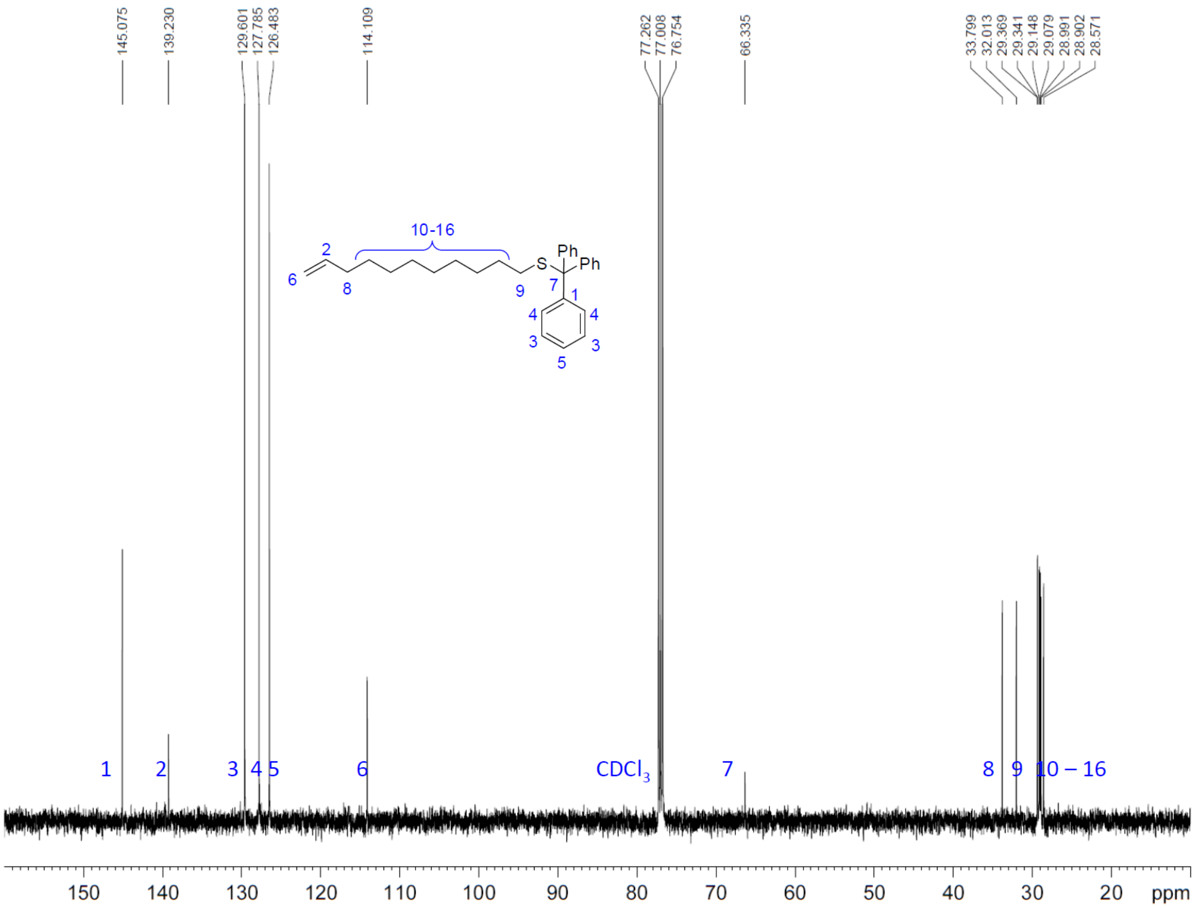

ES-MS (High Resolution):

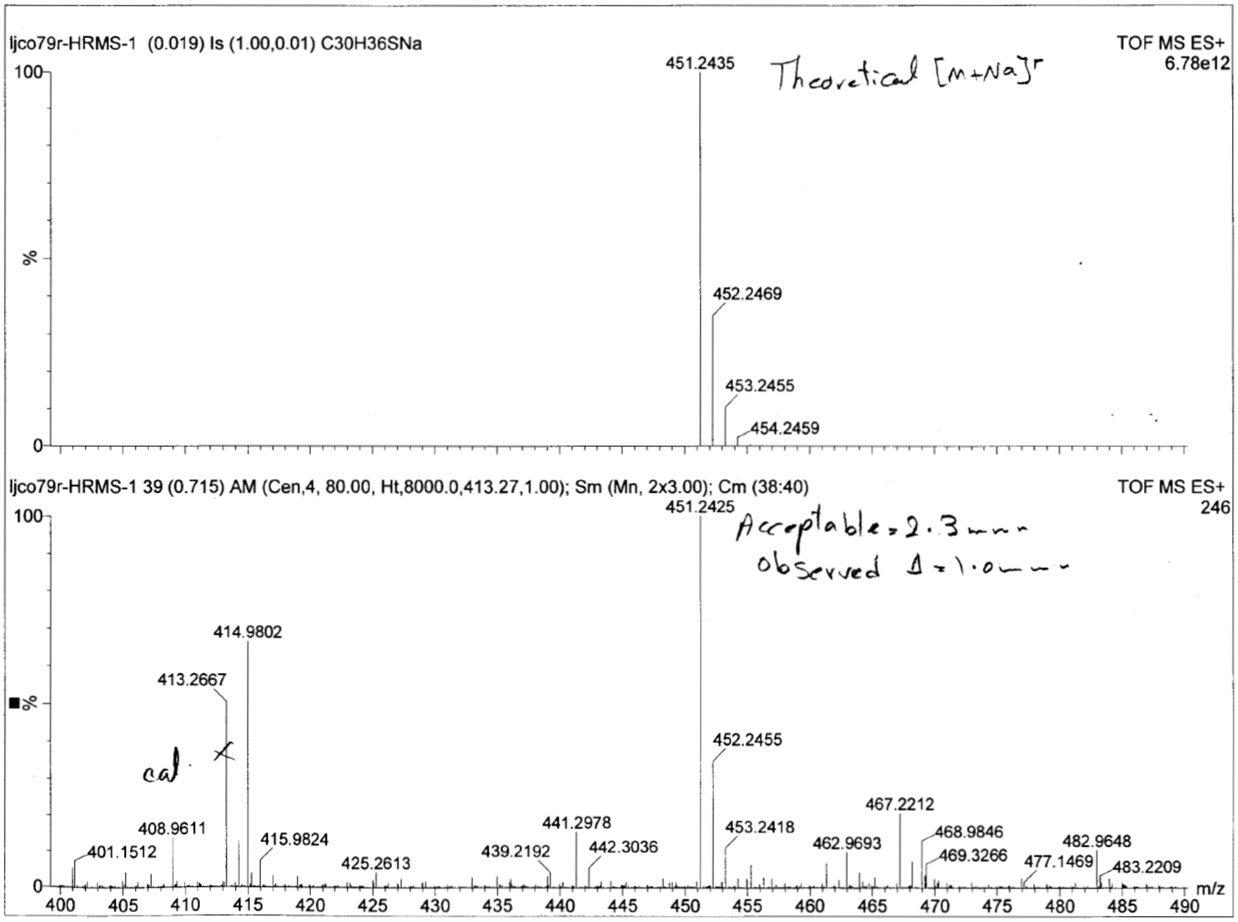

Bis-1-(*S*-trityl)mercaptoundec-10-ene-end-capped SB-UPy-DCL ADMET oligomer (n = 8) (2.11)

^{1}H NMR (500 MHz, $CDCl_3$):

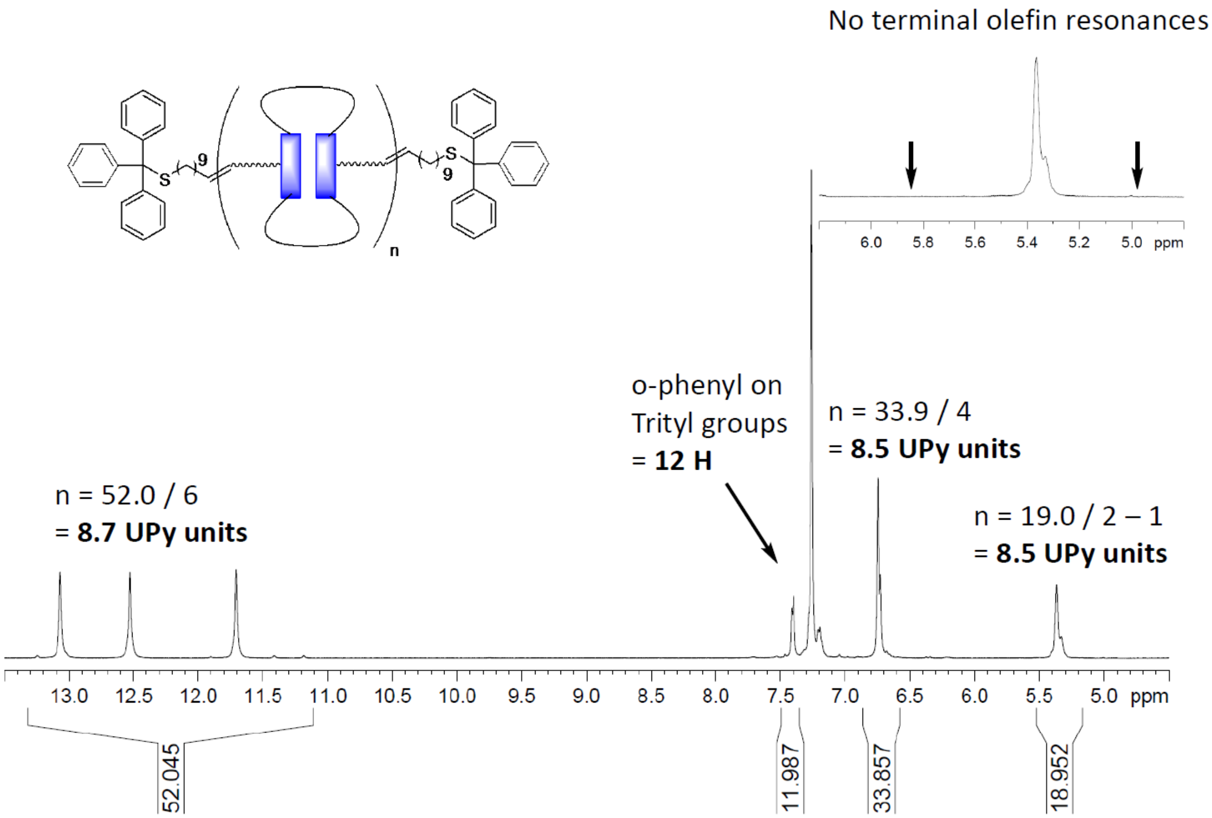

Bis-undec-10-ene-1-thiol-end-capped SB-UPy-DCL ADMET oligomer (n = 8) (2.12)

[1]H NMR (500 MHz, $CDCl_3$):

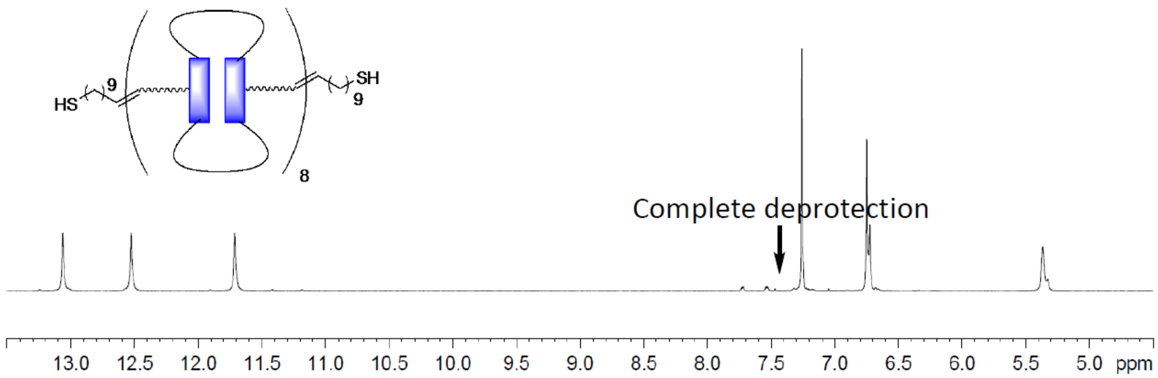

GPC (THF eluent, 1 mL/min, Polystyrene standard):

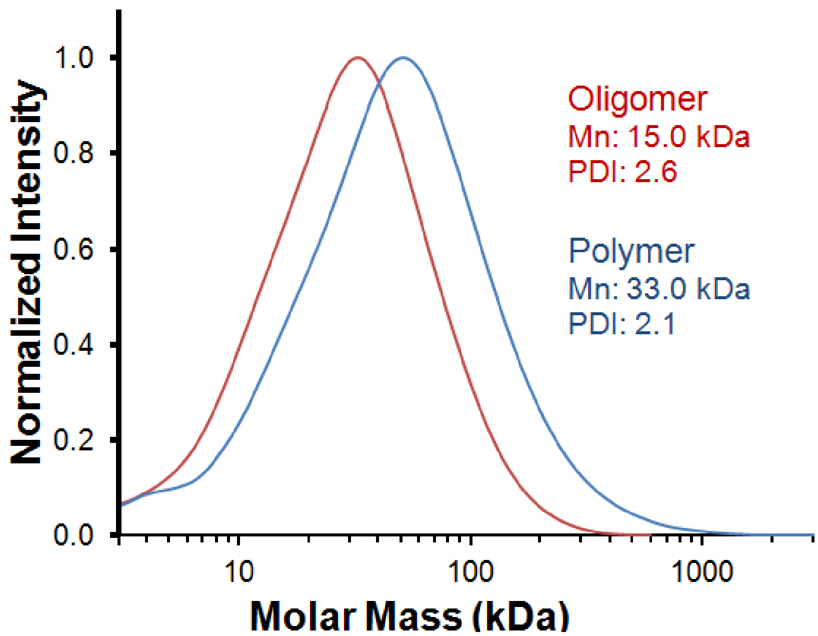

Chapter 3: Malleable and Self-Healing Covalent Polymer Networks Through Tunable Dynamic Boronic Ester Bonds*

**The work presented in this chapter was carried out in equal contribution with Dr. Olivia Cromwell.*

3.1 Introduction

3.1.1 Dynamic Self-healing Materials

Polymeric materials that contain reversible bonds and other dynamic interactions exhibit interesting properties, such as adaptability, malleability, and self-healing. In contrast to traditional thermosets, dynamically crosslinked polymers can be reprocessed and recycled while still maintaining their thermal and chemical stability.[17,103,107,155-157] Moreover, reversible covalent bonds[56,62,63,68,158] and non-covalent bonds[57,70,75,77] have been employed to design self-healing materials. While many dynamic motifs have been developed for such applications,[56,57,62,63,68,70,75,77,158] to our knowledge, systematically tunable motifs whose small molecule kinetics directly correlate to dynamic properties in bulk solid materials largely remain to be explored. Achieving such a goal could aid in the development of novel dynamic materials with tunable properties by simply adjusting the motif's kinetics. Whereas tuning dynamicity of metal-ligand,[111,112,159] imine metathesis,[160] and protein-ligand[161] interactions have been shown to impact various dynamic properties of crosslinked organogels[111,112,159] and hydrogels[161] in solution, such a strategy has rarely been demonstrated in bulk solids for the design of malleable and self-healing materials.[61]

3.1.2 Our Design of Boronic Ester Trans-esterification for Self-Healing

In this study, we used a divalent crosslinker with adjustable exchange kinetics to tune the properties of bulk polymer networks. The dynamics of the functional groups on the small molecule crosslinkers could be kinetically tuned thereby controlling the dynamic and self-healing emergent properties of the resulting networks. In our search for a suitable dynamic motif, the boronic ester bond and its transesterification reaction attracted our attention because of its unique combination of high thermodynamic stability and kinetic tunability. The boronic ester bond has a high bond dissociation energy (B-O bond 124 kcal/mol),[162] and, crucially, the rate of boronic ester transesterification can also be tuned over many orders of magnitude with simple neighboring group effects, ranging from effectively inert to extremely fast.[163] Despite these desirable properties, applications for dynamic boronic ester exchange has been largely limited to aqueous environments,[164,165] often related to sensing technology for sugars.[165-167] For the very few examples of using boronic esters for dynamic[168] or self-healing materials design,[169-171] healing has to be facilitated by water and none has investigated the tunability of boronic ester exchange kinetics for controlling bulk dynamic properties. We envisioned that the boronic ester transesterification reaction provided an untapped potential as a platform for dynamic material design, allowing us the opportunity to develop of a library of materials with tunable transesterification exchange kinetics and emergent malleability and self-healing properties.

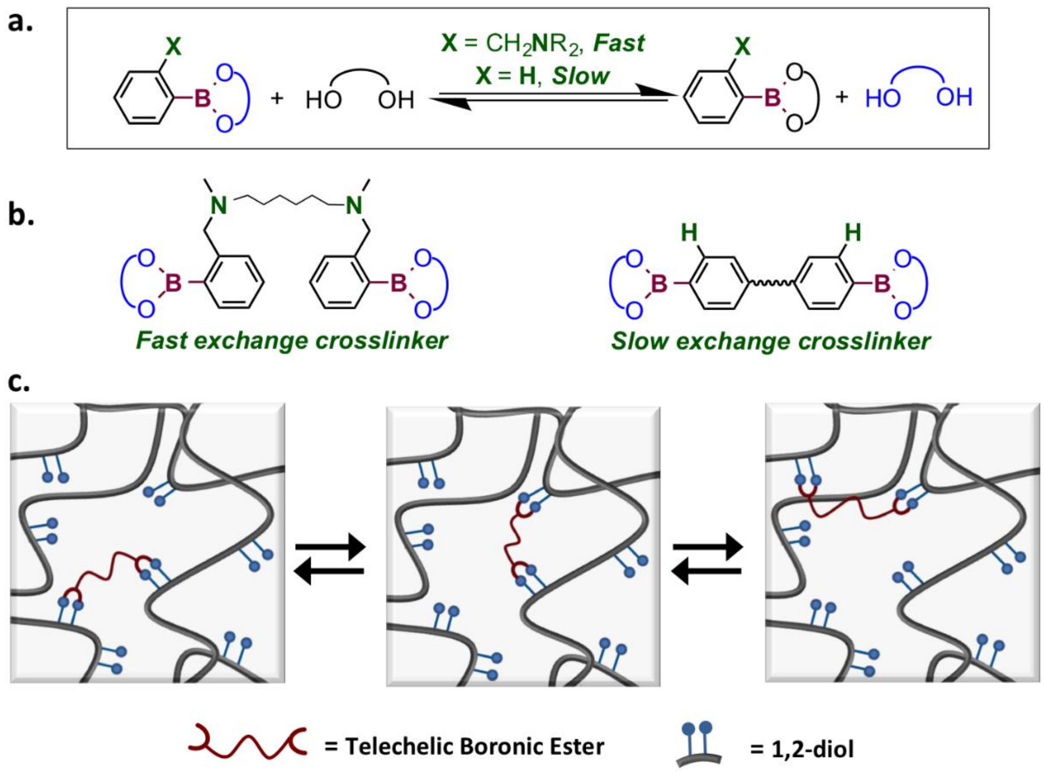

Figure 3.1 Design concept for dynamically crosslinked boronic ester material. **a.** Tuning neighboring group to control the exchange kinetics of boronic ester. **b.** Design of di-boronic ester crosslinkers with tunable exchange kinetics. **c.** Dynamic exchange of boronic ester crosslinkers affords dynamic materials.

Specifically, we demonstrated our concept with a simple polymer embedded with 1,2-diol moieties as attachment sites for boronic esters, crosslinked by telechelic divalent boronic esters. For our initial proof-of-concept, two kinetic variants of di-boronic esters were chosen to serve as dynamically mobile crosslinkers for self-healing (Figure 3.1). Consistent with our hypothesis, both crosslinked polymer networks exhibited malleability and reprocessability. However, the two different variants showed variable efficiencies of self-healing, with the faster exchanging linker showing a significant extent of healing at 50 °C, while the slower exchanging linker showed minimal healing. To our knowledge, our report provides the first direct demonstration of tunable malleability and self-healing efficiency through variations in small molecule design.

3.2 Results and Discussion

3.2.1 Confirmation of Small Molecule Trans-esterification Kinetics

To confirm that the rate of boronic ester transesterification can be tuned by neighboring groups, we synthesized small molecule model compounds and measured the variable exchange rates in solution.[163] We prepared neopentyl glycol esters from phenyl boronic acid and *o*-(dimethylaminomethyl)phenylboronic acid (synthesized through reductive amination between 2-formylphenylboronic acid and dimethylamine) (compounds **3.1** and **3.2**, respectively), and their rates of self-transesterification were monitored in the presence of 1 equivalent excess of neopentyl glycol. The synthesis for these compounds is shown in Scheme 3.1 below.

Scheme 3.1 Synthesis of Model Boronic Ester Compounds for Kinetic Study

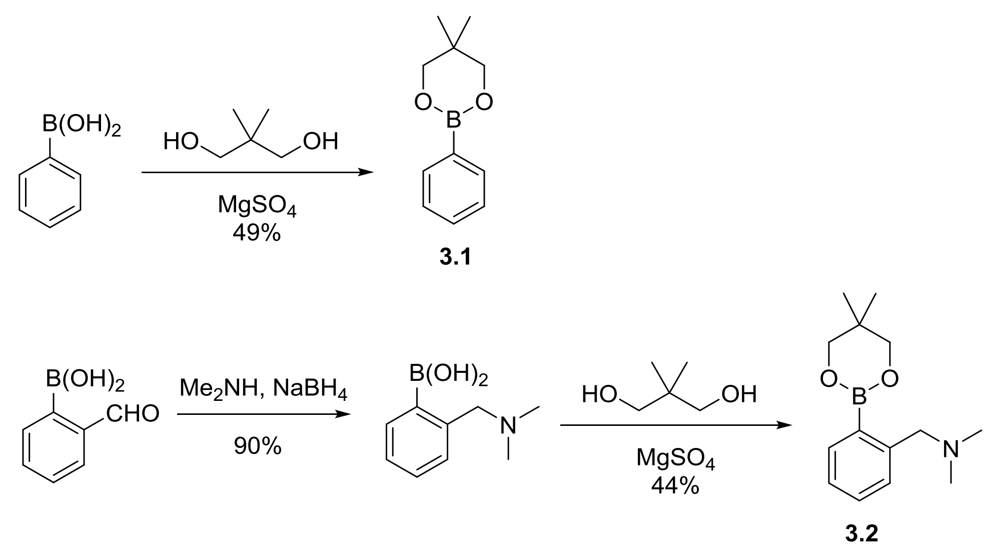

The rate of faster-exchanging boronic ester **3.2** could be monitored through coalescence between bound and unbound glycol methyl resonances in ^{1}H NMR at varied temperatures (Figure 3.2c).[172] The calculated rate of tranesterification was determined to be ~3000/s with an activation energy of 12.6 kcal/mol. The rate of transesterification of the slower exchanging boronic ester **3.1** could not be monitored through coalescence, and was instead determined via 2D EXchange Spectroscopy (EXSY)[173] as 0.016 ± 0.004/s (Figure 3.2b), five orders of magnitude slower than variant **3.2** which has a neighboring *o*-dimethylaminomethyl group, confirming the earlier observation of strong influence of neighboring group on boronic ester exchange kinetics. It is believed that the *o*-aminomethyl acts as a proximal base to facilitate the proton transfer between the leaving group diol on the boronate and the protonated ammonium during transesterification.[163,174,175]

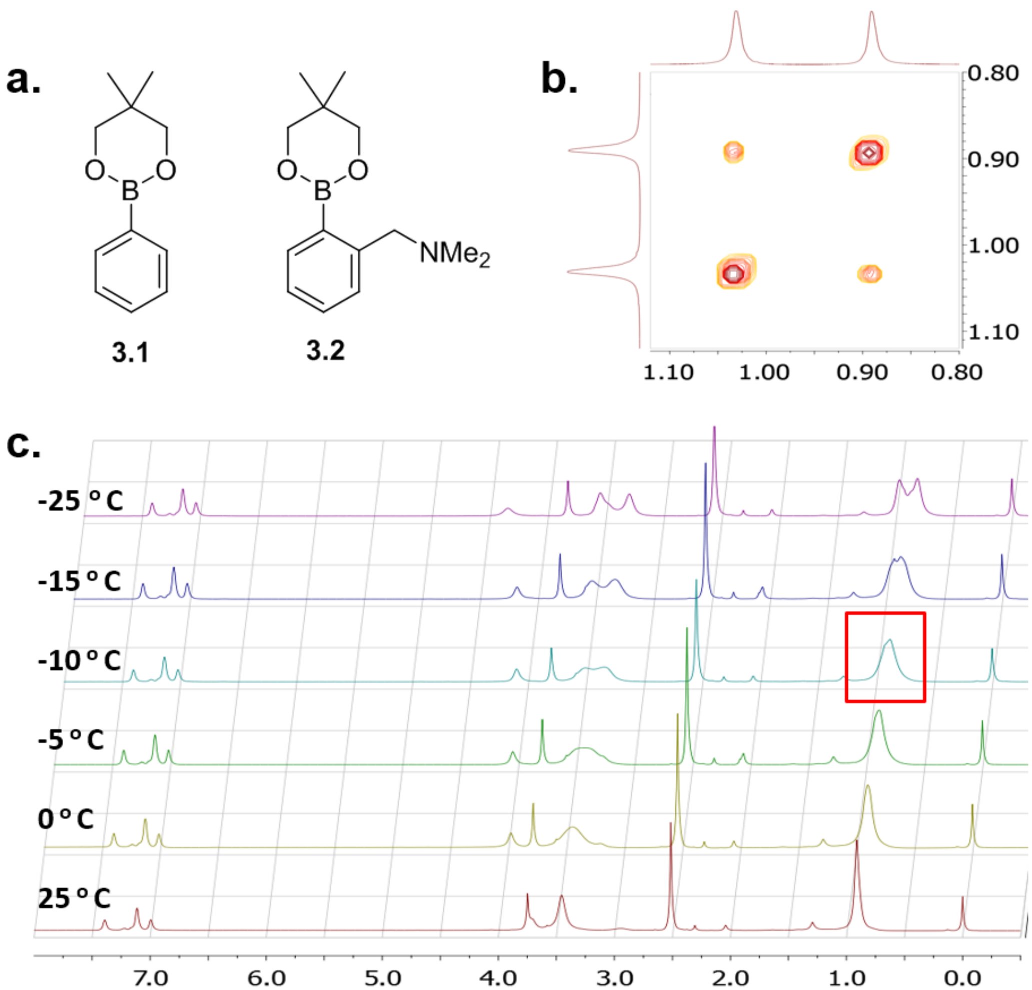

4

Figure 3.2 NMR kinetic study of boronic ester transesterification. **a.** The two model compounds, slower exchanging boronic ester **3.1** and faster exchanging boronic ester **3.2**. **b.** EXSY results for compound **3.1** shows $k = 0.016 \pm 0.004$/s. **c.** Coalescence for compound **3.2** shows $k = \sim 3000$/s.

We then moved to transfer of this molecular design to dynamically crosslinked polymers. First, di-boronic ester crosslinkers of the slow (**3.4**) and fast (**3.6**) variants were synthesized.

Crosslinker **3.4** was synthesized starting from S_N2 substitution of both ends of diethylene glycol with 4-bromobenzyl bromide[176] followed by Miyaura coupling with bis(pinacolato)diboron[37] to form a telechelic di-boronic ester species. The kinetically inert pinacol esters were deprotected with sodium meta-periodate[177] and replaced with the more labile propylene glycol ester[178] for dynamic crosslinking (Scheme 3.2a). Faster-exchanging crosslinker **3.6** was prepared via reductive amination of 2-formyl boronic acid with methylamine followed by nucleophilic substitution of 1,6-dibromohexane, and finally esterification with propylene glycol[178] (Scheme 3.2b) (full details of synthesis and characterization are in Experimental).

Scheme 3.2 Synthesis of Di-boronic Ester Crosslinkers and 1,2-diol Containing Polycyclooctene Polymer[a]

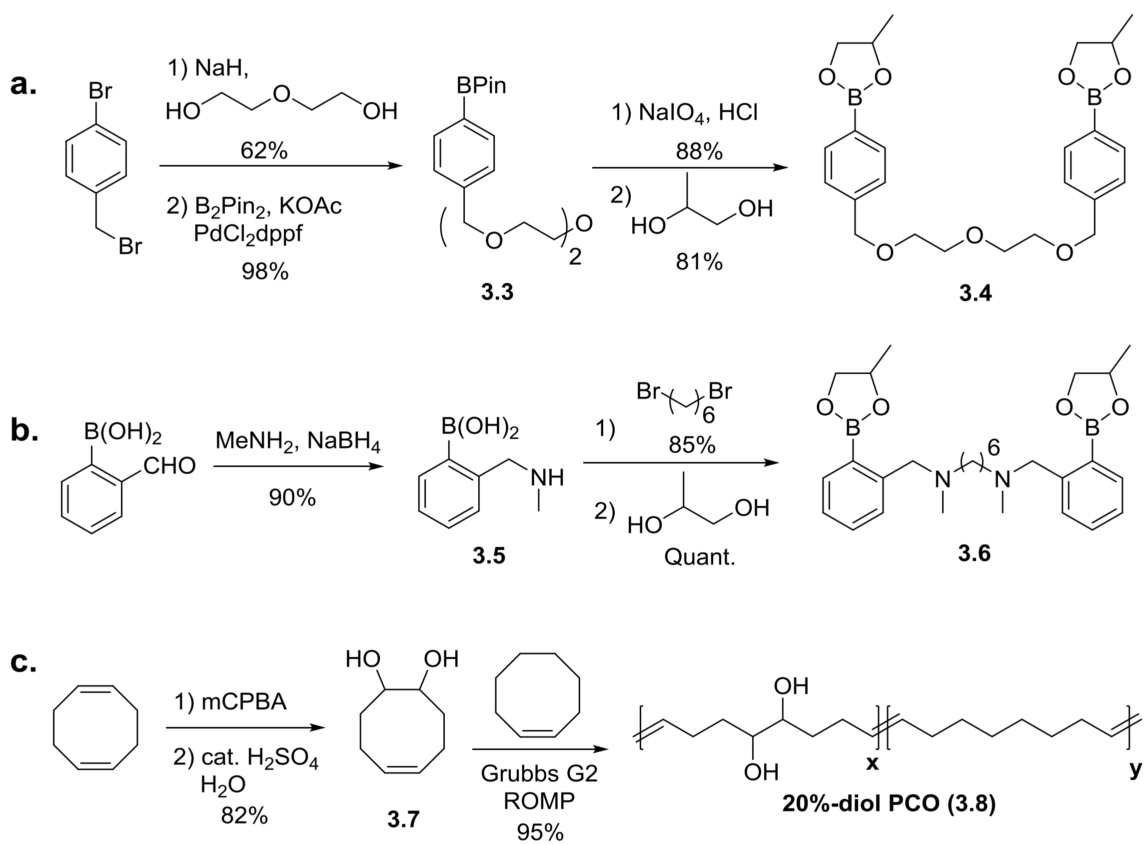

[a]**a.** Synthesis of 'slow' di-phenylboronic ester crosslinker **3.4**. **b.** Synthesis of 'fast' di-*o*-(dimethylaminomethyl) phenylboronic ester crosslinker **3.6**. **c.** Synthesis of 1,2-diol containing polycyclooctene (20%-diol PCO; **3.8**).

We chose to synthesize the 1,2-diol containing polymer backbone using ring-opening metathesis polymerization of cyclooctene-based monomers (ROMP).[179] Dihydroxylated cyclooctene (dHCO) monomer **3.7** was prepared via stoichiometrically controlled epoxidation of cyclooctadiene followed by acid catalyzed epoxide ring opening, which was then copolymerized with cyclooctene to afford 1,2-diol containing polycyclooctene polymer (**3.8**) (M_n 16.5 kDa; PDI 1.89 (GPC shown in Figure 3.3) Scheme 3.2c, with full details of synthesis Experimental).

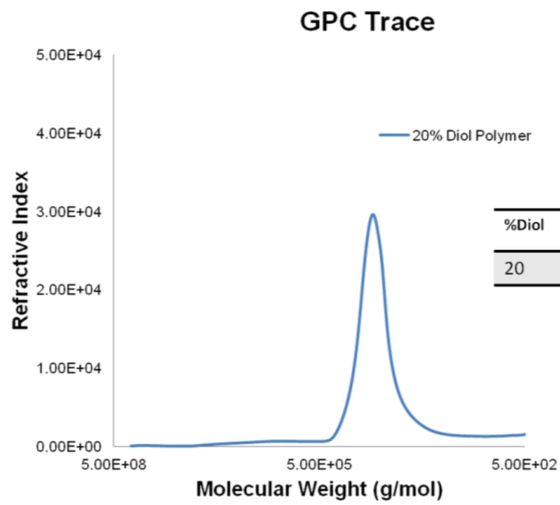

%Diol	%CO	M_n (g/mol)	PDI	T_m (°C)
20	80	1.65×10^5	1.89	35.1

Figure 3.3 GPC trace for 20%-diol PCO polymer

3.2.2. Solution Rheology Studies of Crosslinked Gels & Stress Relaxation of Crosslinked Network

Next, we used solution rheology to monitor the bulk dynamic properties of polymer networks crosslinked by different boronic ester crosslinkers (Figure 3.4a). A solution of polymer **3.8** in toluene was crosslinked with compound **3.4** or **3.6**. This caused gelation in sample with crosslinker **3.4**, while the sample crosslinked by **3.6** showed only a mild increase in viscosity. This is in qualitative agreement with the small molecule exchange kinetics (Figure 3.2), and is reflected in the observed moduli of the samples. The sample with slower crosslinker **3.4** shows a noticeably higher elastic (G') than viscous (G") modulus throughout the range of frequencies tested, showing a high resistance to flow corroborating the relatively inert nature of the crosslinker. On the other hand, the sample crosslinked by **3.6** shows comparable elastic and viscous moduli in the range of tested frequencies, showing a much lower resistance to flow consistent with rapidly shuffling crosslinkers. Finally, the crossover frequency of G' and G" of crosslinker **3.4** sample, corresponding to its gel point, is beyond the lowest frequency tested (0.01 Hz), which is several orders of magnitude lower than the ~1 Hz crossover frequency of sample crosslinked by **3.6**. These results corroborate the difference in rates determined in small molecule exchange and demonstrate the applicability of the concept to the gel state.

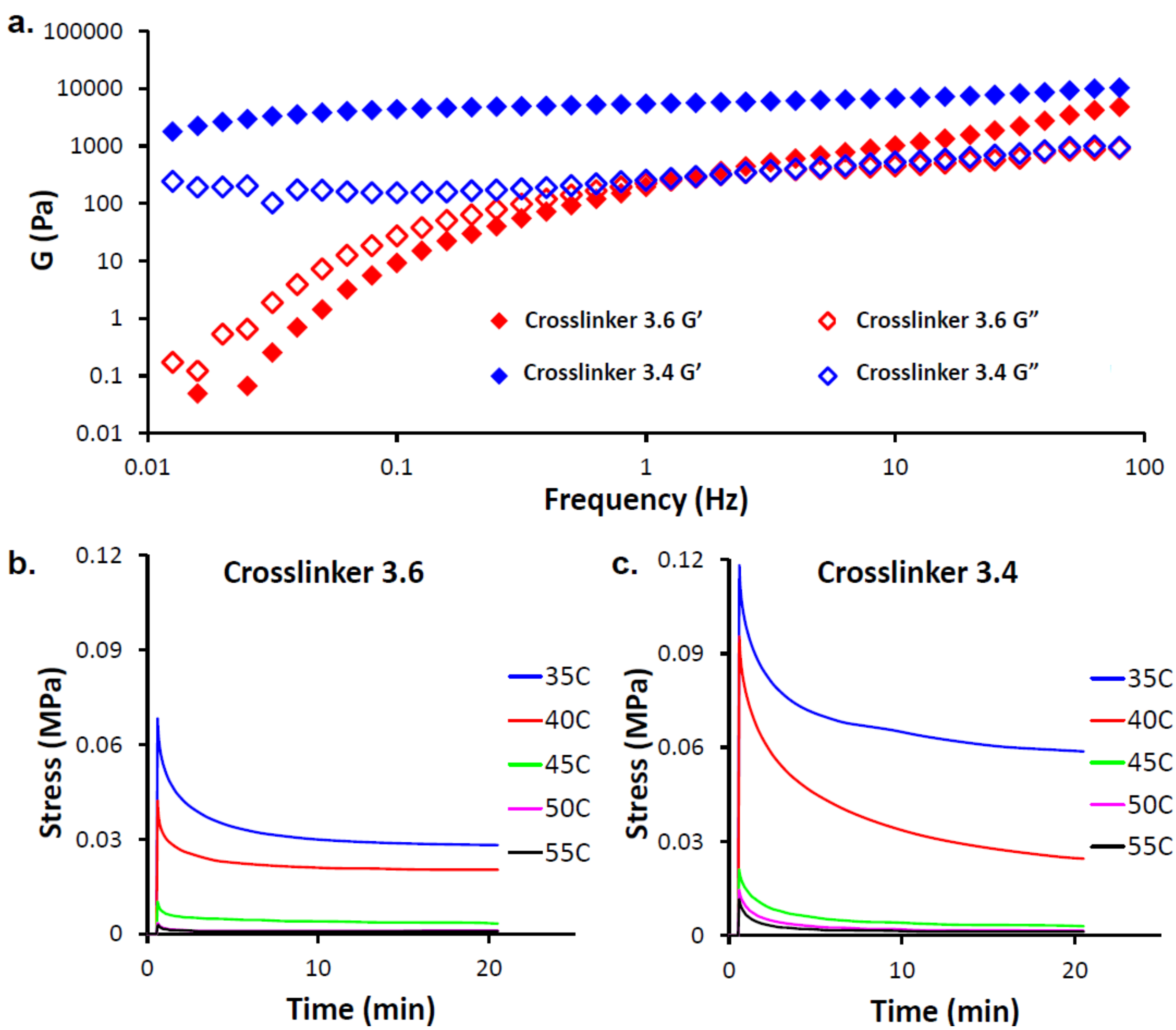

Figure 3.4 Solution rheology and stress relaxation data. **a.** Rheological data showing storage (diamond) and loss (square) moduli for samples crosslinked with compounds **3.6 (**unfilled) and **3.4 (**filled). **b & c.** Stress relaxation data for **3.8** crosslinked with di-boronic esters **3.6** (b) or **3.4** (c).

To further correlate the small molecule kinetics with dynamic properties of the solid polymer, we investigated the malleability of the samples by performing stress-relaxation studies of 20%-diol PCO crosslinked with 1.0% of either crosslinker **3.4** or **3.6** at various temperatures ranging from 35 to 55 degrees. We found, given identical crosslinking percentages, that solid polymer samples crosslinked with crosslinker **3.6** (Figure 3.3b) released stress much faster (within 5 min for 2% strain) than samples crosslinked by **3.4** (>20 min for 2% strain; Figure 3.3c) at all temperatures, providing good evidence that variations in small molecule properties can manifest in tunable malleability for materials in the solid state. The sample containing the fast exchange boronic ester (crosslinker **3.6**) is significantly more malleable than the system crosslinked by the slow exchange boronic ester.

3.2.3 Bulk Self-healing Experiments of Crosslinked Network

We prepared dynamically crosslinked **3.8** samples and performed self-healing experiments on these samples. Crosslinked bulk samples of 20%-diol PCO polymers were prepared using both the fast and slow di-boronic ester crosslinkers. To ensure that there were enough dynamic units present without making the material too stiff through overcrosslinking, crosslinking percentages were empirically chosen to be 0.5 and 1.0% with respect to monomer. Solution cast polymer films were concentrated in a vacuum oven and melt pressed to afford elastomeric samples (details of sample preparation and mechanical property studies are in the Supporting Information). The mechanical properties of the samples are summarized in Table 4.1. For self-healing test, we completely cut through the sample with a razor blade and gently placed the cut interfaces together for one minute and allowed them to heal for 16 hours.

First we tested for the thermal transitions of the crosslinked network to test the temperature at which robust self-healing could occur. Differential scanning calorimetry (DSC) showed a melting transition (T_m) centered at ~35 ºC (Figure 3.5). This semicrystalinity does not allow the efficient chain dynamics that are necessary for self-healing at ambient temperatures, and indeed self-healing was not observed for the material at room temperature (data not shown). In order to overcome the effects of the semicrystaline network, a slightly elevated temperature (50 °C) was required to produce effective healing.

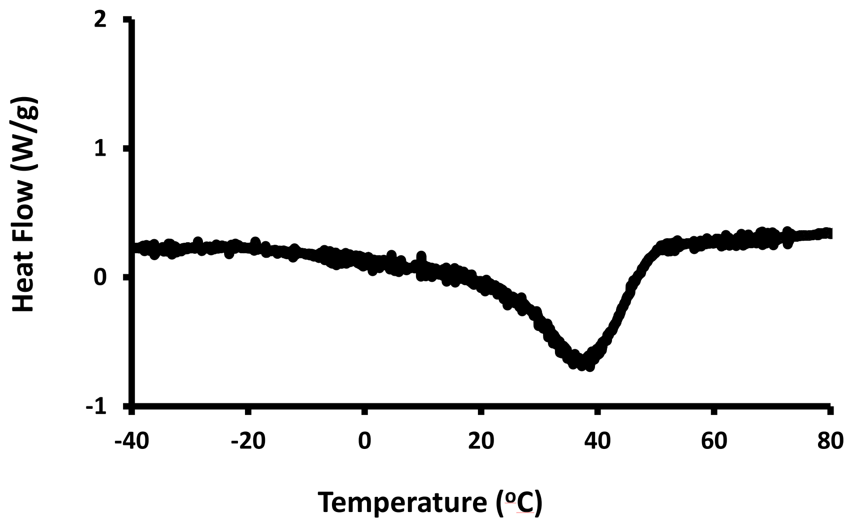

Figure 3.5 Differential scanning calorimetry data of 20%-diol PCO.

Only the sample containing the fast crosslinker **3.6** was able to self-heal, almost quantitatively recovering the material's mechanical properties including Young's modulus, yield strength, ultimate tensile strain and strength (Figure 3.6a&c, and Table 4.1). On the other hand, the sample containing the slow-exchange crosslinker **3.4** showed minimal or no healing (Figure 3.6b&d, and Table 3.1). Furthermore, both uncrosslinked and permanently crosslinked (via 1,4-diisocyanatobutane) **3.8** samples did not display any healing, verifying that healing was not due to other mechanisms, such as through hydrogen bonding of the diol moieties in the PCO backbone (see Figure 3.6e&f, and Table 3.2). Together, these results indicate that dynamic shuffling of the boronic esters is directly responsible for self-healing of our materials. Crucially, the variability in healing efficiencies follows the expected trend based on kinetics of the small molecule boronic ester transesterification reaction, directly demonstrating the effect of small molecule dynamics on emergent bulk self-healing.

Table 3.1 Static Tensile Data for Dynamically Crosslinked Samples

Sample	0.5% Fast (**3.6**)	1.0% Fast (**3.6**)	0.5% Slow (**3.4**)	1.0% Slow (**3.4**)
E^a (pristine)	4.68 ± 0.39	4.86 ± 0.86	4.55 ± 0.45	3.23 ± 0.52
E (healed)	4.63 ± 0.32	4.81 ± 0.40	4.15 ± 0.13	--
ε^b (pristine)	345 ± 80	174 ± 10	446 ± 27	121 ± 31
ε (healed)	344 ± 160	158 ± 21	28.3 ± 7.1	--
δ^c (pristine)	1.85 ± 0.38	1.51 ± 0.27	1.97 ± 0.36	1.12 ± 0.18
δ (healed)	1.75 ± 0.35	1.47 ± 0.51	0.723 ± 0.10	--

[a] Young's modulus calculated from the initial slope of static stress strain curves in (MPa). [b] Ultimate tensile strain (mm/mm). [c] Ultimate tensile strength (MPa).

Table 3.2 Mechanical Properties of Control Samples

Sample Type	Permanent-0.5%	Permanent-1.0%	Uncrosslinked
E^a	0.400 ± 0.071	0.25 ± 0.028	2.23±0.28
ε^b	76% ± 19%	83% ± 9 %	1034% ± 66%

[a] Young's modulus calculated from the initial slope of static stress strain curves in (MPa). [b] Ultimate tensile strain (mm/mm).

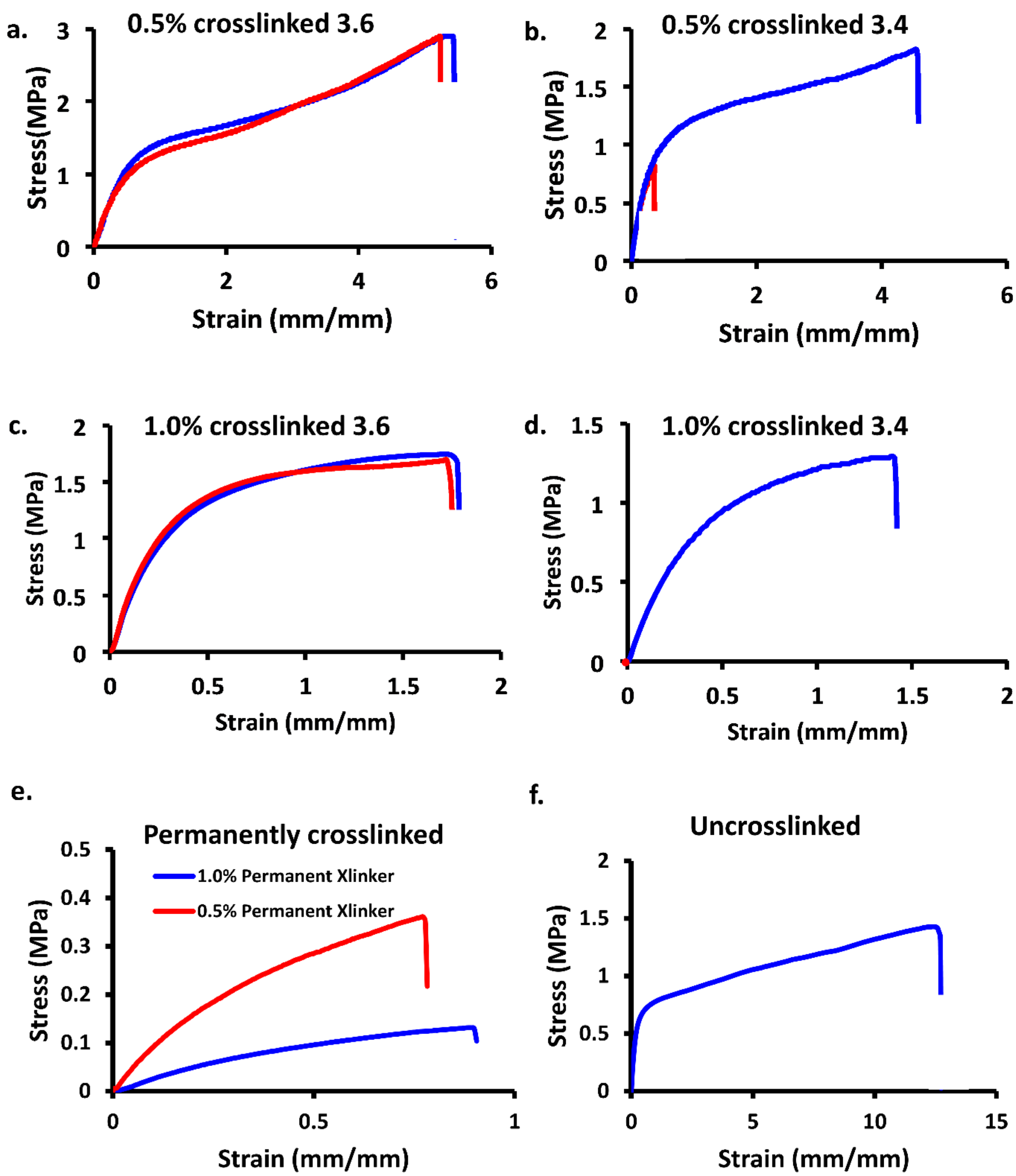

Figure 3.6 Self-healing tests for crosslinked 20%-diol PCO. For a – d, red curves are healed samples and blue curves are pristine samples. **a.** Sample crosslinked by 0.5-mol% compound **3.6**. **b.** Sample crosslinked by 0.5-mol% compound **3.4**. **c.** Sample crosslinked by 1.0-mol% compound **3.6**. **d.** Sample crosslinked by 1.0-mol% compound **3.4.** Absence of red (self-healed) curve is due to complete lack of healing in this particular sample. **e.** Samples crosslinked through 1,4-butanediisocyanate (1.0% blue, 0.5% red). Absence of self-healing curves is due to complete lack

of healing for these samples. **f.** Uncrosslinked sample. Absence of self-healing curves is due to complete lack of healing.

3.2.4 Reprocessability of Crosslinked Network

To prove the thermal stability of the material over multiple cycles of high temperature reprocessing, the crosslinked **3.8** materials were tested through thermogravimetric analysis (TGA). The thermal stability of the materials (Figure 3.7) is high and remains unchanged as a result of the crosslinker, suggesting that the incorporation of boronic esters into the polymer does not decrease the thermal stability.

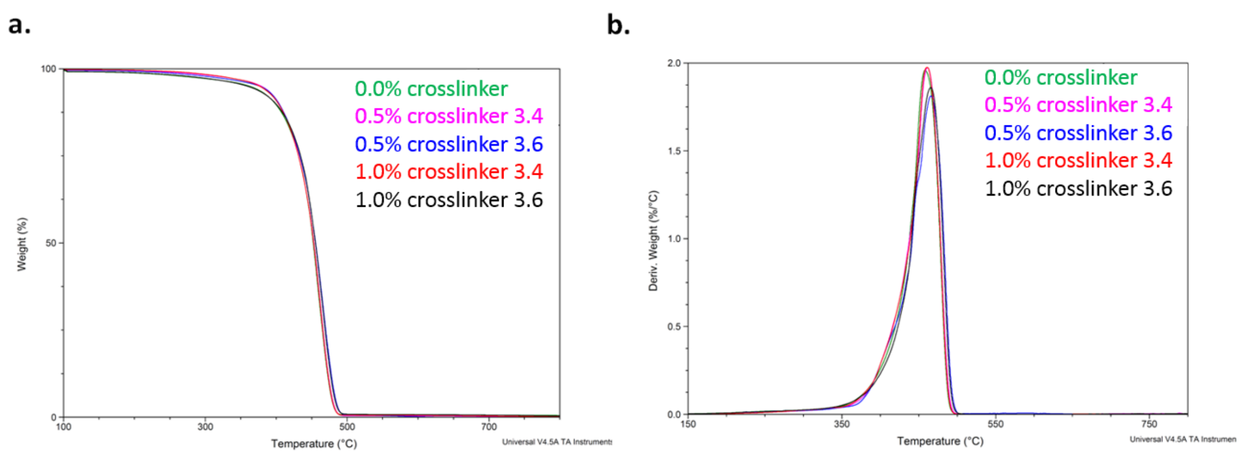

Figure 3.7. TGA for crosslinked polymer samples for 0, 0.5, 1.0-mol% fast (compound **3.6**) and slow (compound **3.4**) (**a**) mass loss versus temperature and (**b**) derivative of mass loss versus temperature.

Given the thermal stability of the crosslinked compounds as well as the dynamic nature of the crosslinked materials, we further envisioned that the dynamic boronic ester crosslinks could allow for reprocessing of the samples. To test this, the **3.8** crosslinked sample by 0.5 mol % **3.6** was cut into small millimeter sized pieces and then melt pressed at 80 ^{o}C to reform the bulk materials (Figure 3.8b). Static tensile tests proved that after multiple cycles, the materials were able to recover most of their mechanical properties (Figure 3.8a).

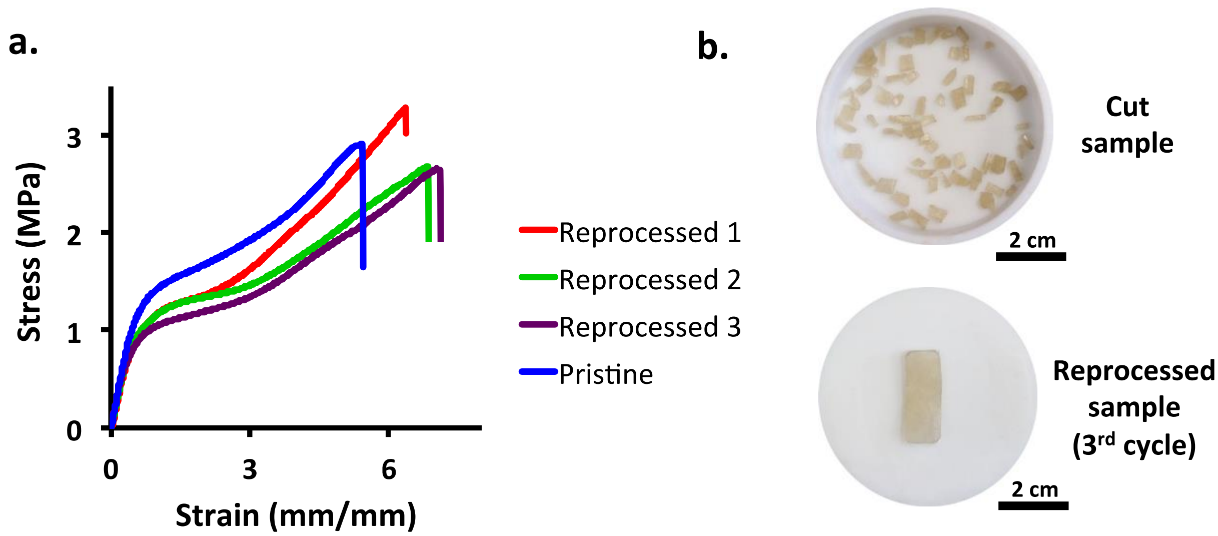

Figure 3.8 Reprocessing (three cycles) of 20%-diol PCO crosslinked by 0.5-mol% fast-exchanging crosslinker. **a.** Static mechanical testing of reprocessed samples. **b.** The image on the top was the sample cut into mm sized pieces and on the bottom was the reprocessed sample after the third repetition.

3.2.4 Hydrolytic stability of the crosslinked network

One potential issue of our design is the hydrolytic stability of boronic ester linkages. To test for this, we immersed our crosslinked samples in water overnight and then monitored any change of mass and mechanical properties. The mass change was negligible for samples before and after water submersion, indicating no appreciable transesterification and dissolution of the resulting small molecules (Table 3.3). Importantly mechanical properties of the samples after submersion in water over night remained unchanged (Figure 3.9), further confirming the hydrolytic stability of boronic ester embedded in our polymer system. Despite the fact that small molecule boronic esters are susceptible to hydrolysis,[162] the relatively hydrophobic local environment of our bulk polymer can prohibit the uptake of water into the crosslinked network, effectively shielding the boronic esters from hydrolysis.

Table 3.3 Mass of Samples Before and After Submerging in Water

Sample	0.5% slow	1.0% slow	0.5% fast	1.0% fast
Before (g)	0.2459	0.3672	0.3992	0.3238
After (g)	0.2462	0.3675	0.3991	0.3238
Δ mass (%)	0.12%	0.08%	-0.02%	0.0%

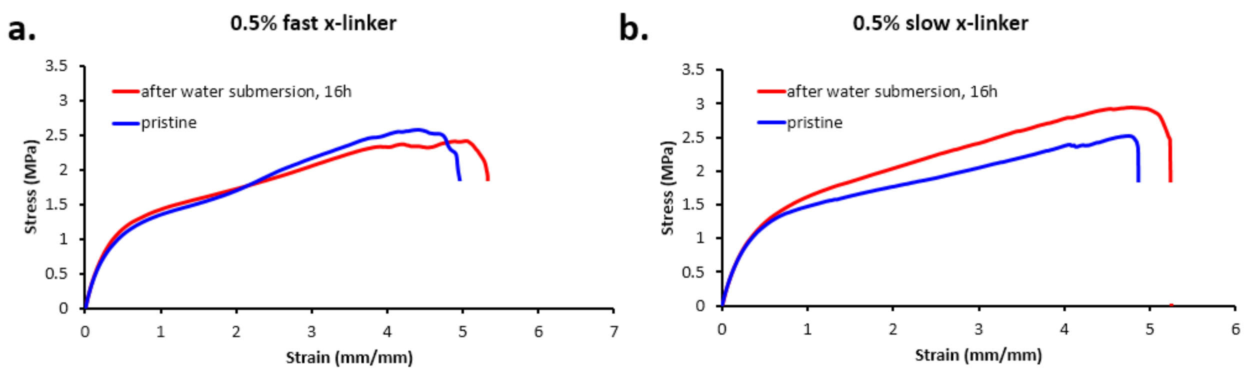

Figure 3.9 Mechanical testing data for crosslinked polymer samples for 0.5-mol% fast (compound **3.6**) (**a**) slow (compound **3.4**) (**b**) crosslinkers shows that mechanical integrity of samples are not compromised after submerging in water.

3.3 Conclusions and Outlook

In conclusion, we have demonstrated that the dynamic boronic ester linkage can be successfully used to prepare malleable, self-healing, and reprocessable covalent network polymers. The dynamic exchange of boronic esters bonds afforded the observed dynamic properties. Significantly, tuning the rates of trans-esterification in the crosslinkers varied the malleability and the efficiency of self-healing, demonstrating a direct link between small molecule kinetics and rate of self-healing. This work shows the possibility of bottom-up rational design of dynamic materials with tunable dynamic properties through simple perturbations of small molecule structure and kinetics, which may give rise to materials with a variety of applications, ranging from robust self-healing elastomers to reprocessable thermosets, described in the next chapter.

3.4 References

(1) Kloxin, C. J.; Scott, T. F.; Adzima, B. J.; Bowman, C. N. Covalent Adaptable Networks (CANs): A Unique Paradigm in Crosslinked Polymers *Macromolecules* **2010**, *43*(6), 2643-2653.

(2) Wojtecki, R. J.; Meador, M. A.; Rowan, S. J. Using the dynamic bond to access macroscopically responsive structurally dynamic polymers *Nat Mater* **2011**, *10*(1), 14-27.

(3) Montarnal, D.; Capelot, M.; Tournilhac, F.; Leibler, L. Silica-Like Malleable Materials from Permanent Organic Networks *Science* **2011**, *334*(6058), 965-968.

(4) Maeda, T.; Otsuka, H.; Takahara, A. Dynamic covalent polymers: Reorganizable polymers with dynamic covalent bonds *Progress in Polymer Science* **2009**, *34*(7), 581-604.

(5) Denissen, W.; Rivero, G.; Nicolaÿ, R.; Leibler, L.; Winne, J. M.; Du Prez, F. E. Vinylogous Urethane Vitrimers *Advanced Functional Materials* **2015**n/a-n/a.

(6) Taynton, P.; Yu, K.; Shoemaker, R. K.; Jin, Y.; Qi, H. J.; Zhang, W. Heat- or Water-Driven Malleability in a Highly Recyclable Covalent Network Polymer *Advanced Materials* **2014**, *26*(23), 3938-3942.

(7) Ghosh, B.; Urban, M. W. Self-Repairing Oxetane-Substituted Chitosan Polyurethane Networks *Science* **2009**, *323*(5920), 1458-1460.

(8) Chen, X.; Dam, M. A.; Ono, K.; Mal, A.; Shen, H.; Nutt, S. R.; Sheran, K.; Wudl, F. A Thermally Re-mendable Crosslinked Polymeric Material *Science* **2002**, *295*(5560), 1698-1702.

(9) Amamoto, Y.; Otsuka, H.; Takahara, A.; Matyjaszewski, K. Self-Healing of Covalently Crosslinked Polymers by Reshuffling Thiuram Disulfide Moieties in Air under Visible Light *Advanced Materials* **2012**, *24*(29), 3975-3980.

(10) Lu, Y.-X.; Guan, Z. Olefin Metathesis for Effective Polymer Healing via Dynamic Exchange of Strong Carbon–Carbon Double Bonds *Journal of the American Chemical Society* **2012**, *134*(34), 14226-14231.

(11) Imato, K.; Nishihara, M.; Kanehara, T.; Amamoto, Y.; Takahara, A.; Otsuka, H. Self-Healing of Chemical Gels Crosslinked by Diarylbibenzofuranone-Based Trigger-Free Dynamic Covalent Bonds at Room Temperature *Angewandte Chemie International Edition* **2012**, *51*(5), 1138-1142.

(12) Cordier, P.; Tournilhac, F.; Soulie-Ziakovic, C.; Leibler, L. Self-healing and thermoreversible rubber from supramolecular assembly *Nature* **2008**, *451*(7181), 977-980.

(13) Chen, Y.; Kushner, A. M.; Williams, G. A.; Guan, Z. Multiphase design of autonomic self-healing thermoplastic elastomers *Nature Chemistry* **2012**, *4*(6), 467-472.

(14) Mozhdehi, D.; Ayala, S.; Cromwell, O. R.; Guan, Z. Self-Healing Multiphase Polymers via Dynamic Metal-Ligand Interactions *Journal of the American Chemical Society* **2014**.

(15) Burattini, S.; Greenland, B. W.; Merino, D. H.; Weng, W.; Seppala, J.; Colquhoun, H. M.; Hayes, W.; Mackay, M. E.; Hamley, I. W.; Rowan, S. J. A Healable Supramolecular Polymer Blend Based on Aromatic Ï€âˆ'Ï€ Stacking and Hydrogen-Bonding Interactions *Journal of the American Chemical Society* **2010**, *132*(34), 12051-12058.

(16) Yount, W. C.; Loveless, D. M.; Craig, S. L. Small-Molecule Dynamics and Mechanisms Underlying the Macroscopic Mechanical Properties of Coordinatively Crosslinked Polymer Networks *Journal of the American Chemical Society* **2005**, *127*(41), 14488-14496.

(17) Yount, W. C.; Loveless, D. M.; Craig, S. L. Strong Means Slow: Dynamic Contributions to the Bulk Mechanical Properties of Supramolecular Networks *Angewandte Chemie International Edition* **2005**, *44*(18), 2746-2748.

(18) Weng, W.; Beck, J. B.; Jamieson, A. M.; Rowan, S. J. Understanding the Mechanism of Gelation and Stimuli-Responsive Nature of a Class of Metallo-Supramolecular Gels *Journal of the American Chemical Society* **2006**, *128*(35), 11663-11672.

(19) Giuseppone, N.; Fuks, G.; Lehn, J.-M. Tunable Fluorene-Based Dynamers through Constitutional Dynamic Chemistry *Chemistry – A European Journal* **2006**, *12*(6), 1723-1735.

(20) Sui, Z.; King, W. J.; Murphy, W. L. Protein-Based Hydrogels with Tunable Dynamic Responses *Advanced Functional Materials* **2008**, *18*(12), 1824-1831.

(21) Ying, H.; Zhang, Y.; Cheng, J. Dynamic urea bond for the design of reversible and self-healing polymers *Nat Commun* **2014**, *5*.

(22) Hall, D. G. *Boronic Acids: Preparation and Applications in Organic Synthesis, Medicine and Materials*; John Wiley & Sons, 2012; Vol. 2.

(23) Wulff, G.; Lauer, M.; Böhnke, H. Rapid Proton Transfer as Cause of an Unusually Large Neighboring Group Effect *Angewandte Chemie International Edition in English* **1984**, *23*(9), 741-742.

(24) Fujita, N.; Shinkai, S.; James, T. D. Boronic Acids in Molecular Self-Assembly *Chemistry – An Asian Journal* **2008**, *3*(7), 1076-1091.

(25) Jäkle, F. Advances in the Synthesis of Organoborane Polymers for Optical, Electronic, and Sensory Applications *Chemical Reviews* **2010**, *110*(7), 3985-4022.

(26) James, T. D.; Sandanayake, K. R. A. S.; Shinkai, S. Saccharide Sensing with Molecular Receptors Based on Boronic Acid *Angewandte Chemie International Edition in English* **1996**, *35*(17), 1910-1922.

(27) Edwards, N. Y.; Sager, T. W.; McDevitt, J. T.; Anslyn, E. V. Boronic Acid Based Peptidic Receptors for Pattern-Based Saccharide Sensing in Neutral Aqueous Media, an Application in Real-Life Samples *Journal of the American Chemical Society* **2007**, *129*(44), 13575-13583.

(28) Bapat, A. P.; Roy, D.; Ray, J. G.; Savin, D. A.; Sumerlin, B. S. Dynamic-Covalent Macromolecular Stars with Boronic Ester Linkages *Journal of the American Chemical Society* **2011**, *133*(49), 19832-19838.

(29) He, L.; Fullenkamp, D. E.; Rivera, J. G.; Messersmith, P. B. pH responsive self-healing hydrogels formed by boronate-catechol complexation *Chemical Communications* **2011**, *47*(26), 7497-7499.

(30) Niu, W.; O'Sullivan, C.; Rambo, B. M.; Smith, M. D.; Lavigne, J. J. Self-repairing polymers: poly(dioxaborolane)s containing trigonal planar boron *Chemical Communications* **2005**(34), 4342-4344.

(31) Cash, J. J.; Kubo, T.; Bapat, A. P.; Sumerlin, B. S. Room-Temperature Self-Healing Polymers Based on Dynamic-Covalent Boronic Esters *Macromolecules* **2015**.

(32) Claridge, T. D. W. In *Tetrahedron Organic Chemistry Series*; Timothy, D. W. C., Ed.; Elsevier: 2009; Vol. Volume 27, p 99-128.

(33) Claridge, T. D. W. In *Tetrahedron Organic Chemistry Series*; Timothy, D. W. C., Ed.; Elsevier: 2009; Vol. Volume 27, p 247-302.

(34) Collins, B. E.; Metola, P.; Anslyn, E. V. On the Rate of Boronate Ester Formation in ortho-Aminomethyl Functionalized Phenyl Boronic Acids *Supramol. Chem.* **2013**, *25*(2), 79-86.

(35) Zhu, L.; Shabbir, S. H.; Gray, M.; Lynch, V. M.; Sorey, S.; Anslyn, E. V. A Structural Investigation of the N−B Interaction in an o-(N,N-Dialkylaminomethyl)arylboronate System *Journal of the American Chemical Society* **2006**, *128*(4), 1222-1232.

(36) Lee, S.-H.; Park, Y.; Wee, K.-R.; Son, H.-J.; Cho, D. W.; Pac, C.; Choi, W.; Kang, S. O. Significance of Hydrophilic Characters of Organic Dyes in Visible-Light Hydrogen Generation Based on TiO2 *Org. Lett.* **2009**, *12*(3), 460-463.

(37) Ding, X.; Chen, L.; Honsho, Y.; Feng, X.; Saengsawang, O.; Guo, J.; Saeki, A.; Seki, S.; Irle, S.; Nagase, S.; Parasuk, V.; Jiang, D. An n-Channel Two-Dimensional Covalent Organic Framework *Journal of the American Chemical Society* **2011**, *133*(37), 14510-14513.

(38) Southwood, T. J.; Curry, M. C.; Hutton, C. A. Factors affecting the efficiency and stereoselectivity of α-amino acid synthesis by the Petasis reaction *Tetrahedron* **2006**, *62*(1), 236-242.

(39) Bielawski, C. W.; Grubbs, R. H. Highly Efficient Ring-Opening Metathesis Polymerization (ROMP) Using New Ruthenium Catalysts Containing N-Heterocyclic Carbene Ligands *Angewandte Chemie International Edition* **2000**, *39*(16), 2903-2906.

3.5 Experimental

General Experimental Information: Unless otherwise noted, reactions were carried out with stirring with a magnetic stir bar at room temperature. Anhydrous solvents were purified through a column of alumina according to the method described by Pangborn *et al*. before use[151]. All commercial reagents were used as received unless otherwise noted. Flash column chromatography was performed by forced flow of indicated solvent using an automated column (CombiFlash, Teledyne Isco). ^{1}H NMR spectra were recorded at 500 MHz on Bruker GN-500 or CRYO-500 spectrometers. ^{1}H NMR chemical shifts are reported as δ values in ppm relative to TMS or residual solvent: $CDCl_3$ (7.27 ppm), and CD_3OD (3.31 ppm). ^{1}H NMR data are reported as follows: chemical shift in ppm, multiplicity (s = singlet, d = doublet, t = triplet, q = quartet), coupling constants in Hz, and relative integration in number of protons. Multiplets (m) are reported over the range of chemical shift at which they appear. For ^{13}C NMR spectra, only chemical shift values are reported. For boronic acid and ester compounds, the ipso carbon resonances were not observed as is consistent with the literature.[180] Mass Spectra were obtained on Micromass LCT (ES-MS, low resolution), and Micromass Autospec (ES-MS and GC-MS, high resolution). Gel Permeation Chromatography (GPC) traces were obtained on an Agilent 1100 SEC system using a PLGel Mixed-C column from Polymer Labs (Amherst, MA). THF was used as eluting solvent at a flow rate of 1.0 mL/min. Number averaged and weight averaged molecular weight distributions (M_n and M_w, respectively) of samples were measured with respect to polystyrene (PS) standards purchased from Aldrich (Milwaukee, WI).

Phenylboronic acid neopentyl glycol ester (3.1). In a round bottom flask, phenylboronic acid (1.00 g; 8.20 mmol), neopentyl glycol (0.854 g; 8.20 mmol), and $MgSO_4$ (~8 g) were suspended over toluene (30 mL), and allowed to stir at room temperature overnight. The resultant mixture was gravity filtered, concentrated *in vacuo* and purified through flash column chromatography (0 – 20% EtOAc in hexanes, eluting fractions ~0 – 10% EtOAc) to yield a white crystalline solid (0.768 g, 49%).

^{1}H NMR (500 MHz, $CDCl_3$): δ 7.82 (d, *J* = 6.9 Hz, 2H), 7.44 (t, *J* = 7.4 Hz, 1H), 7.37 (t, *J* = 7.4 Hz, 2H), 3.79 (s, 4H), 1.04 (s, 6H). ^{13}C NMR (125 MHz, $CDCl_3$): δ 133.9, 130.7, 127.6, 72.4, 31.9, 22.0.

2-((Dimethylamino)methyl)phenylboronic acid. Following a similar strategy from literature,[181] 2-formylphenylboronic acid (0.500 g, 3.33 mmol), and anhydrous magnesium sulfate (~3 g), were combined in anhydrous methanol (20 mL). The reaction mixture was cooled to 0 °C under a nitrogen atmosphere. To this mixture dimethyl amine (2M in methanol, 3.33 mL, 6.66 mmol) was added dropwise and stirred at 0 °C for 30 min followed by 3 h at ambient temperature. The reaction pot was again cooled to 0 °C and $NaBH_4$ (0.190 g, 5.0 mmol) was added in three portions at 10 min intervals. The reaction mixture was then stirred again at room temperature for another 1 h. The reaction mixture was concentrated to 1/3 of its original volume *in vacuo* with the bath temperature at low temperature. Cold deionized water (5 mL) and concentrated aqueous $NaHCO_3$ (5 mL) were added to the above concentrated solution, stirred for 10 min and extracted with dichloromethane (3 x 50 mL). Combined organic phase was dried over Na_2SO_4 and concentrated *in vacuo* to yield at white crystalline solid (0.53 g, 89%).

^{1}H NMR (500 MHz, CD_3OD): δ 7.51 (t, *J* = 5.8 Hz, 1H), 7.20 (m, 3H), 3.99 (s, 2H), 2.61 (s, 3H). ^{13}C NMR (125 MHz, CD_3OD): δ 139.1, 131.3, 126.9, 124.9, 123.9, 65.1, 44.1.

(2-((Dimethylamino)methyl)phenyl)boronic acid neopentyl glycol ester (3.2). (2-((Dimethylamino)methyl)phenyl)boronic acid (0.101 g, 0.564 mmol) was suspended in toluene (10 mL), to which was added anhydrous $MgSO_4$ (1.00 g) and neopentyl glycol (59 mg, 0.564

mmol). The mixture was allowed to stir for 16 h at 70 °C, after which excess solid was filtered through gravity, and the filtrate evaporated *in vacuo*. Yield 65 mg (47 %).

^{1}H NMR (500 MHz, acetone-d^6): δ 7.40 (m, 1H), 7.12 (m, 2H), 7.00 (m, 1H), 3.74 (s, 2H), 3.58 (s, 4H), 2.51 (s, 6H), 1.00 (s, 6H).

4,4'-(2,2'-oxybis(ethane-2,1-diyl)bis(oxy))bis(methylene)bis(bromobenzene). Synthesis of this compound was modified from Lee *et al*.[176] Diethylene glycol (1.36 mL; 1.53 g, 14.4 mmol) was dissolved in anhydrous THF (60 mL), to which NaH (2.07 g, 86.4 mmol) was added in five batches over 20 min. After stirring for 30 min, 4-bromobenzyl bromide (10.8 g, 43.2 mmol) was added. The mixture was allowed to stir overnight (16 h), after which excess NaH was quenched through slow addition of a saturated aqueous solution of NH_4Cl until no more gas evolved. The solution was concentrated to approximately 1/10 volume, diluted with water (~50 mL), and extracted with DCM (~25 mL x 2). The combined organic layer was dried with anhydrous $MgSO_4$, filtered and concentrated under reduced pressure. The product was purified by flash column chromatography (0-100% EtOAc in hexanes, ~70% EtOAc eluting fractions). 3.96 g (62%) yield clear oil.

^{1}H NMR (500 MHz, $CDCl_3$): δ 7.46 (d, J = 8.3 Hz, 4H), 7.22 (d, J = 8.2 Hz, 4H), 4.52 (s, 4H), 3.69 (m, 4H), 3.65 (m, 4H). ^{13}C NMR (125 MHz, $CDCL_3$): δ 137.4, 131.5, 129.4, 121.5, 72.5, 70.8, 69.7. HRMS (ES-MS): *m / z* calcd for $C_{18}H_{20}O_3Br_2$ $(M+Na)^+$ 464.9677, found 464.9684.

2,2'-(4,4'-(2,2'-oxybis(ethane-2,1-diyl)bis(oxy))bis(methylene)bis(4,1-phenylene))bis(4,4,5,5-tetramethyl-1,3,2-dioxaborolane) (3.3). Synthesis of this compound was modified from Ding *et al*.[177] To a solution of compound 4,4'-(2,2'-oxybis(ethane-2,1-diyl)bis(oxy))bis(methylene)bis(bromobenzene) (3.94 g, 8.87 mmol) in anhydrous 1,4-dioxanes (60 mL), bis(pinacolato)diboron (4.96 g, 19.5 mmol) and KOAc (5.88 g, 59.9 mmol) were suspended. The mixture was degassed by bubbling with dry Ar stream for 1 hr, after which the headspace was purged with dry Ar stream for 15 min. (1,1-Bis(diphenylphosphino)ferrocene) dichloropalladium(II), DCM adduct (200 mg) was added, after which the mixture was further degassed through dry Ar stream for 30 min. The mixture was sealed and heated to 80 ºC and allowed to react overnight (16 hr). The reaction was quenched by opening the mixture to air and allowed to cool to room temperature. The reaction mixture was diluted with water (~80 mL) and extracted with EtOAc (~100 mL x 3). The combined organic layer was washed with brine (~100 mL), dried over anhydrous $MgSO_4$, filtered and evaporated to dryness. The product was purified through flash column chromatography (0-100% EtOAc in hexanes, eluting fraction ~65 % EtOAc). 4.67 g (98%) yield off-white oil.

^{1}H NMR (500 MHz, $CDCl_3$): δ 7.79 (d, J = 7.9 Hz, 4H), 7.35 (d, J = 7.8 Hz, 4H), 4.60 (s, 4H), 3.69 (m, 4H), 3.64 (m, 4H), 1.34 (s, 24H). ^{13}C NMR (125 MHz, $CDCl_3$): δ 141.6, 134.9, 126.9, 83.8, 73.2, 70.7, 69.5, 24.9. HRMS (ES-MS): *m* / *z* calcd for $C_{30}H_{44}O_7B_2$ $(M+Na)^+$ 559.3243, found 559.3255.

((((Oxybis(ethane-2,1-diyl))bis(oxy))bis(methylene))bis(4,1-phenylene))diboronic acid. Synthesis of this compound was modified from Ding *et al*.[177] To a solution of compound 2,2'-(4,4'-(2,2'-oxybis(ethane-2,1-diyl)bis(oxy))bis(methylene)bis(4,1-phenylene))bis(4,4,5,5-tetramethyl-1,3,2-dioxaborolane) (4.65 g, 8.64 mmol) in a 4:1 THF (100 mL):water (25 mL) mixture was added $NaIO_4$ (7.39 g, 34.6 mmol), and allowed to stir for 30 min. 1.0 M aqueous HCl was added (12.5 mL) to the mixture and allowed to react for 24 h. The resulting mixture was then evaporated to dryness *in vacuo* and washed under vacuum filtration with the following solvents: water (~1.5 L), hexanes (~1 L), and diethyl ether (~500 mL). 2.85 g (88%) yield off-white solid.

*[1]H NMR (500 MHz, CD_3OD): δ 7.72 (d, *J* = 7.5 Hz, 2H), 7.57 (d, *J* = 7.4 Hz, 2H), 7.34 (d, *J* = 7.6 Hz, 2H), 7.31 (d, *J* = 7.6 Hz, 2H), 4.56 (s, 4H), 3.66 (m, 4H), 3.65 (m, 4H). *[13]C NMR (125 MHz, CD_3OD): δ 133.6, 133.3, 126.6, 126.5, 72.75, 72.65, 70.2, 69.3. ≠HRMS (ES-MS): *m* / *z* calcd for $C_{22}H_{32}O_7B_2$ $(M+Na)^+$ 451.2304, found 451.2305.

*NMR characterization of this compound was performed in CD_3OD due to limited solubility in non-protic solvents, and thus characterization data is a mixture of multi-methoxy esterified boronic acids.

≠ES-MS characterization of this compound was performed in MeOH solvent. The calculated *m / z* value is for the tetra-methyl esterified boronic ester.

2,2'-((((Oxybis(ethane-2,1-diyl))bis(oxy))bis(methylene))bis(4,1-phenylene))bis(4-methyl-1,3,2-dioxaborolane) (3.4). To a suspension of compound ((((oxybis(ethane-2,1-diyl))bis(oxy))bis(methylene))bis(4,1-phenylene))diboronic acid (1.00 g, 2.67 mmol) in toluene (80 mL), anhydrous $MgSO_4$ (2.57 g, 21.4 mmol) was added, followed by racemic propylene glycol (393 μL; 407 mg, 5.35 mmol). The mixture was allowed to react for 6 h, after which the solid was filtered, and the solvent was removed from filtrate *in vacuo*. 980 mg (82 %) yield light orange oil.

[1]H NMR (500 MHz, $CDCl_3$): δ 7.79 (d, *J* = 7.7 Hz, 4H), 7.37 (d, *J* = 7.7 Hz, 4H), 4.73 (apparent sextet, *J* = 6.8 Hz, 1H), 4.60 (s, 4H), 4.46 (dd, *J* = 7.8, 8.8 Hz, 1H), 3.90 (dd, *J* = 7.2, 8.8 Hz, 1H), 3.70 (m, 4H), 3.65 (m, 4H), 1.42 (d, *J* = 6.2 Hz, 3H). [13]C NMR (125 MHz, $CDCl_3$): δ 141.7, 135.0, 127.0, 73.8, 73.2, 72.6, 70.7, 69.6, 21.8. ES-MS: *m* / *z* calcd for $C_{24}H_{32}O_7B_2$ $(M+Na)^+$ 476.23, found 476.22.

(((Hexane-1,6-diylbis(methylazanediyl))bis(methylene))bis(2,1-phenylene))diboronic acid (3.5). In a round bottom flask, 1,6-dibromohexane (2.22 g, 9.09 mmol) and K_2CO_3 (12.6 g, 90.9

mmol) were combined in 300 mL of anhydrous chloroform. To the reaction mixture, 2-((methylamino)methyl)phenylboronic acid (3.00 g, 18.2 mmol) dissolved in 10 mL of anhydrous chloroform, was added dropwise. The reaction mixture was then heated to 40 ^{o}C and allowed to react for 14 hours. The solids were then removed via vacuum filtration and the filtrated was concentrated *in vacuo*. The crude white solid was then purified via reverse phase chromatography 40% acetonitrile, 60% water gradient yielding a white solid. 3.18 g (85 %) white solid.

^{1}H NMR (500 MHz, CD_3OD): δ 7.63 (d, *J* = 7.1 Hz, 1H), 7.28 (d, *J* = 7.2 Hz, 4H), 7.18 (m, 2H), 4.12 (s, 2H), 2.97 (t, , *J* = 8.1 Hz 2H), 2.60 (s, 3H), 1.77 (s, 2H), 1.42 (s, 2H). ^{13}C NMR (125 MHz, CD_3OD): δ 133.3, 128.7, 127.2, 127.1, 126.9, 62.6, 55.0, 38.7, 26.2, 23.5.

N1,N6-dimethyl-N1,N6-bis(2-(4-methyl-1,3,2-dioxaborolan-2-yl)benzyl)hexane-1,6-diamine (3.6). In a flame dried round bottom flask, (((hexane-1,6-diylbis(methylazanediyl))bis(methylene))bis(2,1-phenylene))diboronic acid (1.06 g, 2.57 mmol) and $MgSO_4$ (>5.0 g) were suspended in anhydrous toluene (100 mL) and heated to 100 ^{o}C. Once the reaction mixture was warm, propylene glycol (0.391 g, 0.38 mL, 5.14 mmol) was added dropwise and allowed to react for two hours. The solids were then removed via vacuum filtration and the filtrated was concentrated *in vacuo* yielding a pure white solid. 1.26 g (99%) white solid.

^{1}H NMR (500 MHz, $CDCl_3$): δ 7.95 (d, *J* = 6.5 Hz, 1H), 7.21 (m, 2H), 7.00 (d, *J* = 7.0 Hz, 1H), 4.35 (broad s, 1H), 4.11 (m, 1H), 3.83 (broad s, 2H), 3.55 (broad s, 1H), 2.84 (m, 2H), 2.46 (s, 3H), 1.33 (m, 7H). ^{13}C NMR (125 MHz, $CDCl_3$): δ 139.8, 130.9, 127.7, 127.5, 122.75, 71.7, 60.9, 60.4, 55.3, 41.4, 27.4, 23.2, 14.2.

(Z)-9-oxabicyclo[6.1.0]non-4-ene. This compound was prepared following literature report without any modifications to procedure.[182]

(Z)-cyclooct-5-ene-1,2-diol (3.7). In a round bottom flask, (Z)-9-oxabicyclo[6.1.0]non-4-ene (20.0 g, 161.3 mmol) was dissolved in 320 mL of water with rapid stirring. To the reaction mixture, 10 drops of concentrated H_2SO_4 was added and allowed to react for 12 hours at room temperature. In a separatory funnel, the reaction mixture was added to 500 mL diethyl ether followed by 100 mL of saturated aqueous $NaHCO_3$ solution. The ether layer was then extracted with brine, dried over Na_2SO_4 and was concentrated *in vacuo* yielding a pure, clear and colorless liquid. Yield: 18.81 g (82 %)

^{1}H NMR (500 MHz, $CDCl_3$): δ 5.55 (m, 2H), 3.60 (m, 2H), 3.48 (s, 2H), 2.31 (m, 2H), 2.11 (m, 4H), 1.54 (m, 2H). ^{13}C NMR (125 MHz, $CDCl_3$): δ 129.1, 73.7, 33.3, 22.7. ES-MS: *m* / *z* calcd for $C_8H_{14}O_2$ $(M+Na)^+$ 165.09, found 165.07.

Representative Ring-Opening Metathesis Polymerization (ROMP). In a round bottom flask at room temperature, Grubbs' second generation catalyst (8.6 mg, 0.0101 mmol) was dissolved in 125 mL of anhydrous DCM. In a separate flask, cyclooctene (4.44 g, 40.32 mmol) and (Z)-cyclooct-5-ene-1,2-diol (1.43 g, 10.08 mmol) were combined with 10 mL of anhydrous DCM. The catalyst solution was charged with the monomer mixture and allowed to react for fifteen hours at room temperature. The reaction mixture was quenched with trace amounts of ethyl vinyl ether. The polymer was precipitated from MeOH and characterized by GPC and NMR. Based on NMR, the feed ratio matched the observed diol monomer incorporation. Yield: 5.5g (95%)

^{1}H NMR (500 MHz, $CDCl_3$): δ 5.35 (m, 2H), 3.42 (broad s, 0.39H), 2.01 (m, 4.23H), 1.51 (m, 0.77H), 1.28 (m, 6.52 H) GPC: Mn 1.65×10^5 g/mol, PDI: 1.89.

Representative procedure for preparing crosslinked bulk samples: 20% diol PCO (**3.8**) was dissolved in toluene (54 mg/ mL), 4.4 mL of polymer sample was added to a scintillation vial as well at 0.47 mg of BHT inhibitor. To the stirring solution, either 0.5 or 1.0 mol % of a diboronic ester crosslinker (**3.4** or **3.6**) with respect to olefin was added to the stirring polymer solution at which point the polymer samples became more viscous or gelled. The crosslinked polymer network was then cast into a Teflon mold and allowed to slowly evaporate at room temperature overnight on the bench top. The polymer films were then placed in a vacuum oven at 80 ^{o}C to remove any residual solvent. Boronic ester crosslinked samples were then melt processed and bulk samples were then carried through for self-healing experiments.

For control study, we also prepared non-dynamic permanently crosslinked polymers by adding 0.5 or 1.0 mol% of 1,4-diisocyanatobutane with respect to olefin on PCO for crosslinking. Permanently crosslinked samples were cast into the molds of the desired shape and static mechanical testing was performed after solvent was removed.

Exchange spectroscopy (EXSY) of compound 1 with neopentyl glycol. A solution of phenylboronic acid neopentyl glycol ester in acetone-d^6 (0.5 M) was prepared, to which one equivalent of neopentyl glycol was added. After allowing the reaction to reach equilibrium for 30 min., a NOESY experiment was set up with mixing times of d8 = 0.8, 1, and 1.5 s. The diagonal and cross peaks for the bound and unbound methyl resonances of neopentyl glycol (1.04 and 0.90 ppm) were carefully integrated, and the integration values were plugged into EXSYCalc, a free software developed by MestReNova. The rates thus calculated were k = 0.017, 0.019, and 0.011 /s (for d8 = 0.8, 1, and 1.5 s, respectively) for an average rate of 0.016 ± 0.004 /s.

Coalescence experiment for compound 2 with neopentyl glycol. A solution of (2-((Dimethylamino)methyl)phenyl)boronic acid neopentyl glycol ester in acetone-d^6 (0.5 M) was prepared, to which one equivalent of neopentyl glycol was added. After allowing the reaction to reach equilibrium for 30 min., ^1H NMR spectra of the mixture was taken at temperatures ranging from 25 °C to -25 °C. The spectra were investigated for the coalescence of the methyl peaks of neopentyl glycol in both the esterified and free forms. The peaks in question coalesced at -10 °C.

The activation energy for exchange was calculated using the equation[172]:

$$\Delta G^{\ddagger} = RT_C\,[22.96 + \ln (T_C / \Delta\nu)\,] \,,$$

Where R = 8.314 J/mol K is the universal gas constant, T_c is the coalescence temperature, and $\Delta\nu$ is the separation in Hz of the bound and unbound resonances. In this particular calculation, the methyl resonance of bound and unbound neopentyl glycol were monitored for coalescence, which was found to be -10 °C (263.15 K), and $\Delta\nu$ was found to be 83.5 Hz (determined by taking the ^1H NMR spectrum of the mixture far below coalescence (-50 °C) and measuring the separation of the resonances in question). The $\Delta G^{\ddagger}$ value thus calculated was 12.6 kcal/mol.

Furthermore, the rate at coalescence temperature is[172]:

$$k_{ex} = {}^{\pi}/_{\sqrt{2}}\,(\Delta\nu),$$

Which calculates to k_{ex} = 185 /s at coalescence temperature (263.15 K). Finally, using the activation energy just calculated along with the Arrhenius equation,

$$k = A \cdot exp(-\frac{\Delta G^{\ddagger}}{RT})$$

The rate of the reaction at room temperature can be calculated:

$$\frac{k_{T2}}{k_{T1}} = exp(-\frac{\Delta G^{\ddagger}}{R}\left(\frac{1}{T_2} - \frac{1}{T_1}\right)),$$

Using T_1 = 263.15 K (coalescence temperature), T_2 = 298.15 K (room temperature), $\Delta G^{\ddagger}$ = 12.6 kcal/mol, and k_{T1} = 185 /s, the rate at room temperature (k_{T2}) was calculated to be k = ~3000 /s.

DSC (differential scanning calorimetry) procedure. Differential scanning calorimetry measurements were performed using a TA Q2000 instrument. ~5 mg of polymer sample was placed in a non-hermitic pan and scanned against an empty reference pan. The DSC experiment was performed in a heat-cool cycle (25 to 180 ºC, 20 ºC/min; 180 to -80 ºC, 10 ºC/min; isothermal -80 ºC, 30 min; -80 to 200 ºC, 5 ºC/min), wherein the thermal transitions for the last heating cycle were recorded.

TGA (thermogravimetric analysis) procedure. The thermal stability of the polymers was probed by TGA. The samples were heated from 25 ºC to 105 ºC at 50 ºC/min and held at 105 ºC for five minutes. The sample was then heated from 105 ºC to 850 ºC at 20 ºC/min and then mass loss was plotted versus temperature. For clarity, the derivative of the mass loss is shown as well.

Representative rheology procedure. A 60 mg/mL toluene solution of 20%-diol PCO (**3.8**) (1.5 mL; 90 mg) was stirred in a scintillation vial, to which was added a 110 mg/mL toluene solution of compound **3.6** (3.0 mg, 0.0065 mmol), and the solution was allowed to gel (~30 s). Rheology was performed on an AR-G2 instrument, with a 20 mm standard steel parallel plate – 992561. A frequency sweep test (0.01 to 100 Hz) was performed at fixed strain (1%).

Stress relaxation procedure. Stress relaxation experiments were performed using a TA instruments DMA Q800. Sample dimensions were measured (l,w,t) and loaded into the furnace. The sample was equilibrated to a set temperature (e.g. 35 ºC) for 15 min, after which the sample was displaced and held at 2% strain for 20 min and the decay of stress over time was monitored.

Tensile testing procedure. The bulk static tensile properties of polymer samples were measured using an Instron 3365 instrument with a 500 N load cell with a pulling rate of 100 mm/min. Sample dimensions were measured (l,w,t: 12.0 x 3.4 x 0.20 mm) and the sample was pulled at ambient temperature until break.

Self healing procedure. Samples were prepared via melt pressing with a dimension of ~ 8 x 2.5x 13 mm. The samples were cut completely in half and the cut interfaces were pressed together for one minute and place in a mold in the over at 50 ºC for 16 hours. The samples were removed and allowed to equilibrate at room temperature for 30 minutes at which time static mechanical testing was performed.

Hydrolytic stability experiment. To confirm that our crosslinked polymer samples were stable to the hydrolytic effects of ambient moisture, we submerged our samples (20%-diol PCO (**3.8**) crosslinked with 0.5 % and 1.0 % crosslinkers **3.4** or **3.6**) in deionized water overnight, and monitored the change in mass and mechanical properties of the samples. All the samples look the same in appearance before and submersion. The mass of the samples remain unchanged before and after submerging in water. Mechanical properties also remain uncompromised, demonstrating excellent moisture resistance of these samples. This is presumably due to the hydrophobic nature of the polymer backbone, prohibiting the swelling of sample and the uptake of water into the crosslinked network, shielding the boronic esters from hydrolysis.

3.6 References for experimental

(1) Pangborn, A. B.; Giardello, M. A.; Grubbs, R. H.; Rosen, R. K.; Timmers, F. J. *Organometallics* **1996**, *15*, 1518.

(2) Qiu, D.; Zheng, Z.; Mo, F.; Zhang, Y.; Wang, J. *Can. J. Chem.* **2011**, *90*, 71.

(3) Swamy, K. M. K.; Jang, Y. J.; Park, M. S.; Koh, H. S.; Lee, S. K.; Yoon, Y. J.; Yoon, J. *Tetrahedron Lett.* **2005**, *46*, 3453.

(4) Lee, S.-H.; Park, Y.; Wee, K.-R.; Son, H.-J.; Cho, D. W.; Pac, C.; Choi, W.; Kang, S. O. *Org. Lett.* **2009**, *12*, 460.

(5) Ding, X.; Chen, L.; Honsho, Y.; Feng, X.; Saengsawang, O.; Guo, J.; Saeki, A.; Seki, S.; Irle, S.; Nagase, S.; Parasuk, V.; Jiang, D. *J. Am. Chem. Soc.* **2011**, *133*, 14510.

(6) Hillmyer, M. A.; Laredo, W. R.; Grubbs, R. H. *Macromolecules* **1995**, *28*, 6311.

(7) Kloxin, C. J.; Scott, T. F.; Adzima, B. J.; Bowman, C. N. *Macromolecules* **2010**, *43*, 2643.

(8) Claridge, T. D. W. In *Tetrahedron Organic Chemistry Series*; Timothy, D. W. C., Ed.; Elsevier: 2009; Vol. Volume 27, p 99.

3.7 Chapter 3 Spectra

^{1}H NMR compound 3.1:

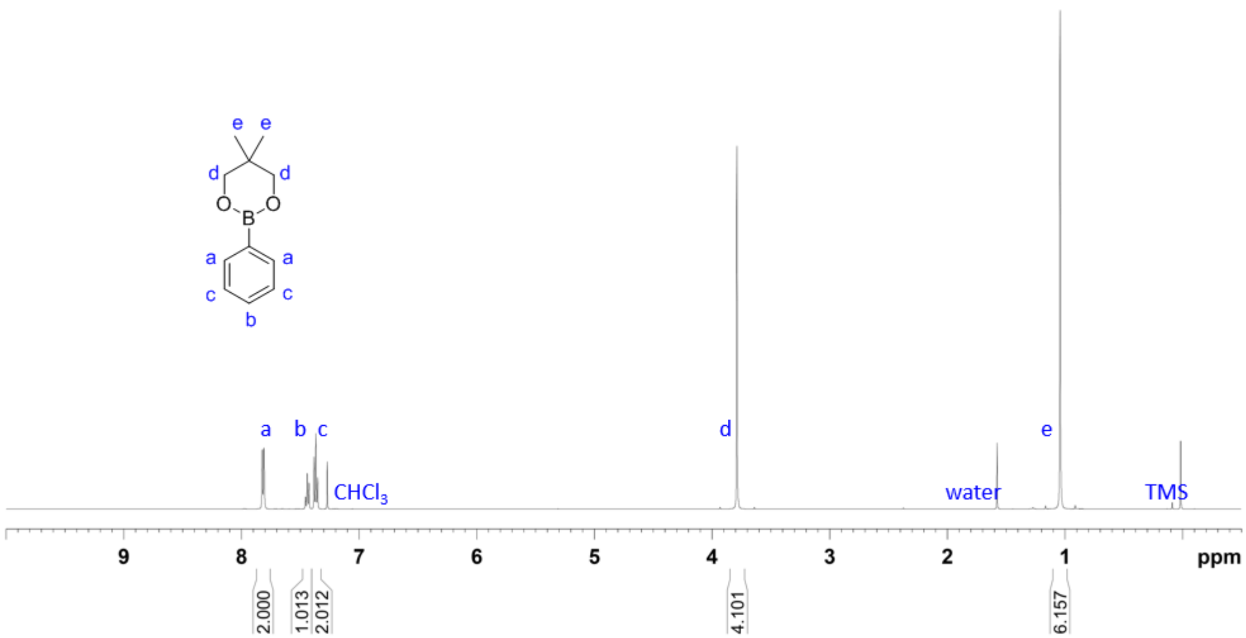

^{13}C NMR compound 3.1:

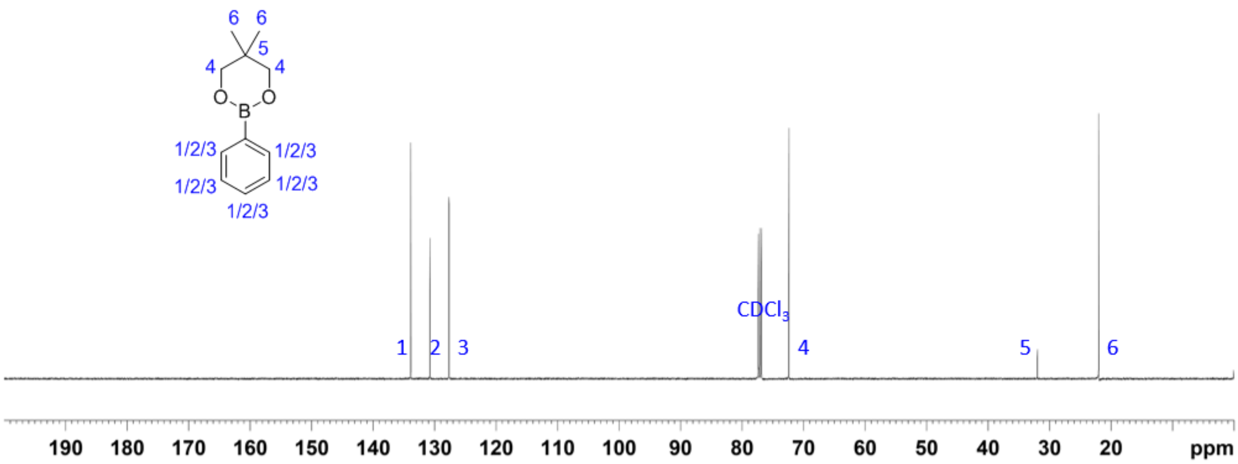

^{1}H NMR compound 2-((Dimethylamino)methyl)phenylboronic acid:

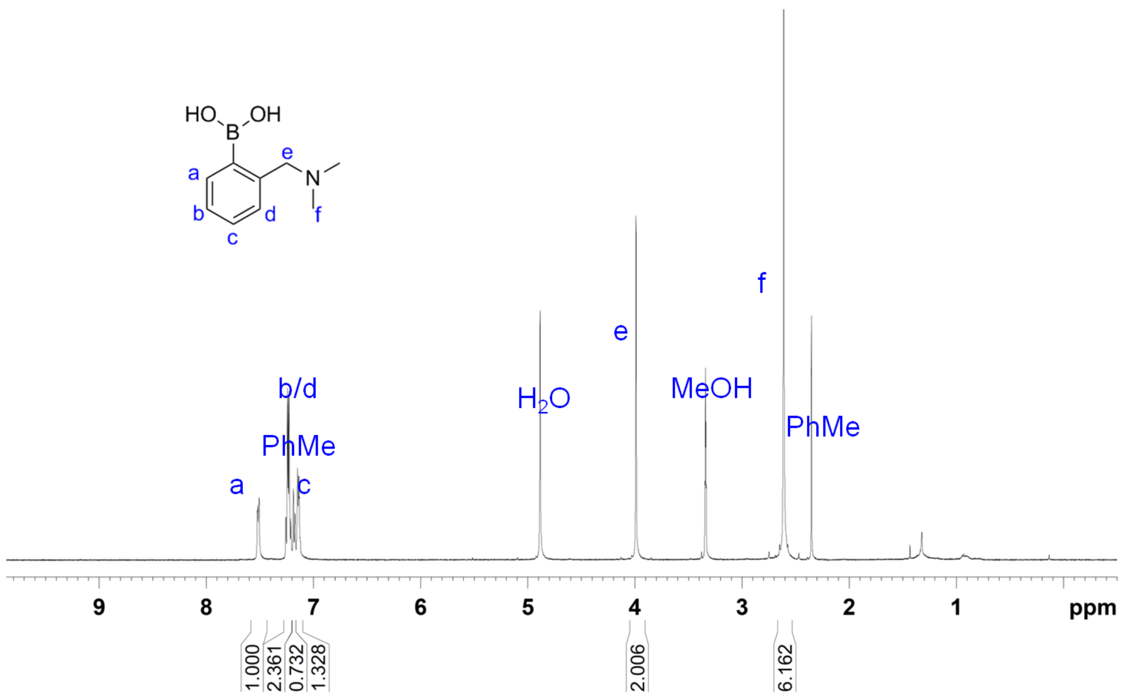

^{13}C NMR compound 2-((Dimethylamino)methyl)phenylboronic acid:

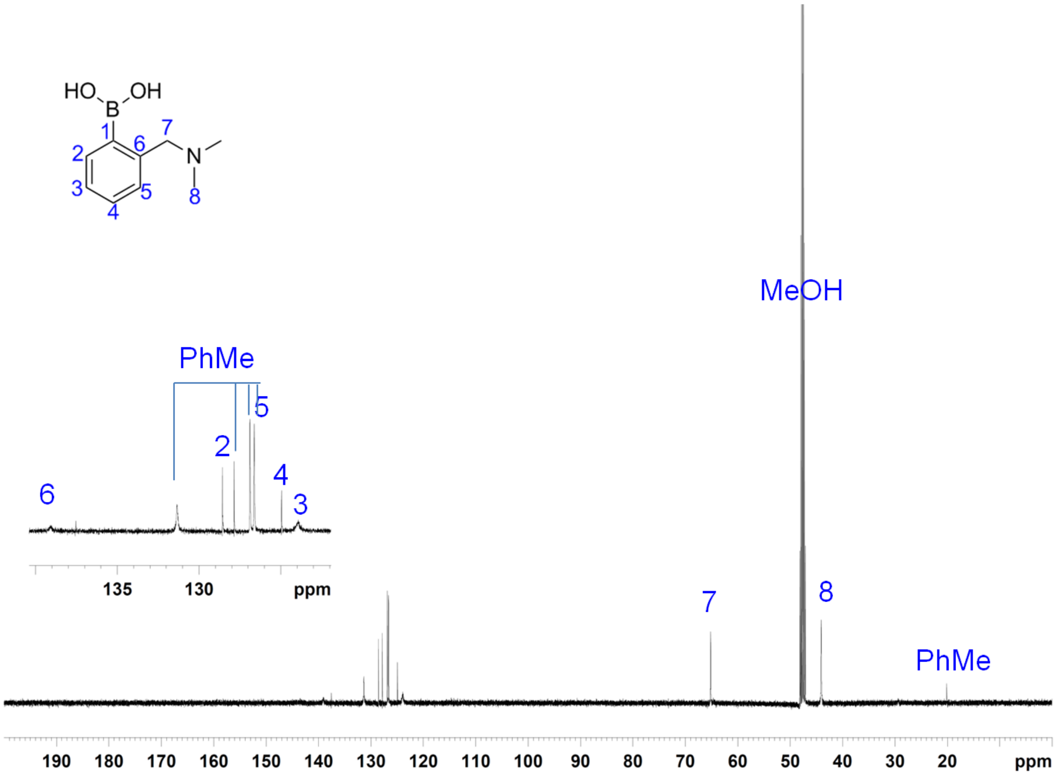

[1]H NMR compound 3.2:

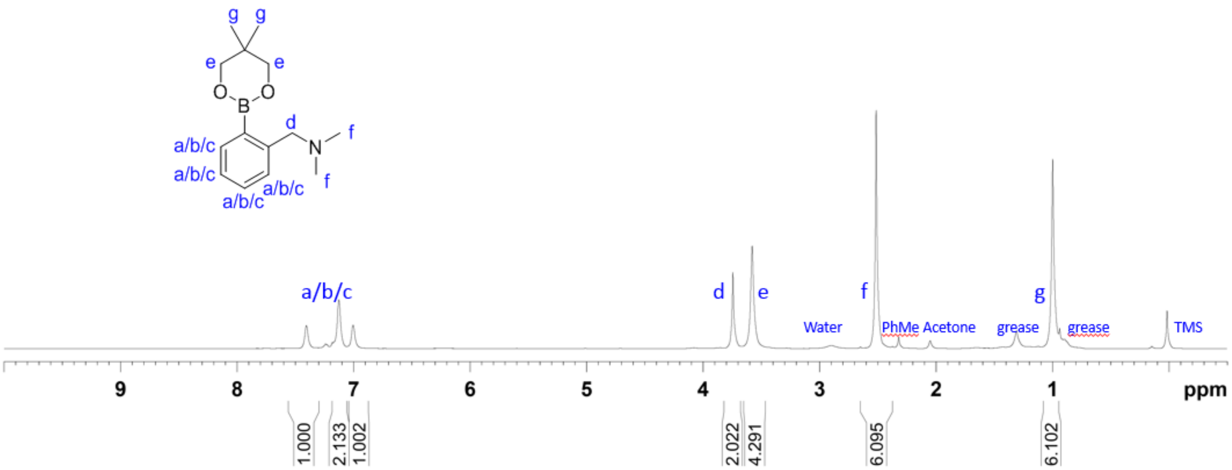

[1]H NMR compound 4,4'-(2,2'-oxybis(ethane-2,1-diyl)bis(oxy))bis(methylene)bis(bromobenzene):

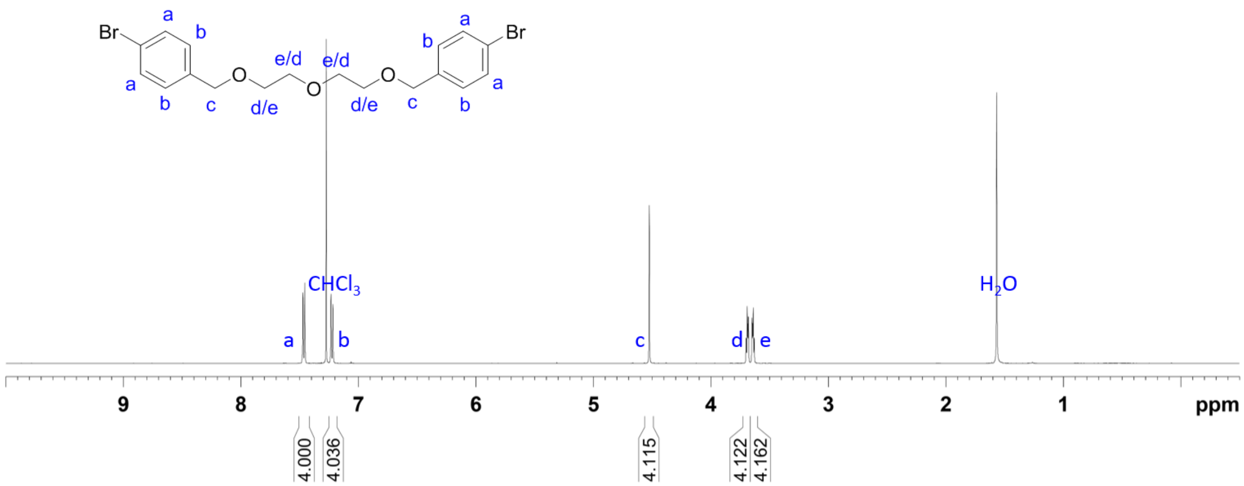

^{13}C NMR compound 4,4'-(2,2'-oxybis(ethane-2,1-diyl)bis(oxy))bis(methylene)bis(bromo-benzene):

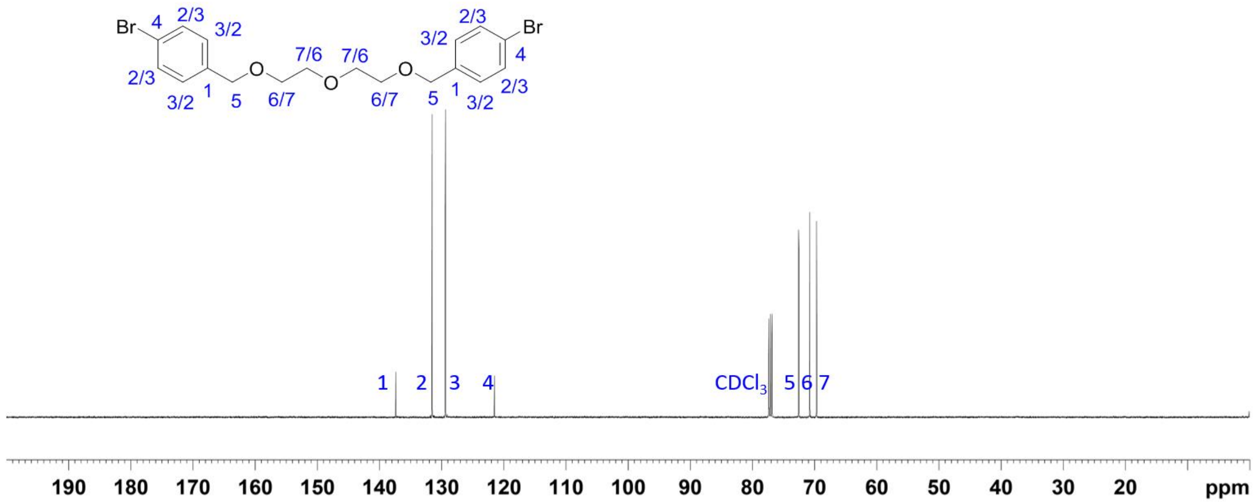

^1H NMR compound 2,2'-(4,4'-(2,2'-oxybis(ethane-2,1-diyl)bis(oxy))bis(methylene)bis(4,1-phenylene))bis(4,4,5,5-tetramethyl-1,3,2-dioxaborolane) (3.3):

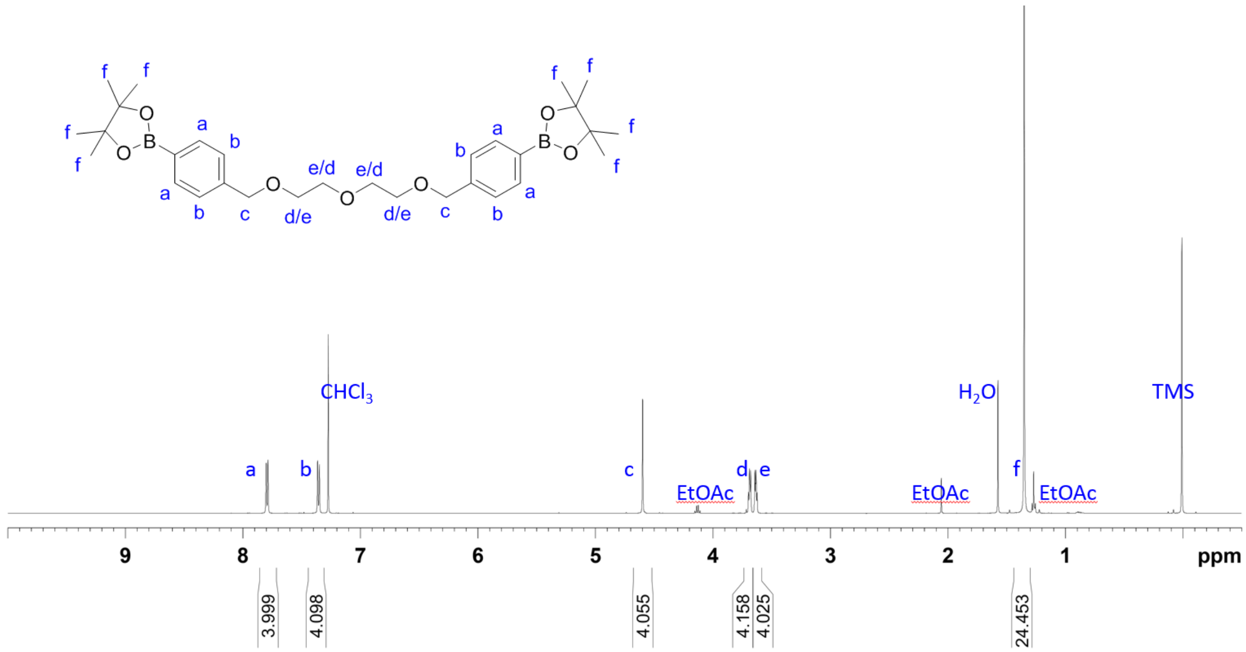

^{13}C NMR compound 2,2'-(4,4'-(2,2'-oxybis(ethane-2,1-diyl)bis(oxy))bis(methylene)bis(4,1-phenylene))bis(4,4,5,5-tetramethyl-1,3,2-dioxaborolane) (3.3):

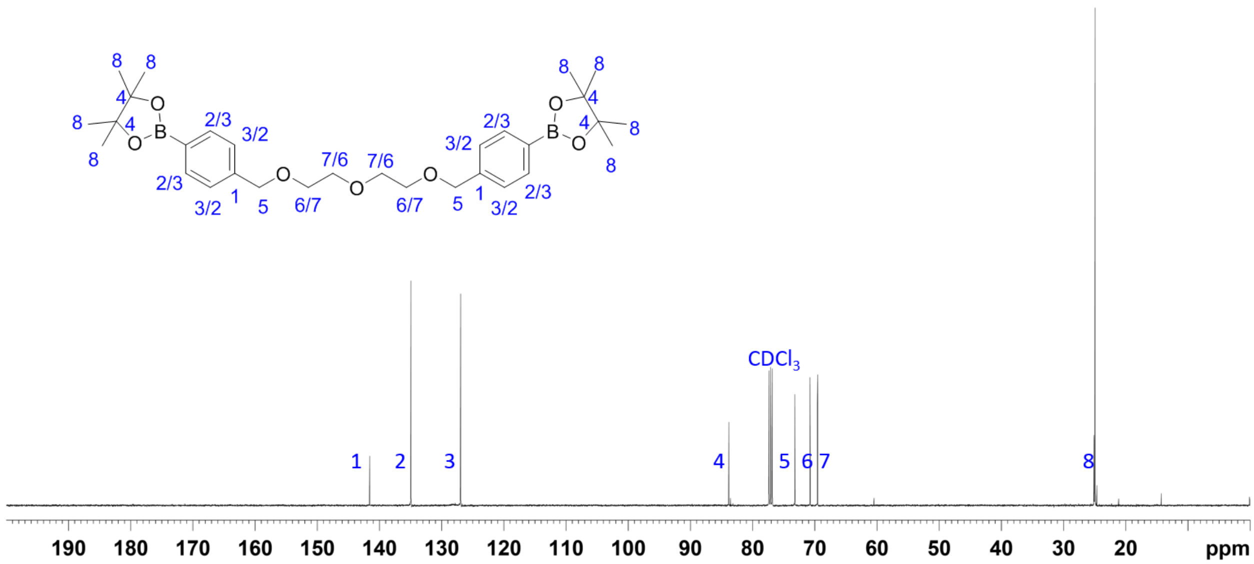

^{1}H NMR compound ((((Oxybis(ethane-2,1-diyl))bis(oxy))bis(methylene))bis(4,1-phenylene))diboronic acid:

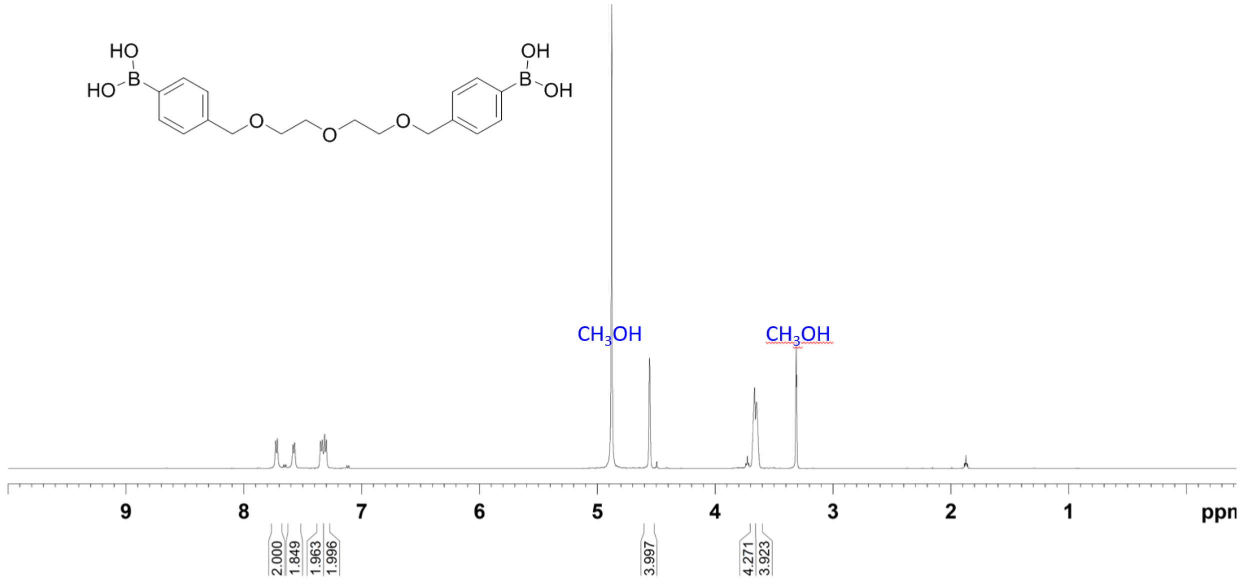

^{13}C NMR compound ((((Oxybis(ethane-2,1-diyl))bis(oxy))bis(methylene))bis(4,1-phenylene))diboronic acid:

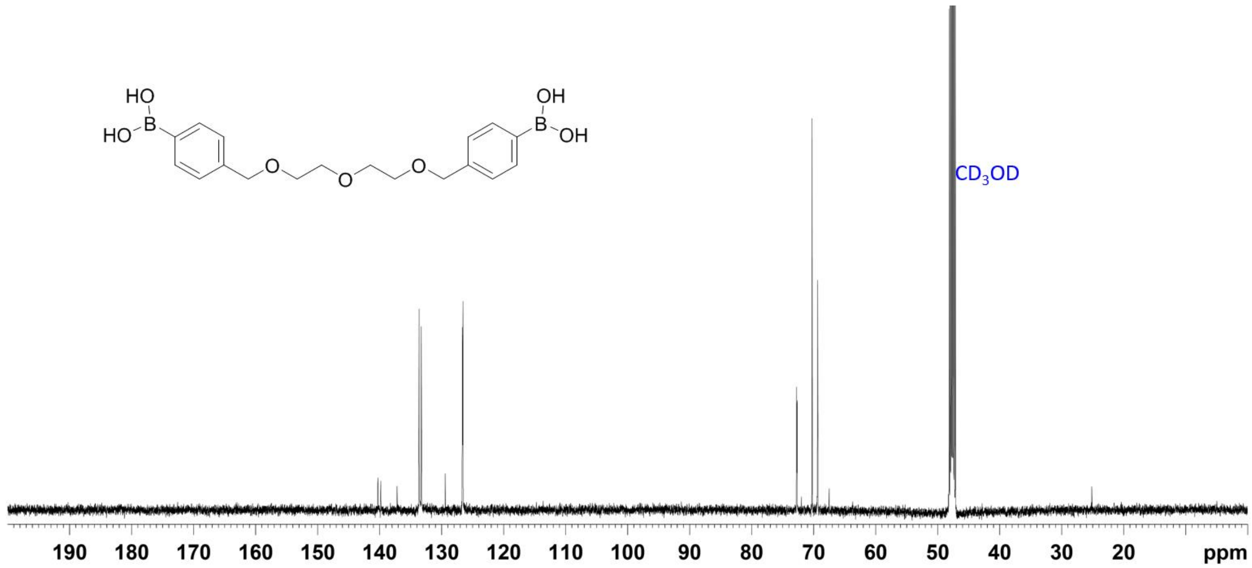

*Species in solution are a mixture of –OCD_3 esterified boronic acids, thus peak-by-peak assignment is difficult.

[1]H NMR compound 3.4:

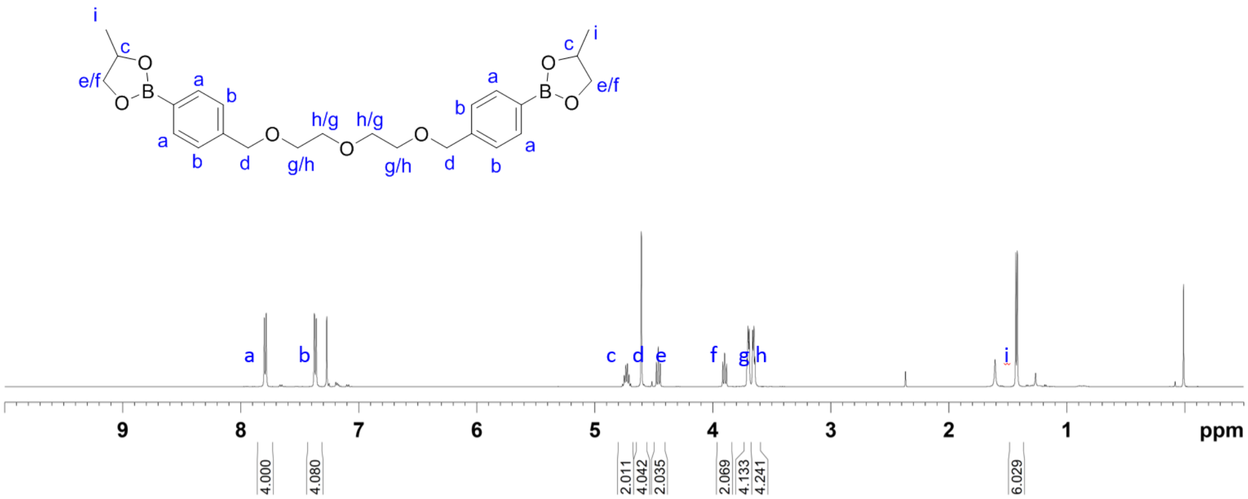

^{13}C NMR compound 3.4:

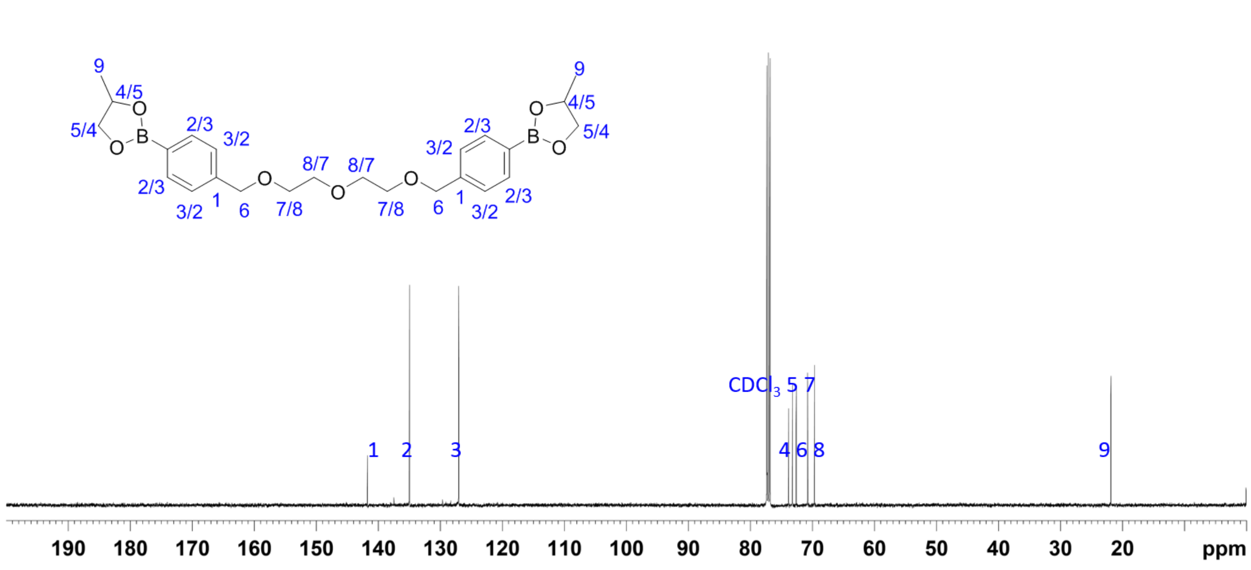

^{1}H NMR compound (((Hexane-1,6-diylbis(methylazanediyl))bis(methylene))bis(2,1-phenylene))diboronic acid (3.5):

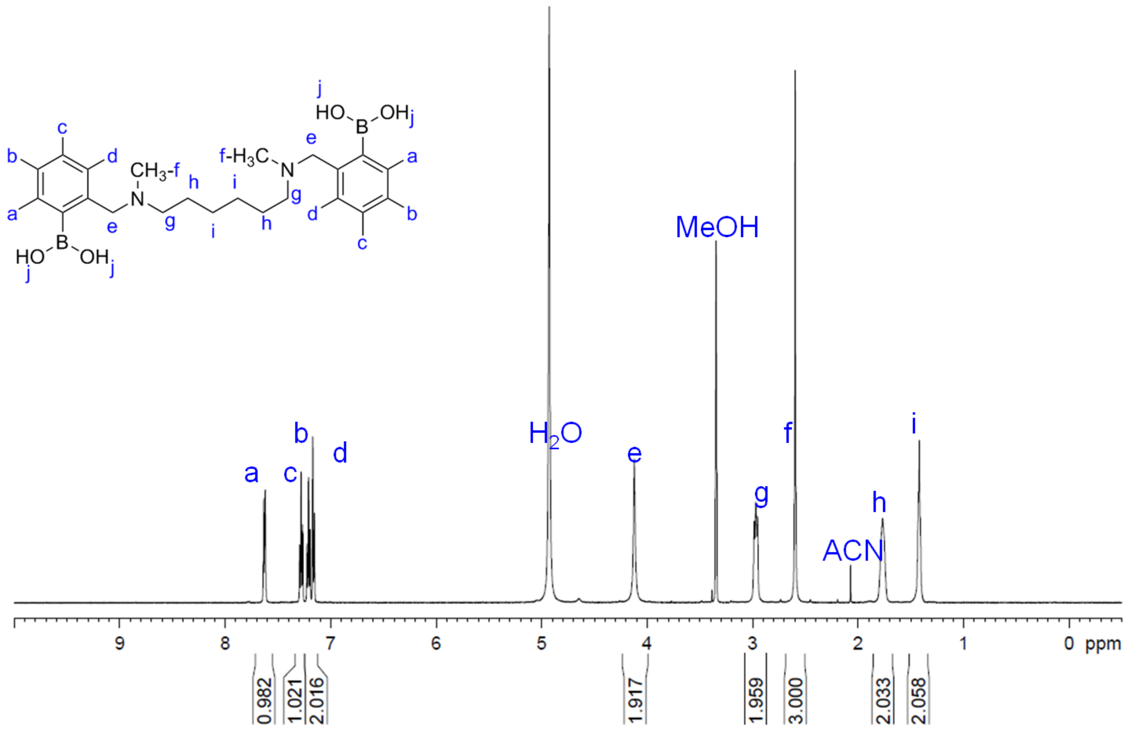

^{13}C NMR compound (((Hexane-1,6-diylbis(methylazanediyl))bis(methylene))bis(2,1-phenylene))diboronic acid (3.5):

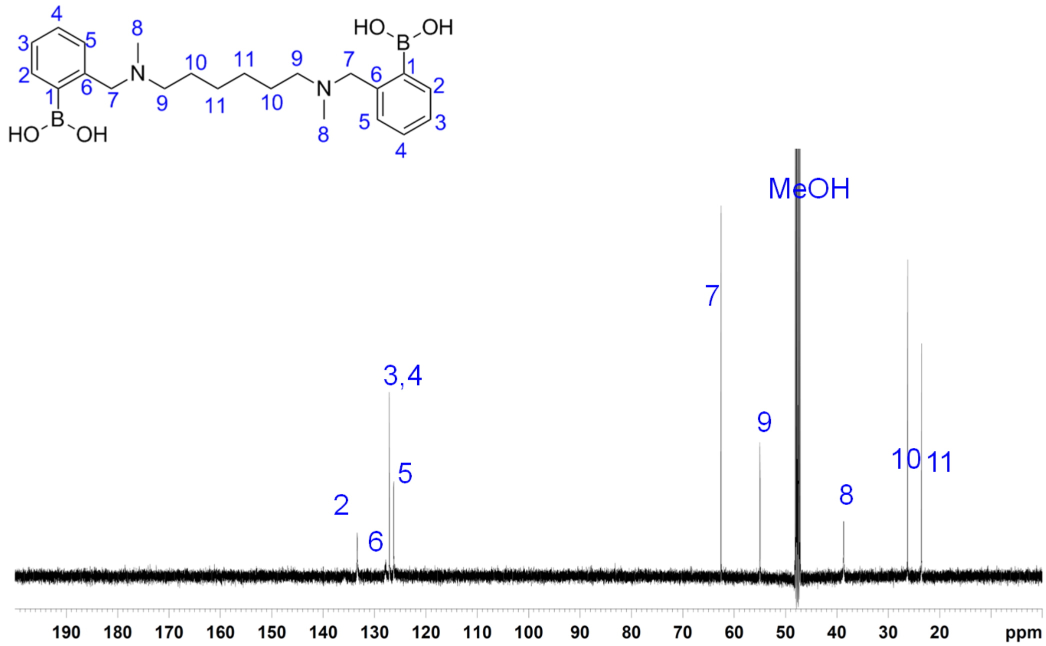

¹H NMR compound 3.6:

:

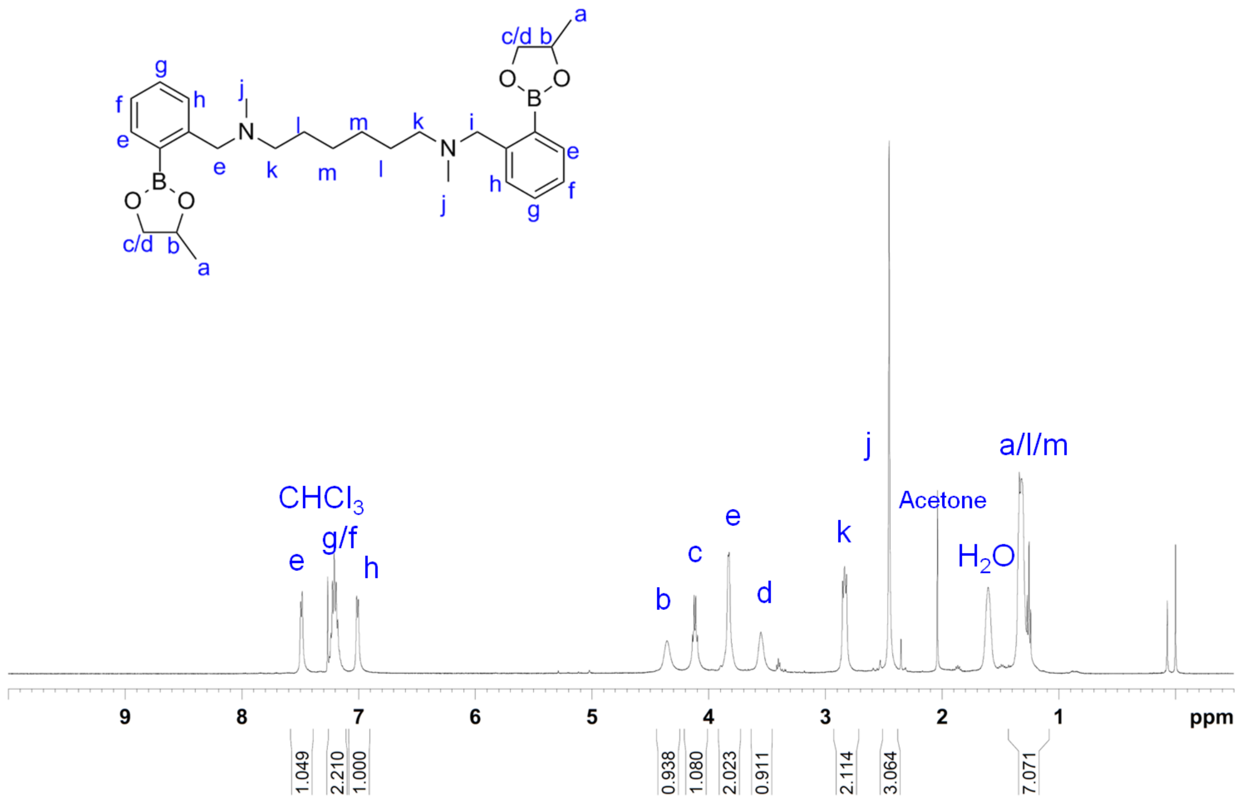

^{13}C NMR compound 3.6:

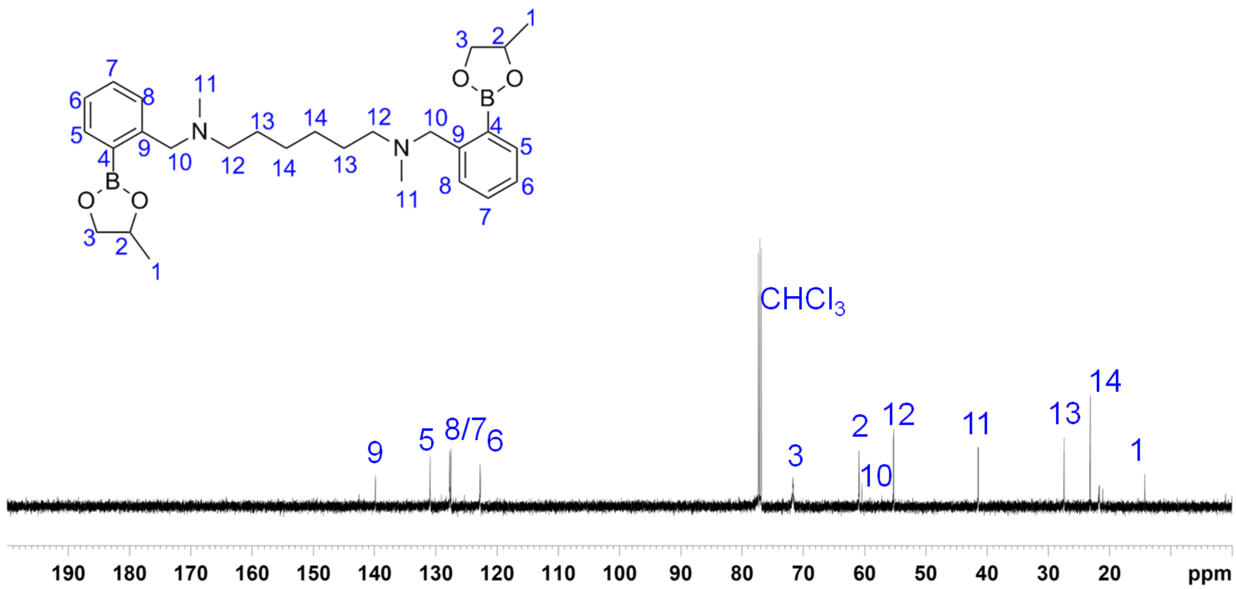

[1]H NMR compound 3.7:

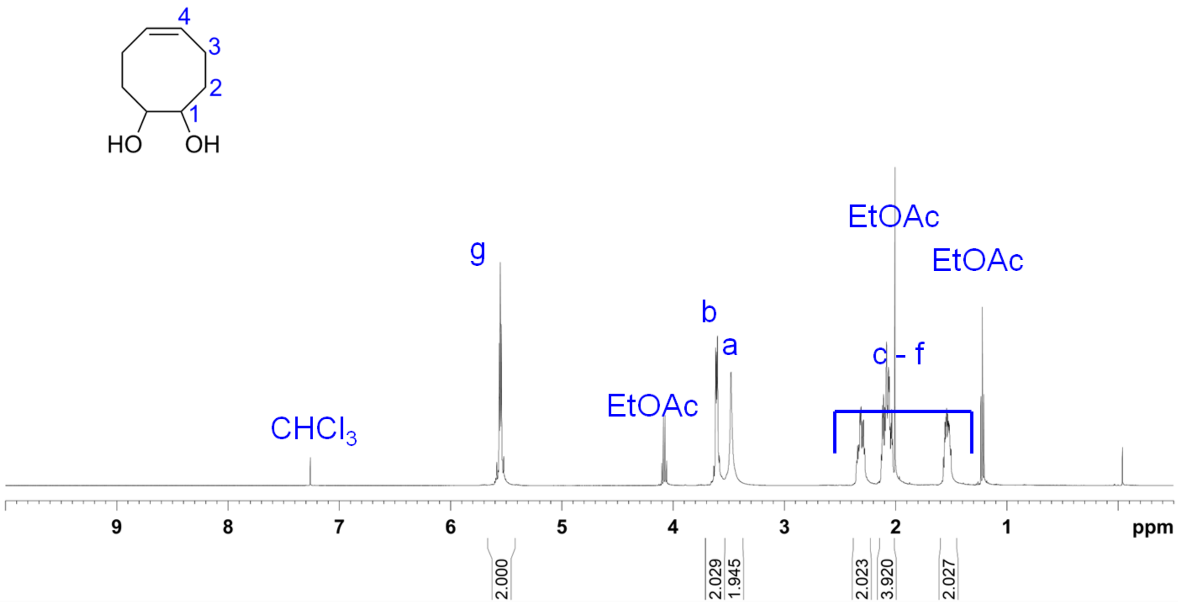

^{13}C NMR compound 3.7:

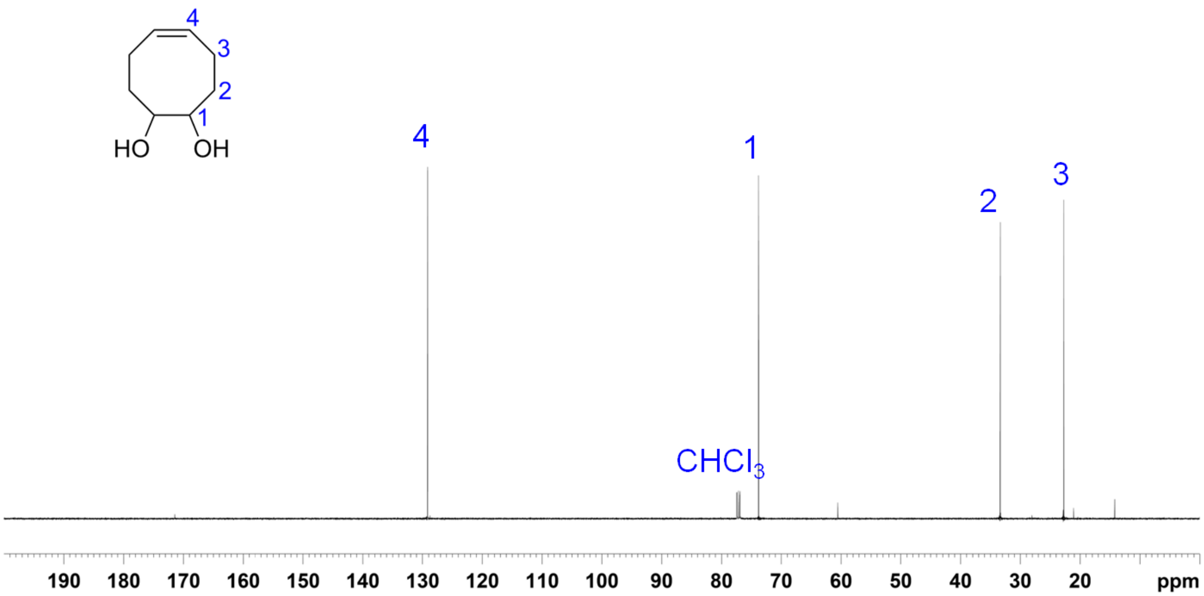

[1]H NMR of 20%-diol polycyclooctene (3.8):

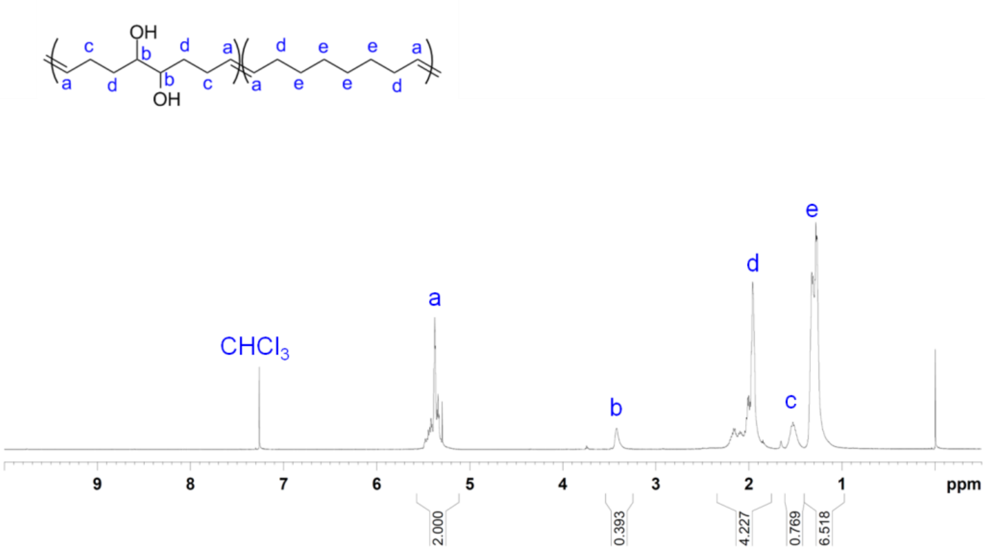

Chapter 4. Progress Towards Boronic Ester-based Vitrimer Materials

4.1 Introduction

In the previous chapter we demonstrated the possibility of using dynamic boronic ester exchange in a condensed bulk material for self-healing.[31] In addition, a correlation between the emergent properties of the material based on different rates of dynamic exchange could be observed, wherein fast trans-esterification of boronic ester resulted in efficient healing while slow trans-esterification did not. Though a good initial demonstration, we wished to take the concept further. In this chapter, we attempt to expand this concept to a vitrimer design,[27] in which monomers are pervasively crosslinked through boronic ester bonds throughout the material. If successful, the much higher mole percentage of boronic ester linkages in the material may offer wider possibilities in tuning the material's dynamicity. Furthermore, variability in the exchange reaction kinetics has been shown to be able to affect the vitrimer thermal transition T_v,[115] which should have the potential to vary the temperature-dependent mechanical properties of the material.

Furthermore, whereas in the boronic ester-based self-healing material described in Chapter 3, the difference in dynamic properties was qualitative,[31] one of the inherent characteristics of vitrimers is that the activation energy of molecular exchange can quantitatively be matched to the activation energy of material flow.[103,107] This type of thorough and numerical match between the molecule-to-bulk activation energy parameters of boronate trans-esterification would be a robust proof of concept in the molecule-to-bulk correlation of material properties. It is noted that a previous report by Capelot *et al.*[115] also demonstrated the tunability of material flow activation energy through tunable kinetics. Nevertheless, their work relied on the use of different external catalysts, whereas the work herein would rely on inherent rate differences of structurally similar monomers. Furthermore, the differences in rates of material flow was not quantified to match the same parameter in small molecule studies. Progress in the development and testing of these boronic ester-based vitrimer materials is described in this chapter.

4.2 Results and Discussion

4.2.1 Crosslinked Networks Synthesized from Neighboring Groups with an *o*-methylene Spacer

We chose to synthesize the network material an A_2B_3 type thermosetting structure. In the proposed design, the chemical bonds crosslinking the material are pervasively saturated with boronic ester bonds, with two distinct variants: one with an amino-group neighboring effect and another without, which are otherwise structurally analogous. The proposed design is depicted in Figure 4.1 below.

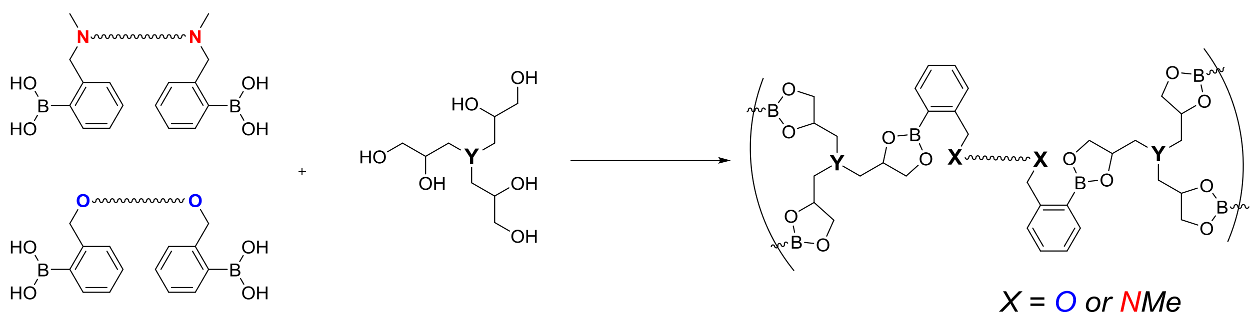

Figure 4.1 Concept design for boronic ester-based vitrimers. A_2B_3 type thermosetting network utilizes two telechelic boronic acids either with amino- neighboring group or without it, crosslinked by tris-diol compounds.

In order to achieve synthesis of the network proposed in Figure 4.1, synthesis of three different monomers is required: two telechelic boronic acid compounds, and one trivalent diol compound. The synthetic scheme for fast- and slow-exchanging telechelic boronic acids are shown in Scheme 4.1 below. Note that structure of the two boronic acids are slightly modified from the previous chapter. First, the two boronic acid variants are more structurally analogous, as the substituents on the phenyl rings are *ortho*- substituted in both monomers. For simplicity of synthesis, the insulating linker between the boronic acid moieties was also changed from a hexyl to an ethylene linker. In this new synthetic scheme, the fast-exchanging ("Wulff-type") monomer **4.1** could be synthesized in one step through reductive amination with commercially available compounds.[183] This monomer could be purified through slow precipitation out of solution after workup in 50:50 MeCN:H_2O. Slow-exchanging ("non-Wulff-type") monomer **4.2** was synthesized in similar strategy as employed in the previous chapter,[31] starting with S_N2 of ethylene glycol to 2-bromobenzyl bromide, followed by lithium-bromide exchange and finally installation of boronic acid moiety through triisopropyl borate and acid workup.[184] Synthesis of multivalent diol compound, TAT tris-diol **4.3**, was followed from literature procedure.[168]

Scheme 4.1 Synthesis of Boronic Acid and Tris-diol Monomers

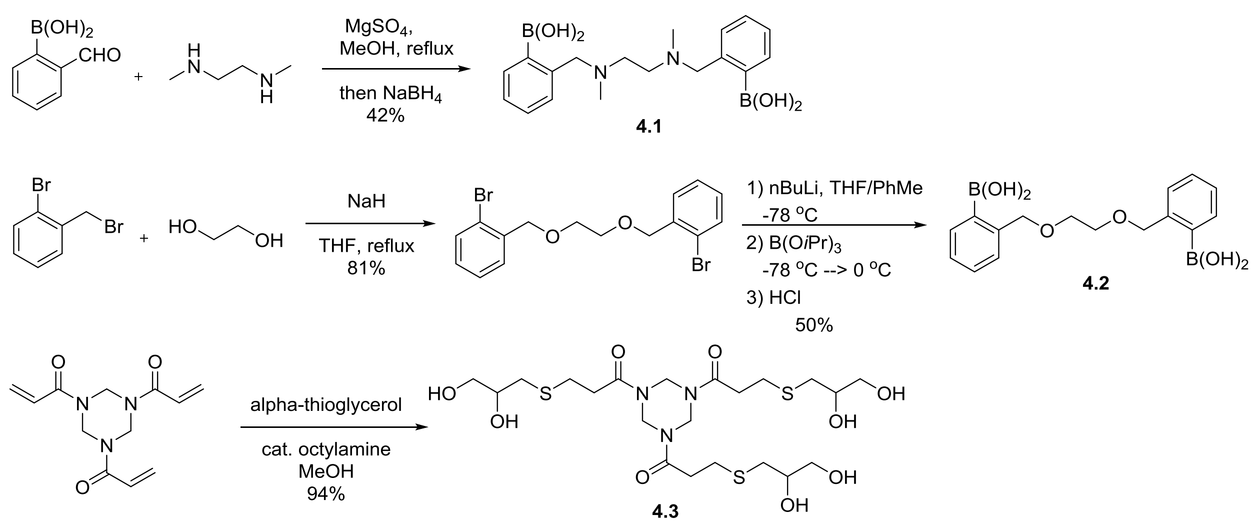

Crosslinked materials were then synthesized through poly-condensation casting from a Teflon mold between either of the boronic acids and the tris-diol compound. For initial testing, the stoichiometry between the bis-boronic acid and the tris-diol compound was chosen to be 3:2.2, in which the equivalents of diol (6.6 equivalents) was in slight (10%) excess to the boronic acid moieties (6 equivalents) in order for dynamic exchange to occur, and thereby allowing the material to have vitrimeric properties.[107] Materials were prepared through solvent casting from DMF, in which slow evaporation (70 ºC, house vacuum, overnight) was followed by thorough removal of solvent and water (100 ºC, high vacuum, 24 h). For both Wulff-type and non-Wulff-type monomers **4.1** and **4.2**, robust thin films were obtained which could easily be hot pressed at 100 ºC into testable materials. Scheme 4.2 below shows the network processing conditions.

Scheme 4.2 Synthesis of Crosslinked Network Through DMF Solvent Casting

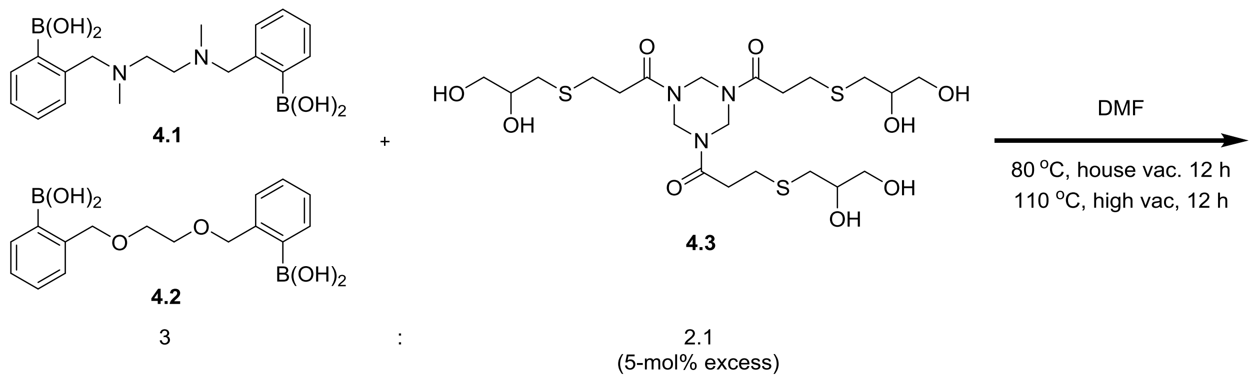

The materials thus obtained were tested thermally and mechanically. Gratifyingly, mechanical testing demonstrated very strong material for both fast and slow boronic acids, with the material synthesized from slow exchanging boronic acid **4.2** not undergoing failure even at a tensile modulus of 25 MPa (Figure 4.2a). We note that these materials are not of the optimal ASTM standard dogbone geometry, hence mechanical properties demonstrated here may not be its optimum potential. Thermal testing demonstrated somewhat different properties between fast and slow exchanging materials. In both DSC and TGA analyses, it was found that the material synthesized from the fast-exchanging boronic acid was thermally more stable. This was evinced by the large exotherm in the DSC curve of the fast exchanging variant at ~150 ºC (Figure 4.2c), similarly reflected in a visible degradation in the fast-exchanging material at a similar temperature on the TGA (Figure 4.2d). As expected of a vitrimer,[103,105-108] both materials were easily reprocessable, recovering their shape and mechanical properties after being broken into pieces and remolded through compression molding (Figures 4.2 e and 4.2 a).

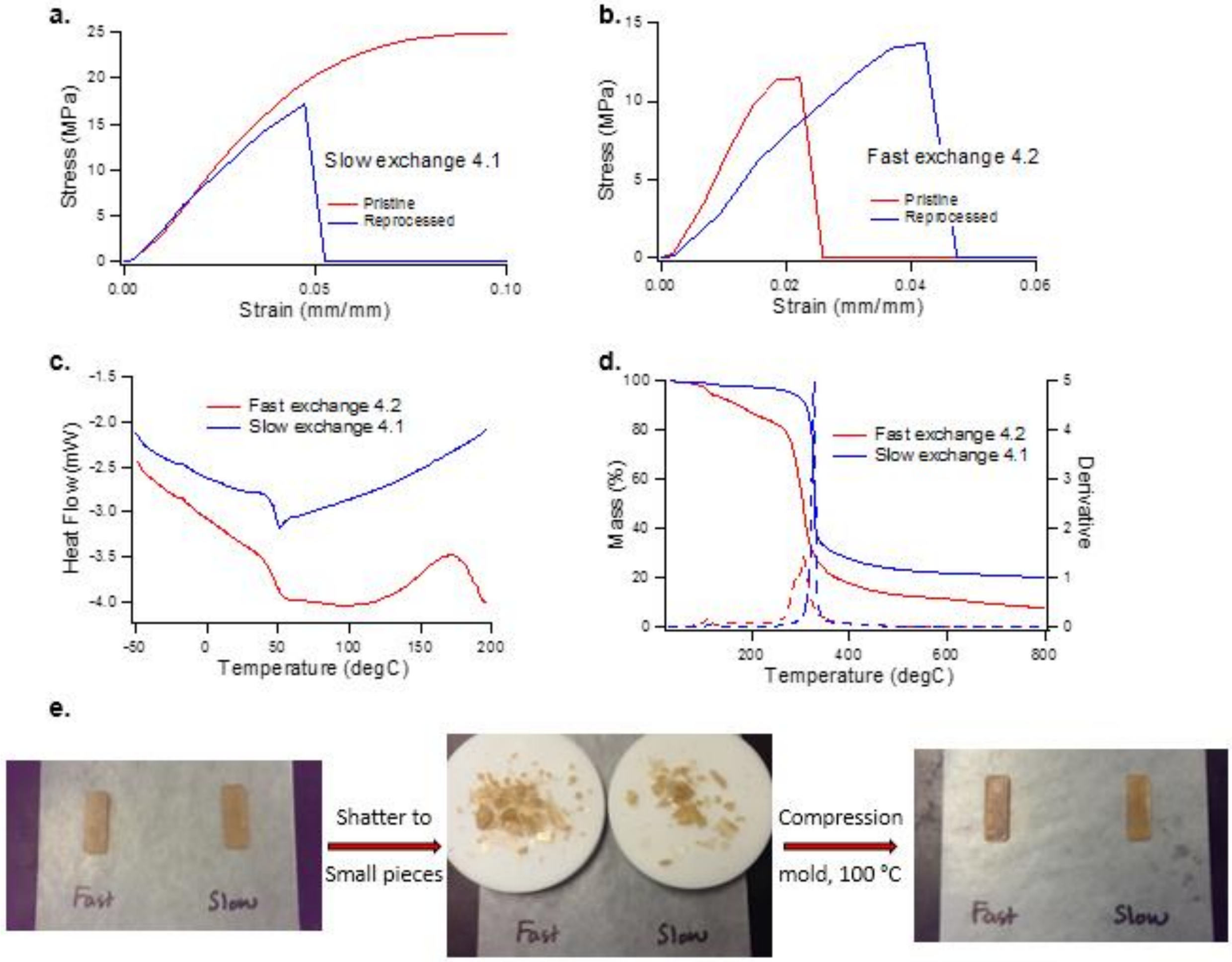

Figure 4.2 Mechanical, thermal, and reprocessing tests for crosslinked materials from monomers **4.1** and **4.2**. **a.** Tensile properties of crosslinked material synthesized from slow-exchanging boronic acid monomer **4.1**, both pristine (blue) and after reprocessing (red). **b.** Tensile properties of crosslinked material synthesized from fast-exchanging boronic acid monomer **4.2**, both pristine (blue) and after reprocessing (red). **c.** Thermal analysis through DSC (slow-exchanging: red, fast-exchanging: blue) shows T_g at approximately 50 ºC for both materials. The fast-exchanging variant shows an exotherm at ~150 – 200 ºC, possibly indicating network degradation. **d.** TGA also show signs of thermal degradation for fast-exchanging material. **e.** Compression molding of material shows robust reprocessing for both variants.

Although these materials were desirable in their mechanical properties as well as their reprocessability, there were a few shortcomings. First was the relative lack of thermal stability of the fast-exchanging material. As described in the previous paragraph, DSC and TGA traces show evidences of possible chemical reaction at around 150 °C, and some discoloration of the fast-exchanging material (Figure 4.2 e) after reprocessing reinforces these observations. Furthermore, we hypothesized that a potential difficulty of the fast-exchanging material is the monomer's propensity to coil around itself into a compact structure through B-N coordination, which we confirmed through ^{11}B NMR (Figure 4.3), wherein a ~13.0 ppm peak indicates a tetrahedral structure.[175,184] Most importantly, submersion of either material in water overnight exhibited marked deterioration in material properties and shape, indicating very poor water stability.

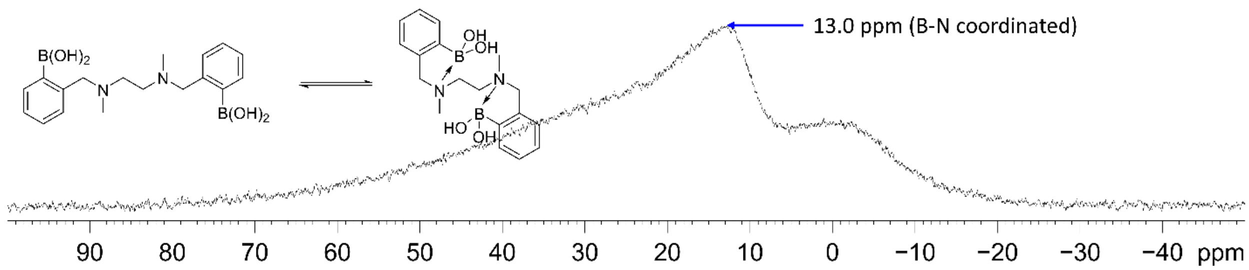

Figure 4.3 ^{11}B NMR of fast-exchanging monomer shows evidence of B-N coordination.

4.2.2 Crosslinked Materials Synthesized with Phenol ether and Aniline derivative Monomers

To address these issues, new synthetic routes were proposed, which are outlined in Scheme 4.3 below. First, in order to avoid the B-N coordination, aniline derivative **4.4** and phenol ether derivative **4.5** monomers were proposed. In Wulff *et al.*'s original report describing neighboring group rate effects on boronate trans-esterification,[163] *o*-aniline boronic esters are reported to have similar trans-esterification rate-enhancement effects, but without the detrimental effects of B-N coordination. Furthermore, the ethylene linker of monomers **4.1** and **4.2** were replaced by a hexyl linker in order to enhance hydrophobicity and potentially mitigate moisture sensitivity.

Scheme 4.3. Synthesis of Phenol- and Aniline- based Boronic Acid Monomers

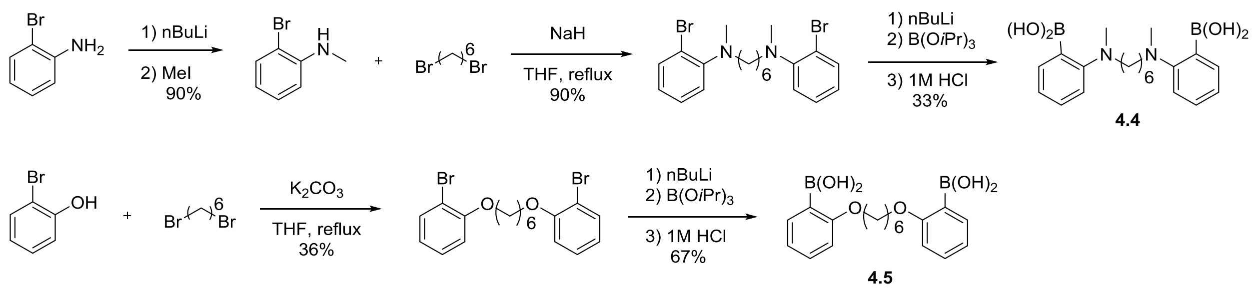

Starting with these monomer units, thermosetting matrix networks were synthesized through poly-condensation of boronic acids and multivalent diols. The stoichiometry was modified from the previous section to have 1% excess of diol units as compared to the boronic acids. The excess of diol was kept small in order to minimize sensitivity to humidity, but non-zero in order to provide a basis for dynamic exchange as needed for vitrimeric properties. The monomer components were mixed in DMF and cast at mild temperatures in house vacuum, followed by curing at elevated temperatures and high vacuum. The obtained films were molded into ASTM Type V dogbone shapes for testing (see Scheme 4.4 below).

Scheme 4.4. Network Synthesis with Phenol- and Aniline- based Monomers

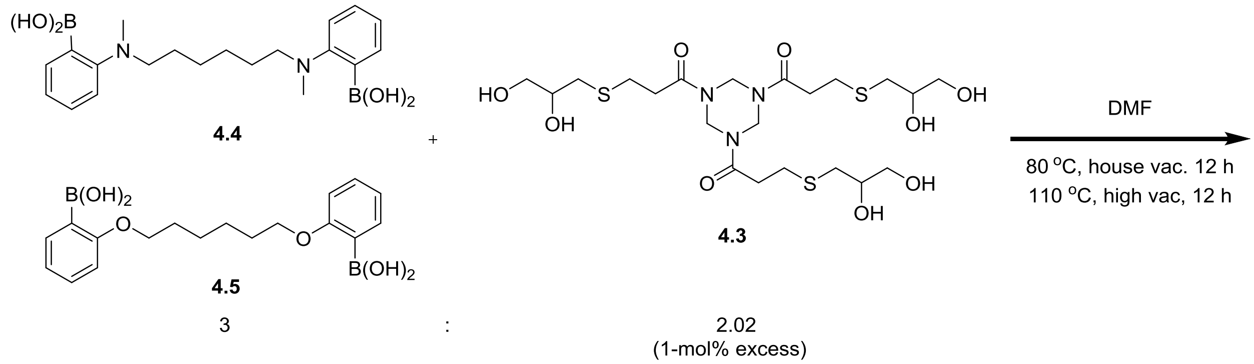

A few emergent properties are needed in order to qualify a material as a vitrimer, and those properties were tested for in the materials synthesized in Scheme 4.5. First, as a highly crosslinked epoxy-like matrix, the mechanical properties often tend towards very strong and somewhat brittle, reaching tens of MPa in ultimate strength, approaching or exceeding a gigapascal in Young's modulus, and typically not exceeding 10% strain.[103,105,106] The mechanical properties of the materials synthesized as shown in Scheme 4.5 meet these criteria, with the material synthesized from slow-exchanging monomer **4.5** demonstrating up to 60 MPa ultimate strength, 1.0 GPa Young's modulus, and 8% strain. The fast-exchanging variety shows slightly weaker but similar properties (Figure 4.4 a). Additionally, an inherent property of vitrimers is its reprocessability, typically at elevated temperatures, without loss of mechanical properties. When tested for the material made from monomer **4.5**, the sample was found to be robustly reprocessable, with modest loss in mechanical properties (Figure 4.4a). This loss in properties may be due to sample defects arising from a greater difficulty in reprocessing material due to low percentage excess of diol.

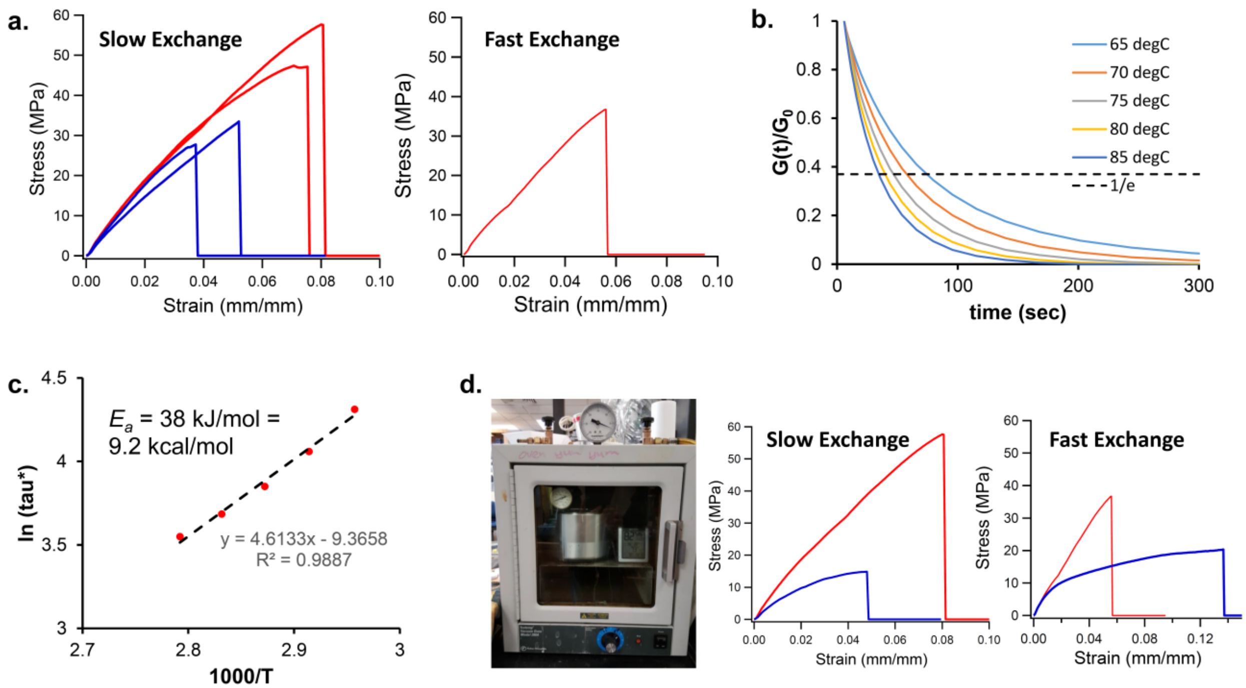

Figure 4.4 Properties of crosslinked samples made from monomers **4.4** and **4.5** **a.** Mechanical properties of fast- (**4.4**) and slow- (**4.5**) exchanging materials. Red curves are for virgin samples, and blue is reprocessed. **b.** Stress relaxation of slow-exchanging material from temperatures ranging from 65 to 85 degrees. **c.** Calculation of activation energy through Arrhenius fit of SR data. d. Humidity chamber (95% humidity) and resultant mechanical properties. Red is virgin samples, and blue is the sample after 12 h in humidity chamber.

Thirdly, vitrimers show a gradual, Arrhenian change in viscosity with changes in temperature above the T_g. This rate of change in viscosity is related to the rate of chemical exchange and not to polymer mobility, and thus a quantitative correlation between the activation energies of material flow and chemical exchange are often possible with vitrimers. The slow exchange material presently described showed an extremely rapid change in viscosity immediately above the T_g according to stress relaxation studies (Figure 4.4b). Furthermore, the activation energy towards flow of this material was 9.2 kcal/mol (Figure 4.4c), slightly less than half the molecular rate of exchange for the slow exchanging boronic ester.

This result was somewhat discouraging and yet complemented by an experiment attempting to verify the fourth property of vitrimers: its solvent stability. Because a vitrimer is a thermosetting network without any loss of network connectivity at all times, it should be resistant to any solvent that does not chemically react with the exchangeable motif. However, both fast- and slow-exchanging variants were shown to rapidly dissolve in DCM. This must mean that the network is not fully formed, with boronic ester oligomers packing in layers to form the material. Additionally, an explanation for the low activation energy of the stress relaxation studies discussed above is provided, as the activation energy towards flow is most likely related to overcoming the Van der Waals forces between the oligomer sheets. Finally, this could potentially explain the low moisture stability of the materials (Figure 4.4d).

Combined, these issues identified the core challenge in the next step: formation of a robust network for a thoroughly crosslinked matrix. In tackling this challenge, we should address not only the surface issue of network formation, but we expect to obtain stress relaxation data more in line with vitrimer material, and also possibly address hydrolytic stability, as the aspect of water penetrating a fully crosslinked network is likely to be much more challenging. The next section addresses these issues.

4.2.3 Improving Solvent Casting Conditions and Formation of Minimal Network

In order to test appropriate conditions for full network formation, we chose to start material synthesis using model small molecules: benzene-1,4-diboronic acid and TAT tris-diol monomer **4.3**. In searching previous literature for formation of similar networks, we found inspiration in work by Yaghi *et al.* with covalent organic frameworks (COFs), wherein boroxine or boronic ester networks were synthesized in a solvent mixture of mesitylene and 1,4-dioxane.[185] Emulating these conditions, a 1:1:5 mixture of mesitylene, 1,4-dioxane, and DMF was used to cast the solution and form the desired network. Though gratifyingly, the film that was cast and cured in this manner was insoluble in DCM over 24 h, the rather complex solvent casting mixture was less than ideal, particularly the large excess of DMF that was required to solubilize the monomer mixture.

It was hypothesized that the ideal solvent mixture would be a two solvent system: one hydrogen bonding polar solvent to solubilize the monomers, and the other an aromatic solvent to solubilize the forming oligomers. Both would need to be high boiling to ensure slow and controlled casting, but ideally the aromatic solvent would be higher boiling, such that, as networks form and monomers disappear, the aromatic solvent would remain to ensure proper mixing and phase behavior for robust formation of pervasive networks amidst lower polarity oligomers. Thus, a 1:1 v/v mixture of DMF and 1,2,4-trichlorobenzene (TCB) was chosen to great effect. The casting and curing conditions are shown in Scheme 4.5 below.

Scheme 4.5 Casting and Curing Condition for Network Formation

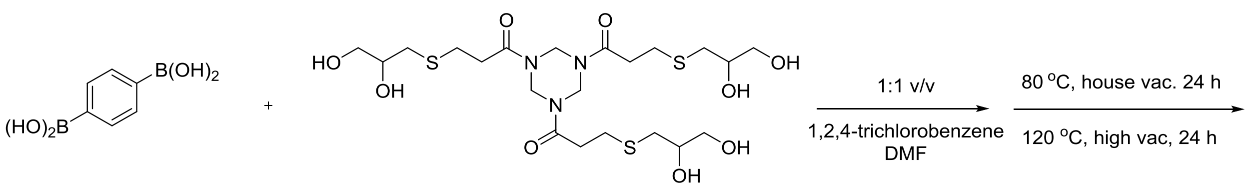

3 : 2.1

We then characterized the full range of properties of the synthesized network. Most crucially, the network was found to be completely insoluble in toluene even at elevated temperature (100 °C) for 48 h, although resistance to solubility in DMF was less robust, losing 78% of its mass to solubilization in identical conditions. Although much care was taken to ensure the DMF was completely anhydrous, it is possible that some residual water in the solvent may have caused depolymerization. Material resistance to water was modest, as ~20% mass was gained in a 95% humidity chamber over 48 h, and close to original mass was regained after applying vacuum (Figure 4.5a). DSC showed a T_g of ~75 °C (Figure 4.5b), and thus multi-temperature stress-relaxation tests were performed at 110 – 140 °C, well above the T_g for optimal results (Figure 4.5c). Relaxation was reasonably slow as expected ($t_{1/2}$ ~ 100 s at 110 °C), and the obtained data fit to an activation energy of material flow of 19 kcal/mol (Figure 4.5d). This activation energy is in perfect agreement with the value calculated for the molecular rate of trans-esterification for slow-exchanging boronic ester, also at 19 kcal/mol,[31] robustly demonstrating the proof-of-concept for boronic ester exchanging vitrimer material. Dynamic mechanical analysis demonstrated a plateau storage modulus at 4.4 MPa (Figure 4.5e), which was used to calculate the topology freezing temperature, T_v, of 16 °C following previously described methods.[103,107] This value is well below the sample's glass transition temperature, which is attributed to the lower rubbery plateau of the material compared to other vitrimer materials, c.f. Leibler's carboxylate epoxy vitrimer.[103] The sample also exhibited robust mechanical properties, at 1.1 GPa Young's modulus and greater than 30 MPa ultimate yield strength (4.5 f). After reprocessing, the material maintained its Young's modulus (1.0 GPa), but lost much of its extensibility and ultimate strength, regaining approximately 40% of both. This is reminiscent of the material created from monomers **4.4** and **4.5**, and though it may be due to sample defects, at this point it is plausible that crosslinking reactions are occurring at high temperatures required for reprocessing, perhaps through a radical mechanism.

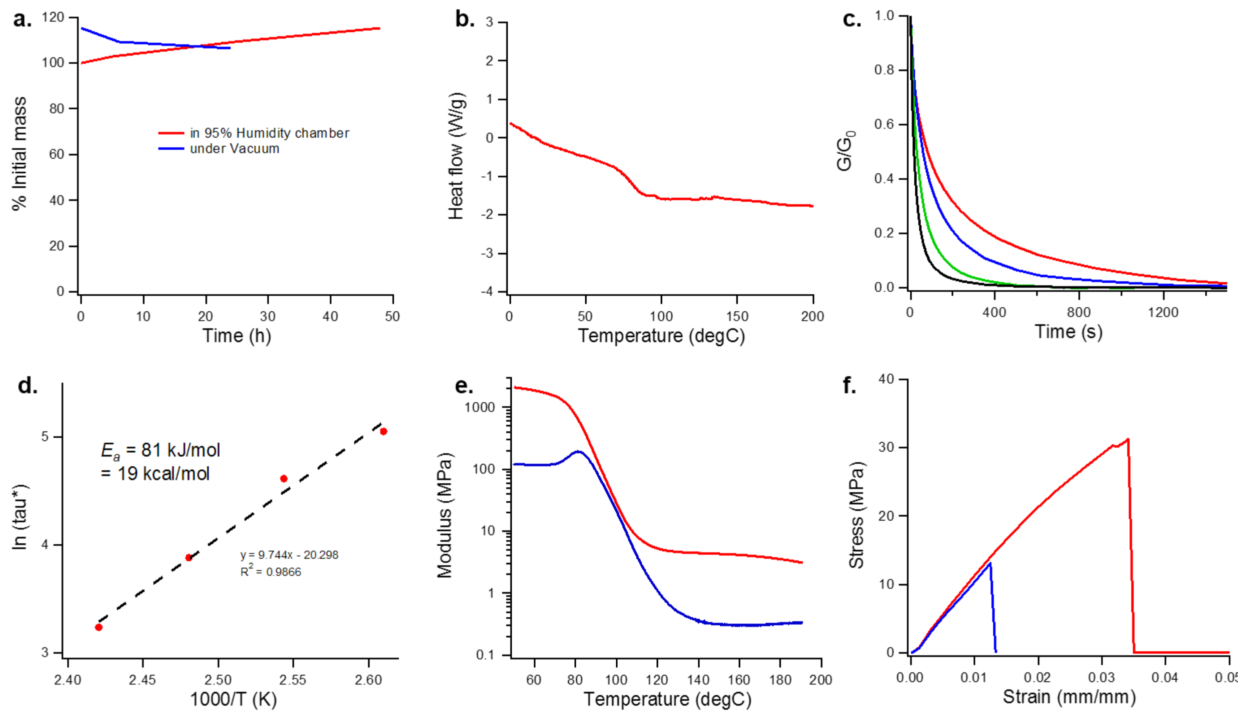

Figure 4.5 Material properties of minimal network. **a.** Mass change from sample's absorption of water in 95% humidity chamber, and removal of water from vacuum. **b.** DSC shows T_g of ~75 °C. **c.** Stress relaxation data at 110, 120, 130, and 140 °C. **d.** Arrhenius fit from decay data shown in 4.5c. Calculated activation energy is 19 kcal/mol. **e.** Iso-strain (0.2 %, 1 Hz) temperature sweep dynamic mechanical analysis (red: storage, blue: loss moduli) shows a plateau in storage modulus above 130 °C at approximately 4.4 MPa. **f.** Tensile properties of pristine (red) and reprocessed (blue) vitrimer.

Unfortunately, the method described in Scheme 4.5 above did not produce networks of the same mechanical integrity when Wulff-type and non-Wulff-type monomers **4.1** and **4.2** were employed in the synthesis. Thermal data (DSC and TGA) were similar to the data that were obtained with previous casting method (see Figure 4.2), but the material synthesized with the slow-exchanging variant showed extremely fast stress relaxation, relaxing all of its stress at the range of tested temperatures (110 – 140 °C) within 100 seconds, inconsistent with a fully formed network. In addition, the material was fully dissolved in hot DMF (100 °C) within 1 hr, also indicating a dominance of oligomeric species instead of a fully crosslinked thermosetting network. As the solvent casting conditions are identical to the minimal network described in Scheme 4.5, incomplete reactivity is an unlikely cause for this behavior, but may be due to favorable loop formation from added flexibility of the linkers in monomers **4.1** and **4.2** compared to benzene-1,4-diboronic acid.

4.3 Conclusions and Outlook

In this chapter, we have demonstrated the novel use of boronic ester bonds to synthesize vitrimer materials. This was achieved through multiple iterations of design, ultimately resulting in an extremely simplified network utilizing benzene-1,4-diboronic acid and a trifunctional diol monomer. The material demonstrated robust mechanical properties reminiscent of commercial epoxies, reprocessability at elevated temperatures due to activated chemistry, and a gradual flow behavior at temperatures above the T_g which robustly fit to an Arrhenius curve with a perfect match to the small molecule exchange kinetics of 19 kcal/mol. Solvent resistance was also evident, however the network had some trouble with especially hygroscopic solvents such as DMF, or high humidity levels. These issues may potentially be addressed with more stable boronic ester bonds, as propylene glycol-type boronic ester bonds are among the least thermodynamically stable boronic ester bonds. Catechol-type or 6-membered ring boronic ester bonds may be an appropriate solution to this issue.

Though we succeeded in describing the first boronic ester-based vitrimer material, we have not yet reached the goal of demonstrating variable kinetics through neighboring group effects, thus affecting T_v, activation energy towards material flow, and temperature-dependent variability in mechanical properties. This may be achieved through changing the molecular design of monomers, such as *para*-substituted linkers in the telechelic boronic acid monomers, disfavoring loop formation, or through further optimization of solvent casting conditions. Further research is underway in the lab by Dr. Gao.

4.4 References

(1) Cromwell, O. R.; Chung, J.; Guan, Z. Malleable and Self-Healing Covalent Polymer Networks through Tunable Dynamic Boronic Ester Bonds *Journal of the American Chemical Society* **2015**, *137*(20), 6492-6495.

(2) Denissen, W.; Winne, J. M.; Du Prez, F. E. Vitrimers: permanent organic networks with glass-like fluidity *Chemical Science* **2016**, *7*(1), 30-38.

(3) Capelot, M.; Unterlass, M. M.; Tournilhac, F.; Leibler, L. Catalytic Control of the Vitrimer Glass Transition *ACS Macro Letters* **2012**, *1*(7), 789-792.

(4) Montarnal, D.; Capelot, M.; Tournilhac, F.; Leibler, L. Silica-Like Malleable Materials from Permanent Organic Networks *Science* **2011**, *334*(6058), 965-968.

(5) Denissen, W.; Rivero, G.; Nicolaÿ, R.; Leibler, L.; Winne, J. M.; Du Prez, F. E. Vinylogous Urethane Vitrimers *Advanced Functional Materials* **2015**n/a-n/a.

(6) Price, E. W.; Cawthray, J. F.; Bailey, G. A.; Ferreira, C. L.; Boros, E.; Adam, M. J.; Orvig, C. H4octapa: An Acyclic Chelator for 111In Radiopharmaceuticals *Journal of the American Chemical Society* **2012**, *134*(20), 8670-8683.

(7) Georgiou, I.; Ilyashenko, G.; Whiting, A. Synthesis of Aminoboronic Acids and Their Applications in Bifunctional Catalysis *Acc. Chem. Res.* **2009**, *42*(6), 756-768.

(8) Bapat, A. P.; Roy, D.; Ray, J. G.; Savin, D. A.; Sumerlin, B. S. Dynamic-Covalent Macromolecular Stars with Boronic Ester Linkages *Journal of the American Chemical Society* **2011**, *133*(49), 19832-19838.

(9) Fortman, D. J.; Brutman, J. P.; Cramer, C. J.; Hillmyer, M. A.; Dichtel, W. R. Mechanically Activated, Catalyst-Free Polyhydroxyurethane Vitrimers *Journal of the American Chemical Society* **2015**, *137*(44), 14019-14022.

(10) Obadia, M. M.; Mudraboyina, B. P.; Serghei, A.; Montarnal, D.; Drockenmuller, E. Reprocessing and Recycling of Highly Crosslinked Ion-Conducting Networks through Transalkylation Exchanges of C–N Bonds *Journal of the American Chemical Society* **2015**, *137*(18), 6078-6083.

(11) Brutman, J. P.; Delgado, P. A.; Hillmyer, M. A. Polylactide Vitrimers *ACS Macro Letters* **2014**, *3*(7), 607-610.

(12) Zhu, L.; Shabbir, S. H.; Gray, M.; Lynch, V. M.; Sorey, S.; Anslyn, E. V. A Structural Investigation of the N−B Interaction in an o-(N,N-Dialkylaminomethyl)arylboronate System *Journal of the American Chemical Society* **2006**, *128*(4), 1222-1232.

(13) Wulff, G.; Lauer, M.; Böhnke, H. Rapid Proton Transfer as Cause of an Unusually Large Neighboring Group Effect *Angewandte Chemie International Edition in English* **1984**, *23*(9), 741-742.

(14) Côté, A. P.; Benin, A. I.; Ockwig, N. W.; O'Keeffe, M.; Matzger, A. J.; Yaghi, O. M. Porous, Crystalline, Covalent Organic Frameworks *Science* **2005**, *310*(5751), 1166-1170.

4.5 Experimental

General Experimental Information: Unless otherwise noted, reactions were carried out with stirring with a magnetic stirbar at room temperature. Anhydrous solvents were purified through a column of alumina according to the method described by Pangborn *et al*. before use.[151] All commercial reagents were used as received unless otherwise noted. Flash column chromatography was performed by forced flow of indicated solvent using an automated column (CombiFlash, Teledyne Isco). ^{1}H NMR spectra were recorded at 500 MHz on Bruker GN-500 or CRYO-500 spectrometers. ^{1}H NMR chemical shifts are reported as δ values in ppm relative to TMS or residual solvent: $CDCl_3$ (7.27 ppm), DMSO-d^6 (2.50 ppm), CD_3OD (3.31 ppm). ^{1}H NMR data are reported as follows: chemical shift in ppm, multiplicity (s = singlet, d = doublet, t = triplet, q = quartet), coupling constants in Hz, and relative integration in number of protons. Multiplets (m) are reported over the range of chemical shift at which they appear.

(((Ethane-1,2-diylbis(methylazanediyl))bis(methylene))bis(2,1-phenylene))diboronic acid (4.1). Synthesis of this compound was modified from a procedure reported by Price *et al*.[183] In a flame dried 50 mL round bottom flask, anhydrous MeOH was collected (20 mL), and 2-formylphenylboronic acid (1.00 g; 6.67 mmol), N,N'-dimethylethylenediamine (359 μL; 3.33 mmol), and activated 4 Å molecular sieves (250 mg) were added to the reaction flask. The reaction mixture was heated to reflux, with slow stirring in order to prevent breaking of the molecular sieves. After 4 h of heating at reflux, the reaction mixture was cooled to 0 °C, and $NaBH_4$ was added (542 mg; 14.3 mmol) in three batches. The reaction mixture was allowed to come to room temperature overnight. The molecular sieves were filtered out, and the solvent was evaporated to dryness *in vacuo*. To the residue was added saturated aqueous $NaHCO_3$ (10 mL), water (10 mL), and chloroform (40 mL). The aqueous layer was extracted twice more with chloroform (20 mL), and the combined organic layers were dried with $MgSO_4$, filtered, and evaporated to dryness. Acetonitrile (~10 mL) was added followed by water (~40 mL), and the mixture was sonicated, from which white precipitate appeared. The mixture was further heated to 50 °C for 2 h, resulting in more precipitate. The white precipitate thus obtained was filtered and dried to obtain pure product. Yield 270 mg (20 %) white flaky solid.

^{1}H NMR (500 MHz, CD_3OD): δ 7.51 (m, 2H), 7.26 (m, 4H), 7.18 (m, 2H), 4.02 (s, 4H), 3.28 (s, 4H), 2.51 (s, 6H). *m* / *z* calcd for $C_{18}H_{26}B_2N_2O_4$ $(M+4Me+Na)^+$ 435.26, found 435.05.

1,2-Bis((2-bromobenzyl)oxy)ethane. In a flame-dried, 250 mL round bottom flask, NaH in 60% mineral oil dispersion (1.60 g, 40.0 mmol) was measured. Under an anhydrous N_2 blanket, mineral oil was washed with hexanes (3 x 10 mL), and dry THF (50 mL) was transferred to the flask. Ethylene glycol (560 μL; 621 mg, 10.0 mmol) was added to the reaction mixture under N_2 purge. The mixture was allowed to stir for ~10 minutes, after which 2-bromobenzyl bromide (2.70 mL; 5.00 g, 20.0 mmol) was added to the reaction mixture, and was heated to reflux for 20 hours. After cooling the reaction mixture to room temperature, excess NaH was quenched through dropwise addition of DI water. After complete quenching, DI water (50 mL) was added, and the organic layer extracted with DCM (4 x 20 mL). The organic layer was dried over Na_2SO_4, filtered, and concentrated *in vacuo*. The resulting residue was purified through silica column chromatography (0 – 70% DCM in hexanes, product fractions ~55 % DCM) to afford product as a yellow oil (3.26 g, 81%).

^{1}H NMR (500 MHz, $CDCl_3$): δ 7.56 – 7.53 (m, 4H), 7.32 (t, J = 7.5 Hz, 2H), 7.16 (t, J = 7.5 Hz, 2H), 4.68 (s, 4H), 3.81 (s, 4H). *m* / *z* calcd for $C_{16}H_{16}Br_2O_2$ $(M+Na)^+$ 422.94, found 422.95.

(((Ethane-1,2-diylbis(oxy))bis(methylene))bis(2,1-phenylene))diboronic acid (4.2). In a flame-dried, 50 mL round bottom flask, a mixture of anhydrous THF and anhydrous PhMe (2 and

8 mL, respectively) were obtained, and 1,2-bis((2-bromobenzyl)oxy)ethane (500 mg; 1.25 mmol) was added. The flask was cooled to -78 °C in a dry ice/acetone bath, and the headspace was backfilled with N_2. 1.6 M nBuLi (1.87 mL; 3.00 mmol) was added dropwise over 15 min, and allowed to react for an additional 15 min. $B(OiPr)_3$ (692 μL; 3.00 mmol) was added dropwise over 15 min, allowed to come to 0 °C over ~1.5 h, then reacted at room temperature for about 45 min. Afterwards, ~10 mL 1M HCl was added, and the organic layer turned cloudy. Addition of more THF (~20 mL) made the solution clear again. The organic layer was collected, dried to near dryness *in vacuo*, and water (~40 mL) was added. The mixture was heated to 50 °C for ~2 h, at which point the resulting white precipitate was filtered. Yield 215 mg (52%) white flaky solid.

^1H NMR (500 MHz, DMSO-d^6): δ 8.02 (s, 4H), 7.52 (d, J = 7.5 Hz, 2H), 7.35 – 7.32 (m, 4H), 7.27 – 7.23 (m, 2H), 4.64 (s, 4H), 3.61 (s, 4H). m/z calcd for $C_{16}H_{20}B_2O_6$ $(M+4Me+Na)^+$ 409.20, found 408.98.

TAT tris-diol (4.3). Synthesis of this compound was followed from literature as reported by Bapat *et al*,[168] with the following exceptions: 1) benzylamine was used as catalyst instead of 1-hexylamine. 2) Recrystallization from cold methanol was performed twice instead of thrice to yield analytically pure product.

^1H NMR (500 MHz, DMSO-d^6): δ 5.25 (br. s. 6H), 4.76 (d, J = 5.1 Hz, 3H), 4.56 (t, J = 5.7 Hz, 3H), 3.57–3.52 (m, 3H), 3.37–3.31 (m, 6H), 2.80–2.73 (m, 6H), 2.73–2.66 (m, 6H), 2.63 (dd, J = 13.4, 4.8 Hz, 3H), 2.46 (dd, J = 13.3, 6.8 Hz, 3H). m/z calcd for $C_{21}H_{39}N_3O_9S_3$ M^+ 573.18, found 573.31.

2-Bromo-N-methylaniline. This compound was synthesized exactly as described in the literature.[186]

^{1}H NMR (500 MHz, $CDCl_3$): δ 7.41 (dd, *J* = 8.3, 1.5 Hz, 1H), 7.21 (td, *J* = 8.0, 1.5 Hz, 1H), 7.16 (dd, *J* = 8.0, 1.5 Hz, 1H), 6.57 (td, *J* = 7.5, 1.5 Hz, 1H), 4.34 (br. s, 1H), 2.89 (s, 3H). *m* / *z* calcd for C_7H_8Br $[M+H]^+$ 185.99, found 185.97.

N1,N6-bis(2-bromophenyl)-N1,N6-dimethylhexane-1,6-diamine. In a flame-dried, 100 mL round-bottom flask, NaH in 60% mineral oil dispersion (658 mg, 16.4 mmol) was measured. Under an anhydrous N_2 blanket, mineral oil was washed with hexanes (3 x 10 mL), and dry THF (45 mL) was transferred to the flask. 1,6-Dibromohexane (1.34 g, 5.48 mmol) was added to the reaction mixture under N_2 purge. The mixture was allowed to stir for ~10 minutes, after which N-methyl-2-bromoaniline (2.14 g, 11.5 mmol) was added to the reaction mixture, and was allowed to stir for 20 hours. Excess NaH was quenched through dropwise addition of DI water. After complete quenching, DI water (50 mL) was added, and the organic layer extracted with DCM (4 x 20 mL). The organic layer was dried over $MgSO_4$, filtered, and concentrated *in vacuo*. The resulting residue was purified through silica column chromatography (0 – 10% EtOAc in hexanes, product fractions ~7% EtOAc) to afford product as a yellow oil (2.25 g, 90%).

^{1}H NMR (500 MHz, $CDCl_3$): δ 7.54 (dd, *J* = 8.0, 1.5 Hz, 2H), 7.24 (td, *J* = 7.0, 1.5 Hz, 2H), 7.07 (dd, *J* = 8.0, 1.5 Hz, 2H), 6.87 (td, *J* = 8.0, 1.5 Hz, 2H), 2.96 (dd, *J* = 8.8, 6.8 Hz, 4H), 2.74 (s, 6H), 1.60 – 1.50 (m, 4H), 1.36 – 1.28 (m, 4H). *m* / *z* calcd for $C_{20}H_{26}Br_2N_2$ $[M+H]^+$ 455.05, found 455.00.

((Hexane-1,6-diylbis(methylazanediyl))bis(2,1-phenylene))diboronic acid (4.4). In a flame-dried, 100 mL round bottom flask, anhydrous THF (20 mL) was added, and N1,N6-bis(2-bromophenyl)-N1,N6-dimethylhexane-1,6-diamine (2.14 g; 4.71 mmol) was added. The flask was cooled to -78 °C in a dry ice/acetone bath, and the headspace was backfilled with N_2. 1.6 M *n*BuLi (6.48 mL; 10.4 mmol) was added dropwise over 20 min, and allowed to react for an additional 30 min. The reaction mixture was heated up to 0 ºC in an ice / water bath over 15 min, then chilled back to -78 ºC in a dry ice/acetone bath for 15 min. The mixture was then cannula transferred to a pre-chilled (-78 ºC dry ice/acetone bath) solution of triisopropyl borate (3.54 g; 18.8 mmol) in anhydrous THF (20 mL) over 1 hr, and the reaction mixture was allowed to come to room temperature overnight. The reaction mixture was quenched with 1M HCl, and the organic layer was extracted with EtOAc (~25 mL x 3). The combined organic later was concentrated *in vacuo* and dissolved in a mixture of 1M NaOH (~200 mL) and DCM (~50 mL) by stirring overnight. The aqueous layer was then collected, pH'ed carefully to 7.00 with 1M HCl, at which point deep red solid flakes appeared. The precipitate was filtered, and washed with water. Yield 591 mg (33%) red-orange flaky solid.

^{1}H NMR (500 MHz, DMSO-d^6): δ 9.29 (s, 4H), 7.72 (dd, J = 8.0, 1.5 Hz, 2H), 7.43 (t, J = 7.0 Hz, 2H), 7.34 (d, J = 8.0 Hz, 2H), 7.15 (t, J = 7.0 Hz, 2H), 2.86 (m, 4H), 2.59 (s, 6H), 1.37 – 1.25 (m, 4H), 1.21 – 1.15 (m, 4H). m / z calcd for $C_{20}H_{30}B_2N_2O_4$ $[M+4Me+Na]^+$ 463.29, found 463.23.

1,6-Bis(2-bromophenoxy)hexane. In a flame-dried, 100 mL round bottom flask, 2-bromophenol (5.00 g; 28.9 mmol) and K_2CO_3 (18.2 g; 131 mmol) were added to a solution of anhydrous THF (50 mL). The mixture was allowed to stir for ~30 minutes, after which 1,6-dibromohexane (3.20 g, 13.1 mmol) was added to the reaction mixture, and was heated to reflux for 18 hours. The reaction mixture was cooled to room temperature, after which excess solid was removed through filtering, and the mixture concentrated *in vacuo*. The residue was purified through silica column (0 – 5% EtOAc in hexanes, product fractions ~2% EtOAc). The fractions with product were pooled and concentrated in vacuo. This residue was diluted in DCM, and washed with 1M NaOH in order to remove residual 2-bromophenol. The organic layer was dried over $MgSO_4$, filtered, and concentrated *in vacuo* to afford product as a white solid (1.82 g, 32%).

^1H NMR (500 MHz, $CDCl_3$): δ 7.53 (dd, J = 7.8, 1.5 Hz, 2H), 7.24 (td, J = 8.5, 1.5 Hz, 2H), 6.89 (dd, J = 8.3, 1.3 Hz, 2H), 6.84 – 6.80 (m, 2H), 4.06 – 4.01 (m, 4H), 1.92 – 1.84 (m, 4H), 1.66 – 1.58 (m, 4H). *m* / *z* calcd for $C_{18}H_{20}Br_2O_2$ $[M+K]^+$ 466.94, found 466.91.

((Hexane-1,6-diylbis(oxy))bis(2,1-phenylene))diboronic acid (4.5). In a flame-dried, 100 mL round bottom flask, anhydrous THF (30 mL) was added, and 1,6-bis(2-bromophenoxy)hexane (1.90g; 4.43 mmol) was added. The flask was cooled to -78 °C in a dry ice/acetone bath, and the headspace was backfilled with N_2. 1.6 M *n*BuLi (6.09 mL; 9.74 mmol) was added dropwise over 15 min, and allowed to react for an additional 15 min. Triisopropyl borate (2.00 g; 10.6 mmol) was added dropwise over 15 min, and the reaction mixture was allowed to come to room temperature overnight. The mixture was dried *in vacuo*, after which white solid was obtained. To the solid residue was then added 1M NaOH (~50 mL), until all the solid dissolved. Then the product was allowed to precipitate by pH'ing to acidic conditions with 1M HCl. The precipitate was filtered, and washed with water. Yield 1.06 g (67%) white flaky solid.

^1H NMR (500 MHz, DMSO-d^6): δ 7.69 (s, 4H), 7.57 (d, J = 7.0 Hz, 2H), 7.37 (t, J = 7.3 Hz, 2H), 6.99 (d, J = 8.0 Hz, 2H), 6.93 (t, J = 7.3 Hz, 2H), 4.07 – 4.01 (m, 4H), 1.83 – 1.73 (m, 4H), 1.52 – 1.47 (m, 4H). *m* / *z* calcd for $C_{18}H_{24}B_2O_6$ $[M+4Me+Na]^+$ 437.23, found 437.12.

Representative procedure for synthesis of pervasively crosslinked network with monomer 4.2. In a scintillation vial, compound **4.2** (300 mg, 0.909 mmol) and tris-diol **4.3** (383 mg, 0.667 mmol) were dissolved in DMF (~10 mL). The mixture was stirred for a few minutes to ensure complete dissolution and a homogeneous solution, after which the solution was poured into a flat pan Teflon mold. The solvent was allowed to evaporate slowly at 80 ºC under house vacuum for 12 h, after which residual solvent was removed by heating to 110 °C under high vacuum for 12 h.

The resulting film could be compression molded and reprocessed at elevated temperatures (100 ºC) into testable materials. The process is similar for monomers **4.1** through **4.4**.

Synthesis of pervasively crosslinked simplified network. In a scintillation vial, benzene-1,4-diboronic acid (166 mg, 1.00 mmol) and tris-diol **4.3** (402 mg, 0.700 mmol) were dissolved in a 1:1 v/v mixture of DMF and 1,2,4-trichlorobenzene (3 + 3 mL). The mixture was stirred for a few minutes to ensure complete dissolution and a homogeneous solution, after which the solution was poured into a flat pan Teflon mold. The solvent was allowed to evaporate slowly 80 ºC under house vacuum for 24 h, after which the material was more thoroughly cured at 120 ºC under high vacuum. The material could be compression molded at elevated temperatures (120 ºC) into ASTM standard dogbone materials.

Representative procedure for synthesis of pervasively crosslinked network through poly-condensation. In a scintillation vial, (((ethane-1,2-diylbis(oxy))bis(methylene))bis(2,1-phenylene))diboronic acid (300 mg, 0.909 mmol) and tris-diol (383 mg, 0.667 mmol) were dissolved in DMF (4 mL). The mixture was stirred for a few minutes to ensure complete dissolution and a homogeneous solution, after which the solution was poured into a flat pan Teflon mold. The solvent was allowed to evaporate slowly overnight at 60 ºC under house vacuum, after which residual solvent was removed by heating to 100 °C high vacuum for 24 h. The material could be compression molded and reprocessed at elevated temperatures (100 ºC) into testable materials.

DSC (differential scanning calorimetry) procedure. Differential scanning calorimetry measurements were performed using a TA Q2000 instrument. ~5 mg of polymer sample was placed in a non-hermitic pan and scanned against an empty reference pan. The DSC experiment was performed in a heat-cool cycle (25 to 180 ºC, 20 ºC/min; 180 to -80 ºC, 20 ºC/min; isothermal

-80 ºC, 30 min; -80 to 200 ºC, 20 ºC/min), wherein the thermal transitions for the last heating cycle were recorded.

TGA (thermogravimetric analysis) procedure. The thermal stability of the polymers was probed by TGA. The samples were heated from 25 ºC to 850 ºC at 20 ºC/min and then mass loss was plotted versus temperature. For clarity, the derivative of the mass loss is shown as well.

Stress relaxation procedure and fitting to Arrhenius plot. Stress relaxation experiments were performed using a TA instruments DMA Q800. Sample dimensions were measured (l,w,t) and loaded into the furnace. The sample was equilibrated to a set temperature (e.g. 110 ºC) for 10 min, after which the sample was displaced and held at 0.2% strain for 30 min and the decay of stress over time was monitored over multiple temperatures (e.g. 110, 120, 130, and 140 ºC). From the raw data, the stress relaxation curves were plotted in G/G_0, and characteristic relaxation time (τ^*), or the time for which the original stress to reach 1/e (37%) its original value, was determined for each temperature. These τ^* values were plotted again 1000/T for each corresponding temperature, and a linear regression plot was made, following the Arrhenius equation:

$$\tau(T) = \tau_0 exp\left(\frac{E_a}{RT}\right).$$

The slope of the plot was multiplied by R = 8.314 J/mol K in order to find the activation energy.

Dynamic mechanical analysis procedure and calculation of *T_v*. Stress relaxation experiments were performed using a TA instruments DMA Q800. Sample dimensions were measured (l,w,t) and loaded into the furnace. The sample was then equilibrated at 50 ºC for 10 min, and ramped at 3 ºC/min to 200 ºC at 0.2% strain, 1 Hz to obtain the temperature-dependent storage and loss moduli of the material. The plateau on the storage modulus at temperatures between 130 and 160 ºC was found to be *E'* = 4.4 MPa, which calculates to a characteristic relaxation time of τ^* = 6.8 x

10^5 s according to the Maxwell relation: $\eta = G{\cdot}\tau^*$, where $G = E'/3$. The corresponding temperature on the Arrhenius plot can then be extrapolated, which is the topology freezing temperature T_v.

Tensile testing procedure. The bulk static uniaxial tensile properties of polymer samples were measured using an Instron 3365 instrument with a 500 N load cell with a pulling rate of 100 mm/min. Sample dimensions were measured (l,w,t) and the sample was pulled at ambient temperature until break.

Hydrolytic stability experiment. In a thermally insulating sealed oven, a dewer filled with water was equilibrated overnight in order to reach a humidity level of 95%. Crosslinked sample was then placed in the equilibrated oven, and the gain in mass was monitored at fixed time points. After 48 hr, the sample was taken out of the oven, and placed under high vacuum, where the loss in mass was again monitored at fixed time points. In a separate experiment, a humidity chamber of 95% was obtained as described previously. Then after 12 hours of exposure to this condition, crosslinked samples were mechanically tested as described above.

4.6 References to Experimental

(1) Staudinger, H. *Ber. Deut. Chem. Ges.* **1920**1073.

(2) Flory, P. J. *Principles of Polymer Chemistry*; 1st ed.; Cornell University Press: Ithaca, NY, 1953.

(3) Doi, M.; Edwards, S. F. *The theory of polymer dynamics*; Oxford University Press: Oxford, UK, 1986.

(4) Rubinstein, M.; Colby, R. H. *Polymer Physics*; Oxford University Press: Oxford, 2003.

(5) Cowie, J. M. G. *Polymers: Chemistry & Physics of Modern Materials*; 2nd ed.; Chapman and Hall: New York, NY, 1991.

(6) Odian, G. *Principles of Polymerization*; 4th ed.; John Wiley & Sons, Inc.: Hoboken, NJ, 2004.

(7) Flory, P. J. *Statistical mechanics of chain molecules*; Interscience Publishers: New York, 1969.

(8) Christensen, R. M. *Theory of Viscoelasticity: an Introduction*; 2nd ed.; Academic Press: New York, NY, 1982.

(9) Matyjaszewski, K.; Xia, J. Atom Transfer Radical Polymerization *Chem. Rev.* **2001**, *101*(9), 2921-2990.

(10) Bielawski, C. W.; Grubbs, R. H. In *Controlled and Living Polymerizations*; Wiley-VCH Verlag GmbH & Co. KGaA: 2010, p 297-342.

(11) Kratky, O.; Porod, G. X-ray investigation of dissolved chain molecules *Rec. Trav. Chim. Pays-Bas* **1949**, *68*1106-1123.

(12) Van Krevelen, D. W.; Hoftyzer, P. J. *Properties of Polymers: Their Estimation and Correlation with Chemical Structure*; Elsevier Scientific Publishing Company: Amsterdam, 1976.

(13) Aida, T.; Meijer, E. W.; Stupp, S. I. Functional Supramolecular Polymers *Science* **2012**, *335*(6070), 813-817.

(14) Brunsveld, L.; Folmer, B. J. B.; Meijer, E. W.; Sijbesma, R. P. Supramolecular Polymers *Chem. Rev.* **2001**, *101*(12), 4071-4098.

(15) De Greef, T. F. A.; Smulders, M. M. J.; Wolffs, M.; Schenning, A. P. H. J.; Sijbesma, R. P.; Meijer, E. W. Supramolecular Polymerization *Chem. Rev.* **2009**, *109*(11), 5687-5754.

(16) Rowan, S. J.; Cantrill, S. J.; Cousins, G. R. L.; Sanders, J. K. M.; Stoddart, J. F. Dynamic Covalent Chemistry *Angew. Chem. Int. Ed.* **2002**, *41*(6), 898-952.

(17) Wojtecki, R. J.; Meador, M. A.; Rowan, S. J. Using the dynamic bond to access macroscopically responsive structurally dynamic polymers *Nature Mater.* **2011**, *10*(1), 14-27.

(18) Caruso, M. M.; Davis, D. A.; Shen, Q.; Odom, S. A.; Sottos, N. R.; White, S. R.; Moore, J. S. Mechanically-Induced Chemical Changes in Polymeric Materials *Chem. Rev.* **2009**, *109*(11), 5755-5798.

(19) Black, A. L.; Lenhardt, J. M.; Craig, S. L. From molecular mechanochemistry to stress-responsive materials *J. Mater. Chem.* **2011**, *21*(6), 1655-1663.

(20) Sijbesma, R. P.; Beijer, F. H.; Brunsveld, L.; Folmer, B. J. B.; Hirschberg, J. H. K. K.; Lange, R. F. M.; Lowe, J. K. L.; Meijer, E. W. Reversible Polymers Formed from Self-Complementary Monomers Using Quadruple Hydrogen Bonding *Science* **1997**, *278*(5343), 1601-1604.

(21) Whittell, G. R.; Hager, M. D.; Schubert, U. S.; Manners, I. Functional soft materials from metallopolymers and metallosupramolecular polymers *Nature Mater.* **2011**, *10*(3), 176-188.

(22) Roy, D.; Cambre, J. N.; Sumerlin, B. S. Future perspectives and recent advances in stimuli-responsive materials *Prog. Polym. Sci.* **2010**, *35*(1–2), 278-301.

(23) Blaiszik, B. J.; Kramer, S. L. B.; Olugebefola, S. C.; Moore, J. S.; Sottos, N. R.; White, S. R. Self-Healing Polymers and Composites *Annu. Rev. Mater. Res.* **2010**, *40*(1), 179-211.

(24) Yang, Y.; Urban, M. W. Self-healing polymeric materials *Chem. Soc. Rev.* **2013**, *42*(17), 7446-7467.

(25) Diesendruck, C. E.; Sottos, N. R.; Moore, J. S.; White, S. R. Biomimetic Self-Healing *Angew. Chem. Int. Ed.* **2015**, *54*(36), 10428-10447.

(26) Liu, C.; Qin, H.; Mather, P. T. Review of progress in shape-memory polymers *J. Mater. Chem.* **2007**, *17*(16), 1543-1558.

(27) Denissen, W.; Winne, J. M.; Du Prez, F. E. Vitrimers: permanent organic networks with glass-like fluidity *Chemical Science* **2016**, *7*(1), 30-38.

(28) Otsuka, H.; Nagano, S.; Kobashi, Y.; Maeda, T.; Takahara, A. A dynamic covalent polymer driven by disulfide metathesis under photoirradiation *Chem. Commun.* **2010**, *46*(7), 1150-1152.

(29) Wang, Q.; Gossweiler, G. R.; Craig, S. L.; Zhao, X. Cephalopod-inspired design of electro-mechano-chemically responsive elastomers for on-demand fluorescent patterning *Nature Commun.* **2014**, *5*.

(30) Chung, J.; Kushner, A. M.; Weisman, A. C.; Guan, Z. Direct correlation of single-molecule properties with bulk mechanical performance for the biomimetic design of polymers *Nature Mater.* **2014**, *13*(11), 1055-1062.

(31) Cromwell, O. R.; Chung, J.; Guan, Z. Malleable and Self-Healing Covalent Polymer Networks through Tunable Dynamic Boronic Ester Bonds *JACS* **2015**, *137*(20), 6492-6495.

(32) Vincent, J. F. V.; Bogatyreva, O. A.; Bogatyrev, N. R.; Bowyer, A.; Pahl, A.-K. Biomimetics: its practice and theory *Journal of The Royal Society Interface* **2006**, *3*(9), 471-482.

(33) Fratzl, P. Biomimetic materials research: what can we really learn from nature's structural materials? *Journal of the Royal Society Interface* **2007**, *4*(15), 637-642.

(34) Tatham, A. S.; Shewry, P. R. Elastomeric proteins: biological roles, structures and mechanisms *Trends Biochem. Sci* **2000**, *25*(11), 567-571.

(35) Granzier, H. L.; Labeit, S. The Giant Protein Titin: A Major Player in Myocardial Mechanics, Signaling, and Disease *Circul. Res.* **2004**, *94*(3), 284-295.

(36) Rief, M.; Gautel, M.; Oesterhelt, F.; Fernandez, J. M.; Gaub, H. E. Reversible Unfolding of Individual Titin Immunoglobulin Domains by AFM *Science* **1997**, *276*(5315), 1109-1112.

(37) Kellermayer, M. S. Z.; Smith, S. B.; Granzier, H. L.; Bustamante, C. Folding-Unfolding Transitions in Single Titin Molecules Characterized with Laser Tweezers *Science* **1997**, *276*(5315), 1112-1116.

(38) Li, H.; Oberhauser, A. F.; Fowler, S. B.; Clarke, J.; Fernandez, J. M. Atomic force microscopy reveals the mechanical design of a modular protein *Proc. Natl. Acad. Sci. U.S.A.* **2000**, *97*(12), 6527-6531.

(39) Lu, H.; Schulten, K. Steered molecular dynamics simulations of force-induced protein domain unfolding *Proteins: Structure, Function, and Genetics* **1999**, *35*453-463.

(40) Lu, H.; Schulten, K. The Key Event in Force-Induced Unfolding of Titin's Immunoglobulin Domains *Biophys. J.* **2000**, *79*(1), 51-65.

(41) Marszalek, P. E.; Lu, H.; Li, H.; Carrion-Vazquez, M.; Oberhauser, A. F.; Schulten, K.; Fernandez, J. M. Mechanical unfolding intermediates in titin modules *Nature* **1999**, *402*(6757), 100-103.

(42) Benichou, I.; Givli, S. The hidden ingenuity in titin structure *Appl. Phys. Lett.* **2011**, *98*(9), -.

(43) Beijer, F. H.; Sijbesma, R. P.; Kooijman, H.; Spek, A. L.; Meijer, E. W. Strong Dimerization of Ureidopyrimidones via Quadruple Hydrogen Bonding *JACS* **1998**, *120*(27), 6761-6769.

(44) Söntjens, S. H. M.; Sijbesma, R. P.; van Genderen, M. H. P.; Meijer, E. W. Stability and Lifetime of Quadruply Hydrogen Bonded 2-Ureido-4[1H]-pyrimidinone Dimers *JACS* **2000**, *122*(31), 7487-7493.

(45) Guan, Z.; Roland, J. T.; Bai, J. Z.; Ma, S. X.; McIntire, T. M.; Nguyen, M. Modular Domain Structure: A Biomimetic Strategy for Advanced Polymeric Materials *JACS* **2004**, *126*(7), 2058-2065.

(46) Roland, J. T.; Guan, Z. Synthesis and Single-Molecule Studies of a Well-Defined Biomimetic Modular Multidomain Polymer Using a Peptidomimetic β-Sheet Module *JACS* **2004**, *126*(44), 14328-14329.

(47) Guzmán, D. L.; Roland, J. T.; Keer, H.; Kong, Y. P.; Ritz, T.; Yee, A.; Guan, Z. Using steered molecular dynamics simulations and single-molecule force spectroscopy to guide the rational design of biomimetic modular polymeric materials *Polymer* **2008**, *49*(18), 3892-3901.

(48) Kushner, A. M.; Vossler, J. D.; Williams, G. A.; Guan, Z. A Biomimetic Modular Polymer with Tough and Adaptive Properties *JACS* **2009**, *131*(25), 8766-8768.

(49) Kushner, A. M.; Gabuchian, V.; Johnson, E. G.; Guan, Z. Biomimetic Design of Reversibly Unfolding Cross-Linker to Enhance Mechanical Properties of 3D Network Polymers *JACS* **2007**, *129*(46), 14110-14111.

(50) Guzmán, D. L.; Randall, A.; Baldi, P.; Guan, Z. Computational and single-molecule force studies of a macro domain protein reveal a key molecular determinant for mechanical stability *Proc. Natl. Acad. Sci. U.S.A.* **2010**, *107*(5), 1989-1994.

(51) Carrion-Vazquez, M.; Oberhauser, A. F.; Fowler, S. B.; Marszalek, P. E.; Broedel, S. E.; Clarke, J.; Fernandez, J. M. Mechanical and chemical unfolding of a single protein: A comparison *Proc. Natl. Acad. Sci. U.S.A.* **1999**, *96*(7), 3694-3699.

(52) Stadelmann, W. K.; Digenis, A. G.; Tobin, G. R. Physiology and healing dynamics of chronic cutaneous wounds *Am. J. Surg.* **1998**, *176*26S-36S.

(53) Versteeg, H. H.; Heemskerk, J. W. M.; Levi, M.; Reitsma, P. H. New Fundamentals in Hemostasis *Physiol. Rev.* **2013**, *93*(1), 327-358.

(54) Eming, S. A.; Krieg, T.; Davidson, J. M. Inflammation in Wound Repair: Molecular and Cellular Mechanisms *Journal of Investigative Dermatology*, *127*(3), 514-525.

(55) Midwood, K. S.; Williams, L. V.; Schwarzbauer, J. E. Tissue repair and the dynamics of the extracellular matrix *The International Journal of Biochemistry & Cell Biology* **2004**, *36*(6), 1031-1037.

(56) Chen, X.; Dam, M. A.; Ono, K.; Mal, A.; Shen, H.; Nutt, S. R.; Sheran, K.; Wudl, F. A Thermally Re-mendable Cross-Linked Polymeric Material *Science* **2002**, *295*(5560), 1698-1702.

(57) Cordier, P.; Tournilhac, F.; Soulie-Ziakovic, C.; Leibler, L. Self-healing and thermoreversible rubber from supramolecular assembly *Nature* **2008**, *451*(7181), 977-980.

(58) Wool, R. P.; O'Connor, K. M. A theory crack healing in polymers *J. Appl. Phys.* **1981**, *52*(10), 5953-5963.

(59) Ling, J.; Rong, M. Z.; Zhang, M. Q. Photo-stimulated self-healing polyurethane containing dihydroxyl coumarin derivatives *Polymer* **2012**, *53*(13), 2691-2698.

(60) Froimowicz, P.; Frey, H.; Landfester, K. Towards the Generation of Self-Healing Materials by Means of a Reversible Photo-induced Approach *Macromol. Rapid Commun.* **2011**, *32*(5), 468-473.

(61) Ying, H.; Zhang, Y.; Cheng, J. Dynamic urea bond for the design of reversible and self-healing polymers *Nature Commun.* **2014**, *5*.

(62) Ghosh, B.; Urban, M. W. Self-Repairing Oxetane-Substituted Chitosan Polyurethane Networks *Science* **2009**, *323*(5920), 1458-1460.

(63) Lu, Y.-X.; Guan, Z. Olefin Metathesis for Effective Polymer Healing via Dynamic Exchange of Strong Carbon–Carbon Double Bonds *JACS* **2012**, *134*(34), 14226-14231.

(64) Yoon, J. A.; Kamada, J.; Koynov, K.; Mohin, J.; Nicolaÿ, R.; Zhang, Y.; Balazs, A. C.; Kowalewski, T.; Matyjaszewski, K. Self-Healing Polymer Films Based on Thiol–Disulfide Exchange Reactions and Self-Healing Kinetics Measured Using Atomic Force Microscopy *Macromolecules* **2011**, *45*(1), 142-149.

(65) An, S. Y.; Noh, S. M.; Nam, J. H.; Oh, J. K. Dual Sulfide–Disulfide Crosslinked Networks with Rapid and Room Temperature Self-Healability *Macromol. Rapid Commun.* **2015**n/a-n/a.

(66) Zheng, P.; McCarthy, T. J. A Surprise from 1954: Siloxane Equilibration Is a Simple, Robust, and Obvious Polymer Self-Healing Mechanism *JACS* **2012**, *134*(4), 2024-2027.

(67) Amamoto, Y.; Kamada, J.; Otsuka, H.; Takahara, A.; Matyjaszewski, K. Repeatable Photoinduced Self-Healing of Covalently Cross-Linked Polymers through Reshuffling of Trithiocarbonate Units *Angew. Chem. Int. Ed.* **2011**, *50*(7), 1660-1663.

(68) Amamoto, Y.; Otsuka, H.; Takahara, A.; Matyjaszewski, K. Self-Healing of Covalently Cross-Linked Polymers by Reshuffling Thiuram Disulfide Moieties in Air under Visible Light *Adv. Mater.* **2012**, *24*(29), 3975-3980.

(69) Lehn, J.-M. Toward complex matter: Supramolecular chemistry and self-organization *Proc. Natl. Acad. Sci. U.S.A.* **2002**, *99*(8), 4763-4768.

(70) Chen, Y.; Kushner, A. M.; Williams, G. A.; Guan, Z. Multiphase design of autonomic self-healing thermoplastic elastomers *Nature Chem.* **2012**, *4*(6), 467-472.

(71) Chen, Y.; Guan, Z. Multivalent hydrogen bonding block copolymers self-assemble into strong and tough self-healing materials *Chem. Commun.* **2014**, *50*(74), 10868-10870.

(72) Chen, Y.; Guan, Z. Self-assembly of core-shell nanoparticles for self-healing materials *Polymer Chemistry* **2013**, *4*(18), 4885-4889.

(73) Williams, G. A.; Ishige, R.; Cromwell, O. R.; Chung, J.; Takahara, A.; Guan, Z. Mechanically Robust and Self-Healable Superlattice Nanocomposites by Self-Assembly of Single-Component “Sticky” Polymer-Grafted Nanoparticles *Adv. Mater.* **2015**, *27*(26), 3934-3941.

(74) Burnworth, M.; Tang, L.; Kumpfer, J. R.; Duncan, A. J.; Beyer, F. L.; Fiore, G. L.; Rowan, S. J.; Weder, C. Optically healable supramolecular polymers *Nature* **2011**, *472*(7343), 334-337.

(75) Mozhdehi, D.; Ayala, S.; Cromwell, O. R.; Guan, Z. Self-Healing Multiphase Polymers via Dynamic Metal-Ligand Interactions *JACS* **2014**.

(76) Burattini, S.; Colquhoun, H. M.; Fox, J. D.; Friedmann, D.; Greenland, B. W.; Harris, P. J. F.; Hayes, W.; Mackay, M. E.; Rowan, S. J. A self-repairing, supramolecular polymer system: healability as a consequence of donor-acceptor [small pi]-[small pi] stacking interactions *Chem. Commun.* **2009**(44), 6717-6719.

(77) Burattini, S.; Greenland, B. W.; Merino, D. H.; Weng, W.; Seppala, J.; Colquhoun, H. M.; Hayes, W.; Mackay, M. E.; Hamley, I. W.; Rowan, S. J. A Healable Supramolecular Polymer Blend Based on Aromatic Ï€âˆ’Ï€ Stacking and Hydrogen-Bonding Interactions *JACS* **2010**, *132*(34), 12051-12058.

(78) Cho, S. H.; Andersson, H. M.; White, S. R.; Sottos, N. R.; Braun, P. V. Polydimethylsiloxane-Based Self-Healing Materials *Adv. Mater.* **2006**, *18*(8), 997-1000.

(79) Xiao, D. S.; Yuan, Y. C.; Rong, M. Z.; Zhang, M. Q. Hollow polymeric microcapsules: Preparation, characterization and application in holding boron trifluoride diethyl etherate *Polymer* **2009**, *50*(2), 560-568.

(80) Esser-Kahn, A. P.; Odom, S. A.; Sottos, N. R.; White, S. R.; Moore, J. S. Triggered Release from Polymer Capsules *Macromolecules* **2011**, *44*(14), 5539-5553.

(81) Yow, H. N.; Routh, A. F. Formation of liquid core-polymer shell microcapsules *Soft Matter* **2006**, *2*(11), 940-949.

(82) Blaiszik, B. J.; Sottos, N. R.; White, S. R. Nanocapsules for self-healing materials *Composites Sci. Technol.* **2008**, *68*(3–4), 978-986.

(83) White, S. R.; Sottos, N. R.; Geubelle, P. H.; Moore, J. S.; Kessler, M. R.; Sriram, S. R.; Brown, E. N.; Viswanathan, S. Autonomic healing of polymer composites *Nature* **2001**, *409*(6822), 794-797.

(84) Brown, E. N.; White, S. R.; Sottos, N. R. Retardation and repair of fatigue cracks in a microcapsule toughened epoxy composite—Part II: In situ self-healing *Composites Sci. Technol.* **2005**, *65*(15–16), 2474-2480.

(85) Brown, E. N.; Kessler, M. R.; Sottos, N. R.; White, S. R. In situ poly(urea-formaldehyde) microencapsulation of dicyclopentadiene *J Microencapsul* **2003**, *20*719-730.

(86) Kirkby, E. L.; Rule, J. D.; Michaud, V. J.; Sottos, N. R.; White, S. R.; Månson, J.-A. E. Embedded Shape-Memory Alloy Wires for Improved Performance of Self-Healing Polymers *Adv. Funct. Mater.* **2008**, *18*(15), 2253-2260.

(87) Kessler, M. R.; Sottos, N. R.; White, S. R. Self-healing structural composite materials *Composites Part A: Applied Science and Manufacturing* **2003**, *34*(8), 743-753.

(88) Chipara, M. D.; Chipara, M.; Shansky, E.; Zaleski, J. M. Self-healing of high elasticity block copolymers *Polym. Adv. Technol.* **2009**, *20*(4), 427-431.

(89) Rule, J. D.; Brown, E. N.; Sottos, N. R.; White, S. R.; Moore, J. S. Wax-Protected Catalyst Microspheres for Efficient Self-Healing Materials *Adv. Mater.* **2005**, *17*(2), 205-208.

(90) Kamphaus, J. M.; Rule, J. D.; Moore, J. S.; Sottos, N. R.; White, S. R. A new self-healing epoxy with tungsten (VI) chloride catalyst *Journal of The Royal Society Interface* **2008**, *5*(18), 95-103.

(91) Wilson, G. O.; Caruso, M. M.; Schelkopf, S. R.; Sottos, N. R.; White, S. R.; Moore, J. S. Adhesion Promotion via Noncovalent Interactions in Self-Healing Polymers *ACS Applied Materials & Interfaces* **2011**, *3*(8), 3072-3077.

(92) Yuan, L.; Liang, G.; Xie, J.; Li, L.; Guo, J. Preparation and characterization of poly(urea-formaldehyde) microcapsules filled with epoxy resins *Polymer* **2006**, *47*(15), 5338-5349.

(93) Keller, M. W.; White, S. R.; Sottos, N. R. A Self-Healing Poly(Dimethyl Siloxane) Elastomer *Adv. Funct. Mater.* **2007**, *17*(14), 2399-2404.

(94) Xiao, D. S.; Yuan, Y. C.; Rong, M. Z.; Zhang, M. Q. Self-healing epoxy based on cationic chain polymerization *Polymer* **2009**, *50*(13), 2967-2975.

(95) Dry, C. *Compos. Struct.* **1996**, *35*263-269.

(96) Bleay, S. M.; Loader, C. B.; Hawyes, V. J.; Humberstone, L.; Curtis, P. T. A smart repair system for polymer matrix composites *Composites Part A: Applied Science and Manufacturing* **2001**, *32*(12), 1767-1776.

(97) Pang, J. W. C.; Bond, I. P. A hollow fibre reinforced polymer composite encompassing self-healing and enhanced damage visibility *Composites Sci. Technol.* **2005**, *65*(11–12), 1791-1799.

(98) Therriault, D.; White, S. R.; Lewis, J. A. Chaotic mixing in three-dimensional microvascular networks fabricated by direct-write assembly *Nature Mater.* **2003**, *2*(4), 265-271.

(99) Toohey, K. S.; Sottos, N. R.; Lewis, J. A.; Moore, J. S.; White, S. R. Self-healing materials with microvascular networks *Nature Mater.* **2007**, *6*(8), 581-585.

(100) Toohey, K. S.; Hansen, C. J.; Lewis, J. A.; White, S. R.; Sottos, N. R. Delivery of Two-Part Self-Healing Chemistry via Microvascular Networks *Adv. Funct. Mater.* **2009**, *19*(9), 1399-1405.

(101) Esser-Kahn, A. P.; Thakre, P. R.; Dong, H.; Patrick, J. F.; Vlasko-Vlasov, V. K.; Sottos, N. R.; Moore, J. S.; White, S. R. Three-Dimensional Microvascular Fiber-Reinforced Composites *Adv. Mater.* **2011**, *23*(32), 3654-3658.

(102) Patrick, J. F.; Hart, K. R.; Krull, B. P.; Diesendruck, C. E.; Moore, J. S.; White, S. R.; Sottos, N. R. Continuous Self-Healing Life Cycle in Vascularized Structural Composites *Adv. Mater.* **2014**, *26*(25), 4302-4308.

(103) Montarnal, D.; Capelot, M.; Tournilhac, F.; Leibler, L. Silica-Like Malleable Materials from Permanent Organic Networks *Science* **2011**, *334*(6058), 965-968.

(104) Pei, Z.; Yang, Y.; Chen, Q.; Wei, Y.; Ji, Y. Regional Shape Control of Strategically Assembled Multishape Memory Vitrimers *Adv. Mater.* **2016**, *28*(1), 156-160.

(105) Brutman, J. P.; Delgado, P. A.; Hillmyer, M. A. Polylactide Vitrimers *ACS Macro Letters* **2014**, *3*(7), 607-610.

(106) Fortman, D. J.; Brutman, J. P.; Cramer, C. J.; Hillmyer, M. A.; Dichtel, W. R. Mechanically Activated, Catalyst-Free Polyhydroxyurethane Vitrimers *JACS* **2015**, *137*(44), 14019-14022.

(107) Denissen, W.; Rivero, G.; Nicolaÿ, R.; Leibler, L.; Winne, J. M.; Du Prez, F. E. Vinylogous Urethane Vitrimers *Adv. Funct. Mater.* **2015**n/a-n/a.

(108) Obadia, M. M.; Mudraboyina, B. P.; Serghei, A.; Montarnal, D.; Drockenmuller, E. Reprocessing and Recycling of Highly Cross-Linked Ion-Conducting Networks through Transalkylation Exchanges of C–N Bonds *JACS* **2015**, *137*(18), 6078-6083.

(109) Serpe, M. J.; Craig, S. L. Physical Organic Chemistry of Supramolecular Polymers *Langmuir* **2007**, *23*(4), 1626-1634.

(110) Yount, W. C.; Juwarker, H.; Craig, S. L. Orthogonal Control of Dissociation Dynamics Relative to Thermodynamics in a Main-Chain Reversible Polymer *JACS* **2003**, *125*(50), 15302-15303.

(111) Yount, W. C.; Loveless, D. M.; Craig, S. L. Small-Molecule Dynamics and Mechanisms Underlying the Macroscopic Mechanical Properties of Coordinatively Cross-Linked Polymer Networks *JACS* **2005**, *127*(41), 14488-14496.

(112) Yount, W. C.; Loveless, D. M.; Craig, S. L. Strong Means Slow: Dynamic Contributions to the Bulk Mechanical Properties of Supramolecular Networks *Angew. Chem. Int. Ed.* **2005**, *44*(18), 2746-2748.

(113) Green, M. S.; Tobolsky, A. V. A New Approach to the Theory of Relaxing Polymeric Media *The Journal of Chemical Physics* **1946**, *14*(2), 80-92.

(114) Tanaka, F.; Edwards, S. F. Viscoelastic properties of physically crosslinked networks. 1. Transient network theory *Macromolecules* **1992**, *25*(5), 1516-1523.

(115) Capelot, M.; Unterlass, M. M.; Tournilhac, F.; Leibler, L. Catalytic Control of the Vitrimer Glass Transition *ACS Macro Letters* **2012**, *1*(7), 789-792.

(116) van Krevelen, D. W.; te Nijenhuis, K. *Properties of polymers: Their correlation with chemical structure; their numerical estimation and prediction from additive group contributions*; 4th ed.; Elsevier: Oxford, UK, 2009.

(117) Hearle, J. W. S. *Polymers and their properties: Fundamentals of structure and mechanics*; Halstead Press: New York, 1982; Vol. 1.

(118) Flory, P. J. *Principles of polymer chemistry*; Cornell University Press: Ithaca, 1953.

(119) Keten, S.; Xu, Z.; Ihle, B.; Buehler, M. J. Nanoconfinement controls stiffness, strength and mechanical toughness of β-sheet crystals in silk *Nature Mater.* **2010**, *9*(4), 359-367.

(120) Meijer, H. E. H.; Govaert, L. E. Mechanical performance of polymer systems: The relation between structure and properties *Prog. Polym. Sci.* **2005**, *30*(8–9), 915-938.

(121) Serpe, M. J.; Craig, S. L. Physical Organic Chemistry of Supramolecular Polymers *Langmuir* **2006**, *23*(4), 1626-1634.

(122) Halary, J.-L.; Lauprêtre, F.; Monnerie, L. *Polymer materials: Macroscopic properties and molecular interpretations*; John Wiley & Sons, Inc.: Hoboken, New Jersey, 2011.

(123) Janshoff, A.; Neitzert, M.; Oberdörfer, Y.; Fuchs, H. Force Spectroscopy of Molecular Systems—Single Molecule Spectroscopy of Polymers and Biomolecules *Angew. Chem. Int. Ed.* **2000**, *39*(18), 3212-3237.

(124) Oberhauser, A. F.; Marszalek, P. E.; Erickson, H. P.; Fernandez, J. M. The molecular elasticity of the extracellular matrix protein tenascin *Nature* **1998**, *393*(6681), 181-185.

(125) Rief, M.; Gautel, M.; Schemmel, A.; Gaub, H. E. The Mechanical Stability of Immunoglobulin and Fibronectin III Domains in the Muscle Protein Titin Measured by Atomic Force Microscopy *Biophys. J.* **1998**, *75*(6), 3008-3014.

(126) Lee, H.; Scherer, N. F.; Messersmith, P. B. Single-molecule mechanics of mussel adhesion *Proc. Natl. Acad. Sci. U.S.A.* **2006**, *103*(35), 12999-13003.

(127) Lu, H.; Isralewitz, B.; Krammer, A.; Vogel, V.; Schulten, K. Unfolding of Titin Immunoglobulin Domains by Steered Molecular Dynamics Simulation *Biophys. J.* **1998**, *75*(2), 662-671.

(128) Chabria, M.; Hertig, S.; Smith, M. L.; Vogel, V. Stretching fibronectin fibres disrupts binding of bacterial adhesins by physically destroying an epitope *Nature Commun.* **2010**, *1*135.

(129) Lv, S.; Dudek, D. M.; Cao, Y.; Balamurali, M. M.; Gosline, J.; Li, H. Designed biomaterials to mimic the mechanical properties of muscles *Nature* **2010**, *465*(7294), 69-73.

(130) Zhang, W.; Zou, S.; Wang, C.; Zhang, X. Single Polymer Chain Elongation of Poly(N-isopropylacrylamide) and Poly(acrylamide) by Atomic Force Microscopy *J. Phys. Chem. B* **2000**, *104*(44), 10258-10264.

(131) Janke, M.; Rudzevich, Y.; Molokanova, O.; Metzroth, T.; Mey, I.; Diezemann, G.; Marszalek, P. E.; Gauss, J.; Bohmer, V.; Janshoff, A. Mechanically interlocked calix[4]arene dimers display reversible bond breakage under force *Nature Nanotechnol.* **2009**, *4*(4), 225-229.

(132) Ortiz, C.; Hadziioannou, G. Entropic Elasticity of Single Polymer Chains of Poly(methacrylic acid) Measured by Atomic Force Microscopy *Macromolecules* **1999**, *32*(3), 780-787.

(133) Zou, S.; Schönherr, H.; Vancso, G. J. Force Spectroscopy of Quadruple H-Bonded Dimers by AFM: Dynamic Bond Rupture and Molecular Time−Temperature Superposition *JACS* **2005**, *127*(32), 11230-11231.

(134) Hentschel, J.; Kushner, A. M.; Ziller, J.; Guan, Z. Self-Healing Supramolecular Block Copolymers *Angew. Chem. Int. Ed.* **2012**, *51*(42), 10561-10565.

(135) Wagener, K. B.; Boncella, J. M.; Nel, J. G. Acyclic diene metathesis (ADMET) polymerization *Macromolecules* **1991**, *24*(10), 2649-2657.

(136) Rief, M.; Pascual, J.; Saraste, M.; Gaub, H. E. Single molecule force spectroscopy of spectrin repeats: low unfolding forces in helix bundles *J. Mol. Biol.* **1999**, *286*(2), 553-561.

(137) Kratky, O.; Porod, G. X-ray investigation of dissolved chain molecules. *Rec. Trav. Chim. Pays-Bas* **1949**, *68*1106-1123.

(138) Marko, J. F.; Siggia, E. D. Stretching DNA *Macromolecules* **1995**, *28*(26), 8759-8770.

(139) Friedsam, C.; Wehle, A., K.; Kühner, F.; Gaub, H. Dynamic single-molecule force spectroscopy: bond rupture analysis with variable spacer length *J. Phys.: Condens. Matter* **2003**, *15*(18), S1709-S1723.

(140) Bell, G. I. Models for the Specific Adhesion of Cells to Cells *Science* **1978**, *200*(4342), 618-627.

(141) Evans, E.; Ritchie, K. Dynamic strength of molecular adhesion bonds *Biophys. J.* **1997**, *72*(4), 1541-1555.

(142) Diezemann, G.; Janshoff, A. Dynamic force spectroscopy: Analysis of reversible bond-breaking dynamics *J. Chem. Phys.* **2008**, *129*(8), 084904.

(143) Cowie, J. M. G. *Polymers: Chemistry & Physics of Modern Materials*; 2nd ed.; Blackie Academic & Professional: Glasgow, UK, 1991.

(144) Brostow, W. *Performance of plastics*; Hanser/Gardner Publications, Inc.: Cincinnati, 2000.

(145) Holden, G.; Kricheldorf, H. R.; Quirk, R. P. *Thermoplastic elastomers*; 3rd ed.; Hanser Gardner Publications, Inc.: Cincinnati, 2004.

(146) Kramers, H. A. Brownian motion in a field of force and the diffusion model of chemical reactions. *Physica (Utrecht)* **1940**, *7*284-304.

(147) Glasstone, S.; Laidler, K. J.; Eyring, H. *The Theory of Rate Processes*; McGraw-Hill: New York, 1941.

(148) Roetling, J. A. Yield stress behaviour of poly(ethyl methacrylate) in the glass transition region *Polymer* **1965**, *6*(11), 615-619.

(149) Rief, M.; Fernandez, J. M.; Gaub, H. E. Elastically Coupled Two-Level Systems as a Model for Biopolymer Extensibility *Phys. Rev. Lett.* **1998**, *81*(21), 4764-4767.

(150) Benichou, I.; Givli, S. The hidden ingenuity in titin structure *Appl. Phys. Lett.* **2011**, *98*091904.

(151) Pangborn, A. B.; Giardello, M. A.; Grubbs, R. H.; Rosen, R. K.; Timmers, F. J. Safe and Convenient Procedure for Solvent Purification *Organometallics* **1996**, *15*(5), 1518-1520.

(152) Weiner, S. J.; Kollman, P. A.; Case, D. A.; Singh, U. C.; Ghio, C.; Alagona, G.; Profeta, S.; Weiner, P. A new force field for molecular mechanical simulation of nucleic acids and proteins *JACS* **1984**, *106*(3), 765-784.

(153) Hutter, J. L.; Bechhoefer, J. Calibration of atomic-force microscope tips *Rev. Sci. Instrum.* **1993**, *64*(7), 1868-1873.

(154) Ray, C.; Brown, J. R.; Akhremitchev, B. B. Correction of Systematic Errors in Single-Molecule Force Spectroscopy with Polymeric Tethers by Atomic Force Microscopy *J. Phys. Chem. B* **2007**, *111*(8), 1963-1974.

(155) Kloxin, C. J.; Scott, T. F.; Adzima, B. J.; Bowman, C. N. Covalent Adaptable Networks (CANs): A Unique Paradigm in Cross-Linked Polymers *Macromolecules* **2010**, *43*(6), 2643-2653.

(156) Maeda, T.; Otsuka, H.; Takahara, A. Dynamic covalent polymers: Reorganizable polymers with dynamic covalent bonds *Prog. Polym. Sci.* **2009**, *34*(7), 581-604.

(157) Taynton, P.; Yu, K.; Shoemaker, R. K.; Jin, Y.; Qi, H. J.; Zhang, W. Heat- or Water-Driven Malleability in a Highly Recyclable Covalent Network Polymer *Adv. Mater.* **2014**, *26*(23), 3938-3942.

(158) Imato, K.; Nishihara, M.; Kanehara, T.; Amamoto, Y.; Takahara, A.; Otsuka, H. Self-Healing of Chemical Gels Cross-Linked by Diarylbibenzofuranone-Based Trigger-Free Dynamic Covalent Bonds at Room Temperature *Angew. Chem. Int. Ed.* **2012**, *51*(5), 1138-1142.

(159) Weng, W.; Beck, J. B.; Jamieson, A. M.; Rowan, S. J. Understanding the Mechanism of Gelation and Stimuli-Responsive Nature of a Class of Metallo-Supramolecular Gels *JACS* **2006**, *128*(35), 11663-11672.

(160) Giuseppone, N.; Fuks, G.; Lehn, J.-M. Tunable Fluorene-Based Dynamers through Constitutional Dynamic Chemistry *Chem. – Eur. J.* **2006**, *12*(6), 1723-1735.

(161) Sui, Z.; King, W. J.; Murphy, W. L. Protein-Based Hydrogels with Tunable Dynamic Responses *Adv. Funct. Mater.* **2008**, *18*(12), 1824-1831.

(162) Hall, D. G. *Boronic Acids: Preparation and Applications in Organic Synthesis, Medicine and Materials*; John Wiley & Sons, 2012; Vol. 2.

(163) Wulff, G.; Lauer, M.; Böhnke, H. Rapid Proton Transfer as Cause of an Unusually Large Neighboring Group Effect *Angew. Chem. Int. Ed. Engl.* **1984**, *23*(9), 741-742.

(164) Fujita, N.; Shinkai, S.; James, T. D. Boronic Acids in Molecular Self-Assembly *Chem. – Asian J.* **2008**, *3*(7), 1076-1091.

(165) Jäkle, F. Advances in the Synthesis of Organoborane Polymers for Optical, Electronic, and Sensory Applications *Chem. Rev.* **2010**, *110*(7), 3985-4022.

(166) James, T. D.; Sandanayake, K. R. A. S.; Shinkai, S. Saccharide Sensing with Molecular Receptors Based on Boronic Acid *Angew. Chem. Int. Ed. Engl.* **1996**, *35*(17), 1910-1922.

(167) Edwards, N. Y.; Sager, T. W.; McDevitt, J. T.; Anslyn, E. V. Boronic Acid Based Peptidic Receptors for Pattern-Based Saccharide Sensing in Neutral Aqueous Media, an Application in Real-Life Samples *JACS* **2007**, *129*(44), 13575-13583.

(168) Bapat, A. P.; Roy, D.; Ray, J. G.; Savin, D. A.; Sumerlin, B. S. Dynamic-Covalent Macromolecular Stars with Boronic Ester Linkages *JACS* **2011**, *133*(49), 19832-19838.

(169) He, L.; Fullenkamp, D. E.; Rivera, J. G.; Messersmith, P. B. pH responsive self-healing hydrogels formed by boronate-catechol complexation *Chem. Commun.* **2011**, *47*(26), 7497-7499.

(170) Niu, W.; O'Sullivan, C.; Rambo, B. M.; Smith, M. D.; Lavigne, J. J. Self-repairing polymers: poly(dioxaborolane)s containing trigonal planar boron *Chem. Commun.* **2005**(34), 4342-4344.

(171) Cash, J. J.; Kubo, T.; Bapat, A. P.; Sumerlin, B. S. Room-Temperature Self-Healing Polymers Based on Dynamic-Covalent Boronic Esters *Macromolecules* **2015**.

(172) Claridge, T. D. W. In *Tetrahedron Organic Chemistry Series*; Timothy, D. W. C., Ed.; Elsevier: 2009; Vol. Volume 27, p 99-128.

(173) Claridge, T. D. W. In *Tetrahedron Organic Chemistry Series*; Timothy, D. W. C., Ed.; Elsevier: 2009; Vol. Volume 27, p 247-302.

(174) Collins, B. E.; Metola, P.; Anslyn, E. V. On the Rate of Boronate Ester Formation in ortho-Aminomethyl Functionalized Phenyl Boronic Acids *Supramol. Chem.* **2013**, *25*(2), 79-86.

(175) Zhu, L.; Shabbir, S. H.; Gray, M.; Lynch, V. M.; Sorey, S.; Anslyn, E. V. A Structural Investigation of the N−B Interaction in an o-(N,N-Dialkylaminomethyl)arylboronate System *JACS* **2006**, *128*(4), 1222-1232.

(176) Lee, S.-H.; Park, Y.; Wee, K.-R.; Son, H.-J.; Cho, D. W.; Pac, C.; Choi, W.; Kang, S. O. Significance of Hydrophilic Characters of Organic Dyes in Visible-Light Hydrogen Generation Based on TiO2 *Org. Lett.* **2009**, *12*(3), 460-463.

(177) Ding, X.; Chen, L.; Honsho, Y.; Feng, X.; Saengsawang, O.; Guo, J.; Saeki, A.; Seki, S.; Irle, S.; Nagase, S.; Parasuk, V.; Jiang, D. An n-Channel Two-Dimensional Covalent Organic Framework *JACS* **2011**, *133*(37), 14510-14513.

(178) Southwood, T. J.; Curry, M. C.; Hutton, C. A. Factors affecting the efficiency and stereoselectivity of α-amino acid synthesis by the Petasis reaction *Tetrahedron* **2006**, *62*(1), 236-242.

(179) Bielawski, C. W.; Grubbs, R. H. Highly Efficient Ring-Opening Metathesis Polymerization (ROMP) Using New Ruthenium Catalysts Containing N-Heterocyclic Carbene Ligands *Angew. Chem. Int. Ed.* **2000**, *39*(16), 2903-2906.

(180) Qiu, D.; Zheng, Z.; Mo, F.; Zhang, Y.; Wang, J. Increments for 1H and 13C NMR chemical shifts in pinacol arylboronates *Can. J. Chem.* **2011**, *90*(1), 71-74.

(181) Swamy, K. M. K.; Jang, Y. J.; Park, M. S.; Koh, H. S.; Lee, S. K.; Yoon, Y. J.; Yoon, J. A sorbitol-selective fluorescence sensor *Tetrahedron Lett.* **2005**, *46*(20), 3453-3456.

(182) Hillmyer, M. A.; Laredo, W. R.; Grubbs, R. H. Ring-Opening Metathesis Polymerization of Functionalized Cyclooctenes by a Ruthenium-Based Metathesis Catalyst *Macromolecules* **1995**, *28*(18), 6311-6316.

(183) Price, E. W.; Cawthray, J. F.; Bailey, G. A.; Ferreira, C. L.; Boros, E.; Adam, M. J.; Orvig, C. H4octapa: An Acyclic Chelator for 111In Radiopharmaceuticals *JACS* **2012**, *134*(20), 8670-8683.

(184) Georgiou, I.; Ilyashenko, G.; Whiting, A. Synthesis of Aminoboronic Acids and Their Applications in Bifunctional Catalysis *Acc. Chem. Res.* **2009**, *42*(6), 756-768.

(185) Côté, A. P.; Benin, A. I.; Ockwig, N. W.; O'Keeffe, M.; Matzger, A. J.; Yaghi, O. M. Porous, Crystalline, Covalent Organic Frameworks *Science* **2005**, *310*(5751), 1166-1170.

(186) Würtz, S.; Lohre, C.; Fröhlich, R.; Bergander, K.; Glorius, F. IBiox[(−)-menthyl]: A Sterically Demanding Chiral NHC Ligand *JACS* **2009**, *131*(24), 8344-8345.

4.7 Chapter 4 Spectra

^{1}H NMR for compound 4.1

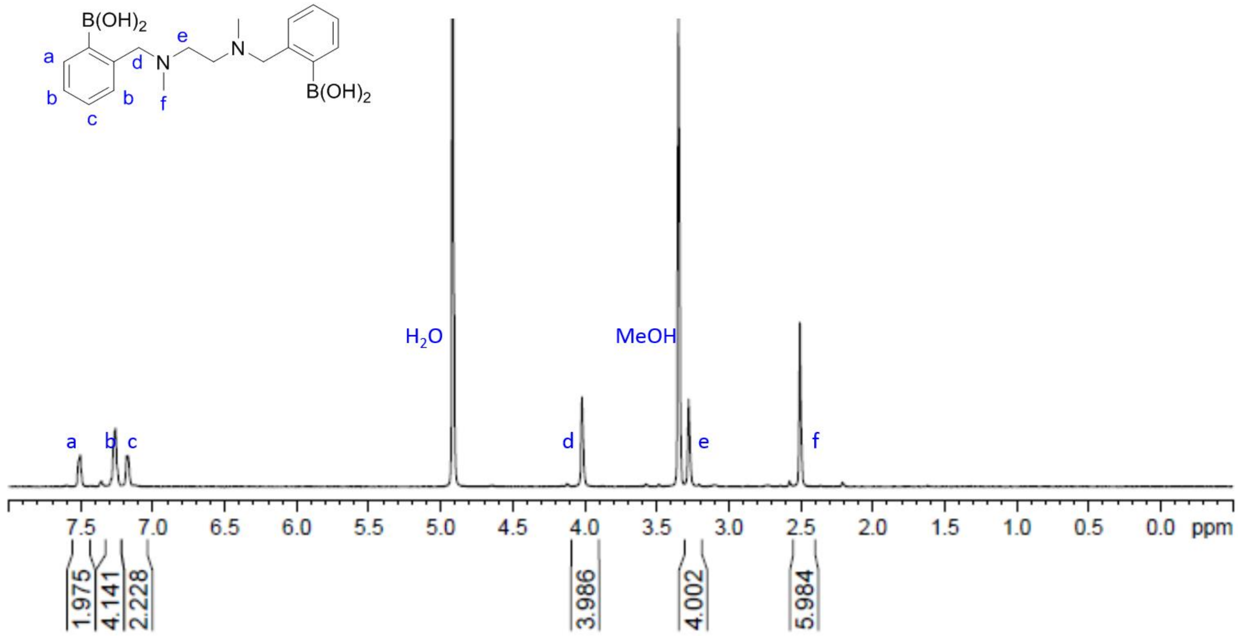

[1]H NMR for 1,2-Bis((2-bromobenzyl)oxy)ethane

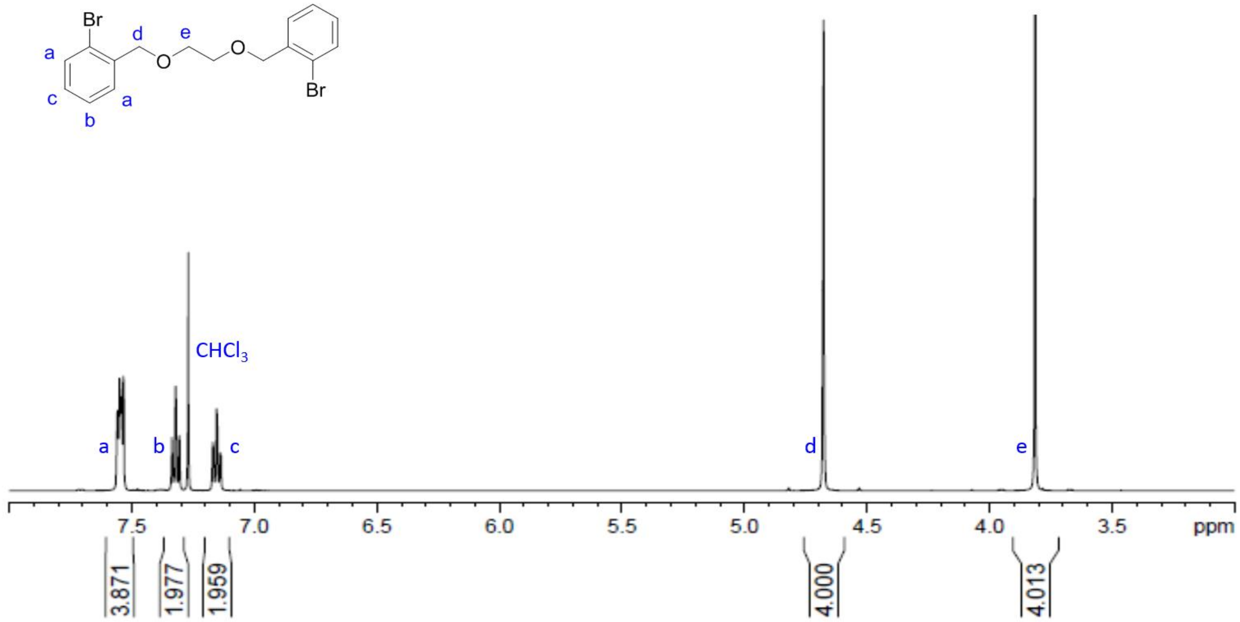

^{1}H NMR for compound 4.2

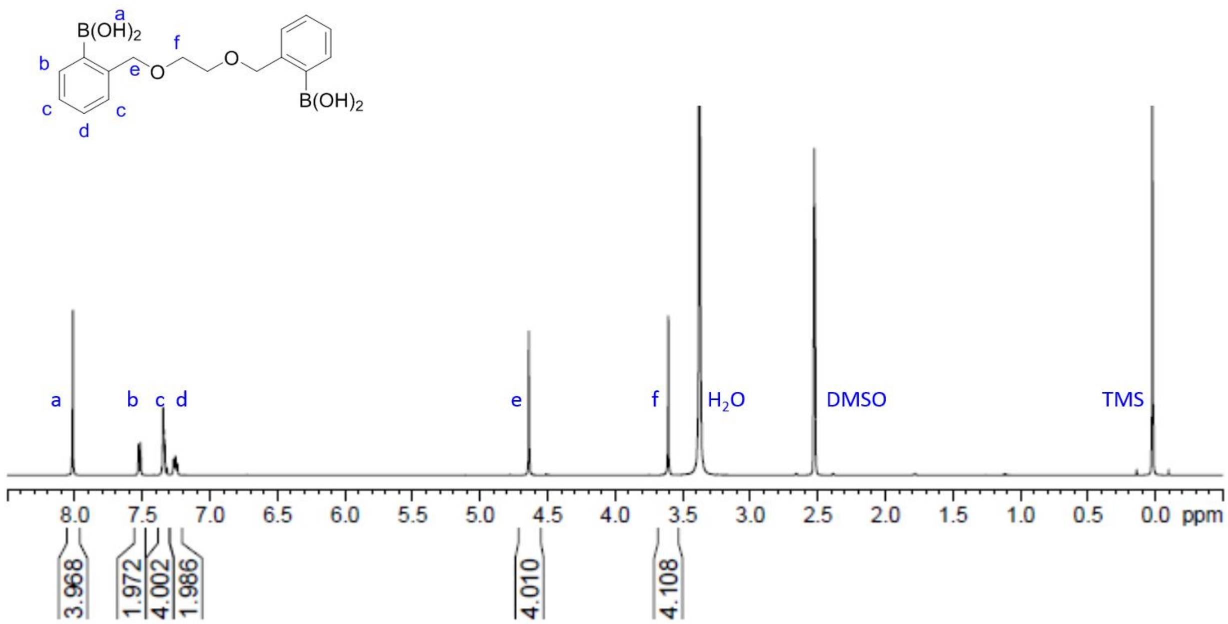

^{1}H NMR for compound 4.3

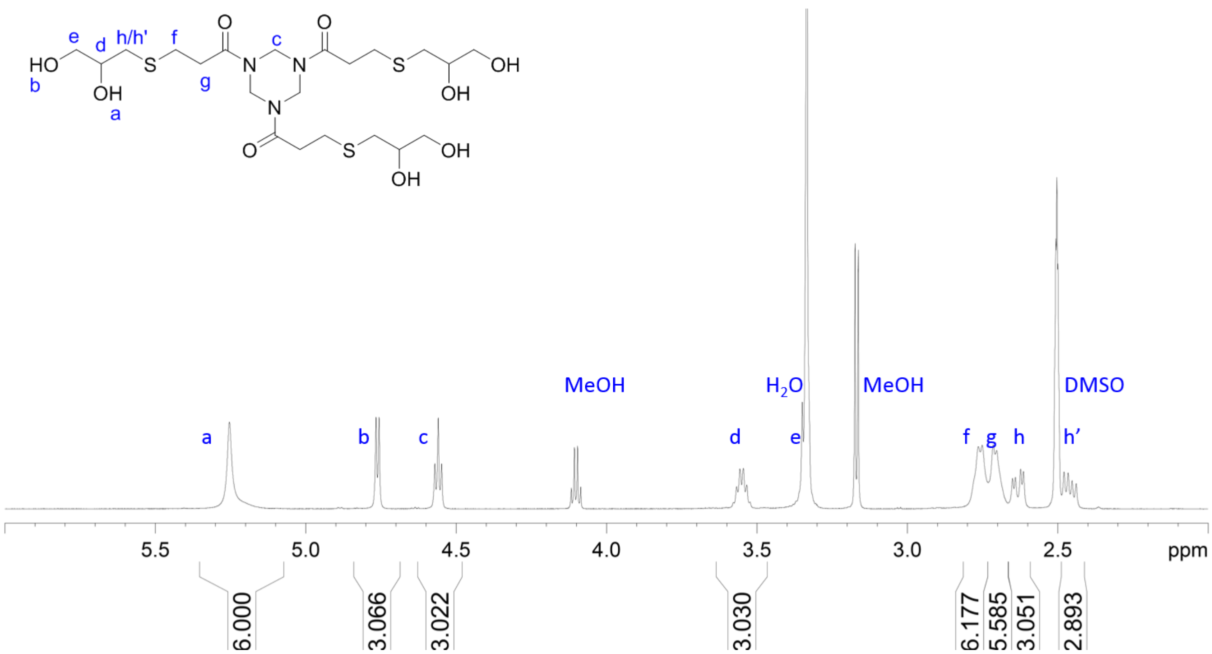

[1]H NMR for 2-bromo-N-methylaniline

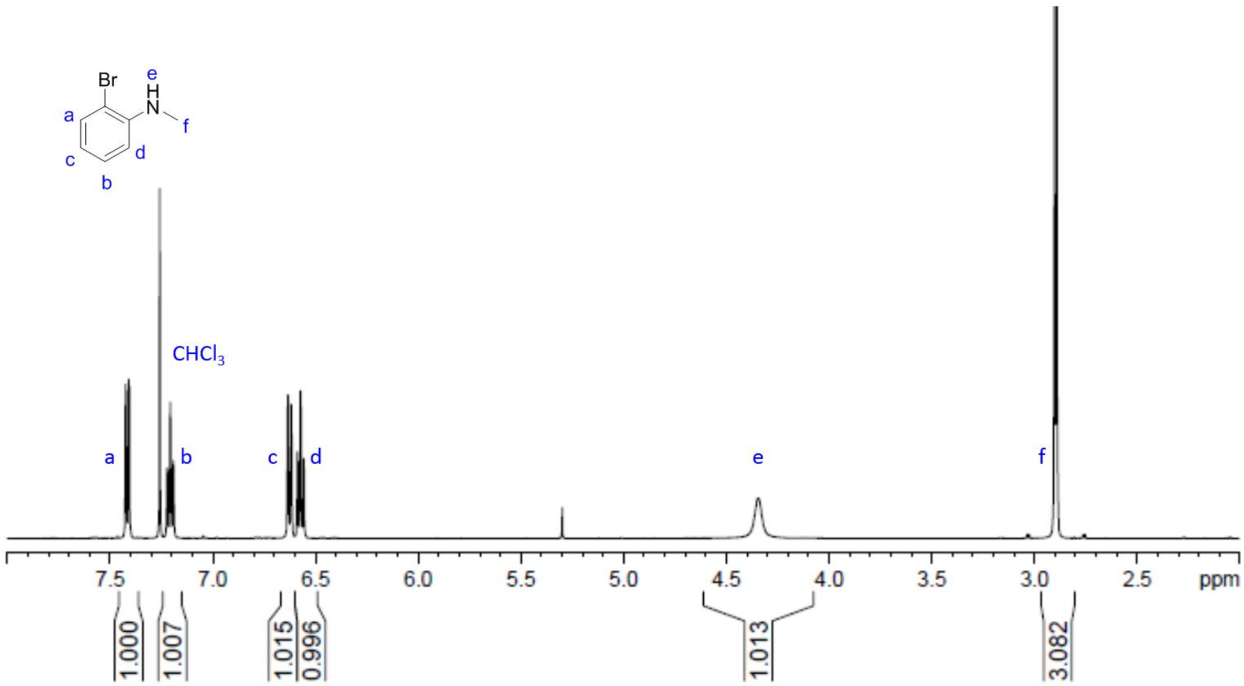

^{1}H NMR for N1,N6-bis(2-bromophenyl)-N1,N6-dimethylhexane-1,6-diamine

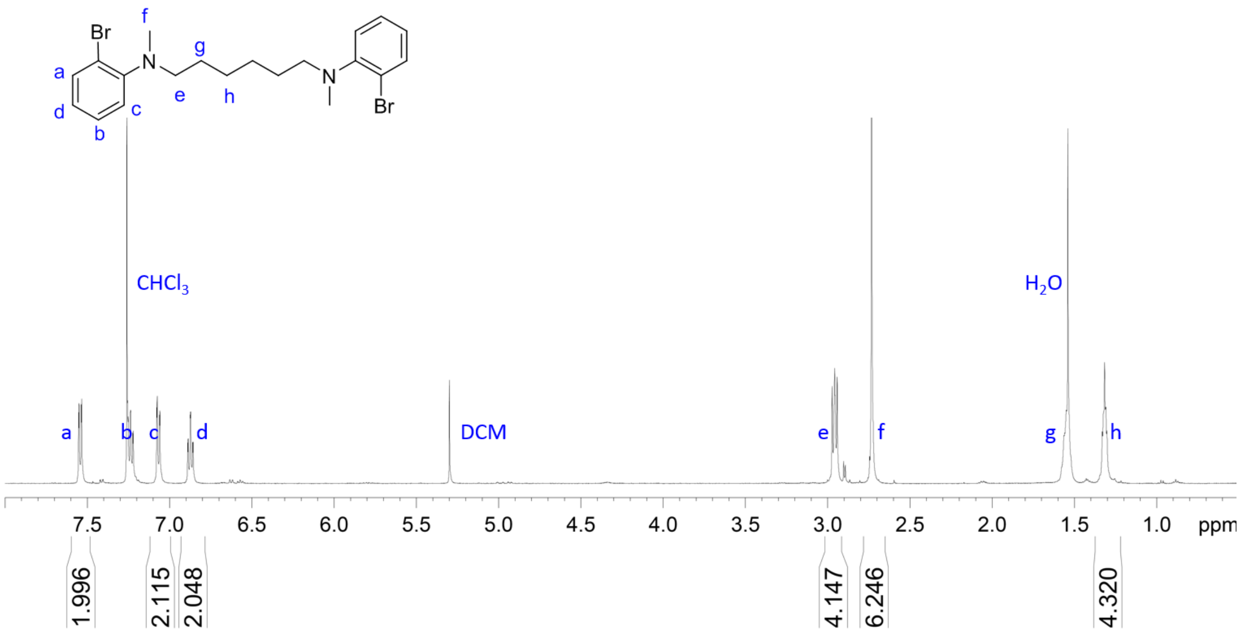

[1]H NMR for compound 4.4

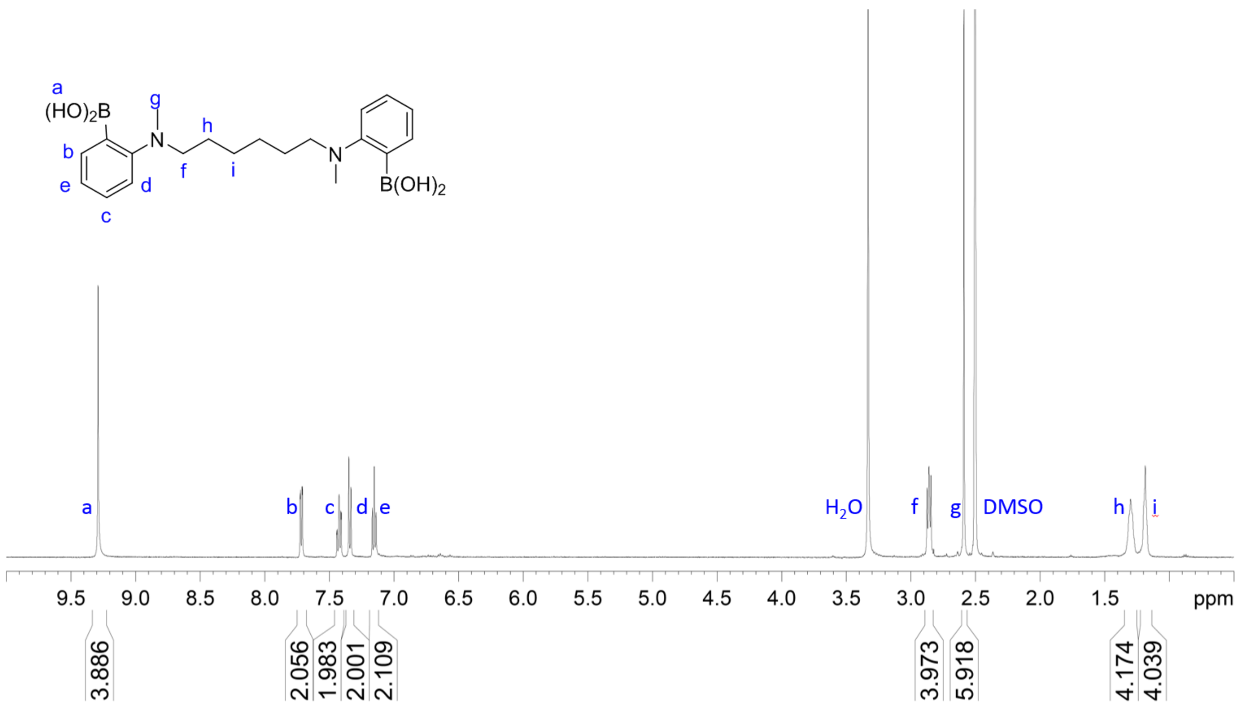

[1]H NMR for 1,6-bis(2-bromophenoxy)hexane

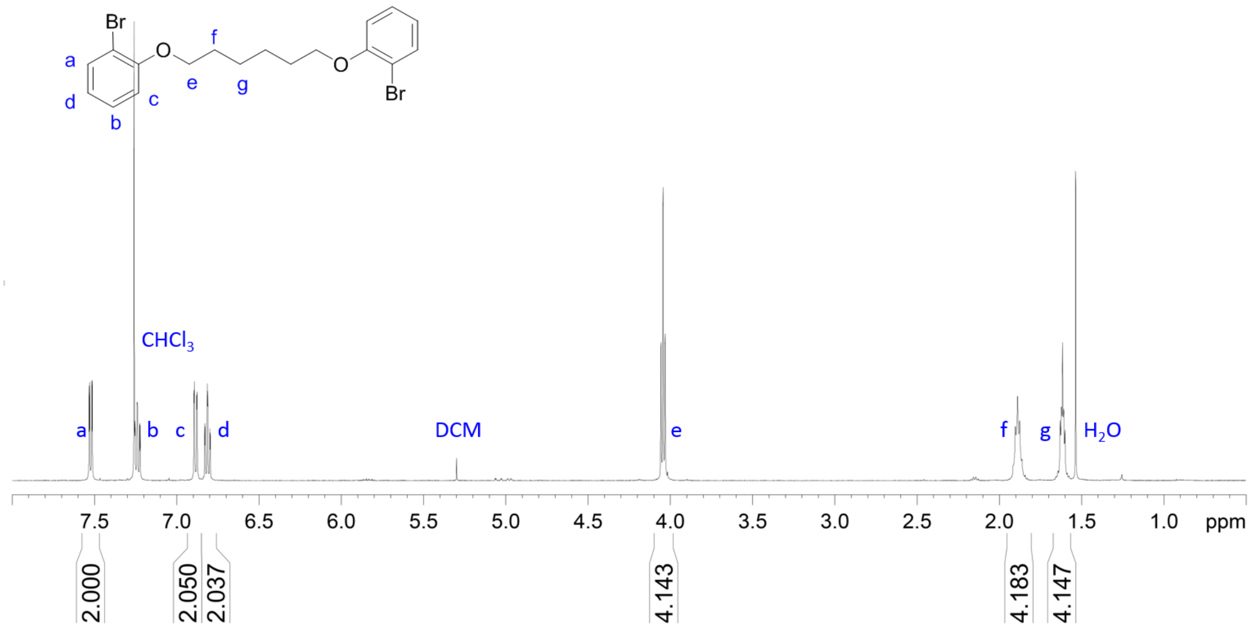

[1]H NMR for compound 4.5